

UNCLASSIFIED

AD NUMBER

AD826192

LIMITATION CHANGES

TO:

Approved for public release; distribution is unlimited.

FROM:

Distribution authorized to U.S. Gov't. agencies and their contractors;
Administrative/Operational Use; 26 SEP 1967.
Other requests shall be referred to Foreign Technology Div., Wright-Patterson AFB, OH 45433.

AUTHORITY

FTD USAF ltr 7 Oct 1971

THIS PAGE IS UNCLASSIFIED

STATEMENT #2 UNCLASSIFIED

FTD-TT-64-991

This document is subject to special export controls and each
government or foreign national may be
required to obtain approval of

CMDR EFD/TOBRD
WPAFB, OHIO, 45433

FOREIGN TECHNOLOGY DIVISION

AD826192



PULSEJET, JET AND ROCKET ENGINES

by

Stanislaw Wojcicki



DDC
RECEIVED
FEB 7 1988
D

~~Distribution of this document is
unlimited. It may be released to
the Clearinghouse, Department of
Commerce, for sale to the general
public.~~

AFMC-WPAFB-JAN 88 136

342

EDITED TRANSLATION

PULSEJET, JET AND ROCKET ENGINES

By: Stanislaw Wojcicki

English pages: 334

Translated under: Contract AF33(657)-14184

STATEMENT #2 UNCLASSIFIED

This document is subject to special export controls and each transmittal to foreign governments or foreign nationals may be made only with prior approval of *CMVR FTD/TDBDR*

WPAFB, OHIO, 45433

TM7001298

THIS TRANSLATION IS A RE rendition OF THE ORIGINAL FOREIGN TEXT WITHOUT ANY ANALYTICAL OR EDITORIAL COMMENT. STATEMENTS OR THEORIES ADVOCATED OR IMPLIED ARE THOSE OF THE SOURCE AND DO NOT NECESSARILY REFLECT THE POSITION OR OPINION OF THE FOREIGN TECHNOLOGY DIVISION.

PREPARED BY:

TRANSLATION DIVISION
FOREIGN TECHNOLOGY DIVISION
WP-APB, OHIO.

Stanislaw Wojcicki

SILNIKI

Pulsacyjne
Strumieniowe
Rakietowe

Wydawnictwo
Ministerstwa Obrony Narodowej

1962

299 pages

FTD-TT-64-991

ITIS INDEX CONTROL FORM

01 Acc Nr TM7001298	68 Translation Nr TT6400991	05 X Ref Acc Nr AM4007084	76 Reel/Frame Nr 1654 1977
97 Header Clas UNCL	63 Clas UNCL, 0	64 Control Markings 0	94 Expansion PO
02 Ctry PO	03 Ref 0000	04 Yr 62	05 Vol 000
06 Iss 000	07 B. Pg. 0001	45 E. Pg. C299	10 Date NONE

Transliterated Title SILNIKY PULSACYJNE, STRUMIENIOWE, RAKIETOWE

09 English Title PULSEJET, RAMJET, AND ROCKET ENGINES

43 Source

MINISTERSTWA OBRONY NARODOWEJ, 1962, 0299 p. (POLISH)

42 Author

WOJCICKI, S.

98 Document Location

16 Co-Author

NONE

47 Subject Codes

01, 07, 21

16 Co-Author

NONE

39 Topic Tags: rocket engine, aircraft engine, nozzle diffuser, combustion theory, combustion

16 Co-Author

NONE

16 Co-Author

NONE

ABSTRACT: This book is intended for engineers and may also be useful to students in technical schools of higher education. The theory, design, and operation of pulsejet, ramjet, and rocket engines are discussed. English translation: 334 pages.

TABLE OF CONTENTS [abridged]

Preface

Foreword

Notations

Chapter 1. Analysis of Engine Operation.....	5
References.....	21
Chapter 2. Characteristic Engine Parameters.....	23
References.....	27
Chapter 3. Flow Problems in Engines.....	28
References.....	74
Chapter 4. Energy Sources.....	75
References.....	101a
Chapter 5. Generation of the Mixture.....	102
References.....	121
Chapter 6. Combustion Theory.....	122
References.....	155
Chapter 7. Pulsejet Engines.....	156
References.....	186
Chapter 8. Ramjet Engines.....	188
References.....	231
Chapter 9. Rocket Engines.....	233
References.....	278

1654 1978

TM7001298

TT6400991

Chapter 10. Compound Engines.....	279
References.....	285
Chapter 11. Engine Cooling.....	286
References.....	296
Chapter 12. Engine Feed Systems.....	297
References.....	306
Chapter 13. Fundamentals of Engine Design.....	307
References.....	315
Chapter 14. Engine Testing.....	317
References.....	332
Appendices.....	333

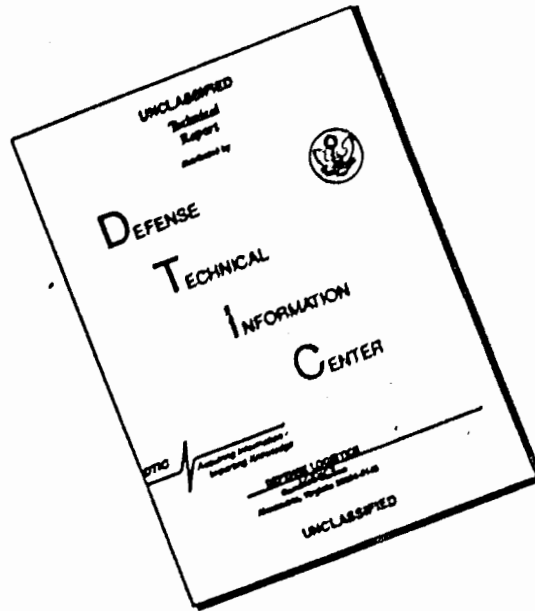
TABLE OF CONTENTS

Preface.....	1
Foreword.....	2
Notations.....	4
Chapter 1. Analysis of Engine Operation.....	5
1.1 The Principle of Pulsejet Engine Operation.....	5
1.2 The Principle of Ramjet Engine Operation.....	6
1.3 The Principle of Rocket Engine Operation.....	8
1.4 The Thrust of Jet Propulsion Engines.....	10
1.5 Power and Efficiency of Propulsion.....	13
1.6 Thermal and Total Efficiency of Flight Engines.....	15
1.7 Velocity Characteristics of Flight Engines.....	16
1.8 Dynamics of the Development of Jet Propulsions Engines - A Short History of Pulsejet Engines- Ramjet Engines and Rocket Engines.....	17
References.....	21
Chapter 2. Characteristic Engine Parameters.....	23
References.....	27
Chapter 3. Flow Problems in Engines.....	28
3.1 Turbulent Flow.....	28
3.2 Diffusers.....	31
3.3 Nozzles.....	55
3.4 Theory of the Gas Ejector.....	63
3.5 Flow with Heat Addition.....	69
References.....	74
Chapter 4. Energy Sources.....	75
4.1 Propellants.....	76
4.2 Free Radicals.....	95
4.3 Nuclear Energy.....	97
References.....	101a
Chapter 5. Generation of the Mixture.....	102
5.1 Injectors.....	102
5.2 Liquid Spray.....	107
5.3 Spray Spectrum.....	110
5.4 Evaporation of Liquid Drops in a Gaseous Medium....	112
5.5 Mixing of the Flows of Sprayed Fuel and Air.....	116
References.....	121

Chapter 6. Combustion Theory.....	122
6.1 Chemical Kinetics of Combustion.....	122
6.2 Combustion of Homogeneous Mixtures in a Laminar Stream.....	125
6.3 Combustion of Homogeneous Mixtures in a Turbulent Stream.....	130
6.4 Flame Stabilization.....	132
6.5 Diffusive Combustion.....	138
6.6 Theory of Combustion of Solid Rocket Fuels.....	146
References.....	155
Chapter 7. Pulsejet Engines.....	156
7.1 Wave Theory of Pulsejets.....	157
7.2 Transient Flow of Gases Through a Pulsejet.....	159
7.3 Analysis of the Output of a Pulsejet Based on the Method of Characteristics.....	161
7.4 Mixture Generation, Ignition and Combustion Development in a Pulsejet.....	163
7.5 Portless Engines.....	167
7.6 Characteristics of Pulsejet Engines.....	171
7.7 Thrust of a Pulsejet Engine.....	176
7.8 Determination of the Characteristic Engine Dimensions.....	178
7.9 Design Solutions of Pulsejet Engines.....	179
7.10 Pulsejet Engine with Detonation Combustion.....	181
7.11 Applications of Pulsejet Engines.....	185
References.....	186
Chapter 8. Ramjet Engines.....	188
8.1 Thermodynamics and Aerodynamics of Ramjets.....	188
8.2 Combustion Chambers of Ramjet Engines.....	199
8.3 Vibrations in the Chamber of a Ramjet Engine.....	209
8.4 Subsonic Ramjet Engines.....	212
8.5 Supersonic Ramjet Engines.....	216
8.6 Hypersonic Ramjet Engines.....	225
8.7 Solid Fuel Ramjet Engines.....	230
References.....	231
Chapter 9. Rocket Engines.....	233
9.1 Thermodynamics of Rocket Engines.....	233
9.2 Solid Propellant Rocket Engines.....	241
9.3 Liquid Fuel Rocket Engines.....	258
9.4 Rocket Engines with Nonchemical Sources of Energy..	271
References.....	278
Chapter 10. Compound Engines.....	279
10.1 Combination of a Turbojet Engine with a Ramjet Engine.....	279
10.2 Tunneling of Pulsejet and Rocket Engines.....	281
References.....	285
Chapter 11. Engine Cooling.....	286

11.1 Heat Conduction Through the Wall.....	287
11.2 Transient Heat Transfer Between Combustion Prod- ucts and Wall.....	292
11.3 Radiative Heat Exchange.....	294
11.4 Composite Heat Transfer.....	295
References.....	296
Chapter 12. Engine Feed Systems.....	297
12.1 Pressure Feed System.....	297
12.2 Force Feed System.....	300
References.....	306
Chapter 13. Fundamentals of Engine Design.....	307
References.....	315
Chapter 14. Engine Testing.....	317
14.1 General Principles of Conducting Developmental Tests.....	317
14.2 Principles of Engine Modeling.....	321
14.3 Test Facilities.....	328
References.....	332
Appendices.....	333

DISCLAIMER NOTICE



THIS DOCUMENT IS BEST QUALITY AVAILABLE. THE COPY FURNISHED TO DTIC CONTAINED A SIGNIFICANT NUMBER OF PAGES WHICH DO NOT REPRODUCE LEGIBLY.

PREFACE

Ryscard Szymani, Professor of Engineering

EDITOR

Jerzy Domanski, Engineer

* * *

This book discusses the problems encountered in the theory, design and research of pulsejets, ramjets, and rocket engines; the basic considerations for the numerical analysis and development of these engines are given; a detailed analysis of the elementary processes is made as they occur in these engines, and the basic directions of their development are shown.

The book is directed towards engineers interested in the technical aspects of aviation and rocketry. It may also serve as a study-guide to graduate students of the different departments in mechanical engineering.

FOREWORD

This book discusses pulsejets, ramjets, and rocket engines with regard to their future in aviation, their present state, and their development in the techniques of rocketry and astronautics. This is the main cause of their continuously increasing significance in the contemporary world.

In this book a first attempt is made to synthesize the problems of these engines encompassing a wide range - where the theory, design and research are treated as undivided factors of equal importance in the formulation of an engine.

This approach arose from the conviction that a great similarity existed among the theoretical and technological problems of these engines. They have in common a very specific and decisive feature in the manner in which they generate thrust: this process, being straightforward and restrained only in one direction of motion, converts thermal energy into the kinetic energy of a jet stream, thus generating thrust.

In this book the elementary processes are at first analyzed as they appear independently in each of the engines under discussion, then the individual features of each engine are pointed out, and those which they have in common are described with regard to their design and research.

This task was the direct result of the adopted approach to discuss these engines as a well-defined, integrated body.

As to the ultimate application of pulsejet, ramjet, and rocket engines, which presently occupy the forefront of heat engine development,

there exists the recognition of two often seemingly opposing ideas: The idea of space flight and the idea of a simple and economical propulsion system for conventional aviation. The author is convinced that these ideas inspire and complement each other, and that they will be achieved during the next ten years as a parallel achievement, and more or less at the same time, by discoveries of designers and scientists.

I am very grateful to the editors of the Technical Books Publishing House MON for their decision to publish this book. The form in which it appeared is to be credited to the scientific editor, Jerzy Domanski, for whose assistance I extend my cordial appreciation.

Warsaw 1961

Stanislaw Wojcicki

NOTATIONS

p [kg/cm ²]	static pressure
p^* [kg/cm ²]	absolute pressure
T [°K]	static temperature
T^* [°K]	absolute temperature
γ [kg/m ³]	specific weight
g [m/sec ²]	acceleration of earth gravity
ρ [kg-sec ² /m ⁴]	density
G [kg/sec]	weight flow rate
S [kg]	thrust
J [sec]	impulse
H_u [kcal/kg]	heat value due to 1 kg of combustible mixture
W_u [kcal/kg]	heat value due to 1 kg of fuel
B [kg/hr]	weight flow rate of propellant
b [kg/kg-hr]	specific fuel consumption
α	excess air coefficient
f	ratio of fuel to oxidizer
F [m ²]	surface area
w [m/sec]	speed
a [m/sec]	speed of sound
M	Mach number
s [kcal/kg-°K]	entropy
i [kcal/kg]	enthalpy

Chapter 1

ANALYSIS OF ENGINE OPERATION

The development of industrial energy sources has always overtaken the development of means of transportation. Because of this observation, engines which are used in transportation are derived primarily from industrial powerplants; and up to this day these two groups of machines have many things in common even in their particular detail. However, jet propulsion, and especially rocket technology, created a requirement for specific transportation engines. And here, for the first time, the situation has become reversed: the internal combustion turbine proved to be the only engine which came to the power industry from the field of transportation.

The approach to most engines from the power industry has left its mark in the theoretical methods by which performance is evaluated, be it a decrease in energy losses or the possibility of an increase in efficiency. However, it is the ultimate purpose of each propulsion engine to develop thrust. It is important, therefore, to examine the change in momentum of the working fluid which in effect creates the thrust; a consideration which is obviously not heeded for industrial powerplants.

1.1. THE PRINCIPLE OF PULSEJET ENGINE OPERATION

The pulsejet engine (Fig. 1.1) consists of a bank of air intake shutters, a combustion chamber with fuel injectors and a spark plug, and of an exhaust nozzle. Fuel is injected continuously into the combustion chamber and forms a combustible mixture with air. The latter

is ignited by an electric spark from the spark plug. As a result of this combustion the burnt gases discharge from the nozzle and, because of their inertia during the last phases of their discharge, an under-pressure is created in the combustion chamber. This opens the array of unidirectional shutters and thus admits a fresh charge of air from the atmosphere to the inside of the engine.

This fresh air, mixed with the injected fuel, again constitutes a burnable mixture which is ignited by some remaining hot gases left over from the preceding sequence. In this manner the cycle repeats itself, and because of the increase in momentum of each ejected charge of air, the thrust of the engine develops.

From a thermodynamic point of view the Lenoir cycle applies to the operation of the pulsejet engine. Accordingly, two theoretical trans-

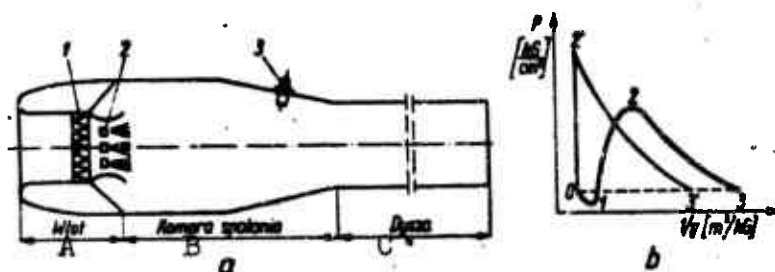


Fig. 1.1. Pulsejet Engine. a) Schematic diagram of engine; b) theoretical and physical cycle diagram; 1) array of unidirectional shutters; 2) fuel injectors; 3) spark plug; A) Inlet; B) combustion chamber; C) discharge nozzle.

formations, namely the isobaric [sic-isochoric] combustion 0-2' and the isentropic expansion 2'-3', stand in place of three physical processes: the expansion 0-1 which takes place during the admission of fresh air to the engine, the combustion 1-2 with a simultaneous increase in pressure and volume, and the adiabatic expansion 2-3.

1.2. THE PRINCIPLE OF RAMJET ENGINE OPERATION

From a thermodynamic point of view the Joule cycle applies to the operation of the ramjet engine (Fig. 1.2). The airstream approaching

at the flight velocity is compressed in the diffuser. The theoretically isentropic process of compression 1-2' is in reality an adiabatic change because of energy losses due to the following conditions: the existence of shock waves in the inlet regions of the diffuser (where $M_0 > 1$) and the loss of energy caused by friction and by turbulence in the subsonic region of the diffuser. Fuel is then injected into the compressed air from injectors which are located upstream of the combustion chamber. Fuel droplets which are thus atomized in the airstream evaporate and with air produce a burnable mixture. This streaming mixture is then ignited by a flame stabilized behind an appropriately constructed flameholder. In this manner is established a flame front which extends throughout the whole cross section of the chamber. Fuel droplets which could not evaporate commence to burn during their passage through the flame front and add to the combustion in the downstream region of the combustion chamber. The theoretically isobaric process of heat addition 2'-3' is in reality a change in state due to the pressure drop 2-3. This pressure drop causes on the one hand the aeromechanical loss of fluid intake. On the other hand, however, it also causes an increase in momentum due to the addition of heat.

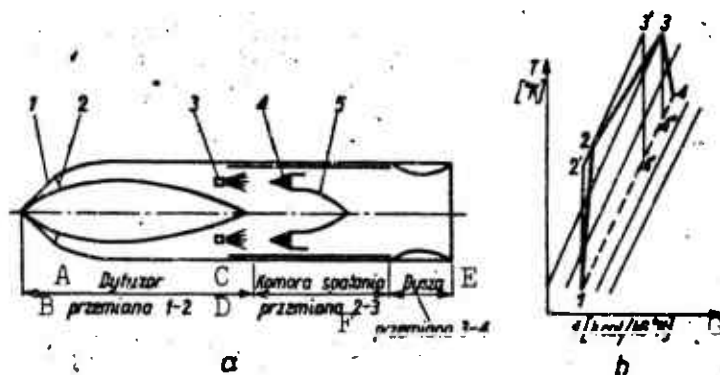


Fig. 1.2. The ramjet engine. a) Schematic diagram of engine; b) theoretical and physical cycle diagram; 1) oblique shock wave; 2) normal shock wave; 3) injectors; 4) flameholder; 5) flame front; A) Diffuser; B) change of state 1-2; C) combustion chamber; D) change of state 2-3; E) exhaust nozzle; F) change of state 3-4; G) s [kcal/kg-°K].

In addition to the mechanical losses, there also exist in the combustion chamber losses due to incomplete burning and due to heat exchange with the environment.

The engine terminates in an exhaust nozzle, wherein the combustion gases expand to atmospheric pressure. Losses which are caused by friction and by turbulence change the theoretically isentropic process of expansion $3'-4'$ to the adiabatic change of state 3-4.

The increase in momentum in the jet stream, as described by the above process, establishes the thrust of the engine.

1.3. THE PRINCIPLE OF ROCKET ENGINE OPERATION

The cycle which can be compared to the operation of the rocket engine is the Rankine cycle. This cycle (Fig. 1.3) can be achieved in two ways, depending upon the type of propellant: in an engine with solid fuel (solid propellant) and in an engine with liquid fuel (liquid propellant).

In the case of an engine with solid propellant the container for the fuel is at the same time the combustion chamber. One employs pre-pellants which are pressed or cast into definite forms which do not change their shape during the reaction time. An ignitor squib is screwed into the bottom of the combustion chamber. It starts the action of the engine by igniting a charge which consists of a sack filled with black powder. On the exhaust side of the combustion chamber is a retainer which protects the exhaust nozzle from being choked by particulate matter and which retains the propellant. The throat of the nozzle is closed with a metal diaphragm. Upon ignition of the black powder charge, both the pressure and the temperature in the combustion chamber are raised by the resulting gases and initiate the ignition of the propellant. Then, as a consequence of the increase in pressure, and partially due to the temperature, the diaphragm bursts in the nozzle

and combustion gases begin to flow to the outside. The pressure in the combustion chamber stabilizes and depends on the equilibrium between the rate of gas generation and the rate of gas outflow.

In the engine with liquid propellant, the oxidizer and the fuel are contained in separate tanks and are brought to the combustion chamber separately with the aid of pumps which are driven by a combustion turbine. One of the liquid propellants (usually the oxidizer, since it appears in greater quantities) cools the exhaust nozzle and the combustion chamber on its way. The fuel and the oxidizer are thus brought to the injectors where they are injected into the combustion chamber and burn following their evaporation and mixture. Combustion gases generated in this manner flow through the nozzle and create thrust.

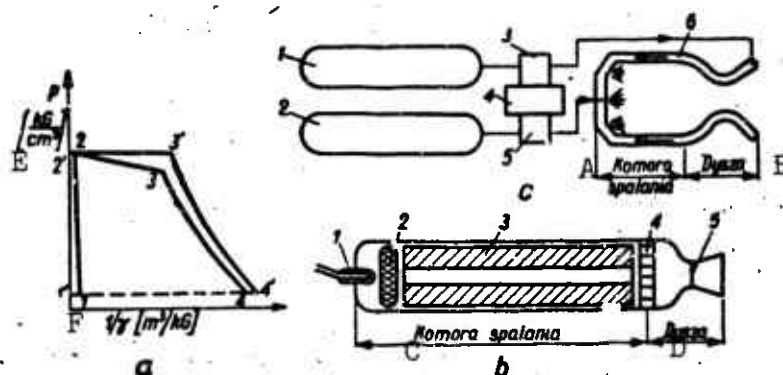


Fig. 1.3. Rocket engine. a) Theoretical and physical cycle diagram; b) schematic diagram of solid propellant rocket engine; 1) ignitor squib; 2) black powder charge; 3) solid propellant; 4) retainer; 5) diaphragm; c) schematic diagram of liquid propellant rocket engine; 1) fuel tank; 2) oxidizer tank; 3) fuel pump; 4) turbine; 5) oxidizer pump; 6) cooling jacket; A) Combustion chamber; B) exhaust nozzle; C) combustion chamber; D) exhaust nozzle; E) $p[\text{kg/cm}^2]$; F) $1/\gamma[\text{m}^3/\text{kg}]$

The theoretical Rankine cycle which consists of the isochor 1'-2', the isentropic line 3'-4' and two isobars 2'-3' and 4'-1' is achieved in the actual engine by the isochor 1-2 which is shifted because of the inherent mass or volume of the solid and by the combustion process 2-3 which droops because of the addition of heat and the opposing aerodynamic forces, and by the polytropic line 3-4 which departs from the

isentropic line due to cooling and friction.

1.4. THE THRUST OF JET PROPULSION ENGINES

Figure 1.4 illustrates the change in speed of air flow in planes A-B and A'-B' which describe the situation ahead of and behind a missile driven by two jet propulsion engines. Away from the unperturbed speed profile there develop lateral perturbations which indicate the areas disturbed by the missile. The missile proceeds with constant speed, so that the aero-dynamic forces are balanced by the thrust of the engines. The static pressures in the plane A'-B' are equalized and are identical to the environmental pressure.

We consider an elementary flow channel with a flow of unit mass of air m_1 , per second. The flow velocities of this mass in the cross sections A-B and A'-B' are accordingly w_1 . The change in mass velocity, which equals the change in momentum, because of the law of the conservation of momentum, produces the unidirectional force

$$S_1 = m_1 (w'_1 - w_1) \quad (1.1)$$

Drag forces effect, of course, a decrease in the momentum of the fluid flow. The increase in the latter immediately establishes the thrust.

Since the missile proceeds with constant speed, as mentioned above, these forces balance each other so that the net force is equal to zero.

$$\sum S_i = \sum m_i (w'_i - w_i) = 0 \quad (1.2)$$

In the preceding analysis, mass changes due to the addition of fuel were disregarded.

We consider now the flow of air through the ramjet engine (Fig. 1.5a) between the reference planes 0-e.

The flow impulses through sections 0 and e are, respectively,

$$S_0 = m_0 w_0 + p_0 F_0 \quad S_e = m_e w_e + p_e F_e$$

where m_0 and m_e are intensities of mass flow, F_0 and F_e are areas of the respective sections, w_0 and w_1 are flow velocities in the respective

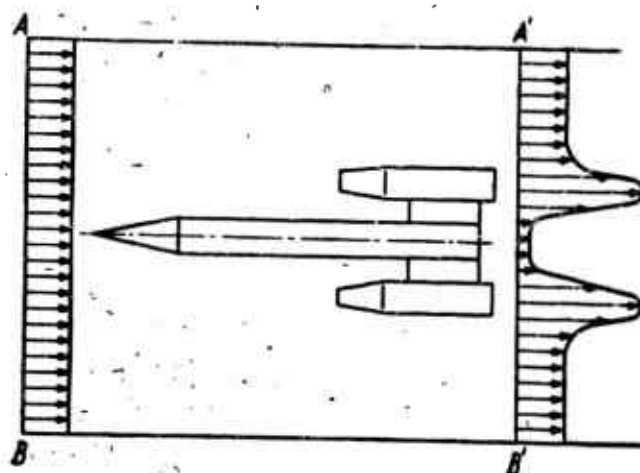


Fig. 1.4. Change in speed of airflow streamlining missile.

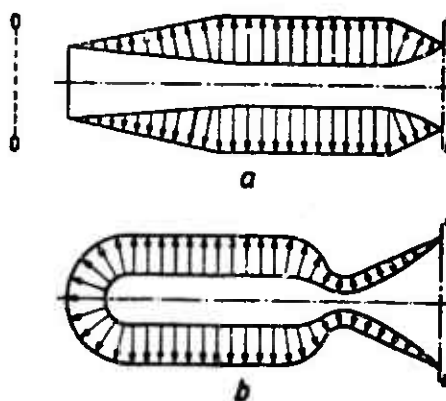


Fig. 1.5. Distribution of pressures acting on the inside engines walls. a) Jet engine; b) rocket engine.

sections.

The atmospheric pressure on the outer contour of the engine is (one neglects the aerodynamic drag forces).

$$\int p_0 dF = p_0 (F_e - F_0)$$

The increase in the impulse of the fluid flow passing through the engine is equal to the thrust of the engine

$$S = S_e - S_0 - \int p_0 dF$$

Substituting the above mentioned relations one obtains

$$S = m_e w_e - m_0 w_0 + F_e(p_e - p_0) \quad (1.3)$$

Since the expansion in the exhaust nozzle approaches the pressure of the environment (i.e. $p_e - p_0 = 0$), and if one neglects the increase in mass due to fuel addition (i.e., $m_e = m_0 = m$), the thrust dependence is given by the equation

$$S = m(w_e - w_0) \quad (1.4)$$

For the rocket engine (Fig. 1.5b) $w_0 = 0$.

The thrust dependence for the rocket engine, therefore, is given by the equation

$$S = m w_e \quad (1.5)$$

If one considers the overpressure of the combustion gases as they leave the exhaust nozzle, one obtains

$$S = m w_e + F_e(p_e - p_0) \quad (1.6)$$

The change in flow velocity along the axis of the engine causes a corresponding pressure profile on the walls. The resultant of these forces is in reality equal to the thrust of the engine.

In the case of the pulsejet engine, with regard to the unstable nature of the fluid flow, the thrust quantitatively equals the J' multiplied by the number of cycles per second ν

$$S = J' \cdot \nu$$

The impulse of each charge of air is

$$J' = m'(\bar{w}_e - w_0)$$

where \underline{m}' is the mass of each individual charge of air, \bar{w}_e is the average velocity of combustion gases passing through the engine.

Substituting $m \nu = m$, one obtains

$$S = m(\bar{w}_e - w_0) \quad (1.7)$$

This expression is analogous to the thrust dependence of the ram jet engine (1.4), inasmuch as the exit flow velocity w_e is replaced by

the average flow velocity \bar{w}_e .

The pulsejet engine and the ramjet engine are called jet propulsion engines.

1.5. POWER AND EFFICIENCY OF PROPULSION

The driving power (N_p) is defined by the product of the thrust and flow velocity

$$N_p = S w_0$$

Substituting the respective relations for the thrust of a jet propulsion engine or a rocket engine one obtains:
for the jet propulsion engine

$$N_{pp} = m(w_e - w_0)w_0 = mw_0^2 \left(1 - \frac{w_0}{w_e}\right) \frac{w_0}{w_e} \quad (1.8)$$

for the rocket engine

$$N_{pr} = mw_e w_0 = mw_0^2 \frac{w_e}{w_0} \quad (1.9)$$

If one seeks the extremum of Function (1.8) one finds that the driving power of the jet propulsion engine tends towards a maximum when w_0/w_e tends towards 0. Whenever $w_0/w_e = 1$, the driving power of the jet propulsion engine is equal to zero, and it is obvious that the thrust of this engine is then also zero.

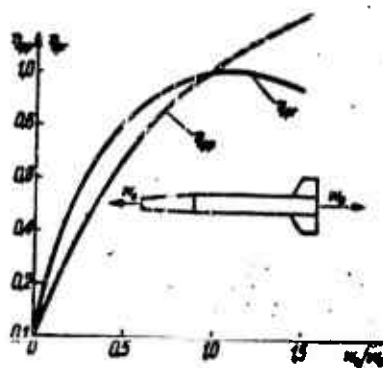


Fig. 1.6. Propulsion efficiency of engines: for rocket engine, η_{pr} , and for jet propulsion engines, η_{pp} , independence upon the flight velocity w_0 and the exit gas velocity w_e .

On the other hand, the driving power of the rocket engine increases continuously with increasing flight velocity and exit-gas velocity.

Figure 1.6 represents a missile which is driven by a jet engine. The missile velocity is w_0 , the velocity of the exit gases from the exhaust nozzle of the engine w_e . The velocity of exhaust gases with respect to the atmosphere is, therefore, $w_e - w_0$. The kinetic energy of the exhaust gases is thus only partially converted into driving power. The energy balance is hence written as follows

$$N_s = \frac{w_e^2}{2g} = N_p + \frac{(w_e - w_0)^2}{2g}$$

By substituting the respective expressions, one obtains for the driving power of the fluid ejected from the engines:
for the rocket engine

$$N_{sr} = \frac{m}{2} w_e^2 \left[1 + \left(\frac{w_0}{w_e} \right)^2 \right]$$

for the jet propulsion engine

$$N_{sp} = \frac{m}{2} w_e^2 \left[1 - \left(\frac{w_0}{w_e} \right)^2 \right]$$

The quantity which takes into account the power losses in the exhaust jet of the combustion gases is the propulsion efficiency η_p . One expresses it through the ratio of the driving power to the jet power

$$\eta_p = \frac{N_p}{N_s}$$

By transforming the above equation, one obtains the respective expressions for the propulsion efficiency of the rocket engine η_{pr} and for the jet engine η_{pp}

$$\eta_{pr} = \frac{2 \frac{w_0}{w_e}}{1 + \left(\frac{w_0}{w_e} \right)^2} \quad \eta_{pp} = \frac{2 \frac{w_0}{w_e}}{1 + \frac{w_0}{w_e}} \quad (1.10)$$

Both of these expressions are illustrated by the graph of Fig. 1.6. One must give attention to the realistic flight of a rocket vehicle with a greater velocity than the exhaust velocity. Therefore, the branch of the curve $\eta_{pr} = (w_0/w_e)$ for $w_0/w_e > 1$ has physical significance. However, there is no apparent physical meaning for the branch of the curve $\eta_{pp} = f(w_0/w_e)$, inasmuch as for $w_0 > 1$ the thrust of the jet propulsion engine is negative.

1.6. THERMAL AND TOTAL EFFICIENCY OF FLIGHT ENGINES

The thermal efficiency takes into account all thermal losses of the engine, which are losses due to the 2nd law of thermodynamics, due to the irreversibility of processes, incomplete combustion and the exchange of heat with the environment. It is expressed by the ratio of the driving power of the exhaust stream to the energy E_w which is added to the engine during one second

$$\eta_t = \frac{N_e}{E_w}$$

For the rocket engine this energy is given by

$$E_{wr} = G \left(JH_u + \frac{w_0^2}{2g} \right)$$

and for the jet propulsion engine by

$$E_{wp} = G \left(JW_u + \frac{w_0^2}{2g} \right)$$

where J is the mechanical equivalent of heat, G is the weight flow rate of fuel or propellant, H_u is the heat value of propellant, W_u is the heat value of fuel.

The total efficiency is the product of the thermal and propulsion efficiencies

$$\eta_o = \eta_t \eta_p$$

For rocket and jet propulsion engines one finds, therefore,

$$\eta_{op} = \frac{m(w_e - w_0)w_e}{G \left(JW_u + \frac{w_0^2}{2g} \right)} \quad \eta_{or} = \frac{mw_e w_e}{G \left(JH + \frac{w_0^2}{2g} \right)} \quad (1.11)$$

1.7. VELOCITY CHARACTERISTICS OF FLIGHT ENGINES

During the selection of a propulsion system for a particular flight vehicle the deciding roles are nearly always played by small fuel consumption and, at the same time, by high overall efficiency of the engine. One seeks small fuel consumption not only because of the decreased costs but primarily (for a given flight range) because of the smaller integrated weight of the vehicle.

The graph of Fig. 1.7 allows us to draw conclusions about the application of the individual types of engines, and in general about the application limits of engines which employ chemical fuels.

It is apparent from the graph that the extent of the applicability of pulsejet engines is limited to subsonic velocities. In this region their efficiency is higher than that of other simple flight engines without moving parts, however, their efficiency is less than that of the turbojet engine.* Ramjet engines have a considerable advantage over other engines (with the exception of the turbojet engine) in the velocity region of 4-13 thousand km/hr. Above this region the rocket engine is most efficient.

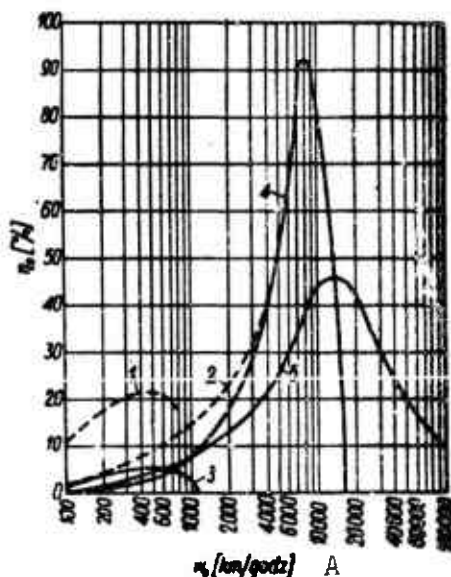


Fig. 1.7. The dependence of the total efficiency η_0 of flight engines on the flight velocity w_0 . 1) Propeller-driven engine; 2) turbojet

engine; 3) pulsejet engine; 4) ramjet engine; 5) rocket engine.
A) w_0 [km/hr].

Considerations other than small fuel consumption often decide the selection of a propulsion system. The factors which then are most frequently taken into account are:

simplified design (application of ramjet engines for rotation of propeller blades, or of pulsejet engines to the propulsion of subsonic target planes);

high thrust-to-weight ratio of engine (application of rocket engines as takeoff assist units for airplanes).

1.8. DYNAMICS OF THE DEVELOPMENT OF JET PROPULSIONS ENGINES - A SHORT HISTORY OF PULSEJET ENGINES- RAMJET ENGINES AND ROCKET ENGINES

One may look upon the development of jet propulsion engines from two viewpoints. First one may consider it as a complex of parallel designs in evolution, and second as a battleground of "fighting" and "mutually exclusive" systems which are subservient to the generation of thrust. It appears that the second method better illuminates the past of flight propulsion and allows insight into its future.

The basic factor which influences the progress of aviation is the battle for ever higher flight velocities. It has decided the direction of engine development where the basic trend was set by the battle over thrust. The thrust of each engine depends primarily upon the flow rate of the working medium, the temperature at the inlet to the exhaust nozzle, the expansion in the nozzle (the ratio between the inlet and exit pressures of the nozzle), and the magnitude of the work of compression of the working medium.

The tendency toward an increase in the flow rate eliminated from competition those engines whose operation did not produce thrust. And since we are also concerned in this book with the pulsejet engine, it

was also the main reason during the design of the turbojet which caused radial-flow (centrifugal) compressors to be eliminated in favor of axial-flow compressors.

The maximum temperature in the engine is limited by the materials and by the properties of the employed chemical fuels. The turbojet engine is burdened with an "organic illness" produced by the high operating temperature of the turbine blades. This basically will spell its quick "defeat" in its competition with the ramjet engine.

The expansion in the exhaust nozzle of a ramjet engine depends on flight velocity, however, for the turbine and the rocket engine it is selected on the basis of thermodynamic analysis of its performance. Therefore, the ramjet can compete with the turbojet only at higher Mach numbers (above $M = 2-3$).

Inasmuch as the compression in the engine defines the thrust and the efficiency for the same fuel consumption, the results of the analysis are derived in the main from the velocity characteristics of flight engines, as described in the preceding chapter.

The last factor which influences the thrust of the engine, namely the work of compression of the working medium, will eventually lead to the replacement of the ramjet by rockets even in stratospheric flights. For high Mach numbers, the efficiency of air compression in the supersonic diffuser of the ramjet engine will be very low and will thus cause a substantial increase of the compression work (as it pertains to the specific energy content of the exhaust jet).

For the rocket engine the work of compression is small (since the compression factor of the liquid phase applies), or it is total equal to zero (when the propellant material is a solid).

Can one foresee the time when certain propulsion systems will "predominate?" To a certain degree the answer to this question is given

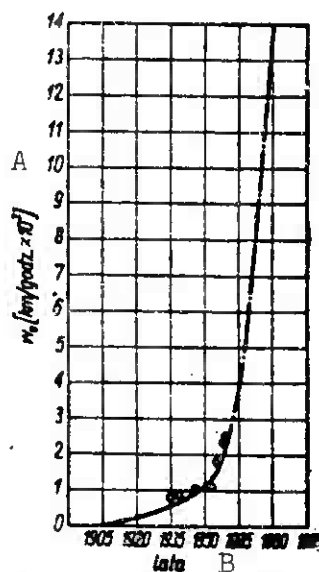


Fig. 1.8. Progress in the achievement of speed records in aviation. o) Significant speed records of the last decades; - . -) extrapolation of speed records for the coming years; A) w_0 , [km/hr. $\cdot 10^3$]; B) year.

by the graph of Fig. 1.8. The curve represents the progress in speed records from the early days of aviation to the present. It characterizes very definitely the advance achieved in aviation. Delineating the speed records, this curve shows a tendency toward an ever steeper ascent. If one performs an extrapolation of this curve over the next 20 years (even if one is not optimistic), one must anticipate that a speed record of 4000 km/hr (the beginning of the ramjet hegemony) will be achievable by conventional means about 1965, although the speed record of 13 thousand km/hr (the beginning of the rocket hegemony) can be expected for the time period of 1975-1980.

Today it is still quite difficult to predict precisely the time when some of the above-mentioned qualitative changes are expected to take place. However, the overall trend in the development of flight propulsion systems remains even today uniquely defined and cannot be a point of dispute. With the intent to illustrate the achievement during the important stages of engine development, as it is here of interest, the most important events in its history are listed:

Year: 848 - Marek Grek mentions rockets in his writings (Byzantium)

1232 - First use of rockets as a weapon of warfare (China)

1259 - Schwarz discovers black powder (Germany)

1290 - First use of rockets in Europe (Spain)

1650 - K. Siemionowics writes his monograph on rockets (Poland)

1687 - I. Newton formulates the law of action and reaction (England)

1816 - First application of rockets for rescue at sea (Germany)

1850 - Series production of rockets with a weight of 20 kg and a range of 3200 m (France)

1880 - Nobel discovers nitroglycerine (Sweden)

1895 - P. Paulet performs the first experiments with solid propellant rockets (Peru)

1903 - K. Ciolkowski writes his work "The Rocket in Cosmic Space" (Russia)

1908 - R. Lorin receives patent for the ramjet engine (France)

1909 - R. Marconnet receives patent for the pulsejet engine (France)

1919 - R. Goddard publishes his work "A Method of Reaching Extreme Altitude (USA)

1923 - H. Oberth writes his work "Die Rakete zu den Planetenraumen" [Rockets To The Planets].

1924 - Opening of an office in the USSR for the study of rocket problems

1931 - First attempts with postal rockets (Switzerland)

1933 - E. Saenger publishes his book "Raketenflugtechnik"

[Rocket Flight Engineering] (Germany)

- 1936 - Establishment of rocket research centers in the USA and in Germany
- 1942 - First liquid-rocket assisted takeoff of an airplane (USA)
- 1944 - Application of a pulsejet engine to the propulsion of an airplane - missile, and liquid propellant rocket engine, applied to the propulsion of a surface-to-surface missile (Germany)
- 1947 - Breaking of sound barrier by an airplane powered by a liquid propellant rocket engine (USA)
- 1951 - First flight by an airplane powered only by a ramjet engine (France)
- 1957 - Launching of the first man-made satellite (USSR)
- 1961 - First man in space (USSR)

REFERENCES

- 1.1 J. Stemmer: Raketenantriebe [Rocket Engines], Schweizer Druck and Verlaghaus A.G. Zurich, 1952.
- 1.2 E. Saenger: Die Physikalischen Grundlagen der Strahlantriebs-technik [Physical Fundamentals of Jet-Propulsion Engineering], V.D.I. Forschungsheft 437 [Assoc. of German Engineers, Research Paper 437] Volume 19/1953.
- 1.3 S. Wojcicki: Kierunki technicznego rozwoju lotniczych zespo-
low napedowych [Trends in Technical Development in Flight
Propulsion Engines]. Najnowsze konstrukcje lotnicze - Napedy
[The Latest Designs in Aviation Propulsion]. PWT, Warsaw
1957.

Manu-
script
Page
No.

[Footnotes]

16 Originally known as a turbine jet (The editor)

Chapter 2

CHARACTERISTIC ENGINE PARAMETERS

For the selection of a propulsion system the designer is especially interested in the following data:

what thrust can be achieved from anticipated available engines,
how high is their fuel consumption,
what are their dimensions,
how much do they weigh.

In order to facilitate a complete analysis, a series of characteristic parameters is introduced which allow a comparison among engines of one propulsion group, or of different propulsion groups among each other. The most important of these parameters are stated below:

The parameter which characterizes the excellence of an engine design for the generation of thrust. This is the thrust coefficient

$$C_t = \frac{S}{pF} \quad (2.1)$$

where $S[\text{kg}]$ is the thrust of the engine, $p[\text{kg}/\text{cm}^2]$ denotes, for the case of the rocket engine, the pressure in the combustion chamber, for the case of the pulsejet engine, the atmospheric pressure; for the case of the ramjet engine, however, it is the dynamic pressure in the free air stream ahead of the engine; $F[\text{cm}^2]$ denotes for the rocket and pulsejet engine the minimum cross sectional area of the exhaust nozzle; for the ramjet engine, the maximum cross sectional area of the engine.

The parameter which characterizes the effectiveness of the fuel consumed by the engine. This is the specific fuel consumption of the

propellant, as described by the relation

$$b = \frac{B}{S} \text{ [kg/kg}\cdot\text{hr]}$$

where B [kg/hr] denotes, for the rocket engine, weight flow rate of fuel-oxidizer mixture; for the pulsejet and ramjet engine, weight flow rate of the fuel alone.

Figure 2.1 shows the dependence of the specific fuel consumption on the Mach number for four types of engines: rockets, ramjets, pulsejets, and turbojets. In the range from $M = 0$ to $M = 2.0$, the most economical of the engines under consideration is the turbojet engine with afterburner; above $M = 2.0$, the least fuel consumption is exhibited by the ramjet engine.

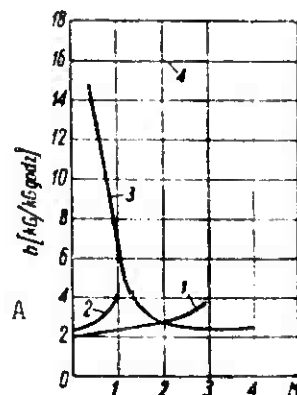


Fig. 2.1. Dependence of the specific fuel consumption on the Mach number for jet propulsion engines. 1) Turbojet engine with afterburner; 2) pulsejet engine; 3) ramjet engine; 4) rocket engine; A) b [kg/kg-hr].

Instead of the above parameter the concept of specific thrust is often used, this is also referred to as the specific impulse. The specific thrust is the inverse of the specific fuel consumption

$$I_{sp} = \frac{S}{B_s} = \frac{3600}{b} = \frac{w}{g} \text{ [sec]} \quad (2.2)$$

where B_s [kg/sec] is the weight flow rate of fuel and oxidizer or of fuel alone, w [m/sec] is the exhaust velocity, g [m/sec²] the acceleration due to earth gravity ,

and can be defined as the thrust due to the specific flow rate. One derives the specific thrust from the weight flow rate of the fuel alone in the case of jet propulsion engines, and from the weight flow rate of the fuel and oxidizer in the case of the rocket engine. Another effective indicator of engine fuel consumption is the range parameter

$$K_r = \frac{w_0}{b} [\text{km}]$$

where w_0 is the flight velocity in km/hr.

The existence of this parameter arises from the well known range expression of aircraft driven by heat engines

$$L = \frac{w_0}{b} \lambda \ln \frac{1}{1-v} [\text{km}]$$

where λ is the aerodynamic excellence of the aircraft; v is the ratio of the initial propellant weight to the total, initial weight of the aircraft.

The magnitude of the range parameter can be derived immediately from the range-limited propellant supply.

In Fig. 2.2 the dependence of the range parameter on the Mach number is shown for the engines here under discussion. It is apparent from the graph that the most economical propulsion system above $M = 2.2$ is the ramjet engine; below this velocity the greatest range for the same propellant load is achieved by the turbojet engine with after burner.

The parameter which characterizes the engine weight. This is the thrust, normalized to the specific weight

$$S_c = \frac{S}{Q} [\text{kg/kg}] \quad (2.3)$$

where Q is the engine weight (without propellant).

The value of the parameter S_c characterizes the engine design from the viewpoint of a specific choice and the resulting utilization

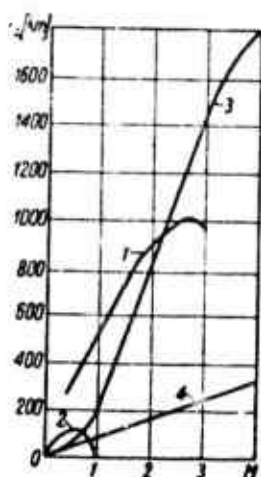


Fig. 2.2. Dependence of the range parameter on the Mach number. The notation of Fig. 2.1 applies.

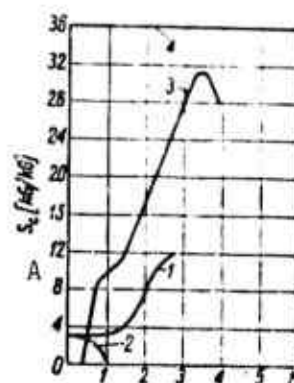


Fig. 2.3. Dependence of the thrust, normalized to the specific weight of the reaction engine, on the Mach number. The notation of Fig. 2.1 applies; A) S_c [kg/kg]

of the construction materials.

Figure 2.3 illustrates the dependence of the parameter S_c on the Mach number. In this case the rocket engine shows itself to be the most advantageous. This mark of the rocket engine explains its frequent use in aviation for takeoff assistance or for sudden demands for increased flight velocity (e.g., in fighter aircraft).

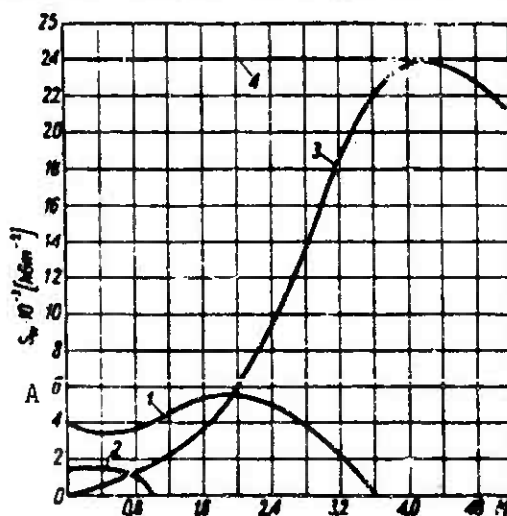


Fig. 2.4. Dependence of thrust, normalized to the specific frontal area of the reaction engine on the Mach number: The notation of Fig. 2.1 apply, except for the turbojet which is without afterburner. A) $S_w \cdot 10^{-3}$ (kg/m²).

Accordingly, the parameter S_c represents a quantity which sheds light upon the cost of the engine to a certain degree. Since the construction cost per kilogram of engine weight is more or less constant for all flight engines, it follows that its price diminishes with the thrust increase per unit weight.

The parameter which characterizes the dimensions of the engine. This is the thrust, normalized to the specific frontal area F of the engine

$$S_* = \frac{S}{F} \text{ [kg/m}^2\text{]}. \quad (2.4)$$

The parameter S_w characterizes the applicability of the engine for highspeed flight. In Fig. 2.4 different flight engines are compared from this viewpoint. Two conclusions are drawn from the comparison:

the highest value of the parameter S_w , over the whole velocity range, is due to the rocket engine;

the ramjet engine exceeds from this point of view the pulsejet engine, beginning with $M \sim 0.75$, and the turbojet beginning $M \sim 2.0$.

REFERENCES

- 2.1 R. Marquardt: Future of Ramjet Engines. American Aviation 1-11, s. 24-28, 1954.
- 2.2 B. Stieczkin, Teoria silnikow odrzutowych [Theory of Reaction Engines]. Published by MON, Warsaw 1961.

Chapter 3

FLOW PROBLEMS IN ENGINES

The characteristic and common feature of pulsejets, ramjets and rocket engines is the utilization of thermodynamic processes through gasdynamics.

The basic assemblies of these engines suffer from turbulence which causes a reciprocating motion. All thermal processes are utilized by the resulting flow of gas through appropriately shaped ducts.

3.1. TURBULENT FLOW

The exchange phenomena between mass, momentum and heat are paramount among processes which take place in one of the most important components of each internal combustion engine, namely the combustion chamber. The primary inrush of air due to vehicle motion, and the intensity of these phenomena, causes turbulence in the gas stream as it passes through the combustion chamber.

Turbulent flow is characterized by a sustained, irregular mixing of flow particles which in turn results in an irregular pulsation of velocity, pressure, temperature and particle density at each location of the gas stream.

3.1.1. Characteristic Parameters of Turbulent Flow

A numerical evaluation of turbulence is made with the aid of the following characteristic parameters:

- intensity of turbulence: This is the ratio of the root-mean-square velocity of fluctuations to the mean flow velocity.

$$i = \frac{\sqrt{\overline{u'^2}}}{\bar{u}}$$

where $\bar{u} = \frac{1}{\tau_0} \int_0^{\tau_0} u(\tau) d\tau$; τ_0 is a time chosen sufficiently long to permit a determination of the mean velocity and u' is the fluctuation velocity;

- degree of turbulence L ; This is a characteristic measure of the volumetric mixing which takes place in the flow per unit length, where in turbulent flow there exists also a dependence between fluctuations at two different locations within the fluid.

Both of these parameters can be described relative to the three axes of a Cartesian coordinate system, designated by w , v , and u .

Exchange phenomena of momentum, heat and mass are described formally by the same equations:

- transport of momentum

$$\frac{\tau}{\rho} = \nu_T \frac{d\bar{u}}{dy}$$

- transport of heat

$$\frac{q}{\rho T} = \alpha_T \frac{d\bar{T}}{dy}$$

- transport of mass

$$m = D_T \frac{d\bar{c}}{dy}$$

where $\frac{d\bar{u}}{dy}$, $\frac{d\bar{T}}{dy}$, $\frac{d\bar{c}}{dy}$; are the gradients of the average velocity, temperature and mass density, ν , α , D ; are the coefficients of eddy viscosity, eddy heat conductivity and eddy diffusion, and where τ , q , m ; are the shear stress, the rate of heat flow and the rate of mass transport.

The subscript T for the transport coefficients signifies that these coefficients pertain to turbulent flow.

3.1.2. Characteristics of Turbulent Flow

Figure 3.1 shows the axial component of turbulent intensity as a function of position in the transverse cross section of a duct.

The axial component of turbulent intensity increases in proportion to the distance from the axis, attains a maximum and decreases thereafter due to the influence of the boundary layer. The dependence of the remaining components is similar.

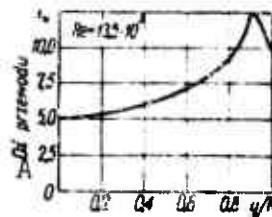


Fig. 3.1. The axial component of turbulent intensity as a function of position in the plane normal to the duct. Here R is the radius of the duct and y the coordinate in the radial direction. A) Duct axis.

Figure 3.2 shows the change in the axial component ϵ_u and the normal component ϵ_v of turbulent intensity along a duct with decreasing cross section.

It is apparent from this figure that the axial component diminishes in size as the flow velocity increases, whereas the normal component passes through a maximum.

The maximum of the normal component occurs at half the duct radius.

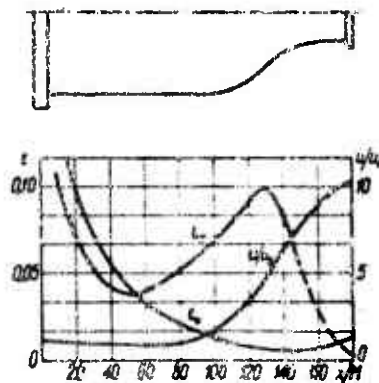


Fig. 3.2. Variations of the axial and normal components of turbulent intensity ϵ_u and ϵ_v in a converging duct. Here, u is the flow velocity at a given cross section, u_0 the inlet flow velocity (0.11 m/sec), and x the coordinate along the core axis. A flow straightener of non-

eycomb construction with square openings was placed at the inlet of the duct. (M is the width of the duct).

Figure 3.3 shows the effects of size and shape of nonstreamlined bodies, inside a stream, upon the magnitude of ϵ_x , as measured on axis at a constant distance. One recognizes from the figure that the shape of the nonstreamlined body has a small effect upon the value of turbulent intensity. However, the value of turbulent intensity rises sharply with an increase of the characteristic size of the body. An example of a body of this type in a gas stream is given by the flame holder in the combustion chambers of a ramjet.

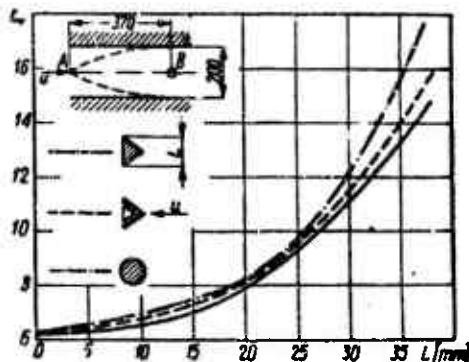


Fig. 3.3. Characteristic effect due to the dimension L of a body, and its shape, upon the axial component of turbulent intensity ϵ_x in the aerodynamic wake of the body. A) Position of body in duct; B) location where turbulence was measured.

3.2 DIFFUSERS

The diffuser in a ramjet takes the place of the compressor in a turbojet.

Its task is to decrease the flow velocity to a value where stable combustion is feasible within the combustion chamber and, at the same time, to compress the air without losses, if possible. The magnitude of this compression has a decisive effect upon efficiency and thrust

of a ramjet.

3.2.1 Diffuser Efficiency

The diffuser is represented by an appropriately shaped duct wherein the ram pressure of the flowing gas is changed into static pressure. One distinguishes three types of diffusers depending upon their flow character: subsonic, sonic and supersonic diffusers. Energy losses in the diffuser can be expressed either by the pressure recovery coefficient

$$\sigma_D = \frac{p_2^*}{p_0^*} \quad (3.1)$$

where p_2^* is the total pressure at the exit of the diffuser; p_0^* the total pressure at its inlet, or by the isentropic efficiency which is defined as the ratio of the actual to the theoretical increase in enthalpy within the diffuser

$$\eta_D = \frac{\Delta i_{rz}}{\Delta i_t} = \frac{\left(\frac{p_2^*}{p_0}\right)^{\frac{\kappa-1}{\kappa}} - 1}{\frac{\kappa-1}{2} M_0^2} \quad (3.2)$$

where Δi_{rz} is the actual enthalpy rise in the diffuser; Δi_t the theoretical enthalpy rise in the diffuser; M_0 the Mach number ahead of the diffuser in the unperturbed flow; p_0 the static pressure ahead of the diffuser; κ the isentropic exponent.

Both of these expressions are related through the equation

$$\eta_D = \frac{\sigma_D^{\frac{\kappa-1}{\kappa}} \left(1 + \frac{\kappa-1}{2} M_0^2\right) - 1}{\frac{\kappa-1}{2} M_0^2} \quad (3.3)$$

3.2.2 One-dimensional, Steady-state Flow Through Ducts with Varying Cross Section.

Beginning with the equation for the continuity of flow

$$\frac{dF}{F} + \frac{dw}{w} + \frac{d\rho}{\rho} = 0.$$

and the equation of momentum

$$w \frac{dw}{dx} = - \frac{1}{\rho} \frac{dp}{dx}$$

we obtain after a transformation, cf. [L3.6]

$$\frac{dF}{F} = (M^2 - 1) \frac{dw}{w} \quad (3.4)$$

where F is the surface of the duct; w the flow velocity; x the longitudinal coordinate; ρ the density; p the static pressure.

It is evident from the preceding relation that, for subsonic flow ($M < 1$) and increasing cross sectional areas ($dF > 0$), the flow velocity decreases ($dw < 0$) whereas the density and the pressure increase ($d\rho > 0$, $dp > 0$); for supersonic flow ($M > 1$) the situation is reversed and one finds for an increasing cross sectional area an increase in flow velocity and a decrease of density and pressure.

3.2.3 Flow Through the Subsonic Diffuser

Figure 3.4 illustrates the flow through a subsonic diffuser. As it is apparent from Eq. (3.4), the compression of subsonic flow manifests itself in a diffuser which diverges in the flow direction. Flow lines at the entrance to the diffuser (section 0-1) depend upon the degree of choking in the chamber which follows the diffuser. In the case of a ramjet, the choking depends upon the cross sectional area of the nozzle and the amount of heat added to the flow in the combustion chamber of the engine. The left part of Fig. 3.4 depicts the characteristic performance of a diffuser. The performance curves are shown for a constant inlet Mach number M_0 and different degrees of choking. Diffuser A and point A on the performance curve pertain to the same case where choking is large (the compression π is great, however, the flow rate G is small). In this case the process of compression commences already ahead of the diffuser. Diffuser B illustrates the case

where compression takes place only within the diffuser. In case C, the exhaust chamber which removes the gas from the diffuser is choked to such an extent that a partial vacuum is created at the inlet to the diffuser (the diffuser behaves like a badly designed Venturi tube).

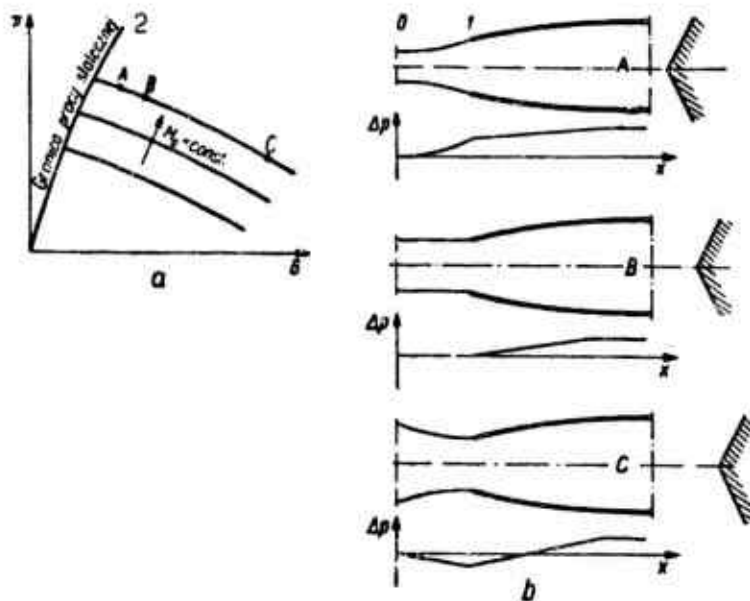


Fig. 3.4. Flow through a subsonic diffuser. α - Characteristic performance of diffuser; π - compression; G - mass flow rate; M_0 - Mach number in the unperturbed flow ahead of the diffuser (the arrow points in the direction of increasing M_0); b - path of flow line ahead of the diffuser, together with the corresponding display of pressure ahead of and inside the diffuser; p - overpressure caused by dynamic compression; x - longitudinal coordinate; 0 - effect of diffuser upon incoming flow line begins to show up; 1) inlet cross section of diffuser. 2) limit of static work.

Compression in a diffuser is a reversible process with regard to the expansion in the nozzle. However, with regard to the different manifestations of the boundary layer in these two processes, the expansion process is much more efficient than the process of compression.

Flow velocities change in the boundary layer, with respect to the stationary wall, from zero at the wall to nearly the nominal flow velocity at a distance δ from the wall (the so-called thickness of the boundary layer). This change in velocity in the boundary layer is caused by friction. When the gas pressure increases in the flow direction (as it is the case in the diffuser, for example), then the retardation of the fluid due to friction is greater in the boundary layer than outside the layer. This can cause within the boundary layer a flow in a direction opposite to the main flow of the fluid, and can give rise to flow separation and vortices.

Whenever the pressure gradient between the boundary layer and the main flow is sufficiently large, vortices begin to enter the main flow and decrease markedly the flow efficiency. The phenomenon of the appearance of vortices at the diffuser wall is sketched in Fig. 3.5.

As shown in Fig. 3.4, the flow through a subsonic diffuser A causes simultaneously a compression outside and inside. In the limiting cases it is possible to reduce the compression in the diffuser to a compression of one type. Figure 3.6 depicts the flow through a diffuser where the compression takes place exclusively outside. The compression between sections 0 - 0 and 1 - 1 can be caused, for example, by the addition of heat (which results in thermal choking) between sections 1 - 1 and $e - e$.

Upon the outside walls of the diffuser, which are shaped similar to airfoils, there acts a compression with a resultant force directed

normal to the flow lines. In this manner a ramjet may function with an outside compression diffuser. The process of external compression may be treated as isentropic, i.e., without losses. However, in diffusers with inside compression, losses are caused by friction and the appearance of vortices.

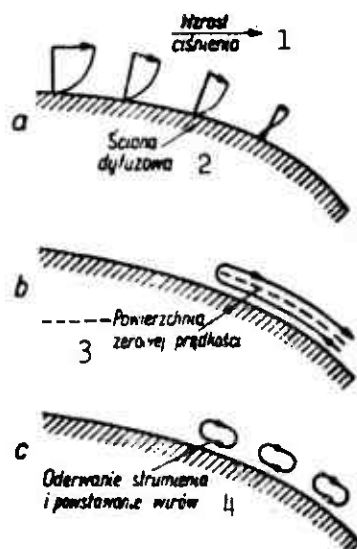


Fig. 3.5. The appearance of flow separation and vortices at the diffuser wall. 1) Pressure rise; 2) diffuser wall; 3) zero-velocity surface; 4) flow separation and appearance of vortices.

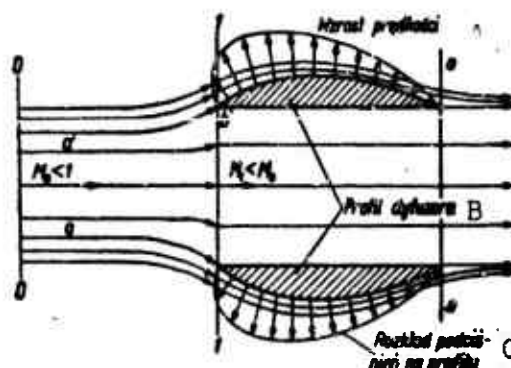


Fig. 3.6. Flow through a diffuser with outside compression only. A) Velocity increase; B) diffuser profile; C) pressure distribution on profile.

Pressure losses due to friction are apparent in the dynamic pressure at the end of the diffuser and are calculated with the aid of the following expression

$$\Delta p_T = \zeta_1 \frac{\rho_2 w_2^2}{2}$$

$$\zeta_1 = \frac{C_t}{2 \sin \frac{\epsilon}{2}} \left[\left(\frac{F_2}{F_1} \right)^2 - 1 \right]$$

where $C_t = 0.005-0.006$ is the coefficient of friction; $\epsilon = 10^\circ-20^\circ$ the diffuser inlet angle; ρ_2, w_2 density and velocity at the exit cross section of the diffuser; F_1, F_2 inlet and discharge areas of diffuser; Δp_T pressure drop in diffuser due to friction; ζ_1 loss coefficient in flow due to friction.

Pressure losses due to flow separation and vortices can be described by the equations below

$$\Delta p_w = \zeta_2 \frac{\rho_2 w_2^2}{2}$$

$$\zeta_2 = K \left[\left(\frac{F_2}{F_1} \right)^2 - 1 \right]$$

where $K = (0.015-0.02) \epsilon$, for $\epsilon = 10^\circ-20^\circ$.

Thus the total pressure loss in the diffuser is calculated as

$$\Delta p = \Delta p_T + \Delta p_w = \frac{\rho_2 w_2^2}{2} (\zeta_1 + \zeta_2) \quad (3.5)$$

whereas the pressure recovery factor is found to be

$$\sigma_D = \frac{p_2^s}{p_1^s} = 1 - \frac{\Delta p}{p_1^s} \approx 1 - \frac{\Delta p}{p_0^s} \quad (3.6)$$

The efficiency of the diffuser is affected decisively by two factors: the shape of the inlet profile and the Mach number M at the inlet cross section. For a rectilinear inlet profile (fig. 3.7), the efficiency is determined, in addition to the Mach number, by the diffuser inlet angle ϵ and by the shape factor φ which is defined as the ratio of the discharge area to inlet area.

$$\varphi = \frac{F_2}{F_1}$$

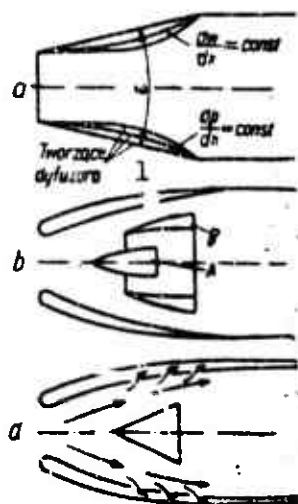


Fig. 3.7 Methods used to shorten diffuser length. *a* - Adequately designed inlet profile; *b* - application of baffles to serve as an array of flame holders; *c* - bleed-off of turbulent boundary layer.

Figure 3.8 shows the dependence of the total pressure recovery factor σ_D upon M_1 and ϵ .

For small inlet angles the compression efficiency is relatively great, however, the diffusers turn out to be then quite long.

There exist the following possibilities to alleviate this situation (Fig. 3.7):

- application of adequately designed diffuser inlet profile;
- application of baffles or flow guides;
- application of bleed-off from the turbulent boundary layer.

Considering the first of the indicated methods, best results are obtained by shaping the diffuser inlet according to a constant pressure gradient or a constant velocity gradient.

An appropriately designed wall profile is shown in Fig. 3.7a. In both versions of this method one subdivides the length of the diffuser into segments and, assuming the correct changes in pressure or velocity, one computes (with the aid of the equations of state, isentropy

and continuity, as well as that of compression efficiency) in sequence the surfaces of the selected segments.

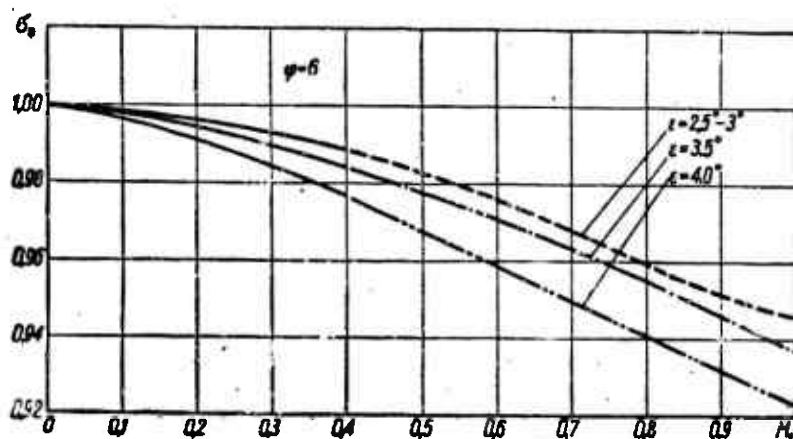


Fig. 3.8. Dependence of the pressure recovery factor σ_D upon the inlet Mach number M_1 and the diffuser inlet angle ϵ for the subsonic diffuser.

The second possibility to increase diffuser efficiency, where at the same time diffuser length is shortened to the utmost, is illustrated in Fig. 3.7b. In an appropriately designed diffuser (where, e.g., $dp/dx = \text{const.}$) the array of flame holders has been incorporated as an integral component (in the shape of a cone A and as an annulus B). Flame stabilizers located in this form affect in a very definite manner the direction of the compressed flow. This diminishes to a large extent the appearance of flow separation and vortices.

Figure 3.7c shows the method of increasing diffuser efficiency by bleed-off from the turbulent boundary layer. The wall of the diffuser is hollow. Slits are cut into the inner wall and are connected by an annular duct with the exhaust of the engine where the pressure is lower than that near the slits inside the diffuser. Through this arrangement a bleed-off of the boundary layer takes place and only laminar flow remains within the diffuser.

3.2.4. Flow Through the Supersonic Diffuser (M 1.5)

The flow through a supersonic diffuser is illustrated in Fig. 3.9. The supersonic diffuser is characterized by the appearance of a normal shock front at its inlet. The normal shock front appears in a position which depends upon the degree of choking: it may show up at the inlet cross section (Fig. 3.9a), it may be sucked to the inside of the diffuser (same figure), or it may be found finally ahead of the diffuser (Fig. 3.9b).

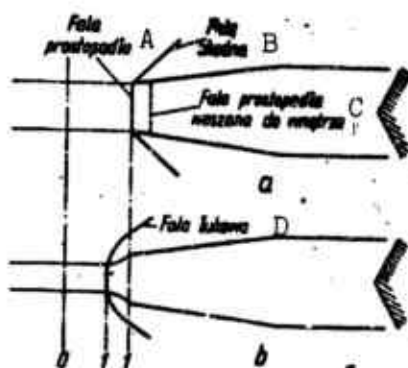


Fig. 3.9. Flow through the supersonic diffuser. *a* - Flow without narrowing of conduit (normal shock at the inlet cross section or inside the diffuser), *b* - flow with narrowing of conduit (normal shock appears ahead of the diffuser and follows the shape of a curved stream line). A) Normal shock front; B) oblique shock front; C) normal shock front sucked to inside; D) curved shock.

In the last example the flow behind the shock behaves like in the subsonic diffuser (the Mach number behind a normal shock front is always smaller than unity), where namely the diverging stream lines cause compression inside. In the case of still greater choking there arises a transgression of the stable range of diffuser performance (the pressure in the diffuser commences to pulse).

Parameters ahead of the shock, and behind the shock, are linked by the relations below:

$$\frac{\rho_{1'}}{\rho_0} = \frac{\rho_{1'}(\kappa + 1) - (\kappa - 1)\rho_0}{\rho_0(\kappa + 1) - (\kappa - 1)\rho_{1'}}$$

$$\frac{\rho_{1'}}{\rho_0} = \frac{\rho_{1'}(\kappa + 1) + (\kappa - 1)\rho_0}{\rho_0(\kappa + 1) + (\kappa - 1)\rho_{1'}}$$

$$\frac{T_{1'}}{T_0} = \frac{\rho_{1'}\rho_0}{\rho_0\rho_{1'}} \quad T_{1'} = T_0$$

(3.7)

$$\frac{\rho_{1'}}{\rho_0} = \frac{\left(\frac{\kappa + 1}{2} M_0^2 \right)^{\frac{\kappa}{\kappa - 1}}}{\left(\frac{2\kappa}{\kappa + 1} M_0^2 - \frac{\kappa - 1}{\kappa + 1} \right)^{\frac{1}{\kappa - 1}}}$$

$$M_{1'} = \sqrt{\frac{1 + \frac{\kappa - 1}{2} M_0^2}{\kappa M_0^2 - \frac{\kappa - 1}{2}}}$$

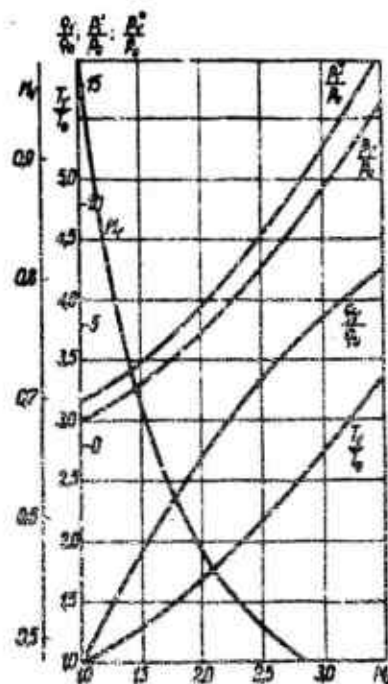


Fig. 3.10. Dependence of parameters fore and aft of the shock wave upon the Mach number ahead of the shock.

where $\rho_0, M_0, p_0, p_0^*, T_0, T_0^*$ are the parameters ahead of the shock (density, Mach number, static pressure, stagnation pressure, static temperature and stagnation temperature); $\rho_1, M_1, p_1, p_1^*, T_1, T_1^*$ are the corresponding parameters behind the shock front.

The graph of Fig. 3.10 shows the results of calculations for a range of Mach numbers 1-3.5.

Single-shock diffusers are not considered for inlet Mach numbers greater than 1.5 because of their low compression efficiency.

3.2.5 Oblique Shock Waves

In supersonic flow against a wedge (Fig. 3.11a), or near a concave corner (Fig. 3.11b), there arises from the apex or the vertex a shock wave which is inclined relative to the flow direction (by the angle σ_0), and which remains stationary with respect to the surface. It is called an oblique shock wave.

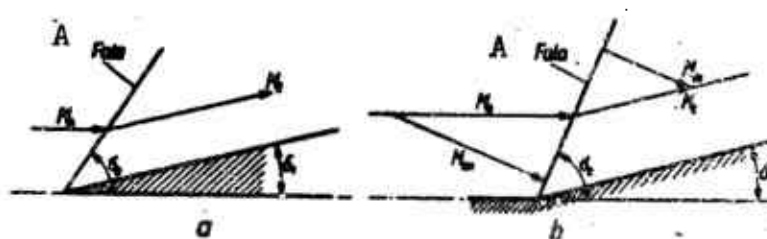


Fig. 3.11 Formation of oblique shock waves.
a - Flow against wedge; b - flow near concave corner. A) Shock.

The direction of flow velocity is parallel to the deflecting surfaces (which form the angle δ_1 relative to the original flow direction).

State parameters fore and aft of the shock are related through the equations below

$$\frac{\rho_1}{\rho_0} = \frac{\frac{\kappa+1}{\kappa-1}}{1 + \frac{1}{M_0^2 \sin^2 \sigma_0} \frac{2}{\kappa-1}}$$

$$\frac{p_1}{p_0} = \frac{2\kappa}{\kappa+1} M_0^2 \sin^2 \sigma_0 - \frac{\kappa-1}{\kappa+1} \quad (3.8)$$

$$\frac{T_1}{T_0} = \frac{\rho_0 p_1}{\rho_1 p_0}$$

$$\frac{M_1}{M_0} = \sqrt{\frac{(\kappa+1)^2 \cos^2 \sigma_0 + \sin^2 \sigma_0 \left[\kappa-1 + \frac{2}{M_0^2 \sin^2 \sigma_0} \right]^2}{(\kappa-1) \left[2\kappa M_0^2 \sin^2 \sigma_0 - \frac{2}{M_0^2 \sin^2 \sigma_0} + \frac{4\kappa}{\kappa-1} - \kappa+1 \right]}}$$

The shock angle and the flow deflection angle, relative to the original flow direction, are governed by the equation

$$\operatorname{tg}(\sigma_0 - \delta) = \left[\frac{\kappa-1}{\kappa+1} + \frac{2}{\kappa+1} \frac{1}{M_0^2 \sin^2 \sigma_0} \right] \operatorname{tg} \sigma_0 \quad (3.9)$$

These equations are explained graphically on Figs. 3.12-3.16.

Oblique shock waves shown in Fig. 3.11 are referred to as attached shock waves (since they originate at the turning point). For the case where the slant angle of the surface $\delta > \delta_{gr}$, the shock separates itself from the wall and forms a detached shock wave (Fig. 3.17) which stands ahead of the slanted surface. The dependence of the limit surface slope angle upon the Mach number in front of the shock wave is shown by a graph in Fig. 3.18.

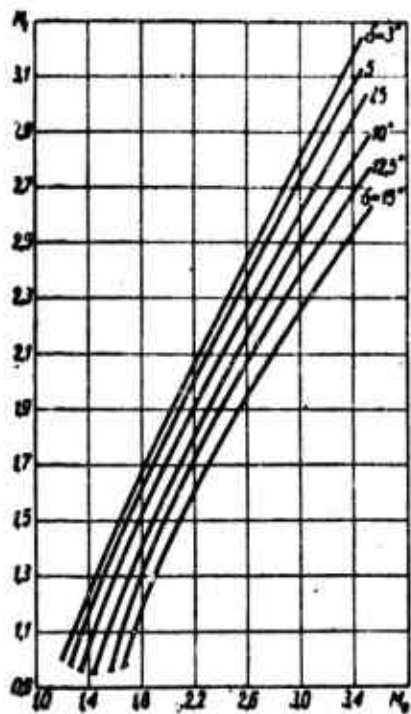


Fig. 3.12 Mach number behind oblique shock M_1 as a function of Mach number in front of shock M_0 .

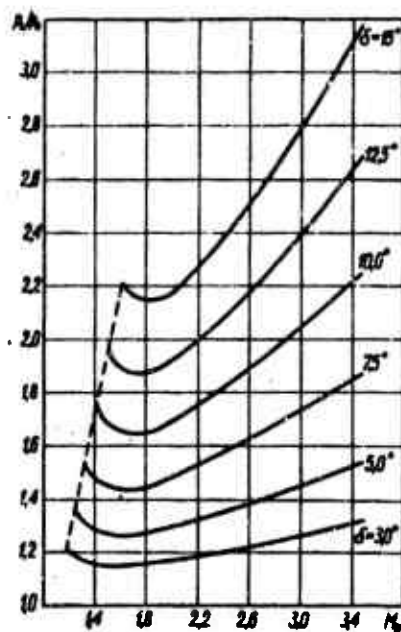


Fig. 3.13 Pressure behind oblique shock as a function of Mach number of original flow.

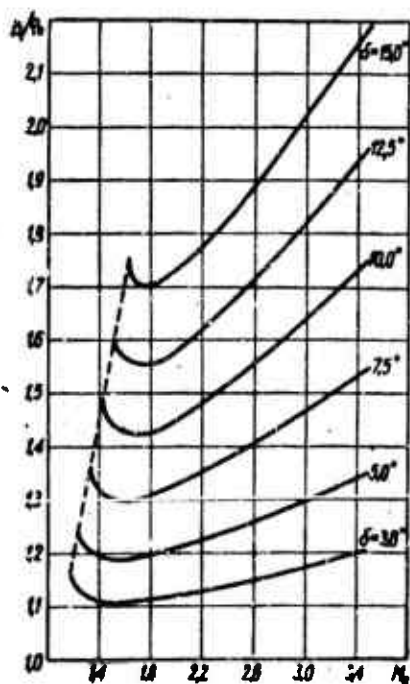


Fig. 3.14 Density behind oblique shock as a function of Mach number of original flow.

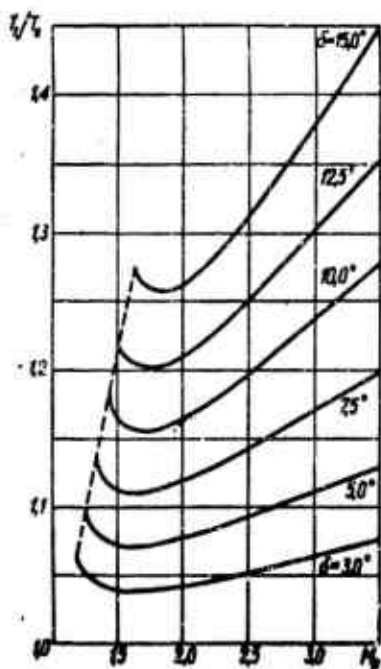


Fig. 3.15 Temperature behind oblique shock as a function of Mach number of original flow.

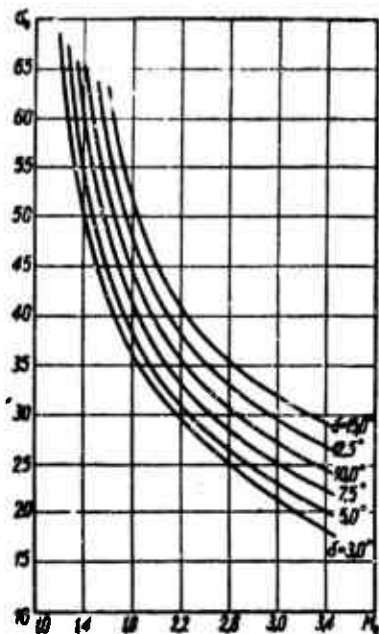


Fig. 3.16 Shock angle σ_0 as a function of Mach number of original flow.

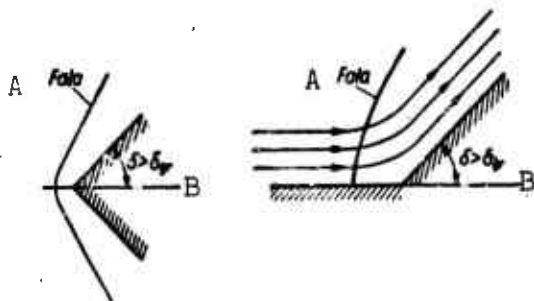


Fig. 3.17 Formation of separated, detached shock wave. A) Shock; B) lim.

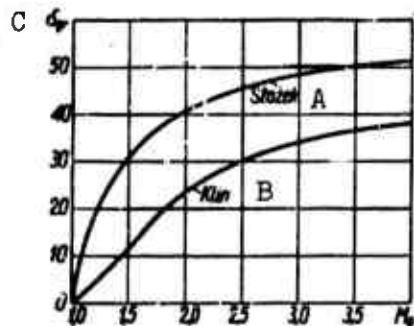


Fig. 3.18 Value of limit surface slope angle as a function of Mach number of original flow. A) Cone; B) wedge; C) lim.

3.2.6 Supersonic Two-Dimensional Diffusers

To improve compression efficiency at high Mach numbers ($M > 1.5$), one substitutes for a single strong normal shock a number of less intense oblique shock waves which are terminated by a weak normal shock (Fig. 3.19).

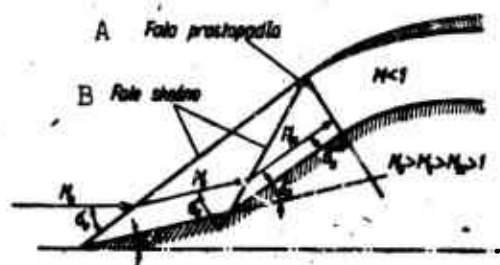


Fig. 3.19 System of oblique shock waves. A) Normal shock; B) oblique shock.

The most advantageous system of shock waves is one where, according to the theory of Oswatitch, the normal component of the Mach number from each shock wave remains unchanged.

$$M_0 \sin \sigma_0 = M_1 \sin \sigma_1 = M_{II} \sin \sigma_{II} \quad (3.10)$$

With this arrangement the diffuser achieves the maximum pressure recovery factor σ_D , which depends now only upon M_0 and the number of shock waves n . The latter can be interpreted as the number of stages in the diffuser.

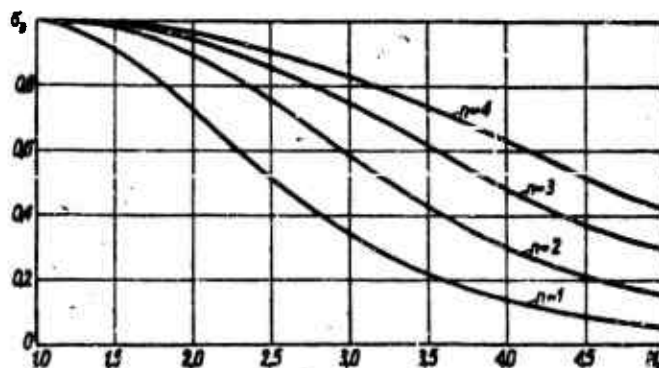


Fig. 3.20 The diffuser pressure recovery factor σ_D as a function of Mach number M_0 in the incident flow and the number of shock waves (or stages) n .

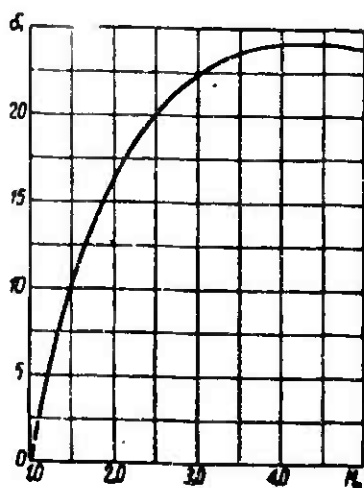


Fig. 3.21 Flow deflection angle δ_1 as a function of Mach number M_0 in the incident flow for a two-stage diffuser.

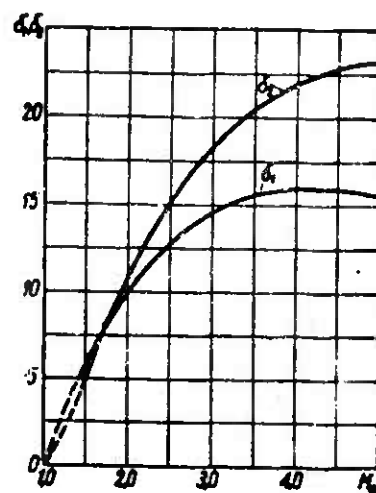


Fig. 3.22 Flow deflection angles δ_1 and δ_2 as functions of Mach number M_0 for a three-stage diffuser.

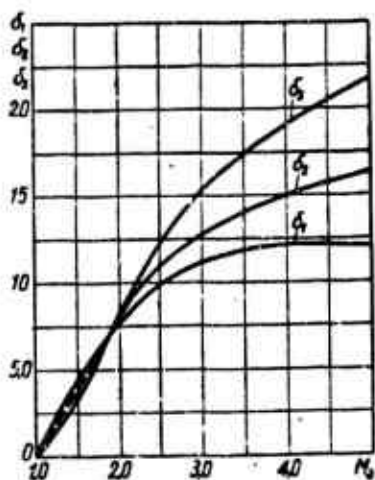


Fig. 3.23 Flow deflection angles δ_1 , δ_2 and δ_3 as functions of Mach number M_0 in the incident flow for a four-stage diffuser.

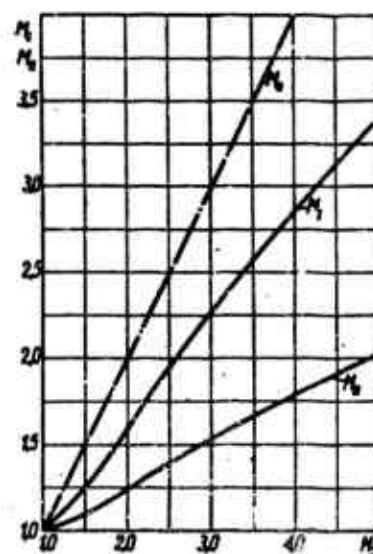


Fig. 3.24 Mach numbers M_I and M_{II} , aft of the oblique shock wave, as functions of the Mach number M_0 in the incident flow, for a three-stage diffuser.

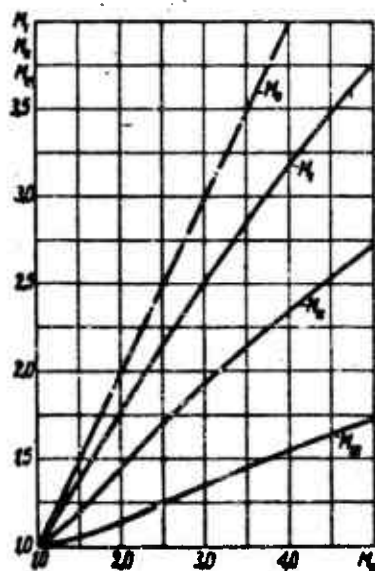


Fig. 3.25. Mach numbers M_I , M_{II} and M_{III} behind oblique shock waves as functions of the Mach number M_0 in the original stream for a four-stage diffuser.

Figure 3.20 shows curves of these relationships.

The calculation of a supersonic diffuser ought to be carried out through the following steps:

- from the graph of Fig. 3.20 one selects the number of diffuser stages n .
- from the graphs of Fig. 3.21, 3.22 and 3.23 one finds the velocity deflection angles, relative to the incident flow direction in front of each shock wave (from Fig. 3.21 for $n = 2$, from Fig. 3.22 for $n = 3$ and from Fig. 3.23 for $n = 4$);

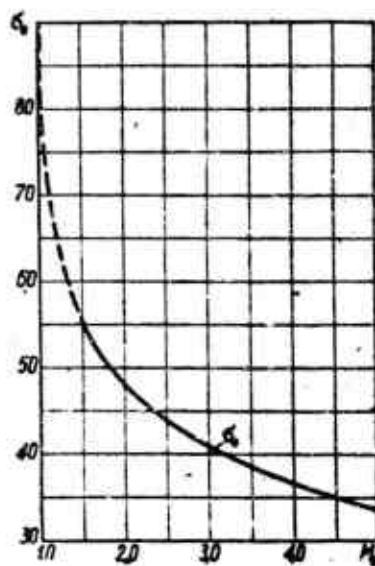


Fig. 3.26. The shock wave deflection angle as a function of M_0 for a two-stage diffuser.

- from the graphs of Fig. 3.24 and 3.25, one reads off the Mach number behind each shock wave;
- from the graphs of Fig. 3.26 and 3.28 one determines the shock wave deflection angles.

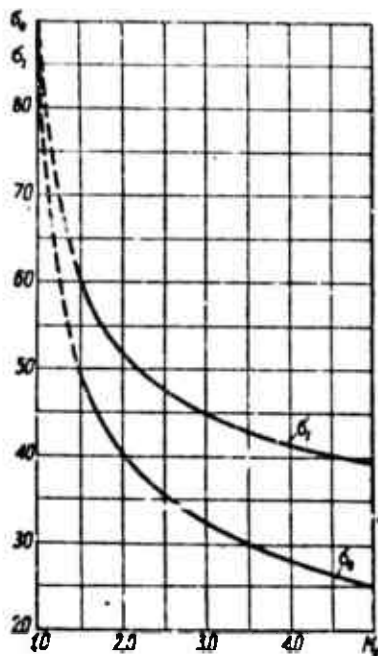


Fig. 3.27 Shock wave deflection angles as functions of M_0 for a three-stage diffuser.

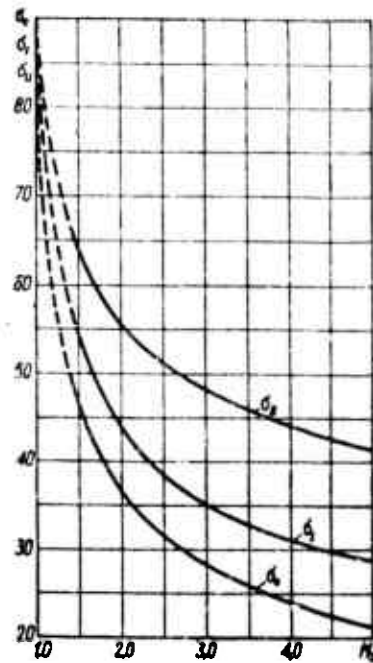


Fig. 3.28 Shock wave deflection angles as functions of M_0 for a four-stage diffuser.

3.2.7 Axially Symmetric Diffusers

The above method of diffuser calculations pertains only to two-dimensional diffusers.

The difference between flat diffusers and axially symmetric diffusers can be derived from the difference in flow past a wedge and a right circular cone.

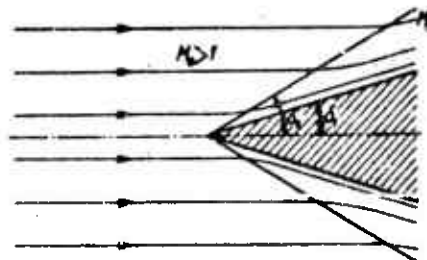


Fig. 3.29 Supersonic flow past a cone.

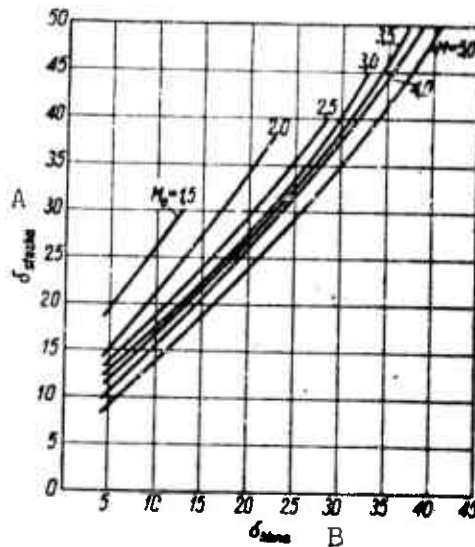


Fig. 3.30 Deflection angles for oblique shock waves of like intensity, for flow past a wedge and cone. A) Cone; B) wedge.

In front of a cone there appears a shock wave similar to that in front of a wedge, however, in this case it is in the form of a conical surface with an apex which is common to that of the cone in the stream. Also, stream lines, having passed through the front of the shock wave, do not assume immediately a direction which is tangent to the surface of the cone but follow curves which approach this condition asymptotically (Fig. 3.29). The shock wave deflection angle σ is smaller in the case of a cone than that of a wedge with the same apex half-angle δ . On the other hand, the apex angle of the cone is greater than that of the wedge for the same shock wave deflection angle. Likewise, the maximum apex angle of the cone is greater than that of the wedge (Fig. 3.18). Streamlines experience a congestion as they flow past the cone, so that the distribution of Mach numbers is uneven in the cross section normal to the flow (Mach numbers rise in proportion to their distance from the cone surface) and the compression of the gas behind the shock wave is isentropic. The compression efficiency for the same pres-

sure ratio is somewhat greater, therefore, for the cone than for the wedge. If we utilize the fact that the flow behind a shock wave of like intensity is similar for the cone and the wedge, we may perform the calculation for the axially symmetric diffuser in the same manner as for the flat diffuser, except for a correction to the apex angle of the cone (Fig. 3.30).

The sequence of calculations for the axially-symmetric three-stage diffuser is apparent from the schematic diagram shown in Fig. 3.31.

One begins to draw the diffuser by selecting at first point A at a distance R_0 from the diffuser axis (where R_0 is the outer radius of the diffuser inlet area); this area is determined by the continuity equation

$$F_0 w_0 \gamma_0 = G$$

where G is the mass flow rate of the gas; F_0 the inlet area; w_0 and γ_0 are the velocity and specific weight of the gas in front of the diffuser;

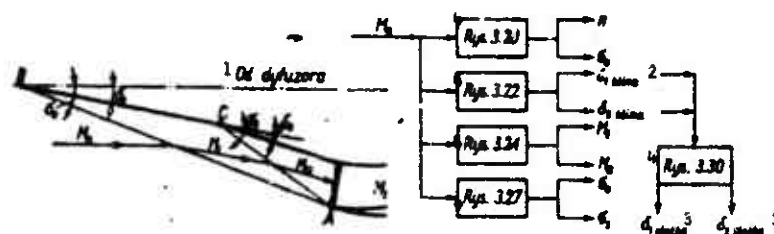


Fig. 3.31 Schematic diagram for the design of an axially-symmetric three-stage diffuser. 1) Diffuser axis; 2) wedge; 3) cone; 4) Fig.

subsequently one finds point B on the diffuser axis at the intersection with a line drawn from A at an angle σ_0 , and finally point C at the intersection of two lines drawn from B (at an angle δ_1) and from A at an angle $\sigma_1 + \delta_1$.

One also notes from the continuity equation that

$$G = w_1 F_1 \gamma_1$$

where w_1 , γ_1 are the velocity and specific weight of the gas behind the last (normal) shock wave; and F_1 the area of the normal shock wave.

3.2.8 The Effect of Viscosity on the Performance of a Supersonic Diffuser

The flow of a viscous gas through a three-stage supersonic diffuser is shown in Fig. 3.32. The boundary layer increases in thickness with its distance from the cone apex and attenuates the passage of gas at the vertex of the concave corner by causing there a number of weak shock waves to appear which merge subsequently into one strong shock wave. The location of these weak shock waves is not stabilized and provides the cause of fluctuations in the passing gas stream.

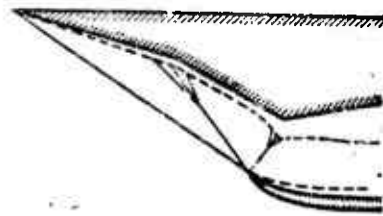


Fig. 3.32 Flow of a realistic gas through an axially symmetric supersonic diffuser.

The normal shock wave behaves in a similar manner. The effect of the boundary layer upon diffuser efficiency is magnified by the number of stages in the diffuser. This diminishes significantly the advantages of these diffusers. Thus in particular one does not strive to employ multi-stage diffusers at low Mach numbers.

3.2.9 Flow Through a Diffuser at Off-Design Conditions

Flow characteristics through a diffuser depend upon the system of shock waves at its inlet. The conditions which influence the system of shock waves are, according to their importance: the Mach number of the

incident flow and the degree of choking in the duct behind the diffuser.

Figure 3.33 shows the case of a diffuser operating at its calculated design Mach number although the choking is greater (a) or smaller (b) than calculated. As can be seen from the figure, the degree of choking has a direct bearing upon the location of the normal shock wave and, at the same time, on the inlet flow area. Under design conditions the whole flow, equal to the inlet flow orifice, enters the diffuser. When the choking is less than calculated (Fig. 3.33b) the flow rate through the diffuser does not change, however, the normal shock wave is drawn immediately inside the diffuser. If the duct

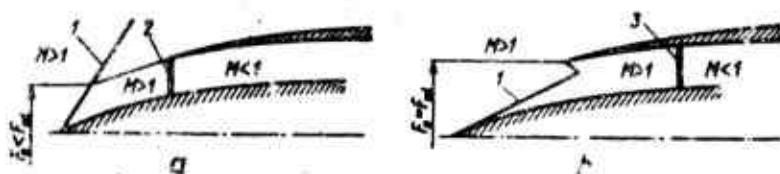


Fig. 3.33. Flow through the diffuser at off-design conditions. Example of flow at design inlet Mach number but with supercritical (a) and relatively subcritical (b) choking: 1 - Oblique shock waves; 2 - normal shock wave pushed upstream (due to increased choking); 3 - normal shock wave drawn inside diffuser (due to decreased choking); F_0 - inlet area of flow incident upon diffuser; F_{w1} - diffuser inlet area.

through which the subsonic flow passes diverges, there occurs an expansion of the flow, an increase of the Mach number, a concurrent rise in normal shock wave intensity and a loss of compression efficiency.

Figure 3.34 illustrates the case where the Mach number of the incident flow is relatively less than (a) or greater (b) than that calculated, whereas the choking in the duct behind the diffuser is held unchanged. When the Mach number is less than that for which the diffuser is designed, the deflection angles of oblique shock waves are greater and the flow rate through the diffuser is less.

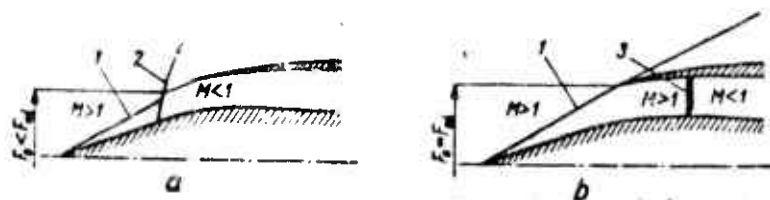


Fig. 3.34 Flow through the diffuser at off-design conditions. Example of flow at designed choking but relatively smaller (a) and greater (b) than calculated Mach number; the legend of Fig. 3.33 applies.

In the opposite case (Fig. 3.34b) the deflection angles of oblique shock waves are smaller than calculated and the shock waves enter inside the diffuser.

The normal shock wave then remains withdrawn deep inside and the diffuser efficiency decreases.

3.3 NOZZLES

The performance of nozzles in jet engines depends upon the change of thermal energy, liberated in the combustion chamber, into kinetic energy. The primary process which conveys this change of energy is the expansion of burnt gases. This basic process, however, is accompanied by a number of side effects. These are: an exchange of heat with the environment, the recombination of gas molecules which became dissociated in the combustion chamber, the transfer of part of the energy into hydro-mechanical losses and the addition of heat from delayed burning of unburnt droplets of the mixture in the combustion chamber. To simplify the analysis of the process one considers it as an isentropic expansion and treats thereby the combustion gases as an ideal gas.

3.3.1 Flow Through Nozzle

The basic equations for the analysis of flow through a nozzle are:
- equation of energy

$$A \frac{w_0^2}{2g} + c_p T_0 = A \frac{w^2}{2g} + c_p T$$

- equation of continuity

$$G = \gamma_0 w_0 F_0 = \gamma w F$$

- isentropic equation

$$\frac{T}{T_0} = \left(\frac{p}{p_0}\right)^{\frac{\kappa-1}{\kappa}} = \left(\frac{\gamma}{\gamma_0}\right)^{\frac{\kappa-1}{\kappa}}$$

where w_0 , T_0 , p_0 , γ_0 - are the velocity, temperature, pressure and mass density of the gas at the inlet cross section of the nozzle; w , T , p , γ - the corresponding parameters at the exit cross section of the nozzle; c_p , κ the specific heat at constant pressure and the isentropic exponent (which remains constant during the whole process of expansion); A the thermal equivalent of work.

By transformation of the above equations one obtains the relation

$$\frac{G}{F} = \sqrt{\frac{2g\kappa}{\kappa-1} p_0 \gamma_0 \left(\frac{p}{p_0}\right)^{\frac{2}{\kappa}} - \left(\frac{p}{p_0}\right)^{\frac{\kappa+1}{\kappa}}}$$

where F is the area of the cross section at the exit of the nozzle.

The ratio G/F achieves a maximum for a particular pressure ratio p/p_0 , known as the critical pressure ratio. This critical pressure ratio determines the relation

$$\left(\frac{p}{p_0}\right)_* = \frac{p_{kr}}{p_0} = \left(\frac{2}{\kappa+1}\right)^{\frac{\kappa}{\kappa-1}}$$

The corresponding critical temperature ratio is then found to be

$$\frac{T_{kr}}{T_0} = \frac{2}{\kappa+1}$$

The velocity which is related to these critical parameters is thus also known as the critical velocity and is equal to the sound velocity in this section.

The value $\frac{p_{kr}}{p_0}$ separates two types of nozzles:

for $\frac{p}{p_0} > \frac{p_{kr}}{p_0}$ the nozzle converges and the discharge velocity is smaller than the sound velocity (Fig. 3.35a);

for $\frac{p}{p_0} < \frac{p_{kr}}{p_0}$ the nozzle is of the converging-diverging type

and the discharge velocity is greater than the sound velocity. This type of a nozzle is called Laval's nozzle (Fig. 3.35b).

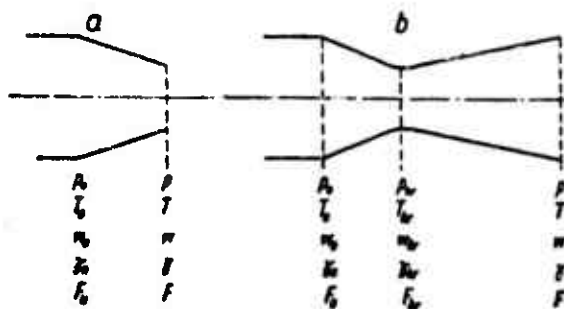


Fig. 3.35 Nozzles. a) converging; b) converging-diverging (Laval's).

The section of the nozzle which is characterized by the critical parameters has been termed the critical section.

Beginning with the energy equation, one may determine the maximum velocity w_{\max} , or that velocity which one obtains for an isentropic expansion to an absolute vacuum

$$w_{\max} = \sqrt{2g_c T_0^*}$$

where T_0^* is the stagnation temperature at the inlet section of the nozzle.

The velocity which one obtains by expanding the gas to the ambient pressure p is determined by the equation

$$w = \sqrt{\frac{2g_c B}{\kappa - 1} \frac{T_0}{\mu} \left[1 - \left(\frac{p}{p_0} \right)^{\frac{\kappa - 1}{\kappa}} \right]} \quad (3.11)$$

where B is the absolute gas constant and μ the molecular weight.

The last two equations are linked by the relation

$$w = w_{\max} \sqrt{1 - \left(\frac{p}{p_0} \right)^{\frac{\kappa - 1}{\kappa}}} \quad (3.12)$$

This dependence is expressed by the curve of Fig. 3.36.

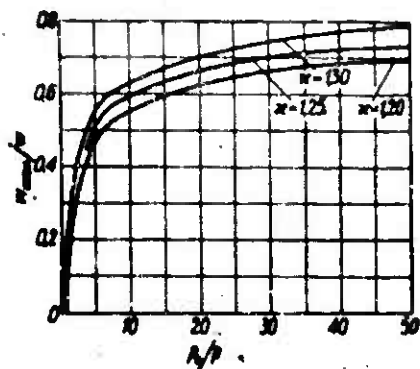


Fig. 3.36 The value of w_{\max}/w as a function of the expansion ratio, for different isentropic exponents κ . The legend of Fig. 3.35 applies.

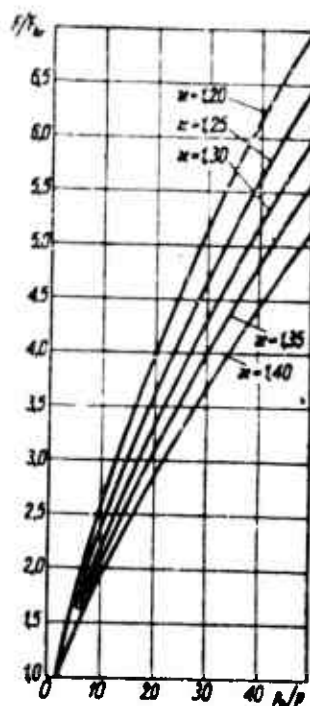


Fig. 3.37 The ratio F/F_{kr} as a function of the expansion ratio for different values of κ . The legend of Fig. 3.35 applies.

The gas discharge velocity rises, therefore, with an increase in the temperature at the nozzle inlet and with a decrease of the molecular weight and the ratio of the exit to inlet pressure of the nozzle.

By transforming the corresponding equations for the exit conditions, as given above, one can derive a relation between the ratio of the exit area to critical area F/F_{cr} and the pressure ratio P/P_0 .

$$\frac{F}{F_{kr}} = \frac{\sqrt{\kappa} \left(\frac{2}{\kappa+1} \right)^{\frac{\kappa+1}{2(\kappa-1)}}}{\left(\frac{P}{P_0} \right)^{\frac{1}{\kappa}} \frac{2\kappa}{\kappa-1} \sqrt{1 - \left(\frac{P}{P_0} \right)^{\frac{\kappa-1}{\kappa}}}} \quad (3.13)$$

This relation is illustrated in Fig. 3.37.

3.3.2 Shapes of Nozzles

The profile of a converging subsonic nozzle is best formed according to the law of Witoszynski

$$r = \frac{r_0}{1 - \left[1 - \frac{r}{r_0}\right]^3 \frac{\left(1 - \frac{3x^2}{l^2}\right)^2}{\left(1 + \frac{x^2}{l^2}\right)^2}} \quad (3.14)$$

where $\beta = \frac{1}{\sqrt{3}}$, and where the remaining quantities are defined by Fig. 3.38.

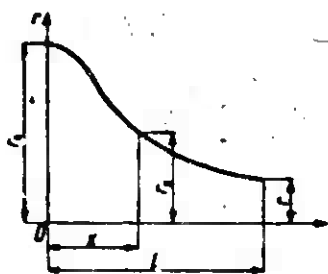


Fig. 3.38 Nozzle profile according to Witoszynski.

The loss coefficient of velocity for a nozzle shaped in this manner is

$$\eta_p = \frac{w_{rs}}{w_t}$$

where w_{rs} is the realistic discharge velocity and w_t the theoretical discharge velocity. This coefficient has a value of 0.985-0.99.

For a nozzle with a conic profile the value of the coefficient is about 0.97.

The nozzle discharge coefficient

$$\eta_g = \frac{G_{rs}}{G_t}$$

where G_{rs} is the realistic mass flow rate and G_t the theoretical flow rate, depends upon the nozzle inlet angle, the ratio of the cross sec-

tions F/F_0 and the expansion ratio p_0/p . This is apparent if we take into account the losses of the mass flow rate through the nozzle due to an uneven velocity profile at the inlet section and due to friction. The above dependence is depicted by the curves of Fig. 3.39.

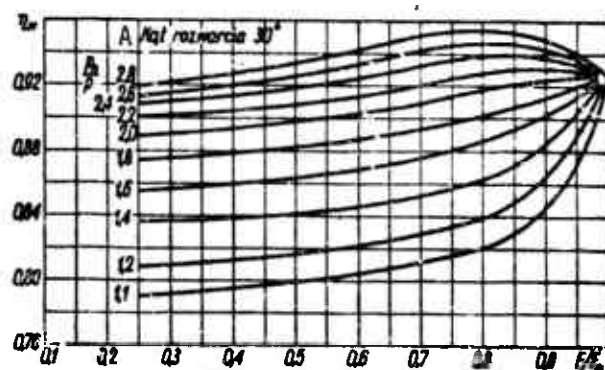


Fig. 3.39 The discharge coefficient of a converging nozzle as a function of the expansion ratio and the area ratio F/F_0 . The legend of Fig. 3.35 applies. A) inlet angle.

De Laval's nozzle profile can best be formulated in accord with the relations expressed in Fig. 3.40.

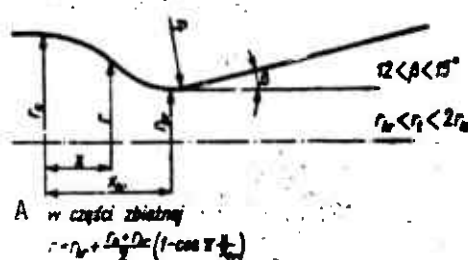


Fig. 3.40 De Laval's nozzle profile. A) For the converging segment of the nozzle.

The velocity loss coefficient for a nozzle of this type amounts to

$$\eta_d = 0.97 \div 0.99$$

3.3.3 Nozzle Performance at Off-design Conditions

The mass flow rate of a gas through a converging nozzle is intimately related to the ratio of pressures which exist at the inlet and

at the exhaust of the nozzle. The pressure at the exhaust of a converging nozzle (disregarding the narrowing of the flow as it is caused by the reaction against the conically oriented stream surfaces near the walls) equals approximately (although it is always somewhat higher) to the pressure outside. This effect is shown by the curve of Fig. 3.41. Whenever it is desired to increase the gas flow rate through a converging nozzle one must increase the pressure at the inlet to the nozzle or, keeping this pressure constant, one must increase the area of the exit section of the nozzle. A change of the back pressure, in the ex-

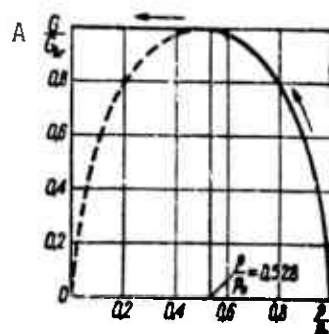


Fig. 3.41 The change of mass flow rate from a converging nozzle as a function of the ratio of outside pressure to inlet pressure.
A) G/G_{kr} .

ample of a converging nozzle, causes a simultaneous change of the mass flow rate and of the pressure at the nozzle inlet.

However, if one starts with the critical pressure ratio (when the exit section of the nozzle assumes the critical value) then the mass flow rate through the nozzle is fixed and the back pressure has no influence. Yet in this case the calculated pressure at the exit section of the nozzle differs from the outside pressure, and one says that the nozzle is operating under off-design conditions.

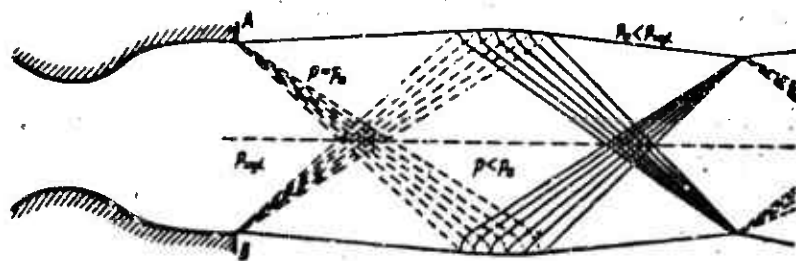


Fig. 3.42 Flow at exit of De Laval's nozzle with an outside pressure smaller than the exit pressure. p_{exit} - Exit pressure (at the exit section of the nozzle); p_a - outside pressure (atmospheric); p - predominant pressure of a given zone.

When the outside pressure is less than the existing pressure at the exit section of the nozzle, then the expansion of the gas continues also in the stream behind the nozzle. A number of rarefaction waves is generated at the trailing edge (dashed lines in Fig. 3.42 which reflect at the jet boundary as compression waves, etc.), thus forming the well-known picture of a system of expansions and compressions in sequence. These processes are nonisentropic in character and thus give rise to losses in energy.

For the case when the outside pressure is greater than the exhaust pressure of the converging nozzle, the phenomena of Fig. 3.43 arise. For a small overpressure (Fig. 3.43a) oblique compression waves appear at the trailing edge of the nozzle and reflect at the stream boundary in the form of a number of expansion waves, etc.

For greater overpressures, compression waves recede into the nozzle and a strong curved compression wave appears in the central region of the flow (Fig. 3.43b). Further pressure rise, responsible for the recession of the compression wave, causes a detachment of the boundary layer behind the wave, thus giving rise to a significant increase in energy losses (Fig. 3.43c). The inception of this effect is expressed

with the aid of Summerfield's criterion. This criterion can be described in the following manner: There exists the danger of flow detachment when the half-angle in the diverging and supersonic region of a De Laval's nozzle is on the order of 15° and when the expansion ratio is greater than 16, i.e., when the ratio of the nominal exit pressure to that outside is less than 0.4.

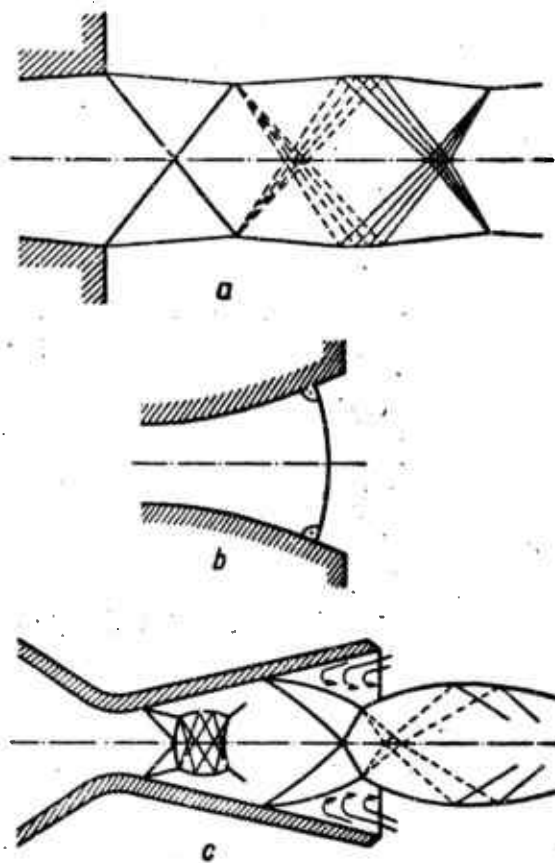


Fig. 3.43 Flow at exit of nozzle with an outside pressure greater than the exit pressure. *a* - Exhaust stream for small pressure difference; *b* - appearance of a receding bowed compression wave; *c* - detachment of flow for great pressure differences.

3.4 THEORY OF THE GAS EJECTOR

The ejector consists in its simplest form (Fig. 3.44) of a nozzle which ejects a primary gas stream of high stagnation pressure, and a chamber wherein energy is transferred from the primary to the second-

ary stream by means of turbulent mixing.

This process results in an increase of the stagnation pressure in the secondary gas stream.

Ejectors found applications in technology as compressors, delivering a greater quantity of gas at lower pressure at the expense of energy from a smaller quantity of gas at higher pressure, also as roughing pumps in vacuum systems for the lowering of pressures in tanks and pipes. In the field of aviation, one hopes to increase with their aid the thrust of jet engines.

3.4.1 Basic Operation of the Gas Ejector

The principle of operation of the gas ejector is described in the following manner. A pressure p_2 exists at the inlet section of the mixing chamber, under steady-state operating conditions, which is lower than the stagnation pressure p_2^* in the secondary gas stream, but which is equal to the static pressure of the primary flow in the down-stream section of the nozzle. The secondary stream accelerates because of the pressure difference and mixes with the primary stream. During this mixing an equalization of parameters takes place in the plane normal to the chamber. The length of the chamber equals 6-10 diameters. Energy losses take place during the process of ejection and are caused not only by aerodynamic resistance but also by the very process of mixing which, from a thermodynamic point of view, is an irreversible process.

The kinetic energy of the exit gas stream can be represented by the equation below (where one assumes the mixing process to occur at constant pressure)

$$E_3 = \frac{G_1 + G_2}{2g} w_3^2 = \frac{1}{2g} \frac{(G_1 w_1 + G_2 w_2)^2}{G_1 + G_2}$$

where w_1 and w_2 are respectively the velocities of the primary and secondary gas stream at the inlet to the mixing chamber and w_3 the ve-

locity of the gas mixture at its exit, and G_1 , G_2 and G_3 the corresponding mass flow rates of the gas.

The sum of kinetic energies of the gas streams can be expressed, at the inlet to the chamber, as

$$E_1 + E_2 = \frac{1}{2} (G_1 w_1^2 + G_2 w_2^2)$$

Subtracting from each other the above relations, one obtains the quantity of energy lost

$$\Delta E = \frac{G_1 G_2}{G_1 + G_2} \frac{(w_1 - w_2)^2}{2g} = G_1 \frac{n}{1+n} \frac{(w_1 - w_2)^2}{2g} \quad (3.15)$$

where $n = G_2/G_1$ is the degree of ejection.

The energy lost during mixing thus depends above all upon the square of the velocity difference between the primary and secondary gas stream.

3.4.2 Ejector Design

The main difficulty in the design of an ejector rests with the parameter determination for the state of the gas stream at the exit of the mixing chamber. One begins with the three equations for the conservation of mass, energy and momentum, as nearly always in the dynamics of gases. If one assumes the mixing process to be adiabatic, and the specific heats of the gas stream to be alike and constant during the whole process, one obtains the following set of equations

$$\begin{aligned} \frac{T_1^*}{T_1^0} &= \frac{n\theta + 1}{n + 1} \\ z(\lambda_1) + n\sqrt{\theta} \cdot z(\lambda_2) &= \sqrt{(n+1)(n\theta+1)} z(\lambda_3) \\ \frac{p_1^*}{p_1^0} &= \frac{\sqrt{(n+1)(n\theta+1)}}{1 + \frac{1}{n}} \cdot \frac{q(\lambda_1)}{q(\lambda_2)} \\ n &= \frac{p_1^*}{p_1^0} \frac{q(\lambda_2)}{q(\lambda_1)} \frac{1}{\alpha\sqrt{\theta}} \end{aligned} \quad (3.16)$$

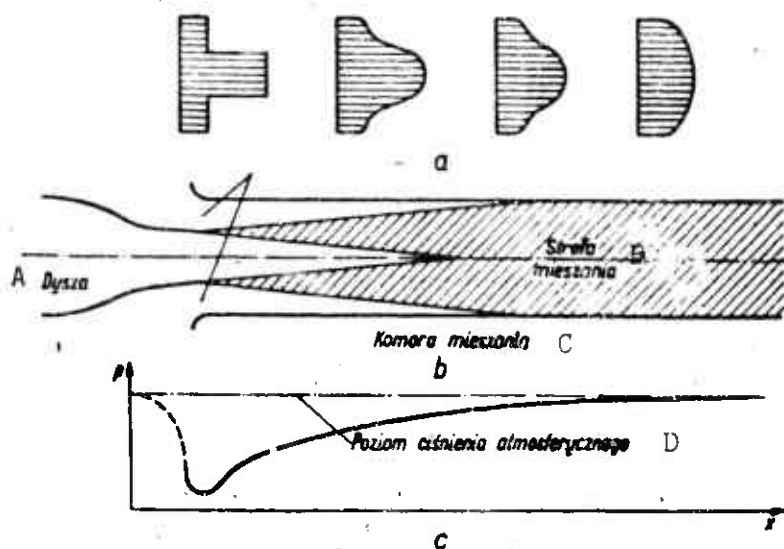


Fig. 3.44 Principle of operation of a gas ejector. a - Velocity profile in characteristic sections of the chamber; b - injector; c - axial pressure distribution in the mixing chamber. A) Nozzle; B) mixing zone; C) mixing chamber; D) level of atmospheric pressure.

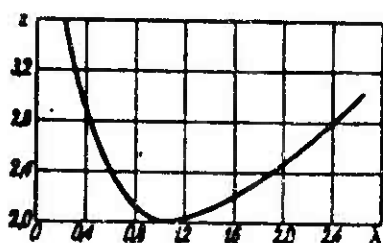


Fig. 3.45 Graph of the function $z = z(\lambda)$.

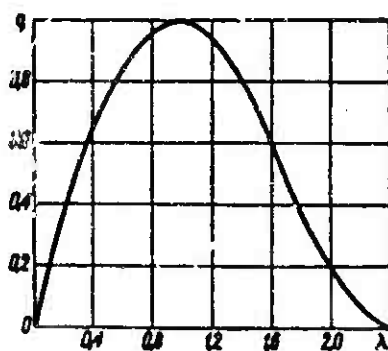


Fig. 3.46 Graph of the function $q = q(\lambda)$.

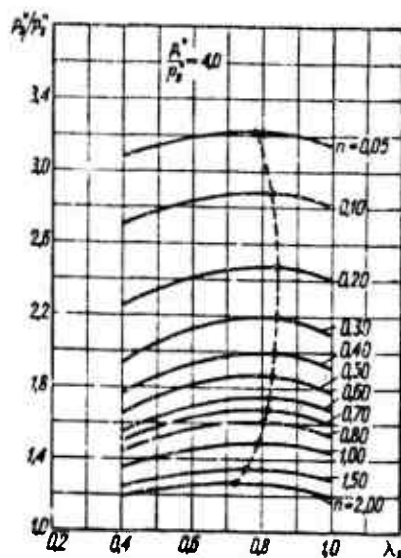


Fig. 3.47 Ejector Characteristics

where T_1^* , T_2^* , T_3^* are the stagnation temperatures of the primary, secondary and final gas stream, and where p_1^* , p_2^* , p_3^* are the corresponding stagnation pressures, furthermore

$$\theta = \frac{T_1^*}{T_2^*};$$

$z(\lambda) = \lambda + \frac{1}{\lambda}$ function illustrated by the curve of Fig. 3.45

$q(\lambda) = \left(\frac{x+1}{2}\right)^{\frac{1}{x-1}} \lambda \left(1 - \frac{x-1}{x+1} \lambda^2\right)^{\frac{1}{x-1}}$ - function illustrated by the curve on Fig. 3.46

$\lambda = \frac{w}{c^*}$ - velocity coefficient (De Laval's number)

c^* - the critical velocity (flow velocity equal to the local sound velocity)

$$\alpha = \frac{F_1}{F_2};$$

$$F_3 = F_1 + F_2.$$

One is in a position to determine missing parameters with the aid of the above equations, when the stagnation temperatures and pressures

are given and when the velocity coefficient is known for the inlet section of the mixing chamber.

Some difficulty arises with the determination of the velocity coefficients λ_1 and λ_2 which depend upon the static pressure at the inlet section to the mixing chamber ($p_1 = p_2$). This pressure does not vary with the given exit parameters and depends upon the assumed operating conditions of the ejector. If one intends to define these conditions, one must estimate the characteristics of the ejector (by assuming a number of values $p_1 = p_2$, and also a number of values for λ_1 and λ_2), and must thus compute, for example, the ratio p_3^*/p_2^* as a function of λ_2 for $n = \text{const}$. A characteristic of this type is shown in Fig.

3.47. One can determine the optimum operating conditions of an ejector (optimum λ_2) when the ejector characteristic is known.

3.3.3 The Ejector as a Means to Increase the Thrust of Jet Engines

If one begins with the momentum equation and utilizes the notation from the diagram of Fig. 3.48, one can determine the thrust of

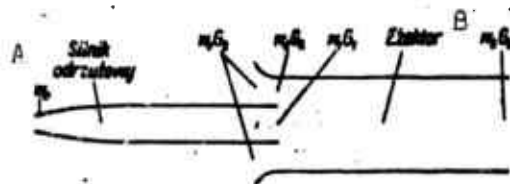


Fig. 3.48 Schematic diagram of jet engine with ejector.
A) Jet engine; B) ejector.

the jet engine without ejector

$$S_0 = \frac{G_1}{g} (w_1 - w_0)$$

the thrust of the jet engine with an ejector

$$S = \frac{G_2}{g} (w_5 - w_0)$$

and the ratio of these thrust values which, after some transformation, amounts to

$$\frac{S}{S_0} = \frac{w_2 - w_0}{w_1' - w_0} \frac{w_1 - w_2}{w_0 - w_2} \quad (3.17)$$

where w_1' is the gas velocity at the nozzle exit for an engine without ejector.

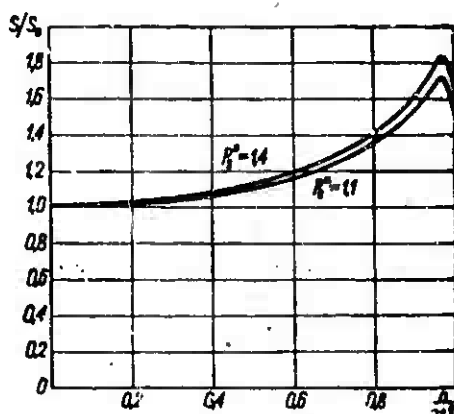


Fig. 3.49 Thrust increase due to application of ejector, as a function of ejector coefficient.

The result of these calculations is shown by the curves of (Fig. 3.49. It was convenient to introduce instead of n the independent variable $n/n + 1$ which is known as the ejector coefficient. It is seen from the graph that the maximum thrust increase amounts to about 80% as a result of ejector addition. This value depends upon the degree of ejection and passes through a maximum at $n \sim 40$.

3.5 FLOW WITH HEAT ADDITION

A flow model for an idealized combustion chamber is illustrated in Fig. 3.50. The combustible gas mixture flows through a cylindrical duct. Its combustion takes place in a definite section. This plane is called the flame front. When the velocity of flame propagation is equal to the flow velocity of the combustible mixture, the position of

the flame front remains steady relative to the duct wherein the flow occurs.

One may begin with the following equations:

Conservation of mass

$$\rho_1 w_1 = \rho_2 w_2$$

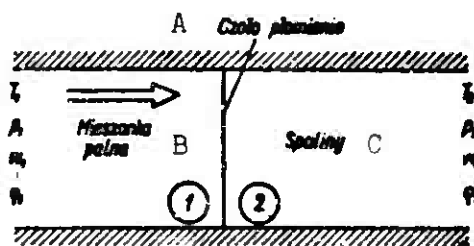
Conservation of momentum

$$\rho_1 w_1^2 - \rho_2 w_2^2 = p_2 - p_1$$

where T_1, w_1, p_1, ρ_1 are the temperature, velocity, pressure and density of the mixture and T_2, w_2, p_2, ρ_2 the temperature, velocity, pressure and density of the combustion products. After some transformation one obtains

$$\rho_1^2 w_1^2 - \rho_2^2 w_2^2 = \frac{p_2 - p_1}{\frac{1}{\rho_1} - \frac{1}{\rho_2}} \quad (3.18)$$

It is apparent from this relation that the pressure and density may either rise or fall across the flame front. Thus, two types of combustion processes are possible, namely, a process where both the pressure and density rise, and one where a drop occurs in pressure and density. The first type of combustion, the second type as a slow-burning combustion or deflagration.



Rys. 3.50. Przepływ ze spalaniem

Fig. 3.50 Flow with combustion. A) Flame front; B) combustion chamber; C) combustion products.

The energy equation assumes the following form for the case of flow in the presence of combustion

$$\frac{1}{2} w_1^2 + \frac{\kappa}{\kappa - 1} \frac{p_1}{\rho_1} = \frac{1}{2} w_2^2 + \frac{\kappa}{\kappa - 1} \frac{p_2}{\rho_2} - Q$$

where Q is the thermal energy liberated during the chemical reaction (expressed in units of its mechanical equivalent) and κ , the isentropic exponent.

One obtains from the preceding equation, after some transformation,

$$p_2 \left(\frac{1}{\rho_2} \frac{\kappa + 1}{\kappa - 1} - \frac{1}{\rho_1} \right) - 2Q - p_1 \left(\frac{1}{\rho_1} \frac{\kappa + 1}{\kappa - 1} - \frac{1}{\rho_2} \right) = 0 \quad (3.19)$$

The graph of this equation, for the system p and $\frac{1}{\rho}$, is the Hugoniot curve for combustion (Fig. 3.51). For $Q = 0$, the Hugoniot curve for combustion transforms into the curve for a normal shock wave. The point with coordinates $(p_1, \frac{1}{\rho_1})$ lies exactly on this curve (0). By drawing an isochore from the point 0 to the point A, and an isobar to the point B (whereby one liberates the same quantity of heat Q in both of these transformations), then both of these points will fall unto the same Hugoniot curve.

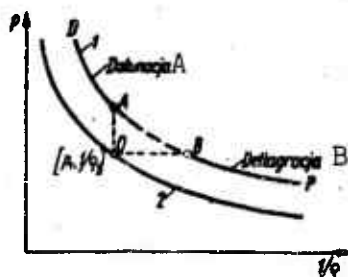


Fig. 3.51 Hugoniot curve. 1 - For combustion; 2 - for a shock wave. A) Detonation; B) deflagration.

The segment A-D of the curve represents the range of detonation, whereas the segment B-P expresses the range of slow combustion. Segment A-B does not have physical significance.

The relation between state parameters, fore and aft of the deflagration flame front, for flow through a duct with constant cross sec-

tion, can be expressed with the aid of corresponding Mach numbers.

These expressions have the following form

$$\frac{\rho_2}{\rho_1} = \frac{1 + \kappa M_1^2}{1 + \kappa M_2^2}$$

$$\frac{T_2}{T_1} = \frac{M_1^2}{M_2^2} \left(\frac{1 + \kappa M_1^2}{1 + \kappa M_2^2} \right)^2$$

$$\frac{p_2}{p_1} = \frac{M_1^2}{M_2^2} \frac{1 + \kappa M_1^2}{1 + \kappa M_2^2} \quad (3.20)$$

$$\frac{T_2^*}{T_1^*} = \frac{M_2^2}{M_1^2} \left(\frac{1 + \kappa M_1^2}{1 + \kappa M_2^2} \right)^{1 + \frac{\kappa - 1}{2} M_1^2} \frac{1 + \frac{\kappa - 1}{2} M_1^2}{1 + \frac{\kappa - 1}{2} M_2^2}$$

$$\frac{p_2^*}{p_1^*} = \frac{1 + \kappa M_1^2}{1 + \kappa M_2^2} \left(\frac{1 + \frac{\kappa - 1}{2} M_1^2}{1 + \frac{\kappa - 1}{2} M_2^2} \right)^{\frac{\kappa}{\kappa - 1}}$$

where T_1^* , p_1^* are the stagnation temperature and pressure of the gas mixture; T_2^* , p_2^* the stagnation temperature and pressure of the combustion products; and M_1 and M_2 the Mach numbers of the gas mixture and the combustion products.

These relations are shown by the curves in Fig. 3.52.

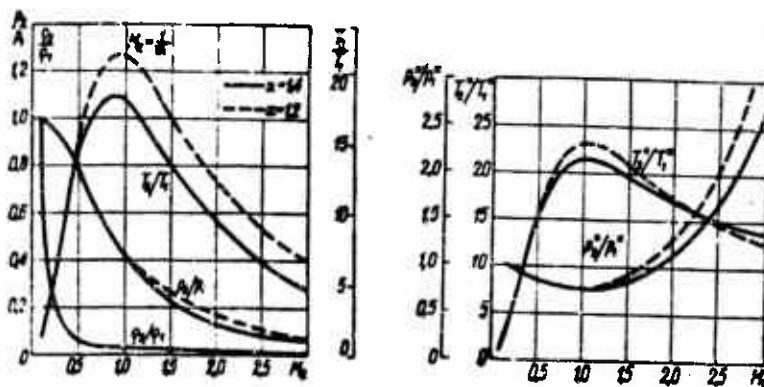


Fig. 3.52 Change of thermodynamic state parameters in an ideal combustion chamber.

The curves illustrate the change in thermodynamic parameters in their dependence from the exit Mach number, for an inlet gas velocity corresponding to $M_1 = 0.1$.

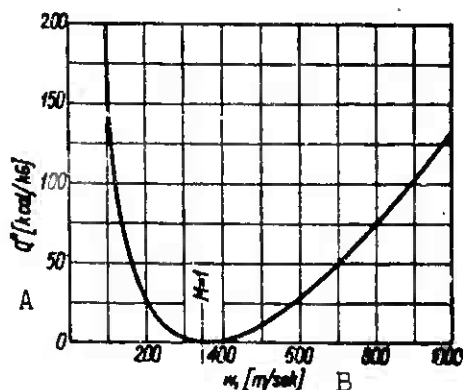


Fig. 3.53 Heat addition, at the condition of flow saturation, as a function of the incident flow velocity. A) Q^* (kcal/kg); B) w_1 (m/sec)

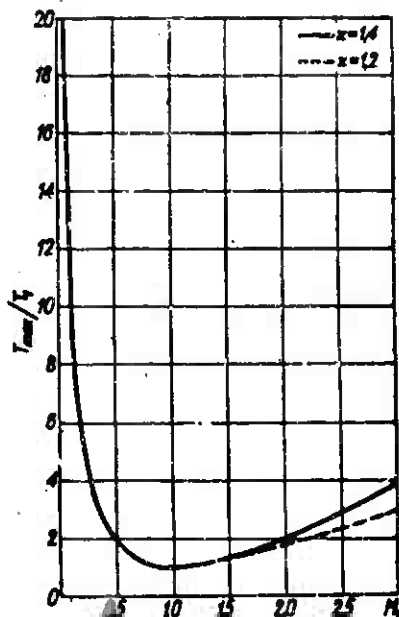


Fig. 3.54 Maximum temperature change as a function of inlet Mach number. T_1 - Inlet temperature.

The addition of heat to a subsonic gas flow, passing through a cylindrical duct, causes a drop in the static and stagnation pressures, a drop in density and an increase of the Mach number.

When the flow is supersonic, the static and stagnation pressures rise, whereas the Mach number and the density decrease. This behavior of the Mach number leads to the corollary that the Mach number $M = 1$ is the limiting value at which heat can be added both in supersonic and subsonic flow. One speaks in this case of a heat-saturated flow of gas. The quantity of heat which can be added to the gas stream, therefore, depends upon the Mach upon the inlet Mach number, and thus upon the flow velocity of this stream. This dependence is illustrated by the curve of Fig. 3.53. The saturation of the flow with heat leads to the existence of a maximum temperature to which the gas may be raised

as it passes through the cylindrical duct. The value of this maximum temperature depends quite clearly also upon the inlet Mach number (Fig. 3.54).

REFERENCES TO CHAPTER 3

- 3.1. K. Oswatitsch: Der Wirkungsgrad von Stossdifusoren [Performance of Thrust-Diffusers]. NACA, TM 1140, 1947.
- 3.2. G. Abramowicz: Prikładnaja gazowaja dinamika [Applied Gas Dynamics]. 1953.
- 3.3. J. Pai Shih: Fluid Dynamics of Jets. 1954.
- 3.4. A. Bonney, M. Zucrow, C. Besserer: Principles of Guided Missile Design - Propulsion. 1956.
- 3.5. O. Lutz: Schuberrhöhung durch Strahlbeimischung [Thrust Augmentation Through Ejector Mixing]. 1957.
- 3.6. J. Rosciszewski: Aerodynamika stosowana [Applied Aerodynamics]. Published by MON, Warsaw 1957.
- 3.7. M. Barrere, A. Jaurnotte, B. Fraeip de Venbeke: La Propulsion par Fussees [Rocket Propulsion]. 1957.
- 3.8. B. Stieczkin: Teoria silników odrzutowych [Theory of Reaction Motors]. Published by MON, Warsaw 1961.
- 3.9. R. Hermann: Supersonic Inlet Diffusers. 1959.
- 3.10. A. Kowalewicz: Praca dyfuzorów wlotowych w zmiennych warunkach [Performance of Inlet Diffusers Under Varying Conditions]. Technika Lotnicza [Technical Aviation] Nos. 5 and 6, 1960.

Chapter 4

ENERGY SOURCES

The basic source of energy, presently used in aircraft propulsion, is the chemical energy of natural or synthetic fuels.

Only in the past few years has work begun on the application of nuclear energy to this purpose. Creative application of these goals will expand our present capability in two main directions:

- first, it will insure that available sources of energy will not be exhausted,

- second, it will allow construction of propulsion units having greater power than at present and with practically unlimited range.

One would expect, however, that in view of the great costs, nuclear energy will not be utilized in transportation until the exhaustion of chemical fuels, except in some special cases where it would be technically justified.

The source of chemical energy is the combustion process which consists of the combination, under appropriate conditions, of two materials which are not in chemical equilibrium. Most often one of these materials is oxygen, and the reaction taking place is one of oxidation. Oxygen in its pure form is rarely used. In aircraft engines it appears as a component in the atmosphere, in rocket engines on the other hand, it appears as a component of a different, usually synthetic oxidizer. The material being oxidized is called a fuel. Together, fuel and oxidizer constitute the propellant. Depending on their consistency, one distinguishes solid, liquid and gaseous propellants. Obviously either

the fuel or the oxidizer can be solid, liquid or gaseous. Gaseous fuels are used only in exceptional cases because of their low density.

4.1 PROPELLANTS

Propellants constitute the one area which has the greatest effect on distinguishing the engines discussed in this book. In pulse and jet engines the oxidizer is atmospheric air and the fuel is gasoline, kerosene or gas oil; however, in the case of pulse jets one mostly uses gasoline. In rocket engines using solid propellants, fuel and oxidizer form a mixture which is ready for combustion without any preliminary processes. In rocket engines using liquid propellants, fuel and oxidizer are stored in separate containers and must be properly prepared before combustion can take place. In both cases of a rocket engine's propellants, fuel as well as oxidizer are synthetically produced or at best are processed from a natural raw material.

4.1.1 Energy Characteristics of Propellants

From the relation of the exhaust velocity from the engine nozzle (3.11)

$$w = \sqrt{\frac{2\kappa B}{\kappa - 1}} \sqrt{\frac{T}{\mu}} \sqrt{1 - \left(\frac{p}{p_0}\right)^{\frac{\kappa - 1}{\kappa}}} \quad (4.1)$$

it follows that this velocity depends on the temperature T (equal to the combustion temperature) at the beginning of the nozzle, on the apparent molecular weight μ of the combustion products, on the ratio of pressures p at the nozzle's outlet and p_0 at the inlet and on the ratio of specific heats κ . Therefore for equal expansion ratios p_0/p , the exhaust velocity of combustion products arising from the combustion of air-hydrocarbon mixtures will depend only on the combustion temperature and therefore on the heating value of the fuel.

In the case of rocket engines, the heating value is not a suffi-

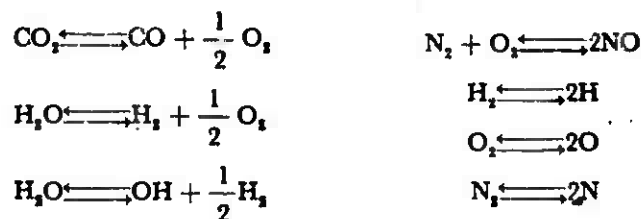
cient quantity to compare various propellants. In this case one takes the exhaust velocity as the criterion, or at least an expression having the greatest influence on its magnitude, namely $\sqrt{T/\mu}$.

4.1.2 Description of Composition, Temperature and Apparent Molecular Weight of Combustion Products.

As a result of complete combustion of commonly encountered propellants, the combustion products consist of the following components: CO_2 , O_2 , H_2O , H_2 and N_2 . Percentage contributions of these various components can be determined from the composition of fuel and oxidizer and from the appropriate stoichiometric equations.

At temperatures on the order of 2000°K one has to take into account the effects of dissociation when computing the composition of the combustion products.

In this case, the quantity of the combustion products is determined from the following equilibrium equations.



Denoting the partial pressures of the individual components of combustion products by p with an appropriate subscript (e.g., partial pressure of oxygen p_{O_2}) one can determine the equilibrium constants corresponding to the seven equilibrium equations given above:

$$\begin{array}{lll} K_1 = \frac{p_{\text{CO}} \cdot p_{\text{O}_2}^{\frac{1}{2}}}{p_{\text{CO}_2}}; & K_2 = \frac{p_{\text{H}_2} \cdot p_{\text{O}_2}^{\frac{1}{2}}}{p_{\text{H}_2\text{O}}}; & K_3 = \frac{p_{\text{OH}} \cdot p_{\text{H}_2}^{\frac{1}{2}}}{p_{\text{H}_2\text{O}}}; \\ K_4 = \frac{p_{\text{NO}}}{p_{\text{N}_2} \cdot p_{\text{O}_2}}; & K_5 = \frac{p_{\text{H}}^2}{p_{\text{H}_2}}; & K_6 = \frac{p_{\text{O}}^2}{p_{\text{O}_2}}; & K_7 = \frac{p_{\text{N}}^2}{p_{\text{N}_2}} \end{array}$$

The above set of equations can be supplemented by the following equations of the conservation of energy and total pressure

$$\begin{aligned}
C_m &= \frac{12}{\sum \mu_i p_i} (p_{CO_2} + p_{CO}) \\
H_m &= \frac{1}{\sum \mu_i p_i} (2p_{H_2O} + 2p_{H_2} + p_{OH} + p_H) \\
N_m &= \frac{14}{\sum \mu_i p_i} (2p_{N_2} + p_{NO} + p_N) \\
O_m &= \frac{16}{\sum \mu_i p_i} (2p_{O_2} + 2p_{CO_2} + p_{H_2O} + p_{CO} + p_{ON} + p_{NO} + p_O) \\
i_{cm} &= [i_m]_{T_s} \\
\mu &= \frac{\sum \mu_i p_i}{P} \\
P &= \sum p_i
\end{aligned}$$

where: C_m , H_m , N_m , O_m are weight percentages of elements constituting the propellants; μ_i is the molecular weight of the given component; i_{cm} is the total enthalpy of the propellants; $(i_{cs})_{T_s}$ is the enthalpy of the combustion products at the combustion temperature; p_i is the partial pressure of the given component.

Total enthalpy of propellants is denoted by the expression

$$i_{cm} = \frac{i_{cu} + f i_p}{1 + f} \text{ [kcal/kg]} \quad (4.2)$$

where: i_{cu} is the total enthalpy of the oxidizer; i_p is the total enthalpy of the fuel; f is the ratio of fuel and oxidizer.

Total enthalpy is a sum of the thermodynamic enthalpy and of chemical energy. The main component of chemical energy is heat of reaction, that is, the heat which must be added or subtracted in order for a compound to be formed from the simple chemical elements. If the heat of reaction of the compound refers to that state in which the given substance is used in the engine, then in the computation of chemical energy one has to take into account the heat of transition from one state to another (therefore, e.g., the heat of sublimation, vaporization, melting, etc.). The difference of total enthalpies of the combustion mixture and combustion products, determined at the same temperature, is called the heating value. Heating value refers to a unit weight of

fuel or a unit weight of propellants.

Total enthalpy of combustion products is determined from the relation

$$[i_{ct}]_{T_g} = \sum M_i i_{ct} = 1000 \frac{\sum i_{ct} p_i}{\mu_i p_i} [\text{kcal/kg}] \quad (4.3)$$

where: M_i is the number of moles i of that gas contained in 1 kg of combustion products; i_{ct} is the total enthalpy i of that gas at the temperature T_g .

In the given set of 14 equations there are 14 unknowns, namely: 11 partial pressures of gases (constituting the mixture), apparent molecular weight of the mixture μ , pressure p and temperature T_g .

There are various methods for solving this set of equations.

One of these, which is most convenient to use if one has a computer available, is to transform all the equilibrium equations into logarithmic form. Then they become simple linear equations suitable for computer solution. Data required for solution of concrete cases has been consolidated in Tables 4.2, 4.7, 4.8 and in Appendices 1 and 2 found at the end of the book.

4.1.3 Determination of the Mean Ratio of Specific Heats of Combustion Products.

The ratio of specific heats of combustion products of a given composition depends in practice only on the temperature. Since temperature changes during expansion, it is necessary to determine the average value of the ratio which will be valid for the given process. Thermodynamic parameters at the inlet and outlet of the nozzle are related by the isentropic equation

$$\frac{T}{T_0} = \left(\frac{p}{p_0} \right)^{\frac{\gamma-1}{\gamma}}$$

where: T and p are temperature and pressure at the inlet; T_0 and p_0 are temperature and pressure at the nozzle's outlet.

If one assumes that the composition of the combustion products does not change during expansion (that means that a process of redissociation does not occur) then one can postulate the following relations in order to determine the average ratio of specific heats:

$$\kappa = \frac{\bar{c}_p}{\bar{c}_p - AR}$$

$$\bar{c}_p = \frac{i - i_0}{T - T_0}$$

$$R = \frac{848}{\mu}$$

where: κ is the ratio of specific heats; \bar{c}_p is the average heat of combustion products, at constant pressure; A is the heat equivalent of mechanical energy; R is the gas constant of combustion products; μ is the apparent molecular weight; i and i_0 are the thermodynamic enthalpies of combustion products at inlet and outlet of nozzle.

4.1.4 Kinetic Properties of Propellants

Kinetic properties of propellants influence the time required to the liberation of the energy contained in the propellants. One differentiates two operational ranges in the analysis of which kinetic properties should be taken into account. They are: acceleration, steady-state energy.

In both cases, ignition lag has great influence on quality of the processes. Ignition lag is defined as the time interval between contact of active ingredients and their ignition (this is the total ignition delay τ_0). Ignition process takes place after the occurrence of appropriate auxiliary conditions; these are, first of all, evaporation, mixing of the vapors, and heating them to the appropriate temperature, called ignition temperature. Only then do initial chemical reactions take place between particles of fuel and oxidizer, which lead to the flaming reactions. This leads to the subdivision of the total ignition

lag into a physical lag τ_f and chemical lag τ_{ch} . Obviously

$$\tau_c = \tau_f + \tau_{ch}$$

Chemical ignition lag depends on thermodynamic parameters of the mixture, namely

$$\tau_{ch} \sim e^{\frac{1.987 E}{T}}; \quad \tau_{ch} \sim p^{-n}$$

where: p is the mixture pressure; T is its temperature; E is the activation energy; n is a constant.

It follows from these relations that chemical ignition lag decreases with an increase in mixture pressure and temperature. Ignition lag in liquid fuel rocket engines governs the acceleration curve of these engines. Too great an ignition lag causes an accumulation of propellants in the combustion chamber, which, if they explode, could ruin the engine. Furthermore, ignition lag influences the size of the combustion chambers, for all engines. Obviously as the lag increases, the combustion chamber must be longer.

4.1.5 Working Properties of Propellants

Working properties of propellants are a function of the operating conditions of the engine and of the conditions under which they are used. From a usage point of view, propellants should be nontoxic and should have as low a corrosion activity as possible. For these reasons, for example, hydrocarbons must be rid of soda and sulphur, and nitric acid which is used as an oxidizer in rocket engines should contain additives (e.g., solutions of heavy organic acids) to decrease its activity. Chemical stability of the propellants should be as high as possible, from a storage point of view. Propellants should also be insensitive to sudden temperature changes or to shocks.

Propellants should not leave any deposits in the plumbing nor any carbon deposits in the combustion chamber. In liquid fuel rocket en-

gines, the oxidizer or the fuel are used to cool the engine. From this point of view then, they should have a high specific heat, a high latent heat of vaporization and should not decompose easily at higher temperatures. In order to reduce hydromechanical resistance in feeding the propellants, they should have low viscosity. In order to maintain a constant ratio of fuel and oxidizer during operation, it is necessary to select the two components in such a way that their viscosity should change in the same manner with changes in temperature. Furthermore, it is required that solid fuels be easily formed into charges of arbitrary size and shape. From military considerations, one also requires that the combustion gases be nonsmoky and nonluminous. This condition is not one of the most important, and is not always satisfied.

The last requirements are: low cost and a possible natural derivation of the propellants.

4.1.6 Solid Propellants

Solid propellants are subdivided into two categories depending on their composition and physical structure: homogeneous and composite. Fundamental components of homogeneous propellants are nitric acid esters forming colloidal mixtures: nitroglycerin and nitrocellulose.

This composition is derived from the smokeless artillery gun powder which has already been used for many years. Besides the above mentioned components, homogeneous propellants also contain small quantities of other substances. In this group one includes stabilizers used to reduce the decomposition rate in storage, inhibitors to reduce burning speed as well as other substances to lower burning temperature, to increase plasticity and grain endurance.

Because of a number of disadvantages, homogeneous propellants are being superseded by composite propellants. These disadvantages consist of: low shelf life, strong dependence of burning rate on pressure,

high cost of raw materials and dangerous manufacturing process.

These disadvantages exist to a lesser degree in composite propellants. Composite propellants have various compositions. Their common feature is the distribution of a finely powdered oxidizer in a resin, elastomer or plastic substrate.

The structure of these propellants is clearly nonhomogeneous, having local areas rich or poor in oxygen. Common oxidizers in composite propellants are nitrates and perchlorates.

Of all these compounds, lithium perchlorate containing 60% oxygen appears to have greatest promise. The composition of two sample solid propellants is given in Table 4.1.

Development of solid propellants tends toward a search for more efficient oxidizers (e.g., ozone compounds) and an increase in the heating value by addition of high caloric-content metals and boron. These additives increase the heating value of the fuel, but they also raise the apparent molecular weight of the combustion products. Therefore there is an optimum percentage for these additives, beyond which further increases do not pay.

4.1.7 Fuels

Hydrocarbons. The majority of presently used hydrocarbon fuels derive from crude oil. The actual components of crude oil consist of three hydrocarbon groups: paraffins, naphthenes and aromatic compounds. Their relative ratios depend on the crude oil origin. Processing of crude oil consists of fractional distillation and refining under the action of sulfuric acid, sodium hydroxide or liquid sulfur hydrate and separation of paraffins. During distillation one gets: up to a temperature of 150°C — gasoline; from 150 to 300°C — kerosene; from 300 to 350°C — gas oil; above 350°C — other oils (used as lubricants and not as fuels).

TABLE 4.1

Properties of Solid Propellants

1 Rodzaj	2 Skład [%]	3 Ciężar właściwy [G/cm ³]	4 Impuls właściwy I _{sp} [sek]	5 Temperatura spalania T _s [°K]	6 Wydajność procesu politropowego Równ. [6.17]	7 Ciężar molekularny [kg/mol]	8 Wydajność izentropowa
9 Jednorodny prasowany (J.P.N.)	Nitroceluloza 1.1. .51,50 Nitrogliceryna 1.2. .43,00 Dietylfталат 1.3. . 9,25 Centralit 1.4. 1,00 Siarczan potasu 1.5. .1,25 Sód 1.6. 0,20 Wosk 1.7. 0,08	1,62	220	3125	0,69	26,4	1,215
10 Niejednorodny	NH ₄ ClO ₄ 80 Lepiszczko organiczne liczone jako C ₂ H ₄ O . . . 20	1,72	236	2790	0,4	25,4	1,22

1) Kind; 2) composition; 3) specific weight; 4) specific impulse; 5) combustion temperature; 6) polytropic process constant; 7) molecular weight; 8) ratio of specific heats; 9) extruded homogeneous; 10) composite; 11) nitrocellulose; 12) nitroglycerin; 13) diethylphthalate; 14) centralite; 15) potassium sulfate; 16) carbon black; 17) candelilla wax; 18) organic binders counted as C₂H₄O.

Hydrocarbons are fuels which are used in all types of combustion engines. Pulse jets use gasoline, axial flow jet engines usually use kerosene, and rocket engines use either kerosene or gas oil. Properties of hydrocarbon fuels are presented in Table 4.2.

Hydrocarbon fuels are stored in metal tanks. They do not react with the container's material, but proper precautionary measures must be taken in view of their high vaporization and low ignition temperature. They have a harmful effect on human organisms only at relatively high concentrations in air; and the aromatic hydrocarbons are the most toxic.

Liquid hydrogen. Liquid hydrogen is an especially attractive fuel because of its high heating value, and at the same time because of its high specific impulse. So far it has been used in rocket engines and

TABLE 4.2

Properties of Hydrocarbon Fuels

1 Jednostki	2 Ciężar molekowy —	3 Ciężar właściwy [kg/l]	4 Wartość opałowa [kcal/kg]	5 Zapotrzeb. powietrza [kg/kg]	6 Skład			
					C	H	O ₂ +N ₂	S
7 Benzyna	140	0,74	10370	15,03	0,84	0,16	—	—
8 Nafta	140	0,8 ÷ 0,81	10300	14,8	0,85	0,141	0,006	0,003
9 Olej ga- zowy	140	0,86	10000	14,3	0,863	0,13	0,001	0,004

1) Type; 2) molecular weight; 3) specific weight; 4) heating value; 5) air requirements; 6) composition; 7) gasoline; 8) kerosene; 9) gas oil.

jet engines designed to operate at high Mach numbers. Properties of hydrogen as an element and as a fuel are presented in Table 4.3 and 4.4.

Hydrogen liquefaction is a difficult problem because of its low critical temperature. Presently two methods are used to produce liquid hydrogen: — high pressure, consisting of cooling hydrogen compressed to 140 atmospheres with liquid air or nitrogen, and then expanding it; — low pressure with cooling by means of helium.

In this method, gaseous helium, circulating in the fixture, is cooled by appropriately chosen thermodynamic exchanges to a temperature lower than the hydrogen's boiling temperature (-253°C). This causes condensation of the hydrogen under a very low pressure.

Serious difficulties arise not only in obtaining liquid hydrogen, but also in storing it. Containers used for storing liquid hydrogen are made of stainless steel having a high nickel content and resistant to low temperature effects (which cause brittleness). These containers have multilayer walls. Spaces between individual layers are filled

with insulating materials, and the entire container is cooled with liquid nitrogen or helium.

TABLE 4.3
Properties of Liquid Hydrogen

1 Temperatura wracania (przy 710 mm Hg)	2 Temperatura krytyczna	3 Ciężnienie krytyczne	4 Ciężar właściwy	5 Ciepło parowania
[°C]	[°C]	[kG/cm ²]	[kG/m ³]	[kcal/kg]
-253	-229	13,5	70,9	108

1) Boiling point (at 710 mm Hg); 2) critical temperature; 3) critical pressure; 4) specific weight; 5) latent heat of vaporization.

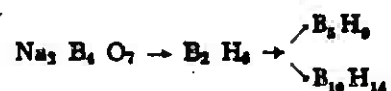
TABLE 4.4
Propellants with Liquid Hydrogen as Fuel

1 Materiał pędny	2 Stosunek utleniacza do paliwa	3 Temperatura spalania [°C]	4 Impuls właściwy [sek]
6 Wodór - tlen	2,80	2141	363
6 Wodór - fluor	3,42	4466	371
7 Wodór - ozon	2,65	2360	373

1) Propellants; 2) ratio of oxidizer to fuel; 3) combustion temperature; 4) specific impulse; 5) hydrogen-oxygen; 6) hydrogen-fluorine; 7) hydrogen-ozone.

Boron hydrides. Boron hydrides, otherwise known as boranes, on the average have a 40 to 60% higher heating value than the corresponding carbon-hydrogen compounds, i.e., hydrocarbons.

Borax is the raw material for the production of boron fuels. A typical process for obtaining boron hydrides is shown in the reaction diagram below:



This process consists of two stages: - obtaining diborane (diborohexahydride) from borax; - transforming it into pentaborane (penta-

boronnanohydride) or decaborane ($B_{10}H_{14}$).

TABLE 4.5
Properties of Boron Fuels

1 Nazwa	2 Wzór	3 Ciężar właściwy [kg/dm ³]	4 Temper. krzepnięcia [°C]	5 Temperatura wrzenia [°C]	6 Ciepło spalania [kcal/kg]
1. Borowodory 7					
8 Dwuboran	B_2H_6	0,43	-166	- 93	17750
9 Pentaboran	B_5H_9	0,61	- 47	48	16650
10 Dekaboran	$B_{10}H_{14}$	0,94	99	213	15550
2. Alkiloborowodory 11					
12 Metyldwuboran	$CH_3B_2H_5$	-	-	-	14400
13 Etyldwuboran	$C_2H_5B_2H_5$	-	-	-	13900
3. Metaloborowodory 14					
15 Borowodorek berylowy	$Be(BH_4)_2$	-	123	91,3	-
16 Borowodorek glinowy	$Al(BH_4)_3$	-	-65,4	44,5	-

1) Name; 2) equation; 3) specific weight; 4) melting point; 5) boiling point; 6) heating value; 7) boron hydrides; 8) diborane; 9) pentaborane; 10) decaborane; 11) alkylborohydrides; 12) methyldiborane; 13) ethyldiborane; 14) metallo borohydrides; 15) beryllium borohydride; 16) aluminum borohydride.

In further processing, the products can be alkalized (compounded with alkali, that is, radicals derived from aliphatic hydrocarbons by subtraction of one hydrogen atom, e.g., methyl - CH_3 from methane CH_4 , ethyl C_2H_5 from ethane C_2H_6) or compounded with metals such as aluminum, sodium, lithium and beryllium in the form of metallo-borohydrides. The properties of a few typical boron fuels are presented in Table 4.5.

Boron fuels are not presently exploited on a large scale. Their production costs are still high, but in view of the stress being applied to the study of these fuels and the development of new techniques, one should expect an early increase in their significance as technically useful fuels.

Alcohols. Alcohols have a very much lower heating value than hy-

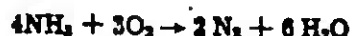
drocarbons, they also yield a somewhat lower combustion temperature. However, their specific impulse does not differ much from that of the hydrocarbon fuels (this results from a similar T/u ratio).

Alcohols owe their rather extensive applications as rocket fuels primarily to their ease of manufacture.

The alcohols most often used are: methyl, ethyl and furfuryl. This latter is usually used in self-igniting mixtures with nitric acid as oxidizer.

Nitrogen compounds. Nitrogen compounds are often used as rocket fuels. This group is mostly represented by ammonia and hydrazine hydrate.

Ammonia burns in oxygen according to the reaction:



and yields high combustion temperatures and a large amount of gaseous combustion products. Toxic and corrosive properties as well as high vapor pressures impede its wider applicability.

Hydrazine hydrate $\text{N}_2\text{H}_4 \cdot \text{H}_2\text{O}$ is an azeotropic mixture which boils at a temperature of 120.3°C and contains 68.5% of hydrazine by weight. Higher concentration hydrazine is obtained by extractive distillation.

From a chemical point of view, hydrazine is a strong reducing agent and a weak base. In the absence of oxidizers, hydrazine decomposes under the influence of temperature according to the equation:



At room temperature this decomposition takes place at the rate of 0.01% per hour; at a temperature of 250°C , on the other hand, it takes place at a rate of 10% per minute.

Hydrazine is a highly poisonous compound. It is stored in stainless steel or aluminum containers; furthermore to guard against the possibility of explosion, the space above the liquid surface is filled

with an inert gas, and the container is stored at a temperature below 40°C.

Metals. Metal additives to either liquid or solid propellants in the form of colloidal solutions or suspensions in fuel structures greatly increase the latter's heating value, especially in comparison with unit volume. Oxides are formed as a result of metal combustion in oxygen; at normal temperatures these oxides are solids; fluorine, on the other hand, combines with some of these metals to form gaseous compounds. Most commonly used metal additives are lithium, beryllium, magnesium, aluminum and silicon.

TABLE 4.6
Heating Value of Kerosene-Nitric Acid-Beryllium Mixtures.

¹ Składniki mieszanki	² Wartość opałowa [kcal/kg]
³ Nafta + kwas azotowy	1440
" + " " + 3,6% ⁴ berylu	1790
" + " " + 7,2% berylu	2190
" + " " + 10,0% berylu	2480

1) Mixture components; 2) heating value; 3) kerosene + nitric acid; 4) beryllium.

The effect of beryllium additives on the heating value of a kerosene-nitric acid mixture, when referred to 1 kg of the mixture, is shown in Table 4.6.

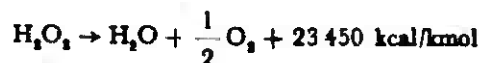
Pyrophoric propellants are fuels which ignite spontaneously upon contact with air. The most commonly encountered form of pyrophoric fuels are metalloorganic compounds (e.g., trimethyl aluminum). The domain of application of pyrophoric propellants will be the future hypersonic axial flow jet engines.

4.1.8 Rocket-Engine Liquid Propellants.

Liquid propellants used for rocket engines are subdivided, depending on composition, into monocomponent and bicomponent.

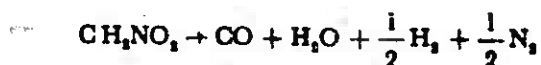
In monopropellants one further distinguishes two groups: catergolic and monergolic propellants.

Catergolic propellants are exothermic. A typical example of a catergolic propellant is hydrogen peroxide decomposing in the presence of calcium permanganate into superheated steam and oxygen:



An 80% solution of hydrogen peroxide creates a gaseous mixture at 470°C temperature. Since in this case no combustion takes place, the reaction is called "cold" as opposed to a "hot" reaction of combustion of kerosene, for instance, with hydrogen peroxide.

Monergolic propellants are monopropellants; the liquid contained in them is a mixture of compounds, some of which play the role of oxidizer, and the others the role of fuel. There are also monergolic propellants consisting of a single compound, which supply energy during interstitial oxidation. Nitromethane is an example of such a monergolic propellant; it undergoes internal combustion under a pressure of 40 atmospheres. This reaction takes place according to the following equation.



Bipropellants are subdivided into self-igniting propellants, called hypergolics, and normal propellants which are nonself-igniting.

In bipropellants, fuel and oxidizer are kept in two separate containers and are fed independently to the combustion chamber. In the case of hypergolics, ignition occurs spontaneously when the fuel and oxidizer streams come into contact in the combustion chamber. In the case of normal propellants, the combustion chamber is equipped with an ignition system (pyrotechnic igniter, sparkplug or initial injection of hypergolics).

TABLE 4.7

Properties of Two-Component Liquid Propellants

¹ Założenia: spalanie adiabatyczne, rozprężanie izentropowe, ciśnienie w komorze spalania $p_2 = 35,15 \text{ kg/cm}^2$, ciśnienie na końcu dyszy $p_e = 1,033 \text{ kg/cm}^2$

2 Utleniacz	3 Paliwo	4 Stosunek paliwa do utleniacza f	5 Teoretyczna temperatura spalania T_s [°K]	6 Współczynnik izentropowy	7 Ciężar molekularny spalin	8 Ciężar właściwy [kg/dm ³]	9 Impuls właściwy I_{sp} [sek]
10 Fluor	11 Hydrazyna	0,500	4555	1,33	19	1,3	316
"	12 Wodór	0,222	3033	1,33	8,9	0,32	374
13 90% Nadtlenek wodoru	11 Hydrazyna	0,526	2572	1,25	18	1,2	253
14 Kwas azotowy dymiący	15 Amoniak	0,465	2600	1,24	21	1,12	237
"	16 Nafta	0,244	3116	1,23	25	1,30	238
17 Tlen	75% alkohol etylowy	0,789	3116	1,22	23	0,99	248
"	16 Nafta	0,455	3522	1,24	22	0,96	264
"	15 Amoniak	0,789	2983	1,25	19	0,88	266
"	11 Hydrazyna	1,429	3072	1,25	18	1,06	262
"	12 Wodór	0,286	2735	1,26	9,0	0,26	364
18 Ozon	16 Nafta	0,526	3800	1,25	21	1,17	283

Propellant density is described by the relation

$$\gamma = \frac{1+f}{\frac{1}{\gamma_u} + f \frac{1}{\gamma_p}}$$

where: γ_u is the oxidizer density; γ_p is the fuel density.

1) Assumptions: adiabatic combustion, isentropic expansion, pressure in the combustion chamber $p_2 = 35.15 \text{ kg/cm}^2$, pressure at nozzle outlet $p_e = 1.033 \text{ kg/cm}^2$; 2) oxidizer; 3) fuel; 4) ratio of fuel to oxidizer f ; 5) theoretical combustion temperature; 6) ratio of specific heats; 7) molecular weight of combustion products; 8) density; 9) specific impulse; 10) fluorine; 11) hydrazine; 12) hydrogen; 13) 90% hydrogen peroxide; 14) fuming nitric acid; 15) ammonia; 16) kerosene; 17) oxygen; 18) ozone.

Table 4.7 shows the properties of a number of propellants.

4.19 Oxidizers

Atmospheric air. Atmospheric air is the oxidizer most often used in engineering applications. It is a mixture of oxygen and nitrogen, with 23.1% of oxygen by weight. Atmosphere parameters change with altitude, as shown in Fig. 4.1. It is more than certain that air will always be used as the basic oxidizer for engines used for terrestrial

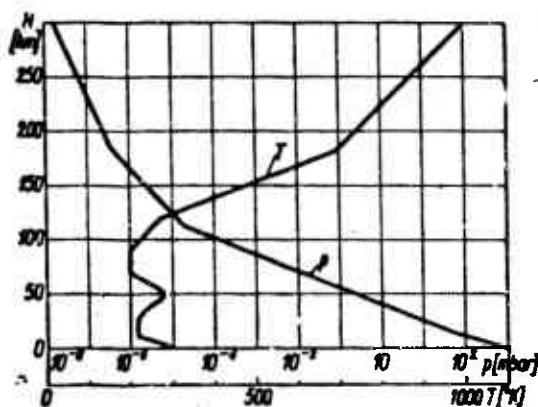


Fig. 4.1 Dependence of atmospheric pressure and temperature on altitude.

travel; this is so for two obvious reasons: - first of all, it need not be carried along; - second, it does not cost anything.

However, one should foresee in the future the possibility of changes in air composition due to pollution from combustion taking place to such a degree as to render it harmful to living organisms. This matter is worth mentioning, since in the last 50 years such composition changes have already been noticed. In future years these changes will undoubtedly take place at a much faster rate in view of the development of energy transformation technology and of travel.

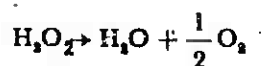
Liquid oxygen. Liquid oxygen is obtained from atmospheric air by condensation and further distillation. In addition to industrial methods, devices have been developed to produce liquid oxygen under field

conditions; this is very important for topping off missile rocket engines since it decreases losses due to transportation and storage. Liquid oxygen is stored in Dewar flasks or other properly insulated tanks. Surfaces with which liquid oxygen comes in contact must be clean, since contact with greases or other organic substances results in a violent oxidation which may cause an explosion.

Liquid oxygen is used mainly as an oxidizer for alcohol or hydrocarbon fuels, but with these it does not form any self-igniting compounds. Very high combustion temperatures are obtained as a result of combustion in pure oxygen, so much so that in many cases it must be lowered by diluting the fuel with water.

Ozone is an allotropic state of oxygen, which yields an even higher heating value. Ozone is obtained from oxygen by subjecting the latter to electrical discharges at 10 to 15 kv. An oxygen-ozone mixture arises then, having a 20% ozone content. Taking advantage of the different boiling points of liquid oxygen (- 180°C) and liquid ozone (- 111°C), mixtures with higher ozone content can be obtained.

Hydrogen peroxide. The oxidizing action of hydrogen peroxide consists of it giving up oxygen, in the presence of catalysts or under higher temperatures, according to the reaction



In rocket technology one uses hydrogen peroxide having a concentration of 70 - 100%. It is obtained most often by means of a method consisting of electrolytic oxidation of sulfuric acid into peroxydisulfuric acid. As a result of hydrolysis of the above compound, 30% hydrogen peroxide is formed. The desired concentration of hydrogen peroxide is obtained by means of distillation and rectification or by freezing. It is most often stored in glass, porcelain or aluminum con-

tainers; in the latter case 99.5% pure aluminum is required. In storage, hydrogen peroxide decomposes at a rate of 1 to 2% per year. In order to decrease this decomposition, stabilizers in the form of phosphoric acid are added at the rate of 120 - 150 mg/l.

Nitric acid. In rocket technology 98 - 99% concentrated nitric acid is used; it also contains 0.5 - 1.5% water and around 0.5% of nitrogen oxides. In order to increase the acid's activity it is often saturated with nitrogen oxides ranging from a few per cent to twenty per cent. In view of nitric acid's high corrosive action, it is often used as a mixture with a small quantity of concentrated sulfuric or hydrofluoric acids which decrease this activity somewhat. Just as hydrogen peroxide, nitric acid is stored in aluminum, glass or porcelain containers.

Fluorine. Fluorine is an example of an oxygenless oxidizer. It reacts violently upon contact with a majority of organic substances, and this reaction is strongly exothermic.

Difficulties in practical applications of fluorine result from its low boiling point (- 188°C), its high corrosive action upon container materials and its high toxicity. On a commercial scale, fluorine is obtained by electrolysis of a mixture of potassium fluoride and fluorine hydride. Fluorine is stored in steel or nickel bottles.

The most promising oxidizer of all the fluorine compounds appears to be trichlorofluoride (ClO_3F). This oxidizer yields high specific impulses. Rocket fuels do not form self-igniting mixtures with it, but they are easily ignited and burn very uniformly. This compound is easily stored and has no toxic or corrosive properties.

Properties of most commonly used oxidizers are shown in table 4.8.

TABLE 4.8

Physical Properties of Most Commonly Used Fuels and Oxidizers

1	2	3	4	5	6	7	8	9	10	11	12	13
Czynnik	Wzór	Ciepota molowa [kJ/mol]	Punkt krzepnięcia [°K]	Punkt wrzenia [°K]	Ciepło krzepnięcia [kJ/mol]	Ciepło parowania [kJ/mol]	Ciepota właściwa [G/cm ³ · °K]	Ciepota tworzenia [kJ/mol] (298°K)	Ciepota właściwa [kJ/kg] (°K)	Lepkość [CP] (°K)	Przewodność cieplna [°K]	Napięcie powierzchniowe [dyn/cm] (°K)
14 Tlen	O ₂	32,0	54,39	90,19	0,106	1,630	1,14(91)	0	0,4(919)	0,19(53) 0,67(90)	0,0182(93)	13,2(90)
15 Fluor	F ₂	38,0	55,20	85,24	0,372	1,51	1,64(55) 1,54(77) 1,51(85)	0	0,36(86)	0,414(69) 0,257(85)	0,0213(273) (1 atm)	17,9(69) 14,6(81)
16 Kwas azotowy	HNO ₃	63,02	231,5	359	—	7,23	1,52(283)	-41,40	0,422	2(269) 0,45(449)	0,236(283) 0,260(338)	42,7(284,6)
17 Nadtlenek wodoru	H ₂ O ₂	54,016	273,5	423,7	2,516	13,01	1,45(293)	-44,84	0,580	1,13(291)	0,54(320)	71,1(291)
18 Ozon	O ₃	48,0	89	162,63	—	2,99	1,57(90)	34,0	0,190	1,55(93) 4,2(432)	—	—
19 Amoniak	NH ₃	17,032	195,42	239,6	1,351	5,381	0,68(299)	-11,04	1,05(219)	0,253(239)	0,043(273)	23,4(284)
20 Alkohol etylowy	C ₂ H ₅ OH	46,06	158,6	351,7	1,20	3,22	0,785(298)	-67,2	0,62(293)	1,4(293)	0,144(293)	21,5(303)
21 Hydrazyna	N ₂ H ₄	32,05	274,7	366,7	3,023	0,2	1,011(288)	12,05	0,75(300)	1,29(274) 1,12(283) 0,97(293)	0,18(293)	91,5(298)
22 Nafta	C ₁₂ H ₂₆	140	230	—	—	—	0,8(298)	-59	0,5	1,6(268)	0,134(273) 0,100(443)	—
23 Wodór	H ₂	2,016	13,96	20,39	0,028	0,216	0,071(30,5)	0	1,75(14) 2,19(20)	0,024(14) 0,019(20)	0,057(100)	2,51(18)

1) Factor; 2) equation; 3) molecular weight; 4) melting point; 5) boiling point; 6) latent heat of melting; 7) latent heat of vaporization; 8) density; 9) heat of formation; 10) specific heat; 11) viscosity; 12) thermal conductivity; 13) surface tension; 14) oxygen; 15) fluorine; 16) nitric acid; 17) hydrogen peroxide; 18) ozone; 19) ammonia; 20) ethyl alcohol; 21) hydrazine; 22) kerosene; 23) hydrogen.

4.2 FREE RADICALS

Investigations of the possibility of increasing the specific impulse of propellants have led to the idea of employing free radicals.

Free radicals are atoms or groups of atoms characterized by a very short chemical existence. Thus they either combine to form larger molecules or conversely they disintegrate into smaller groupings. As a result of the process of the disappearance of the radicals, a large quantity of heat is generated, much greater than the heat generated during combustion. This phenomenon can be explained by referring to the commonly known mechanism of chemical reactions. For combustion to take place, particles of fuel and oxidizer must first disintegrate into free radicals. In the next phase, these free radicals react with each other, thus forming the terminal products of the chemical reaction. The process of formation of free radicals involves absorption of large quantities of energy, of the same order as is later created during their recombination. Therefore the output energy created during the average duration of chemical reactions cannot be too large, since it represents only the excess of the total energy created, decreased by the energy used for the creation of the free radicals.

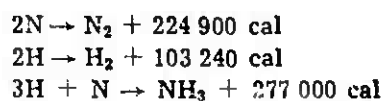
Various sources of energy can be exploited to create free radicals, e.g., an electric arc, high frequency electric discharges, ultraviolet radiation or fission reactors. From a practical point of view, it would be necessary to store the industrially produced free radicals in containers, just as presently used propellants are stored.

One of the presently known methods of prolonging the life of free radicals to a matter of hours or even days (but which is not yet beyond the stage laboratory investigations) consists of freezing them to an appropriate temperature, e.g., -180°C .

Recent studies conducted by means of rockets have shown that starting from an altitude of 80 km air contains a large percentage of dissociated oxygen. Oxygen's dissociation (that is, disintegration of oxygen particles into free radicals) takes place under the action of ul-

traviolet radiation. An idea has already been advanced for the construction of an axial flow jet engine where advantage would be taken of the free radicals to accelerate the flow of air passing through.

A few sample reactions showing the combination of free radicals are shown below:



4.3 NUCLEAR ENERGY

All energy sources discussed until now are insufficient to achieve all the ideas of the applications of aircraft and rocket technology. In particular, cosmic flights will require greater specific impulses than can be produced by presently used chemical fuels. Furthermore, one should take into account the fact that oil and coal deposits, which as an exception are not in chemical balance with the earth, will be exhausted in the near future. Therefore, the search for new fuels has become a necessity. These sources were discovered as a result of detailed physicochemical studies of the structure of matter, and in particular the structure of the atom and its elements.

The starting point of these studies is the orbital model of the atom, according to which negatively charged electrons revolve around a central positively charged nucleus.

An atom's properties are described by two types of forces: electromagnetic forces and nuclear forces.

Electromagnetic forces are almost completely known already, and are incorporated into general theory; all knowledge of nuclear forces, on the other hand, is based on experimental facts and working hypotheses.

One of the fundamental properties of nuclear forces is their short range of action ($\sim 10^{-13}$ cm) which makes their measurement im-

possible and which renders a closer study more difficult.

According to present understanding, the nucleus consists only of protons and neutrons. On that basis one assumes that they form a two-parameter union and that they can be represented as a set of two factors.

The most commonly used factors are:

Z , a cardinal number, that is, the number of protons; and A , a mass number, that is, the total number of neutrons. When representing the nucleus by means of the chemical symbol of its atom, one adds Z on the left-hand side as a subscript, and A on the right-hand side as a superscript. Thus in general a nucleus is represented by the expression:

$${}_Z^AX$$

In accordance with this notation, a neutron is denoted as ${}_0n^1$, a proton as ${}_1H^1$, and a deuteron (deuterium's nucleus) as ${}_1H^2$. Natural nuclei fall on the (Z, A) plot with a very small deviation from the so-called stability curve (Fig. 4.2).

A number of nuclei arising in nature are not stable, which means that they emit rays (e.g., the uranium nucleus ${}_{92}U^{238}$ or the thorium nucleus ${}_{90}Th^{232}$).

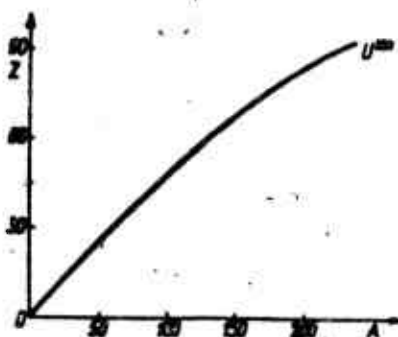


Fig. 4.2 Stability curve.

Stability problems lead directly to energy problems. Namely, it has been verified that the atom's mass is always smaller than the sum of the masses of which it is made: protons, neutrons and orbiting electrons. These differences are explained by the existence of bonding en-

ergy and Einstein's relativity:

$$E = mc^2$$

from which it results that mass and energy are equivalent, but are expressed in units differing in magnitude by the square of the velocity of light c .

A nucleus, whether as an atom or as a particle, has a quantum representation and therefore can exist at various energy levels. Due to collisions, the nucleus is knocked out of its fundamental state and goes into an excited state which is distinguishable by its higher level. The nucleus can return to its fundamental state, from an excited state, after emitting the quantum of energy absorbed during the collision. A nucleus in an excited state is denoted by the symbol:

$$x^*()^A$$

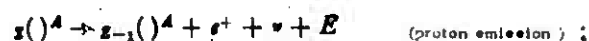
Nuclear reactions, just as all processes occurring in nature, are limited by the laws of conservation. These are the law of conservation of charge and the law of the conservation of the number of nucleons. Nuclear reactions can be subdivided into two groups: spontaneous reactions can be subdivided into two groups: spontaneous reactions and reactions caused by collisions. In spontaneous reactions one differentiates the following processes: - gamma radiation, that is, emission by the nucleus of a photon during its transition from an excited state to its fundamental state.

$$x^*()^A \rightarrow x()^A + \gamma + E$$

The liberated energy E is carried away by λ radiation; beta radiation, that is, emission of an electron e and a neutrino ν by a nucleus which is not on the stability curve. During this process the mass number A remains unchanged, whereas Z increases or decreases depending on whether the emitted electron is e^- or e^+

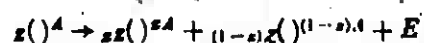
$$x()^A \rightarrow x_{+1}()^A + e^- + \nu + E \quad (\text{electron emission})$$

or



- fission process, that is, nucleus disintegration into two elements (and sometimes also into a certain number of neutrons).

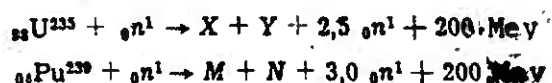
If one can assume that both fragments, after fission, conserve the same ratio of Z to A , then this reaction can be represented by the equation:



where x can vary from 0 to 0.5, and E is the energy liberated during the fission process and is transferred to the nuclear fragments as kinetic energy.

Nuclear reactions of interest to the technology of rocket propulsion are subdivided into fission reactions of heavy nuclei or fusion reactions of light nuclei.

The fission process of heavy nuclei of uranium and plutonium takes place according to the following reaction:



where: X, Y, M, N are fission products; U, P_u are symbols for uranium and plutonium elements; ${}_0n^1$ is the neutron whose collision with the U or P_u nucleus causes the reaction.

The practical achievement of this process takes place in fission reactors (Fig. 4.3).

The main component element of a fission reactor is the core. The core contains an appropriate quantity of fissionable material, so that a chain reaction can take place. To initiate and maintain the reaction it is necessary to create and continuously replenish a stream of nucleus splitting neutrons. To achieve this goal, it is sufficient to enrich the natural U^{238} uranium which absorbs neutrons, with its isotope

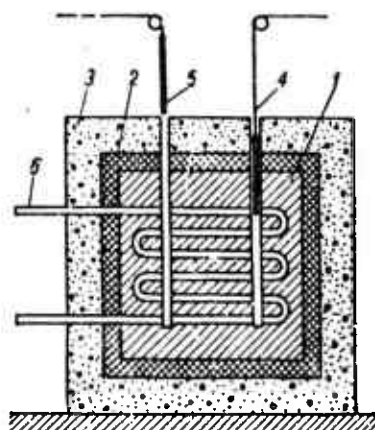
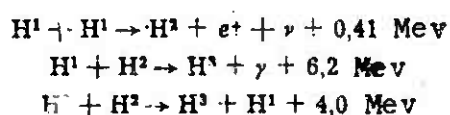


Fig. 4.3 Diagram of a (nuclear) fission reactor: 1) Core; 2) reflector; 3) shielding; 4) control rod; 5) safety rod; 6) cooling system.

U^{235} which is a source of neutron emission. An uncontrolled fission reaction has a snow-balling effect and ruins the reactor. In order to facilitate control of the reaction rate, one uses control rods made of substances which are strong neutron absorbers, such as cadmium or boroncarbonates. By changing the penetration depth of the control rods inside the reactor, the course of the fission reaction can be properly controlled. The thermal energy created inside the reactor is extracted by means of an appropriate cooling system.

Another method of liberating nuclear energy consists of fusing the lightest nuclei, and mainly hydrogen's isotopes: protons, deuterons and tritium. In order to accomplish this fusion in practice, it is necessary to impart to the nuclei an appropriately high kinetic energy. Nuclei achieve such an energy after being heated to a temperature of several million degrees (e.g., one takes advantage of the fission process to achieve these temperatures). That is why fusion reactions are called thermonuclear. The following equations show a few sample thermonuclear reactions:



REFERENCES TO CHAPTER 4

- 4.1. B. Lewis, R. Pease, H. Taylor: Combustion Processes. Princeton University Press. 1956.
- 4.2. G. Siniariew, M. Dobrowolski: Silniki rakietowe na paliwo plynne [Liquid Fuel Rocket Engines]. Published by MON, Warsaw 1958.
- 4.3. J. Stanuch, J. Swidzinski, A. Wachal, O. Wolczek: Rakiety - Srodki napedowe [Rockets - Means of Propulsion]. PWT, Warsaw 1960.

Chapter 5

GENERATION OF THE MIXTURE

The mixture in axial-flow, pulse and rocket engines using liquid propellants is generated as a result of simple processes such as liquid injection, liquid spray, drop evaporation and mixing of the vapors generated, with each other or with an air stream.

The range of combustion chamber steady-state output, and its behavior depend on the mixture composition and its decomposition.

5.1 INJECTORS

Liquid injection is achieved by means of injectors, which depending on their construction and operating mode are subdivided into flow and swirl injectors.

5.1.1 Flow Injectors

A flow injector consists of a pipe terminated by an orifice (Fig. 5.1). The pressure difference between the pressure acting on the flow and the surrounding pressure causes the flow of liquid to the outside. The classical relation between the flow G , the pressure drop Δp and density γ is given by the equation

$$G = \mu F \sqrt{2g\gamma \Delta p} \quad (5.1)$$

where: μ is the jet contraction coefficient; g is the acceleration of gravity; F is the orifice area.

The contraction coefficient μ is a function of orifice shape and of the pressure drop across the orifice (Fig. 5.2).

Flow injectors have been used mainly in liquid propellant rocket engines.



Fig. 5.1 Flow injector. 1) Fuel

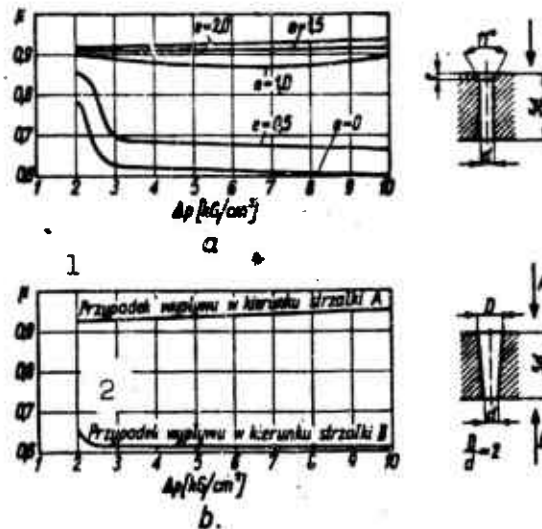


Fig. 5.2. Dependence of contraction coefficient on orifice shape and pressure drop across it: a) Cylindrical opening preceded by a cone (influence of cone height); b) conical orifice. 1) Flow in the direction of arrow A; 2) flow in the direction of arrow B.

5.1.2 Spray Injectors

The operation of spray injectors depends on inducing a vortex flow in the liquid prior to its discharge. This can be achieved by utilizing a swirl chamber (Fig. 5.3) into which fuel is introduced tangent to the walls. Each fluid particle issuing from the injector has two velocity components; i.e., an axial and a radial component. As a result of this, a liquid cone is obtained whose included angle is a function of injector geometry. In the first flow phase, the liquid forms a continuous film as if constituting the lateral area of a cone. This film gets thinner and thinner as it moves away from the

orifice and breaks up into flakes which later coalesce into drops. Under the influence of the dynamic pressure of the flow core in which the spray takes place, the drops are further subdivided.

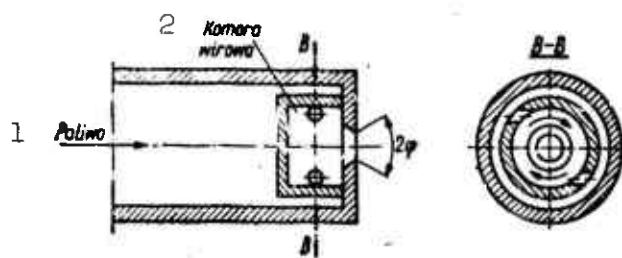


Fig. 5.3 Spray injector.
1) Fuel; 2) swirl chamber

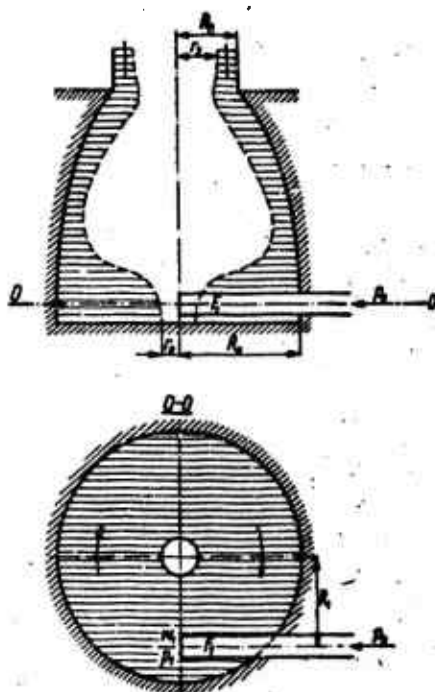


Fig. 5.4 Cross section of
the swirl chamber

Under the influence of the vortex motion, the liquid in the combustion chamber assumes the shape shown in Fig. 5.4. Starting with the continuity equation

$$\mu' F_1 w_1 = (R_1^2 - r_1^2) \pi w \cos \varphi$$

and the equation of the conservation of rotation

$$w_1 R_1 = w \sin \varphi \frac{R_1 - r_1}{2}$$

traction coefficient as a function of the dimensions characterizing the injector geometry

$$\tan \varphi = \frac{R_1 R_2 \pi}{\mu' F_1} ; \quad \mu = f\left(\frac{\pi R_1 R_2}{\mu' F_1}\right) \quad (5.2)$$

where: μ is the contraction coefficient of the flow, obtained from Eq. (5.1); F is the injector exit area; F_1 is the cross sectional area of the pipe feeding the liquid to the spray chamber; μ' is the contraction coefficient of the flow issuing from this pipe. The other quantities are defined in Figs. 5.3 and 5.4. Both functions are illustrated in Fig. 5.5.

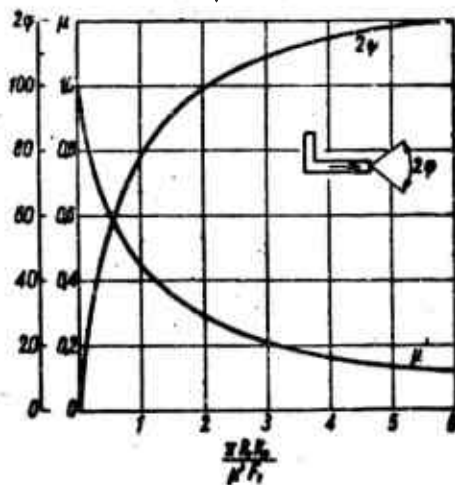


Fig. 5.5 Dependence of the flow contraction coefficient μ and of the injection angle 2φ on the dimensions characterizing the injector geometry.

5.1.3 Spill-Control By-Pass Injector

The flow rate in the case of the two injectors discussed so far is a function of the square root of the pressure drop. For a given in-

jector and liquid flowing through the injector, we get:

$$\frac{G}{\sqrt{\Delta p}} = k = \text{const} \quad (5.3)$$

where k is the injector constant.

If the injector is to operate over a prescribed range of flow rates, then it is necessary to obtain the appropriate range of pressures which is related to the flow by a quadratic law (for instance, if the ratio of maximum to minimum injector flow rates is n , then the ratio of corresponding pressure drops across the injector is n^2).

In a case of wide range of flow rates, it may occur that for a given minimum injection pressure the required maximum pressure will be higher than can be allowed (e.g., in view of pump constraints). The only solution to this problem is the building of an injector with a smoother flow-pressure drop characteristic. One such injector, the spill-control (by-pass) injector is shown in Fig. 5.6. The liquid introduced into the swirl chamber is subdivided into two streams: one of them flows (just as in a normal spray nozzle) through the injector orifice (having diameter d), and the other flows through the spill orifice (having diameter s). By throttling the spill (by changing the diameter s) it is possible to control the injection flow rate. The liquid flowing through the spill orifice is directed to the pump intake manifold. The quantitative characteristic of the spill-control injector

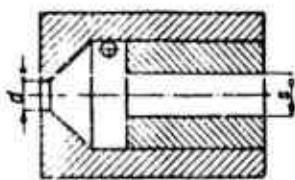


Fig. 5.6 Spill-control injector.

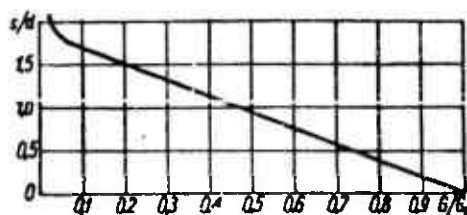


Fig. 5.7 Characteristic of a spill-control injector: G is the flow rate with the spill orifice open (orifice diameter is s); G_0 is the flow rate with the spill orifice closed.

is shown in Fig. 5.7.

This graph illustrates the relationship between the ratio of diameters of injector and spill orifices and the ratio of injector flow rates with open and closed spill orifice. When the ratio of diameters of injector and spill orifices increases, the ratio of flow rates in the two extreme cases of open and closed spill decreases.

Spill-control injectors are used in axial flow jet engines designed to operate over a wide range of speeds and altitudes.

5.2 LIQUID SPRAY

A liquid flow injected into a gaseous environment is at first dispersed into independent particles of various shapes, and then is further subdivided into drops of ever decreasing diameters. The dispersion mechanism of a solid flow tube is as follows. The undisturbed contact surface between the liquid and the environment is in dynamic equilibrium. If, however, a disturbance occurs on the liquid surface, due to the turbulent motion of individual liquid or gaseous particles, then two types of forces start to act on this surface: forces resulting from surface tension, which strive to reestablish the state of equilibrium; aerodynamic forces (which are present because air has a velocity relative to the fluid) which tend to increase the disturbance and result in unstable equilibrium.

The waves so produced exhibit an exponentially increasing amplitude and lead to a disintegration of the liquid into ever smaller segments, which eventually assume the shape of drops. The liquid drops moving with respect to the gaseous medium are subject to the above-mentioned forces of surface tension and aerodynamics. Surface-tension forces tend to give the drops a spherical shape, whereas aerodynamic forces tend to "flatten" the drops. In the presence of a sufficiently high dynamic pressure, drop disintegration takes place. The individual

phases of this process are shown in Fig. 5.8 in an idealized fashion. If the surface tension of a drop of diameter d_k is σ , then the force f due to which one half of the drop is bound to the other is equal to

$$f = \pi d_k \sigma$$

This force creates a pressure p which acts on the drop's entire surface area. In view of this we can write

$$f = \int_{\frac{F}{2}} p dF \cos \varphi = p \int_{\left(\frac{\pi}{2} d_k^2\right)} dF \cos \varphi = \frac{\pi}{4} d_k^2 p$$

Where: F is the drop's lateral surface, φ is the angle of the directed ray, which establishes the position of the element dF on the drop's surface.

Comparing these two equations, we obtain an expression for the internal pressure caused by surface tension

$$p = \frac{4\sigma}{d_k}$$

If the dynamic pressure $\gamma u^2/2g$ caused by the relative velocity of the drop and the medium is greater than the internal pressure, then the drop will disintegrate. From the condition

$$\frac{\gamma u^2}{2g} = \beta \frac{4\sigma}{d_k}$$

the following relation is obtained

$$\frac{\gamma u^2 d_k}{8\sigma} = D_k \quad (5.4)$$

where: β is an empirical quantity describing the ratio between dynamic and internal pressures; γ is the density of the medium; u is the drop velocity relative to the medium; D_k is the disintegration criterion.

According to Dltjakin and Borodin (L.5.2), the drops subdivide into two starting with $D_k = 8.5$, whereas starting with $D_k = 11.3$ the drops simultaneously disintegrate into a number of smaller ones. From the above equation the maximum diameter of the drops which will arise

under given conditions with a specified drop velocity relative to the medium can be determined:

$$d_{cr} = \frac{g \sigma D_k}{\gamma u^2} \quad (5.5)$$

and the minimum velocity required to break up the drop into drops of given diameter is given by:

$$u_{cr} = \sqrt{\frac{g \sigma D_k}{\gamma d_k}} \quad (5.6)$$

In these equations u is expressed in m/sec, σ in kg/m, γ in kgf/m³, d_k in m and g in m/sec².

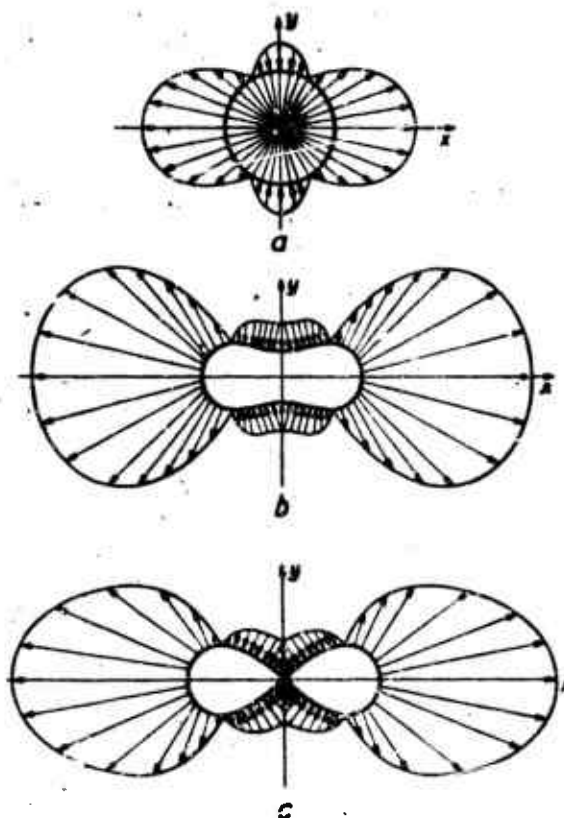


Fig. 5.8 Distribution of pressure acting on drop surface during the various phases of its disintegration.

The spray theory presented above is used in the determination of the drop diameter in a liquid jet spray, which is created by a flow nozzle.

In the case of spray injectors, disintegration conditions are more advantageous (instead of a nearly cylindrical flow, there is a thin conical surface) and the velocities required to obtain a given drop diameter are much smaller.

5.3 SPRAY SPECTRUM

The spray spectrum refers to the experimentally obtained distribution of drop diameters. All drops generated during a given time interval are segregated according to size (e.g., each 20 μ) into groups and one defines their percentage by weight. The graph in Fig. 5.9 illustrates a spray spectrum. Drop diameter is plotted along the abscissa, while along the ordinate we have the weight percentage of drops whose diameter is less than the given diameter. The graph was made for

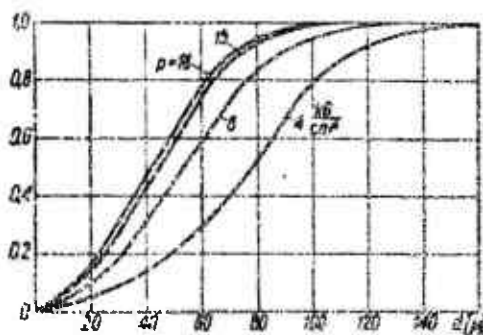


Fig. 5.9 Spray spectrum

several pressures. An obvious conclusion can be reached from this graph and namely, that the percentage of small diameter drops increases with spray pressure. The spectrum is characterized by spray quality; a direct index of this quality is the average drop diameter defined by Sauter as that diameter which would be assumed by identical size drops if their total area $\sum \pi d_i^2$ and total volume $\sum \pi d_i^3/6$ were the same as those in flow consisting of drops of various dimensions. According to this definition, the average drop diameter is

$$d_m = \frac{\sum d_i^3}{\sum d_i^2}$$

In both the hypothetical and actual cases the number of drops is the same.

There are a number of empirical models which allow us to compute the average diameter as well as the spray spectrum for the case of the spray injector. The relationships given by Longwell (L.5.4) are commonly used

$$\frac{d_m}{d_0} = \frac{0.22 \mu^{0.5}}{\rho^{0.5} \sin \phi} \text{ or } K \times \frac{G_{d > d_m}}{G} = \exp\left(-\left(\frac{d}{d_m}\right)^2\right) \quad (5.7)$$

where d_0 is the diameter of the exit orifice of the spray injector; μ is the liquid viscosity; ϕ is the injection half-angle; p is the injection overpressure; $G_{d > d_m}$ is the weight of the drops whose diameter is greater than d ; G is the weight of all the drops; K is the experimental coefficient of the distribution uniformity, a function of d_m (Fig. 5.10), κ is the weight percentage of drops whose diameter is greater than d .

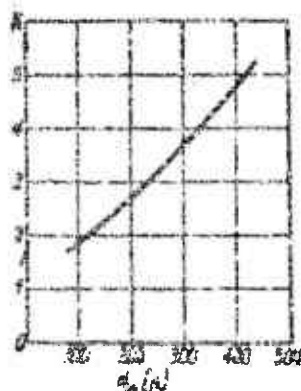


Fig. 5.10 Dependence of distribution uniformity coefficient on the average drop diameter.

It follows from the cited relationships that the average drop di-

ameter increases with an increase in the viscosity of the sprayed liquid and decreases with an increase in the pressure drop across the injector.

Furthermore, average drop diameter decreases with an increase in the injection angle. The coefficient of distribution uniformity K characterizes the width of the drop size distribution. As the coefficient K increases, the distribution spread narrows and therefore its uniformity increases.

5.4 EVAPORATION OF LIQUID DROPS IN A GASEOUS MEDIUM

The course of the combustion process taking place in the mixture stream depends to a large extent on the degree of drop evaporation. The quantity of the liquid components of the propellants which will eventually evaporate is influenced mainly by their volatility and enthalpy. Even though it is rarely possible to reach an equilibrium state before initiating the combustion process, it is still worthwhile to compute the degree of evaporation corresponding to the equilibrium state so that one could determine approximately, *a priori*, the maximum quantity of evaporation to be expected from the various components. It is simplest, in this case, to use prepared graphs. Figure 5.11 shows as an example the evaporation of kerosene in an air stream, where the

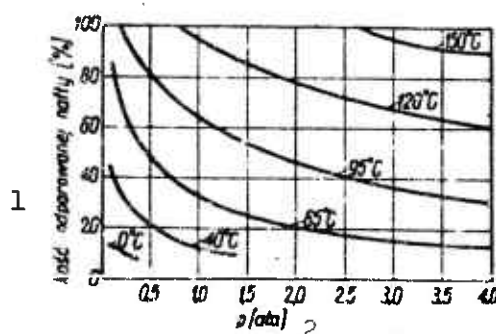


Fig. 5.11 The entry represents the equilibrium of the portion of kerosene which evaporated, expressed as a function of pressure and temperature. 1) Quantity of evaporated kerosene; 2) p , atm. abs.

relation between the percentage of kerosene evaporated and the air temperature and pressure for a stoichiometric mixture has been indicated. In considering the climbing flight of a jet engine, for instance, at a constant Mach number, an interesting phenomenon is observed. With an increase in altitude, the influence of a temperature decrease is greater than the influence of decreased pressure, so that the capability of fuel evaporation decreases. As the airplane reaches the stratosphere, temperature stabilizes while pressure keeps on decreasing and this increases the quantity of fuel evaporation. It follows from the above that the conditions of poorest evaporation occur in the range of altitudes from 9 - 12 km.

In order to compute the evaporation rate it is necessary to know the distribution of drop sizes as well as the physical characteristics of the liquid and of the vapor components in the propellants. The computational method is based on a simplified model of the physical process of evaporation. First of all it is assumed that evaporation rate is a function of the rate at which heat can be supplied to the drop. This heat is used to cover the latent heat of vaporization. The evaporation rate is so slow that the vapors in the immediate vicinity of the drop surface are in equilibrium with the liquid of the drop. The drop reaches an equilibrium temperature lower than the boiling point of the liquid, and this temperature results mainly from the conditions of heat exchange.

The rate of heat exchange $dq/d\tau$ on the given radius r is given by the equation:

$$\frac{dq}{d\tau} = -\lambda F \frac{dT}{dr} + m_0 c_p T$$

where λ is the coefficient of thermal conductivity in the drop; m_0 is the weight yield due to vaporization; c_p is the specific heat of the

vapor; T is the vapor temperature; F is the drop area.

The first expression in this equation describes the quantity of heat transferred by means of conduction, and the other expresses the heat carried away by diffusing fuel vapors.

After transformation we get:

$$m_0 = \frac{4\pi r_0}{q_p} \lambda_0 (T_1 - T_0)$$

$$\tau = \frac{c_p \rho_c [r_1^2 - r_0^2]}{2\lambda \ln \left[1 + \frac{\lambda_0}{\lambda} \frac{c_p}{q_p} (T_1 - T_0) \right]}$$

where ρ_c is liquid density; r_1 is the initial drop radius; r_0 is the drop radius at the instant τ ; q_p is the heat of vaporization; c_p and λ are the average values of the specific heat and of the thermal conductivity in the temperature range from T_1 to T_0 ; τ is the evaporation time for the drop radius to go from radius r_1 to r_0 ; λ_0 is the value of thermal conductivity at the drop temperature T_0 ; T_1 is the ambient temperature.

The first of the above-obtained equations describes the evaporation rate as a function of the heat transfer rate. From the second equation it follows that the time required for evaporation is proportional to the square of the initial drop radius

$$\tau = C(r_1^2 - r_0^2) \quad (5.8)$$

where

$$C = \frac{c_p \rho_c}{2\lambda \ln \left[1 + \frac{\lambda_0}{\lambda} \frac{c_p}{q_p} (T_1 - T_0) \right]}$$

In an actual case, drops of widely varying sizes are injected into the combustion chamber. An interesting problem involves the manner in which the evaporation of such a stream of drops of different diameters change with time. As was shown in the preceding paragraph, the qualitative drop distribution is governed by the uniformity coefficient

K. Low coefficient values indicate a wide distribution. Figure 5.12 shows the evaporation rate of the liquid in streams having the same average drop diameter but a different distribution. The highest initial evaporation rate is obtained from the stream having the widest distribution. In general such a distribution is advantageous in achieving ignition. However, after evaporation of 75% of the liquid, the situation is reversed. In a wide-distribution stream, large drops remain and these reduce the evaporation rate.

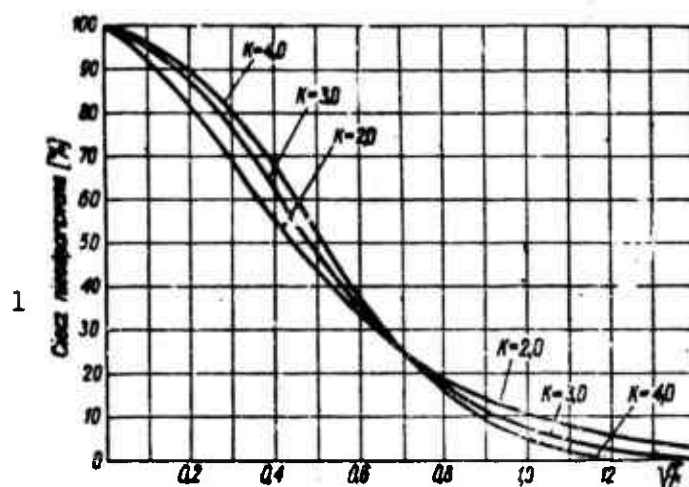


Fig. 5.12. Evaporation rate of a liquid in streams of same average drop diameter but different distribution. 1) Nonevaporated liquid (%).

This has an important effect on the course of the combustion process, on which this phenomenon imposes the characteristic of a multi-phase process. The significance of individual factors influencing the evaporation rate varies within wide limits. In order to illustrate the influence of the most important parameters on the evaporation rate of fuel drops, Figs. 5.13 and 5.14 show the influence of the distance from the point of injection and of the flow velocity.

In both cases the fuel was injected against the flow. From Fig. 5.13 we see that in the case of an air velocity of 150 m/sec the evapo-

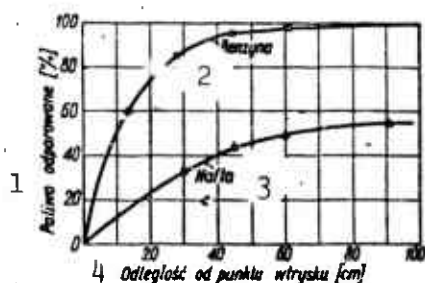


Fig. 5.13. Evaporation of a sprayed fuel stream as a function of the distance from the injection point. 1) Evaporated fuel (%); 2) gasoline; 3) kerosene; 4) distance from the injection point (cm).

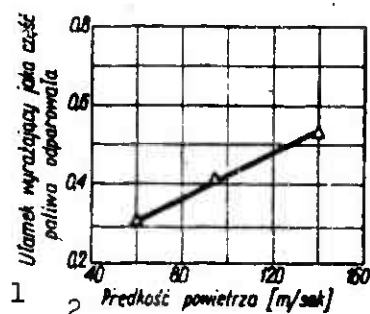


Fig. 5.14. Influence of flow velocity on degree of evaporation. 1) Fraction expressing the portion of evaporated fuel; 2) air velocity (m/sec).

ration is virtually completed within a distance of approximately 0.5 m from the point of injection. At that point, gasoline has evaporated almost completely, whereas only around 50% of kerosene has evaporated. A further increase in the distance has only a slight effect on kerosene evaporation. Figure 5.14 shows that an increase in flow velocity increases the degree of evaporation. This is due to an increase in the heat and mass exchange coefficients which depend mainly on velocity.

5.5. MIXING OF THE FLOWS OF SPRAYED FUEL AND AIR.

For proper progress of the combustion process, particles of fuel and air should be thoroughly mixed on the molecular level. This function is ultimately achieved by particle diffusion, but its effective influence is shortlived. In practice, fuel injection points are widely separated, so that during the mixing process one can rely only on fuel

spray and on the turbulence of the air stream. This latter mixing method is called mixing by means of turbulent diffusion. It is not limited only to the mixing of particles of fuel vapors with air particles, as is the case with molecular diffusion, but it also causes the mixing of entire drop particles. Turbulent diffusion is described by the equation:

$$\frac{\partial M}{\partial \tau} = - D_T F \frac{\partial f}{\partial r}$$

where $\partial M / \partial \tau$ is the mass transfer rate; F is the transfer surface; $\partial f / \partial r$ is the fuel concentration gradient in the flow; D_T is the coefficient of turbulent diffusion; $f = B/G$ is the fuel-to-air ratio in the mixture stream.

The coefficient of turbulent diffusion is determined by the relation:

$$D_T = L \sqrt{(u')^2} \quad (5.9)$$

where L is the turbulence scale; $\sqrt{(u')^2}$ is the mean square pulsation rate which is a measure of turbulence intensity.

The coefficient of turbulent diffusion is over one hundred times greater than the coefficient of molecular diffusion.

If we solve the diffusion equation in the assumption that the fuel issues from a point without an initial velocity, the following relation is obtained:

$$f = \frac{B}{\pi G} \cdot \frac{\pi}{4 D_T x} e^{-\frac{r^2}{4 D_T x}} \quad (5.10)$$

where x is the distance from the injection point; r is the distance from the injection axis; u is the flow velocity; f is the fuel-to-air ratio at a given point (x, r) .

From the above relation we see that the mixture concentration distribution within the stream is governed by the parameter D_T/u . It is known empirically that turbulence intensity is a fixed fraction of the

flow velocity ($\sim 3\%$). In view of this (see Eq. (5.9)) parameter D_T/u should not be a function of velocity. Similarly, in view of the high Reynolds numbers (10^5 to 10^6) present in jet engines, large variations in the diffusion constant should not be expected because of changes in mixture temperature or concentration. From the above it follows that for the given geometrical shapes of the systems, the parameter D_T/u is approximately constant. This means that fuel distribution will be essentially independent of the operating conditions, if it is assumed that the method of fuel injection is unchanged. The above conclusions refer to evaporated fuel. In the case in which fuel drops are present in the mixture, the stream's diffusivity, compared to vapor diffusivity, will be smaller, the larger the drops and the lower the frequency of turbulent velocity fluctuations. The dependence of the ratio D_T/u on velocity, for the case of mixtures with evaporated and nonevaporated fuel, is shown in Fig. 5.15.

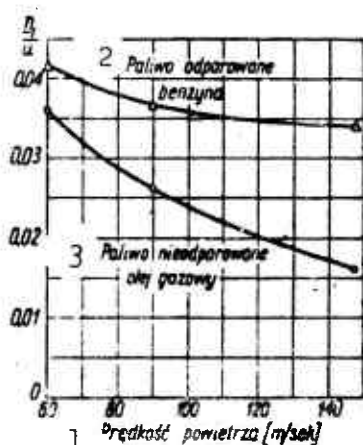


Fig. 5.15. Influence of flow velocity on the diffusion parameter D_T/u : pipe diameter 150 mm, air temperature 150°C . 1) Air velocity (m/sec); 2) evaporated fuel, gasoline; 3) unevaporated fuel, gas oil.

It is seen from the graph that at low velocities the diffusivities of evaporated and unevaporated mixtures differ slightly. The difference occurs only at high flow velocities due to a marked decrease in the

diffusivity of the unevaporated mixture. Mixture diffusivity increases (by a factor of as much as two) when the flow is interrupted by obstacles.

The point source model described above represents a good approximation to actual conditions if the fuel enters the air stream at a very low velocity through a small pipe. In the cases in which the fuel

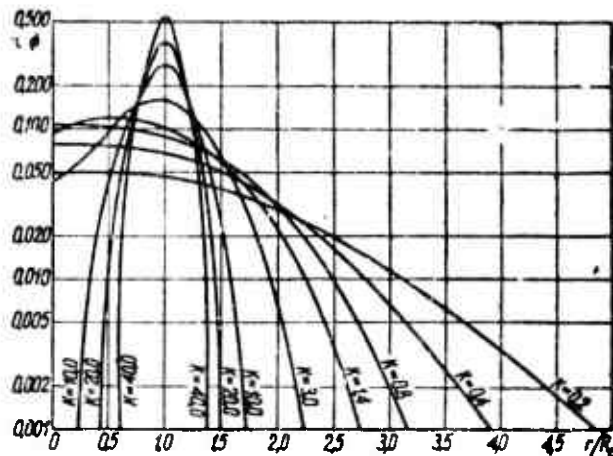


Fig. 5.16. Fuel distribution behind a ring source.

is introduced in a counterflow or parallel-flow manner by means of a stream injector or in counterflow fashion by means of a spray injector, it is more convenient to assume a ring source, assuming that point sources are uniformly distributed on the circumference of a circle of radius R_0 . In this case the equation assumes the form:

$$n = \frac{B}{GR_0^2} \frac{K}{\pi} \left[J_0 2K \frac{r}{R_0} \right] e^{-K \left(1 + \frac{r^2}{R_0^2} \right)} = \frac{B}{GR_0^2} \Phi$$

$$\tilde{\kappa} = \frac{uR_0^2}{4D_T x}$$

Function Φ is plotted in Fig. 5.16.

It has been established empirically that R_0 can be taken as the radius of the sprayed fuel flow which is observed visually or measured in photographs (Fig. 5.17).

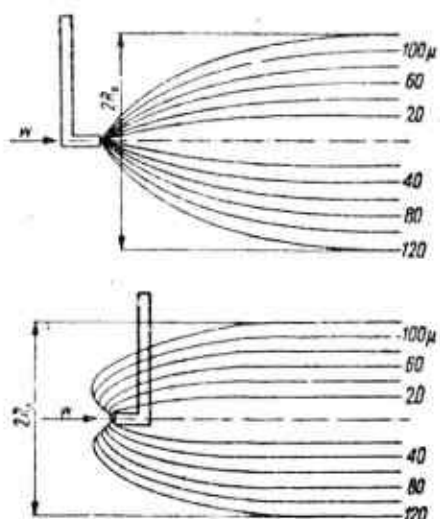


Fig. 5.17. Trajectories of fuel drops sprayed by spray injectors: a) parallel to the flow; b) counterflow. Fuel drop distribution according to size, in a cross section of the sprayed stream.

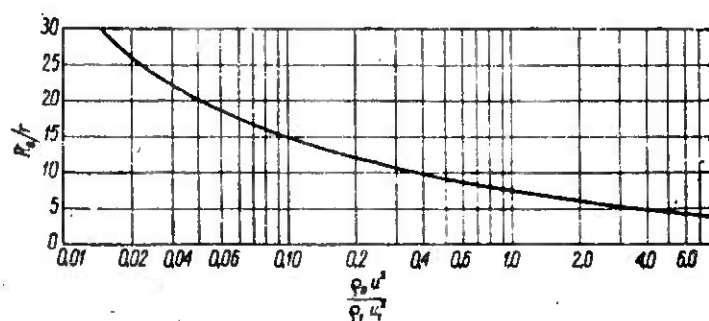


Fig. 5.18. Radial penetration of sprayed fuel injected with counterflow by a stream injector.

In the case of a stream injector operating with counterflow, the magnitude of the radius R_0 can be determined from the experimental curve given in Fig. 5.18. That curve represents the radial ratio of the fuel stream to the injector orifice as a function of air stream velocity divided by the velocity of the fuel stream.

A similar relation for counterflow spray injectors is illustrated in Fig. 5.19. This figure shows the influence of the excess pressure Δp and of the diameter d of the injector exit orifice on the maximum radial penetration R_0 of fuel drops.

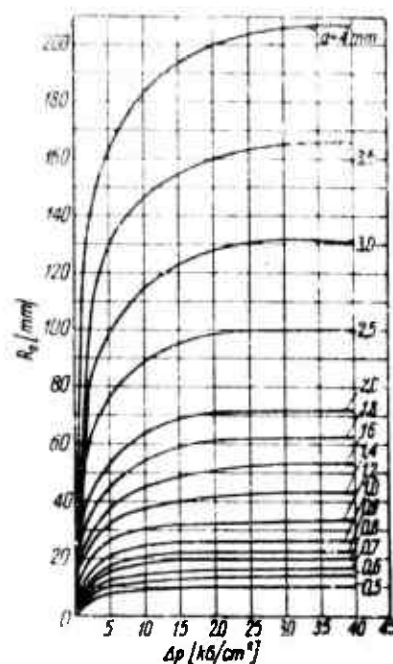


Fig. 5.19. Radial penetration of sprayed fuel injected with counter-flow by a spray injector.

REFERENCES TO CHAPTER 5

- 5.1. E. Sängér: Smiesobrazowanie w kamierach sgorania [Mixing in Combustion Chambers]. Woprosy Rakietnoj Tiekhniki [Problems of Rocket Engineering], No. 5 (17) 1953.
- 5.2. J. Ditjakin, W. Borodin: K tieorii razrywa zydkoj niti i kapli w potokie wozducha [Toward a Theory of Detachment of Liquid Filaments and Drops in a Jet of Air]. M.A.P. Trudy [Trans. Ministry of Aviation], No. 192.
- 5.3. B. Lewis, R. Pease, H. Taylor: Combustion Processes. Princeton University Press, 1956.
- 5.4. M. Barrère, B. Veubeke, A. Jaumotte, J. Vadenkerckhove: La Propulsion par Fussées [Rocket Propulsion]. Dunod, Paris 1957.
- 5.5. M. Bondariuk, S. Iljaszenko: Priamotocznyje wozdusznorieaktywnyje dwigatieli [Ramjet Engines], G.J.O.P. [State Defense Industry Press], 1958.

Chapter 6

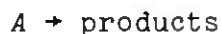
COMBUSTION THEORY

The essence of the combustion process consists in a rapid exothermic chemical reaction taking place between fuel and oxygen.

The combustion mechanism depends most of all on the concentration of the reacting substances and on the aeromechanical conditions under which the process takes place.

6.1. CHEMICAL KINETICS OF COMBUSTION

If a reaction of a single type takes place in the mixture under consideration, without any simultaneous secondary reactions occurring to complicate the picture, then this reaction is called an elementary reaction. In theory, every reaction is reversible only if the conditions are right. It may occur then that an elementary reaction could be complicated by a simultaneous occurrence of the reverse process. Furthermore, the products of the first reaction can be subject to further reactions, the result of which will be new products. Such a complicated set of reactions is called a simultaneous reaction. An elementary reaction is characterized by the reaction order which is expressed by a mathematical equation linking the observed reaction rate with the concentration of the reagents. Reactions of the first order encompass the transformation of a single particle. For this type of reaction, having the general form:



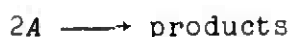
the reaction rate can be expressed by the differential equation

$$\frac{dx}{dt} = k_1(a - x)$$

where a is the initial concentration of the substance A; x is the quantity of the substance A which was subjected to the transformation during the time t .

At each instant of time the reaction rate is proportional to the first power of the concentration of the reacting substance. The constant k_1 is the coefficient of proportionality and is called the reaction rate.

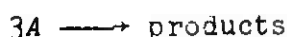
A reaction of the second order consists in obtaining products by means of a reaction between two particles or between an atom and a particle. A reaction of the second order, having the general form



leads to an equation in which the reaction rate is at all times proportional to the square of the reacting substance's concentration:

$$\frac{dx}{dt} = k_2(a - x)^2$$

Reactions of the third order encompass simultaneous interactions of three atoms or molecules. Such reactions are very unlikely and therefore occur very rarely. The corresponding equations for a reaction of the third order have the form:



and

$$\frac{dx}{dt} = k_3(a - x)^3$$

or



and

$$\frac{dx}{dt} = k_3(a - 2x)^2(b - x)$$

as well as



and

$$\frac{dx}{dt} = k_3(a-x)(b-x)(c-x)$$

The time in which the concentration of a given component of the reaction drops to one half of its initial value is called its half life τ_0 . From the equations presented above, it turns out that for a reaction of the n th order

$$\tau_{0,5} \sim \frac{1}{a^{n-1}}$$

The half life is therefore inversely proportional to the initial concentration raised to the power of the reaction order, decreased by one.

The reversible reaction



represents a simple form of simultaneous reactions. The differential equation for identical concentrations of A and B assumes the form:

$$\frac{dx}{dt} = k_1(a-x)^2 - k_2'x^2$$

where k_2 , k_2' are the reaction rates for second order processes, taking place from left to right and in the opposite direction.

According to what has been said above, the half life is inversely proportional to the concentration of the given reactant. In view of this, two opposite reactions of the second order take place, just like a simple process of the same order.

The effect of temperature on the rate of chemical reactions taking place in homogeneous mixtures has been formulated empirically by Arrhenius.

According to his equation the reaction rate is

$$k = A_e^{-\frac{E}{RT}} \quad (6.1)$$

where B is the absolute gas constant; E is the activation energy; A_0 is the proportionality constant.

6.2. COMBUSTION OF HOMOGENEOUS MIXTURES IN A LAMINAR STREAM

The flame propagation mechanism in the laminar flow of a fuel and oxidizer mixture is illustrated in Fig. 6.1.

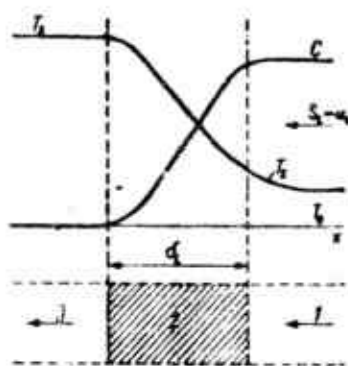


Fig. 6.1. Flame front in laminar flow of a homogeneous mixture: 1) mixture; 2) flame; 3) products of combustion.

The mixture entering at a velocity u_L is ignited on contact with the hot products of combustion which have arisen from the combustion of the preceding layer. Two curves characterize the process: the change of oxygen concentration in the mixture along the flow, and the change of temperature. The rate of flame propagation (in this case, the so-called laminar combustion rate or normal combustion rate) is given by the equation:

$$S_L = u_L = \lim_{\Delta t \rightarrow 0} \frac{\Delta x}{\Delta t} = \frac{dx}{dt}$$

where Δx is the displacement along the x -axis, perpendicular to the combustion surface.

The factor initiating ignition in successive mixture layers is, on the one hand, the phenomenon of heat conduction from the combustion side, and on the other hand, the diffusion of active particles such as

free atoms or radicals, formed during combustion of preceding layers. Which of the two phenomena is the controlling one is not known, so there are still two sets of theories on laminar combustion of homogeneous mixtures: the set of diffusion theories and the set of thermal theories.

The simplest thermal theory is presented below. The quantity of heat required to heat the mixture from a temperature T_0 to the ignition temperature T_z per unit flame area and per unit time is equal to

$$q = c_p \rho_0 u_L (T_z - T_0)$$

where c_p , ρ_0 are the specific heat at constant pressure and the density of the mixture.

The quantity of heat transferred out of the reaction region is

$$q = \lambda \frac{T_s - T_z}{\delta_x}$$

where λ is thermal conductivity; $(T_s - T_z)/\delta_x$ is the average temperature gradient; δ_x is the width of the reaction zone; T_s is the combustion temperature.

From these equations we obtain:

$$c_p \rho_0 u_L (T_z - T_0) = \lambda \frac{T_s - T_z}{\delta_x}$$

Let $\tau_x = \delta_x / u_L$ be the chemical reaction time and $a = \lambda / c_p \rho$ be the coefficient of temperature equalization; the above equation can be rearranged to yield the normal combustion rate as:

$$S_L = u_L = \sqrt{\frac{T_s - T_z}{T_z - T_0}} \sqrt{\frac{a}{\tau_x}} \quad (6.2)$$

It is seen from this equation that the normal combustion rate is directly proportional to the square root of the temperature equalization coefficient and inversely proportional to the square root of the chemical reaction time. The theory's weak point is its treatment of the mixture ignition temperature T_z as a physicochemical constant,

when in reality this temperature is a function of the conditions under which the process takes place. However, even the most complicated theories do not provide a rigorous method for the computation of the normal combustion rate as a function of the thermodynamic parameters and physical properties of the mixture.

Therefore, in practical cases one should operate with experimentally determined quantities. In this regard, the so-called Bunsen burner method is utilized (Fig. 6.2).

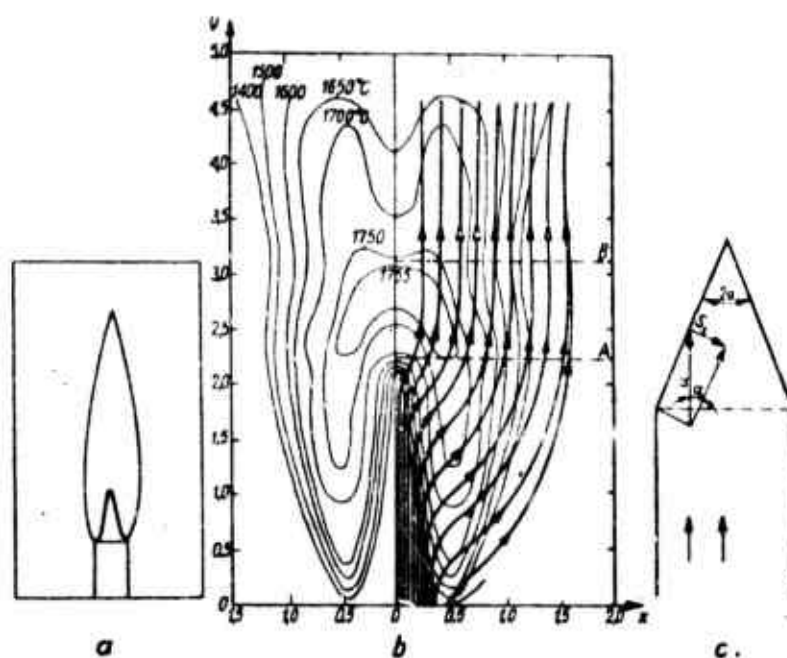


Fig. 6.2. Flame of a Bunsen burner: a) profile of inside and outside cone; b) isotherms and flow lines; c) method of determining the rate of laminar combustion.

The mixture flowing through the burner burns over the burner's exit cross section. In the laminar flame so created, two cones can be distinguished: an external flame and an internal one. The basic combustion process takes place on the lateral surface of the internal cone which has a grayish-blue tinge. The particles not burned on the internal cone finish burning in the luminous space between the cones.

Figure 6.2a shows the flame of a Bunsen burner. Figure 6.2b shows the speed, temperature and streamline distribution in the flame. Figure 6.2c on the other hand shows the method of determining the laminar combustion rate.

From the flow continuity equation one gets:

$$S_L F_b \gamma = u F_p \gamma = u F_b \gamma \sin \alpha$$

where S_L is the speed of laminar combustion; u is the velocity of the mixture in the burner; 2α is the included angle of the internal cone; γ is the mixture's specific weight before combustion; F_b is the cone's lateral surface area; F_p is the cone's base surface area.

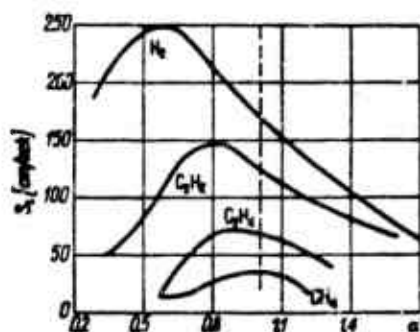


Fig. 6.3. Dependence of laminar combustion rate on fuel type and on the coefficient of excess air.

After rearrangement one finally gets:

$$S_L = u \sin \alpha$$

In order to determine the rate of laminar combustion, it is sufficient to measure the mixture velocity through the exit cross section (e.g., by means of measurements of stagnation pressure and measurement of the mixture's thermodynamic parameters) and the included angle of the internal cone (for instance, by projecting the cone's shadow on a screen, which facilitates the measurement). On the basis of such studies, it has been verified that the rate of laminar combustion is

primarily a function of fuel type and of the coefficient of excess air (Fig. 6.3). The highest combustion rate is obtained in the case of hydrogen. In the case of hydrocarbon fuels, the combustion rate decreases with an increase in the degree of saturation of structural chains. In the case of gasoline and kerosene mixtures, the highest laminar combustion rate amounts to ~40 cm/sec. An increase in mixture temperature upstream of the flame front increases the combustion rate. In the case of propane-air mixtures, as well as other hydrocarbon mixtures (including gasoline and kerosene) the following empirical relation (which holds at 1 atm) is important:

$$S_{L0} = 10 + 0,000342 T^2$$

where S_{L0} is the maximum laminar combustion rate (cm/sec); T is mixture temperature before combustion ($^{\circ}\text{K}$).

The influence of pressure on combustion rate is indicated qualitatively by the following empirical relationship:

$$S_L \sim \frac{1}{p^{0.25}}$$

From this we see that the rate of laminar combustion increases with a decrease in mixture pressure.

In depth the flame front consists of a layer in which the mixture is heated up to the ignition temperature, and of a second layer in which the combustion process takes place. From the condition that the heat transferred from the combustion area to the mixture is equal to the heat which raises the mixture temperature, we obtain:

$$\lambda \frac{dT}{dx} = S_L \rho c_p (T - T_0)$$

We assume that

$$\frac{dT}{dx} \sim \frac{T - T_0}{\delta_L}$$

and obtain the following relationship for the flame front depth, in

the case of laminar combustion:

$$\delta_L \sim \frac{a}{S_L} \quad (6.3)$$

where a is the coefficient of temperature equalization.

We see from Eq. (6.3) that the depth of the combustion zone is inversely proportional to the speed of flame propagation.

6.3. COMBUSTION OF HOMOGENEOUS MIXTURES IN A TURBULENT STREAM

In the analysis of the combustion process in a turbulent stream we distinguish two characteristic cases:

— when the turbulence scale is small compared to the forward depth of the laminar flame,

— when the turbulence scale is large.

The second case occurs mainly in technical applications, and it will be considered below. In this case the flame's zone assumes the shape illustrated in Fig. 6.4. The boundary of the unburned mixture, on the flame side, is very wavy and furthermore, separate pockets of fresh mixture are formed in the midst of the combustion products; these pockets have various volumes.



Fig. 6.4. Schematic diagram of the flame zone in the case of turbulent combustion of homogeneous mixtures: 1) mixture; 2) turbulent flame; 3) products of combustion.

Assuming that the flame's surface area increases as the ratio u'/S_L , where u' is the pulsation rate in the direction of flame propagation, and that the protuberances on the combustion surface assume a conical shape, we have derived the following relation:

$$\frac{S_T}{S_L} = A \sqrt{1 + B \left(\frac{u'}{S_L} \right)^2}$$

where A and B are constants; S_T is turbulent combustion rate.

After taking into account the experimental results, we find that this equation assumes the following form:

$$\frac{S_T}{S_L} = 1 + 5.9 \left(\frac{u'}{S_L} \right)^{0.6 \div 0.7} \quad (6.4)$$

Therefore, the turbulent combustion rate of a homogeneous mixture depends on the laminar combustion rate and on the pulsation rate in the direction of flame propagation.

Figure 6.5 shows the qualitative influence of the thermodynamic parameters of state on the rate of turbulent combustion.

The increase in the rate of turbulent combustion with an increase in pressure and temperature can be explained by means of the following relationships:

- dependence of the pulsation rate on pressure

$$u' \sim p^{0.25} \quad (6.5)$$

- dependence of rate of laminar combustion on temperature

$$S_L \sim T^2$$

The effect of Eq. (6.5) is offset by the relation determining the influence of pressure on the rate of laminar combustion

$$S_L \sim p^{-0.25}$$

However, in accordance with the theory discussed above (see Eq. (6.4)) the influence of pulsation rate on the rate of turbulent combustion is greater than the influence of S_L and therefore S_T increases with increasing p .

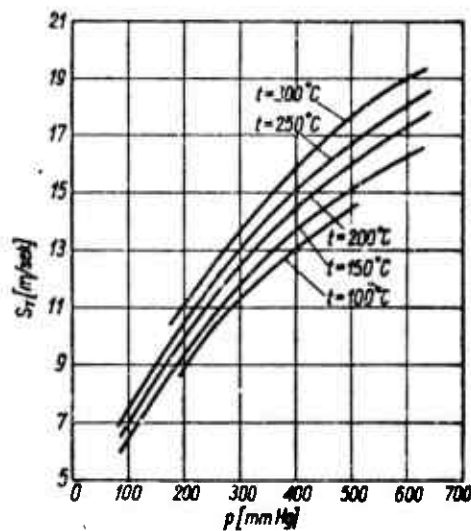


Fig. 6.5. Dependence of the rate of turbulent combustion on the mixture pressure and temperature.

6.4. FLAME STABILIZATION

In all cases where the flow velocity is greater than the rate of flame propagation, a device must be introduced into the mixture flow to stabilize the flame. The function of this device is to create, in a certain section of the combustion chamber, conditions leading to steady combustion. This is achieved most often by placing in the flow a blunt body behind which a recirculating vortex is created. The recirculation region becomes "the point of attachment" of the turbulent flame front which in turn encompasses the entire mixture flowing through (Fig. 6.6).

A realistic picture of the phenomena occurring in the combustion zone, behind a stabilizer of circular cross section, is shown in the diagram of Fig. 6.7 which is based on photographic data. A fresh mixture flowing about the stabilizer slides over the aerodynamic shadow of the stabilizer formed by the turbulent region of vortex motion of hot combustion product particles. A layer is formed on the boundary

between this region and the fresh mixture, into which particles of fresh mixture penetrate as a result of turbulent motion and burn up. This process constitutes the initiation of the flame front which will subsequently encompass the entire combustion chamber.



Fig. 6.6. Typical model of a combustion chamber with a flame stabilizer: 1) flame stabilizer; 2) recirculation region; 3) flame front.

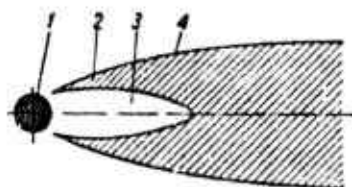


Fig. 6.7. Realistic picture of the phenomena occurring in the combustion zone behind a flame stabilizer: 1) stabilizer; 2) mixing region; 3) recirculation region; 4) flame front.

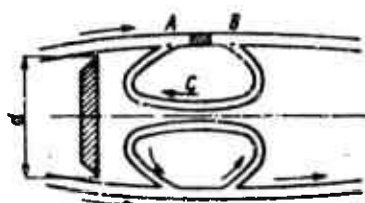


Fig. 6.8. Model of flame stabilization by means of a recirculating vortex.

There are a number of theories explaining the mechanism of flame stabilization described above.

The majority of these, however, are based on the following physical model of the phenomenon (Fig. 6.8).

The mixture flowing around the flame stabilizer (in the shape of a flat circular target) creates in its aerodynamical shadow a toroidal vortex. The path of a fluid element in this vortex can be subdivided into two parts. In the first part (A-B) heating of the fresh mixture takes place as a result of mixing with combustion products from the previous dose and as a result of radiation from the hot recirculating region. In the second part (B-C-A) combustion of the mixture preheated to the proper temperature takes place. Starting with this model, Spalding [6.2] assumed that the phenomenon controlling the stabilization process is the heat-exchange rate in the recirculation region. It has been assumed therefore that the mathematical equation describing this process is the heat-transfer equation, with a heat source:

$$a \frac{\partial^2 T}{\partial x^2} - u \frac{\partial T}{\partial x} + z p^{n-1} f(T) = 0 \quad (6.6)$$

Using the method of dimensional analysis, and transforming the above equation, the following dimensionless groups can be formed:

$$Pe_u = K Pe_s^m \quad (6.7)$$

where $Pe_u = ud/a$ is the Peclet number referred to the flow velocity; $Pe_s = S_L d/a$ is the Peclet number referred to the rate of laminar combustion; K and m are experimental constants; z is a chemical constant; n is reaction order; p and T are pressure and temperature; a is the coefficient of temperature equalization.

Equation (6.6) explains the change in enthalpy of a fluid element (2nd expression) as a result of conductive heat transfer (1st expression) and as a result of the release of the chemical heat of reaction (3rd expression). The Peclet numbers in Eq. (6.7) determine the physical conditions in the stabilization region. The Peclet number referred to the flow velocity determines the conditions of heat transfer, whereas the Peclet number referred to the rate of laminar combustion deter-

mines the conditions for generation of thermal energy. Figure 6.9 shows experimental results gathered by Spalding. It is seen from the graph given in this figure that at $Pe_u = 10^4$ a change in the exponent occurring in Eq. (6.7) takes place; it goes from 1.5 to 2.0.

Starting with a similar model, De Zubay [6.1] assumed that the condition for flame stabilization is a net energy excess resulting from the comparison of the heat generated in the recirculation region and the heat conducted away from this region by the mixture flow passing the flame stabilizer. Based on the equation so obtained, and taking into account the experimental coefficients, the following stability criterion is obtained:

$$a = f\left(\frac{u}{p^{0.85} d^{0.856}}\right) \quad (6.8)$$

where a is the coefficient of excess air; p is the ambient pressure in the combustion chamber (kgf/cm^2); u is the flow velocity in the stabilizer plane (m/sec); d is the stabilizer's characteristic dimension (target diameter or hydraulic diameter of a stabilizer of a different shape (mm)).

Measurement results are shown in Fig. 6.10.

The question of flame stabilization in a completely different plane has been analyzed by Zukoski and Marble [6.4]. Adhering strictly to the picture of the phenomena occurring in the stabilization region, which has been presented earlier (Fig. 6.7), they have assumed that the factor governing flame stability is the ignition lag of the mixture flowing past the recirculation region.

In this case the stability condition reduces to the equation

$$\frac{u}{L} \leq \tau \quad (6.9)$$

where u is the mixture velocity past the stabilizer; L is the length of the recirculation region; τ is ignition lag.

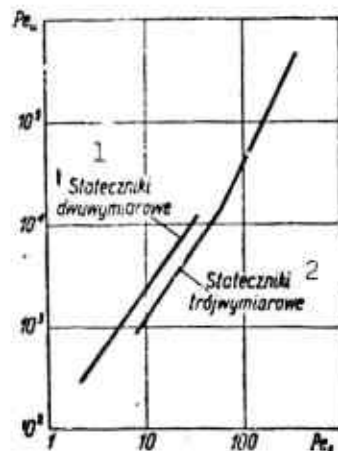


Fig. 6.9. Characteristics of flame stabilizers according to Spalding. 1) Two-dimensional stabilizers; 2) three-dimensional stabilizers.

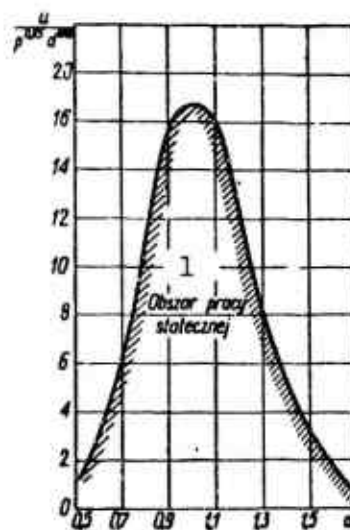


Fig. 6.10. Characteristics of flame stabilizers according to De Zubay: u (m/sec), p (kgf/cm²), d (mm). Region inside the graph determines the range of stabilization energy. 1) Region of stabilization energy.

It is seen from experimental evidence that the length of the recirculation region is a function of the Reynolds number (Fig. 6.11). However, from $Re = 1.5 \cdot 10^4$ on, the ratio of region length to the characteristic stabilizer dimension is constant and equal to 2.3. On the other hand, ignition lag is a function of the coefficient of excess

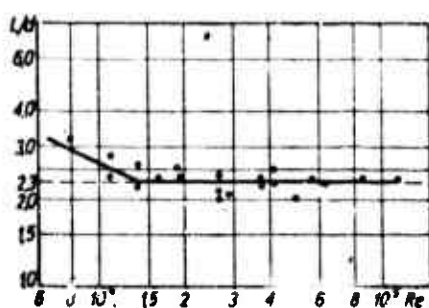


Fig. 6.11. Dependence of the relative length of the recirculation region on the Reynolds number.

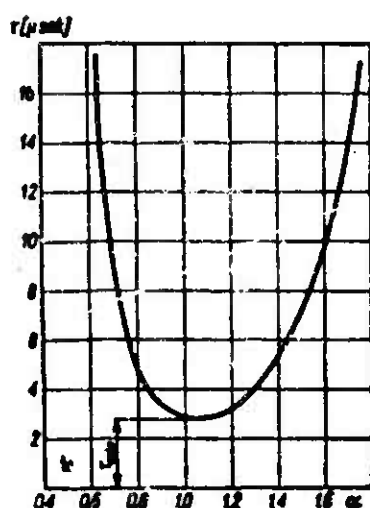


Fig. 6.12. Dependence of ignition lag on mixture composition: conical stabilizer, gasoline-air mixture.

Kashit stabilizer	1	d (mm)	r_{min} [$\cdot 10^{-3}$ sec.]
		3.8	3.08
		4.4	2.35
		6.5	2.80
		6.5	2.38
		8.4	2.70
		12.7	2.65
		12.05	2.54
		12.5	1.46
		12.7	1.12
		12.7	1.05
		14.05	1.02
		14.05	1.05
		14.05	2.70

Fig. 6.13. Dependence of minimum ignition lag on stabilizer shape and size. 1) Stabilizer shape.

air (Fig. 6.12) and of the shape and size of the stabilizer (Fig. 6.13). In the general case, the stability condition can be written in the form of a function of the dimensionless groups:

$$Re = f(D_{II}) \quad (6.10)$$

where $Re = ua/v$ is the Reynolds number; $D_{II} = u\tau/d$ is Damköhler's second number; v is the mixture's kinematic viscosity; d is a characteristic dimension of the flame stabilizer.

6.5. DIFFUSIVE COMBUSTION

In cases most often encountered in practice, the combustion process takes place simultaneously with the process of mixture generation. This type of combustion is commonly known as diffusive combustion. Typically, diffusive combustion takes place in liquid-fuel rockets and in pulsejets.

Only in a few instances of axial-flow jet-engine design can it be assumed that the combustion process approximates the nature of homogeneous mixtures.

6.5.1. Diffusive Combustion in a Laminar Stream

Figure 6.14 shows an idealized diagram of diffusive combustion. The fuel flows through the inner cylindrical conduit with diameter d_1 with a velocity u . Air flows (with the same velocity) through the annular region between the inner and outer conduits. Mixing of the fuel and air takes place at the end of the inner conduit. After ignition of the mixture, a flame front arises in a region of appropriate concentrations; air on the one hand and fuel on the other hand diffuse toward this flame front (Fig. 6.15).

If the following assumptions are introduced

- air and fuel diffusion coefficients are the same and equal to D ;
- fuel and air diffuse only in a radial direction;
- the combustion region is infinitely thin, and by the same token the combustion process takes place infinitely fast;
- air and fuel velocities are equal;

then the phenomenon of diffusive combustion can be described by the equation:

$$\frac{\partial c}{\partial \tau} = u \frac{\partial c}{\partial s} - D \left(\frac{\partial^2 c}{\partial r^2} + \frac{1}{r} \frac{\partial c}{\partial r} \right) \quad (6.11)$$

where c is the concentration of the combustible mixture, and is related

to the concentration of air and fuel by the equation

$$c = C_p - \tau C_0$$

C_p is fuel concentration; C_0 is oxygen concentration; τ is the number of moles of oxygen required to burn one mole of fuel; τ is time; z and r are cylindrical coordinates as per Fig. 6.14; D is the diffusion coefficient.

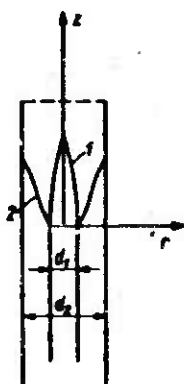


Fig. 6.14. Shape of a diffusive laminar flame: 1) with excess air; 2) with fuel excess.

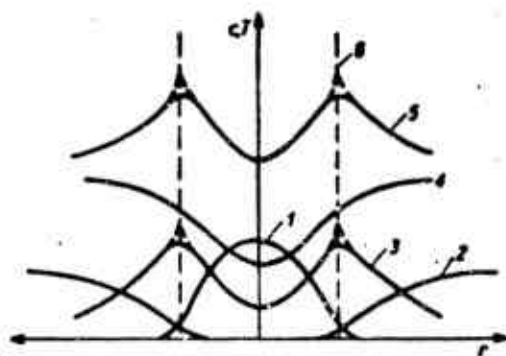


Fig. 6.15. Distribution of gas concentration c and temperature T in a diffusive flame: 1) concentration of the fuel; 2) oxygen concentration; 3) concentration of combustion products; 4) nitrogen concentration; 5) temperature distribution; 6) flame front position.

Equation (6.11) has two solutions illustrated in Fig. 6.14 by two curves (1 and 2).

The result is a function of the coefficient α , the air excess in the mixture. When $\alpha > 1$ the flame surface closes on the flow centerline

(curve 1). When $\alpha > 1$, that is, when there is an air excess, the flame surface approaches the wall of the outer conduit.

Based on (Fick's) diffusion equation:

$$\frac{\partial M}{\partial \tau} = - DF \frac{\partial c}{\partial r} \quad (6.12)$$

where M is the mass of the diffusing gas; F is the diffusion area; r is the diffusion path, and using dimensional analysis, we can define the following relationship:

$$\tau = \frac{r^2}{D}$$

In the case of diffusive flames with excess air, flame height is determined by the position of its peak on the burner's axis. Then the oxygen diffusion path is equal to the radius of the inner conduit

$$R = d_1/2$$

and the diffusion time amounts to

$$\tau \sim R^2/D$$

If flow velocity does not change and is equal to u , then the flame height is

$$L = \tau \sim \frac{uR^2}{D} \sim \frac{Q}{D} \quad (6.13)$$

where $Q \sim uR^2$ is the volumetric efficiency of the fuel gas.

It is seen from Eq. (6.13) that the height of a diffusive laminar flame increases with an increasing flow velocity and burner radius and with a decreasing diffusion coefficient. Flame height decreases with a decrease in pressure (in the case of nondecreasing volumetric efficiency), since then the diffusion coefficient increases. In the case of constant gravimetric efficiency, flame height is not a function of pressure.

Figure 6.16 shows an actual picture of the influence of fuel efficiency on the height of a diffusive flame. Beyond the range of laminar

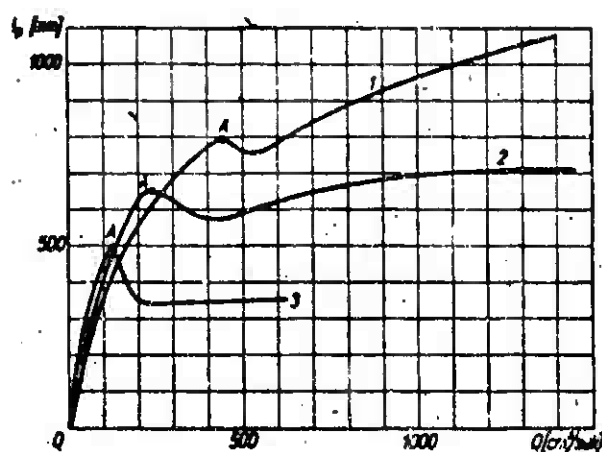


Fig. 6.16. Influence of gas efficiency (city gas, Q) and of burner diameter d_1 on flame length l_p : 1) $d_1 = 10.2$ mm; 2) $d_1 = 6$ mm; 3) $d_1 = 3.4$ mm. A is the boundary of the diffusive laminar flame.

combustion, these curves also encompass turbulent combustion (the range of laminar combustion terminates at the curve apex, i.e., at point A in Fig. 6.17). The following conclusions can be reached from this graph:

- in the case of short flames ($l_p < 150$ mm) the relationship of Eq. (6.13) is important; it yields the proportionality between flame length and fuel efficiency;

- in the case of longer flames, the rate of flame length increase decreases with an increase in efficiency, which must be interpreted as a drop in gas velocity and an increase in the diffusion coefficient as a function of distance from the burner edge.

This latter influence illustrates the relationship used in practice:

$$D = D_0 + kz$$

where D_0 is the diffusion coefficient at the burner edge; z is the distance from the burner edge, measured along its axis; k is an experimental constant.

6.5.2. Diffusive Combustion in a Turbulent Stream

As can be seen from Fig. 6.16, an increase in gas efficiency (and thereby an increase in its velocity in the terminal burner cross section) causes an elongation of the flame in the range of laminar combustion. After exceeding a certain limit velocity, vortices appear first in the apex region and then in the entire flame, and these shorten the flame and simultaneously change the nature of the process. Such combustion is called turbulent combustion. Figure 6.17 shows the dependence of the flame length and of the length of the laminar region on the gas flow velocity in the terminal burner cross section. As the velocity increases, the laminar segment decreases until it disappears completely, which occurs when gas flow becomes turbulent inside the burner. Thus diffusive turbulent flames can be subdivided into two groups:

- mixed flames (the flow at burner exit has a laminar character),
- completely turbulent flames (the flow at burner exit has a turbulent character).

A characteristic feature of turbulent flames is the weak effect of flow velocity on their length.

This fundamental experimental result can easily be explained theoretically. As has been shown in the preceding section, the height of a diffusive laminar flame is directly proportional to flow velocity and to the square of the burner radius, and it is inversely proportional to the diffusion coefficient. In the case of turbulent flow the role of the diffusion coefficient D is filled by the coefficient of turbulent diffusion

$$D_T = L \sqrt{(u')^2}$$

where L is the turbulence scale; $\sqrt{(u')^2}$ is the mean square pulsation rate.

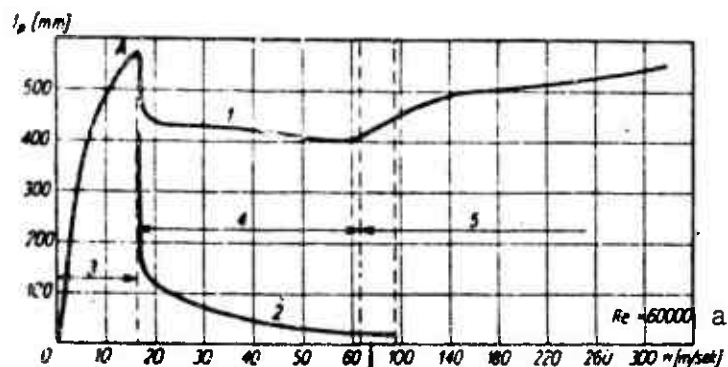


Fig. 6.17. Influence of gas velocity in exit section of combustion chamber on height of diffuse flame: 1) height of diffuse flame; 2) height of laminar part of flame; 3) laminar-flame region; 4) mixed-flame region; 5) turbulent-flame region. a) m/sec.

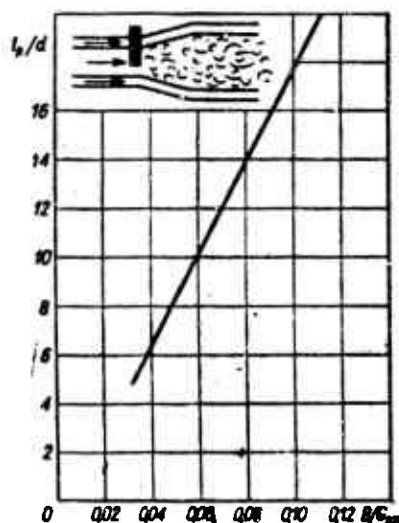


Fig. 6.18. Influence of the ratio of fuel efficiency to primary air efficiency on flame length in model combustion chambers: B) fuel efficiency; G_{pp}) efficiency of primary air; l_p) flame length; d) diameter of incandescent chamber.

In the case of a turbulent flow it is assumed that

$$\tau \sim R$$

$$\sqrt{\overline{(u')^2}} \sim u$$

From which

$$L \sqrt{\overline{(u')^2}} \sim Ru$$

and the flame height is

$$l_p \sim \frac{uR^2}{L\sqrt{(u')^2}} \sim \frac{uR^2}{Ru} \sim R$$

or

$$\frac{l_p}{R} \sim \text{const}$$

(6.14)

Therefore the nondimensional height of a completely turbulent diffusive flame is a constant. The height of turbulent flames can be decreased by two methods:

- by addition to the stream of fuel gas of the so-called primary air in front of the combustion zone; this shortens the diffusion path of the secondary air particles. In this case the flame has a diffusion-mixture character;

- by increasing turbulence while maintaining the flow velocity constant.

The first method of flame shortening is illustrated in Fig. 6.18.

From this graph it is seen that by preserving the ratio of fuel and total air, the relative flame length decreases when the efficiency of primary air increases. The influence of increased turbulence on flame shortening can be explained by an intensification of the mixing process of fuel gas and oxidizer.

The result of the existence of turbulent flow is that mixing of air and fuel occurs due to a mutual penetration of elementary volumes of gas, the size of which is a function of the turbulence scale.

The combustion process starts at the contact surface of the reacting elements; further flame propagation is governed by the rate of molecular particle diffusion. Therefore, the rate of diffusive combustion is a function of turbulence intensity and of the molecular diffusion coefficient.

6.5.3. DIFFUSIVE COMBUSTION THEORY OF LIQUID FUEL DROPS IN AN OXIDIZING ATMOSPHERE

The combustion process of fuel drops in an oxidizing atmosphere can be illustrated by means of the model shown in Fig. 6.19a. The drop temperature is equal to the fuel's boiling temperature. Fuel vapors

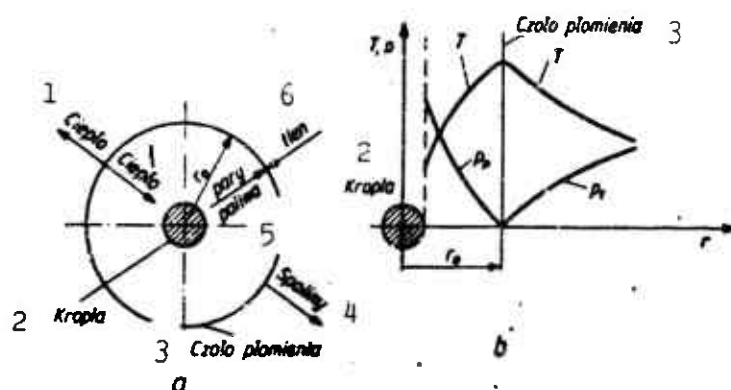


Fig. 6.19. Combustion model of a liquid fuel drop in a gaseous oxidizing medium. 1) Heat; 2) drop; 3) flame front; 4) combustion products; 5) fuel vapors; 6) oxygen.

diffuse toward the flame front which stabilizes itself at a distance r_0 from the drop center. Oxygen diffuses similarly toward the flame front, but from the outside. The heat created at the point of contact between the fuel vapors and oxygen is transmitted partially to the drop and partially, together with the combustion products, to the outside. Figure 6.19b shows the temperature distribution as well as the distribution of partial pressures of fuel vapors and oxygen in the drop's surface layer. In the described model, the combustion rate is rigorously related to the evaporation rate which in turn is a function of the heat-transfer rate between the drop and the flame front.

If it is assumed that the phenomenon governing the process is the diffusion of fuel vapors from the drop toward the surrounding flame front, then the result of the mathematical analysis is analogous to that obtained in Chapter 5 for the case of an evaporating liquid fuel

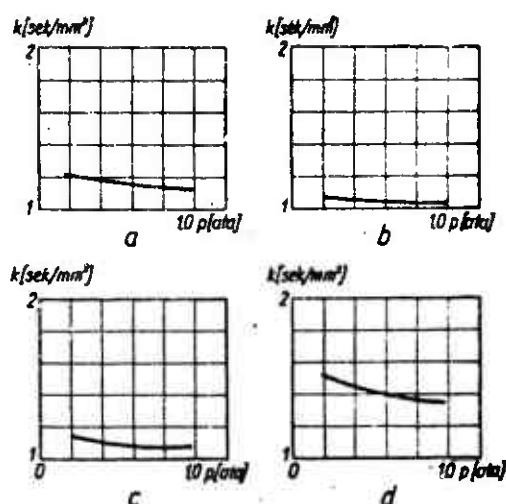


Fig. 6.20. Influence of pressure and type of hydrocarbon fuel on the value of the combustion rate constant: a) gasoline; b) isooctane; c) kerosene; d) ethyl alcohol.

drop in a gaseous medium (Eq. (5.8)).

$$\tau = k (d_0^2 - d^2) \quad (6.15)$$

where k is the combustion rate constant; d_0 is the initial drop diameter; d is the drop diameter at time τ , reckoned from initiation of combustion.

The combustion constant k is a function of the fundamental thermodynamic parameters and of the fuel type. The corresponding relationships are illustrated by the graphs in Fig. 6.20.

6.6. THEORY OF COMBUSTION OF SOLID ROCKET FUELS

Solid rocket propellants consist of a mixture of fuel and oxidizer, shaped into a charge whose form is a function of the desired burning rate.

The term "combustion of solid propellants" refers to a series of chemical processes as the result of which the solid propellants are transformed into gaseous products because of the action of an initial ignition process. An appropriately shaped charge of solid propellant is called a grain. Grain combustion occurs at its surface.

The burning rate of a solid propellant has been defined as the distance traveled by the flame front per unit time in a direction perpendicular to the open surface of the grain.

As has already been discussed in Chapter 4, solid propellants are subdivided into two groups: homogeneous and composite.

The combustion mechanism of these two types of propellants is different and therefore will be considered separately.

6.6.1. Combustion of a Solid Propellant Having a Homogeneous Structure

Combustion of solid propellants occurs in parallel layers, and therefore it can be treated as a one-dimensional process varying along an axis perpendicular to the burning surface (Fig. 6.21). Since the combustible material exhibits low thermal conductivity, changes in the propellant caused by surface combustion do not reach deeply into the propellant mass. Heat transfer from the flame toward the material in the solid phase should be sufficient to maintain the temperature of the reacting substances in the individual layers at the level required to preserve the reaction's continuity.

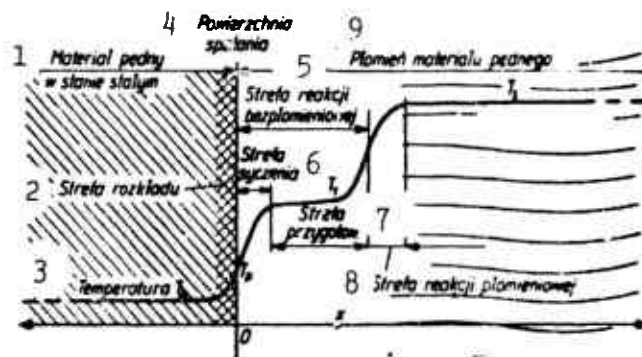


Fig. 6.21. Illustration of the combustion of a homogeneous propellant. 1) Solid propellant; 2) decomposition zone; 3) temperature T_0 ; 4) combustion surface; 5) flameless reaction zone; 6) hissing zone; 7) ready zone; 8) flame reaction zone; 9) propellant flame.

In this fashion is created a steady state which is characterized by constant rates of mass and energy flow through the combustion zone

and by constant temperature and concentration gradients. The first material zone subjected to the flame's action is the surface layer called the decomposition zone. A temperature increase in this zone causes an exothermal decomposition of nitrocellulose and of nitroglycerine into gaseous products. Another source of heat raising the temperature of the subsurface layer is the reaction taking place between nitric acid esters and the stabilizer (e.g., ethyl centralite). The stabilizer's function is to react with the nitrogen oxides which occur in spontaneous decomposition of nitric acid esters during the fuel manufacturing process and thus to prevent an accelerated autocatalytic reaction.

At high temperatures, stabilizers can react directly with nitric acid esters; this reaction has an exothermic character.

The heat balance on an arbitrary plane in the combustion zone is described by the relation

$$\lambda \frac{\partial^2 T}{\partial x^2} - m c_p \frac{\partial T}{\partial x} + q_x = 0$$

where x is the distance from the flame front; λ is the thermal conductivity; m is the mass combustion rate; q_x is the heat flux in the plane x caused by the chemical reaction.

The first term in the equation represents the rate of change in heat energy per unit volume due to conduction; the second term represents the agent's rate of change of enthalpy, and the third represents the rate of liberation of heat energy as a result of combustion. This equation can be easily solved by assuming that $q_x = 0$, which is nearly the case for planes further away from the combustion surface. After integration one gets:

$$T - T_0 = (T_p - T_0) e^{\frac{m c_p x}{\lambda}} \quad (6.16)$$

where T_0 is the initial propellant temperature; T_p is the temperature at the combustion surface.

Figure 6.22 shows the experimentally obtained temperature distribution in the vicinity of the combustion surface for the case of nitrocellulose with a 1% additive of ethyl centralite. If it is assumed that temperature distribution in the fuel, underneath the surface layer, is described by Eq. (6.16) then the quantity of stored heat is given by

$$Q = \int_{-\infty}^0 (T - T_0) \rho c_p dx = (T_p - T_0) \rho c_p \int_{-\infty}^0 e^{-\frac{\rho u x}{\lambda}} dx$$

whereas the surface temperature is given by

$$T_p = T_0 + \frac{q_m}{\rho \lambda}$$

In this way (substituting actual values), we find that the temperature at the combustion surface of a double base propellant is $330 \pm 45^\circ\text{C}$. The mechanism responsible for the creation of the gaseous

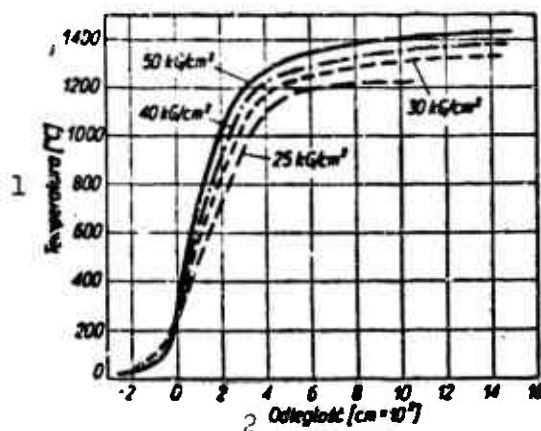


Fig. 6.22. Temperature distribution in the vicinity of the combustion surface as a function of pressure, in the case of a solid propellant. 1) Temperature ($^\circ\text{C}$); 2) distance ($\text{cm} \times 10^2$).

mixture as a result of the reaction, in the decomposition zone, is considered to be the process which governs the combustion rate of solid propellants. Unsaturated particles arising in the decomposition zone are expelled toward the gaseous phase in a direction perpendicular to the grain's surface. These particles initiate a secondary reac-

tion in the next zone, called the hissing zone. The reaction products in this case are: nitrogen oxides, as well as individual organic compounds together with such stable terminal products as nitrogen, water vapor, carbon monoxide and dioxide. Present reactions release energies on the order of 500 kcal/kgf which is less than half of the total heating value. Terminal temperature in the hissing zone is $\sim 1500^{\circ}\text{C}$. Subsequently, transformations having a preparatory character take place (readying zone), where activated products are created without heat generation.

In the terminal reaction stages, nitrogen oxides react with the remaining materials to be oxidized, and the products tend toward thermodynamic equilibrium. Flame temperature then reaches its maximum value of about 3000°K , and the reaction zone glows intensely. The hissing zone together with the preparatory zone constitute the flameless reaction zone. The width l (mm) of this zone is a function of pressure p (kgf/cm²) and is given by the empirical equation:

$$l = 8790/p^3.$$

At low pressures, the area of high temperature is fairly distant from the combustion surface in order to supply a greater amount of energy to the initial decomposition in the surface layer (in the combustion of solid fuels, radiation has much lower significance than conduction).

This phenomenon is the reason for the existence, for a given solid fuel, of a minimum pressure below which a stabilized combustion process cannot be achieved. When pressure drops below the minimum level, the zone of flameless reaction widens, the activity in the decomposition and hissing zones decreases, the concentration of activated products in the preparatory zone decreases and the flame zone disappears.

But initial reactions take place nevertheless and the grain is used up; however, the reaction does not run its full course and the temperature in the lower layers is low. This phenomenon is the beginning of an intermittent operation of combustion chambers operating at pressures that are too low.

6.6.2. Combustion of a Solid Propellant Having a Composite Structure

The variety of solid propellants having a composite structure is so great that a general treatment of the combustion processes of this group of fuels is impossible. However, a majority of propellants of this type exhibit a similarity from the point of view of physical structure and ballistic properties. A common feature of these propellants is among others the relative insensitivity of the combustion rate to pressure and temperature. The inhomogeneous structure of the fuels under discussion results in an inhomogeneity on the combustion surface and in the flame-reaction zone. The basic oxidizing agent in composite solid propellants is in general potassium perchlorate which is disseminated in a resin substrate. Perchlorate's thermal distribution on the combustion surface leads to a gaseous mixture containing oxygen and potassium chloride. Simultaneously, the substrate enveloping the potassium perchlorate generates a fuel gas mixed with carbon particles. The rate of the reaction between these components and therefore the distance between the flame's hot zone and the propellant surface are functions of the flow's mixing rate. The more the perchlorate is subdivided, the more tiny sources of oxygen will be created, and this will decrease the diffusion mixing path and will increase the reaction rate by improving heat exchange with the combustion surface.

Since diffusion rate decreases with a pressure increase, then to a certain degree it equalizes the strong dependence of the substrate's combustion rate on pressure, and by the same token it lessens the pres-

sure's influence on the combustion rate of solid fuel propellants having a composite structure.

6.6.3. Combustion Law Governing Solid Propellants

Rocket technology preserves the old artillery traditions. This has contributed to the fact that many concepts and formulations, which today are either untimely or have a strange sound, suffer by their strict relation to the terminology of this scientific discipline. We are not surprised therefore by the discrepancy between this section's title and its modest and simple equation describing the relation between the combustion rate of solid propellants and pressure, in which this process takes place.

This equation has the following form:

$$w = bp^n \quad (6.17)$$

where w is combustion rate; p is pressure; n is an experimental exponential coefficient which is a function of the propellant's composition; b is an experimental constant which is a function of the initial propellant's temperature.

This is an approximate equation valid in the experimentally described ranges. However, based on many studies the following generalizations can be made:

- at high pressures (above 20-140 atm) the equation is adhered to rigorously;
- in the medium pressure range, irregularities occur (regions are encountered in which combustion rate is not a function of pressure or even decreases with an increase in pressure);
- in the range of lowest pressures the equation is not valid, since the propellants cease to burn at pressures below 0.3-20 atm.

These phenomena can be explained on the basis of the previously described theory of the combustion of solid propellants. At high pres-

sures the greater portion of the energy required to achieve decomposition in the subsurface layer comes from the flame zone. The rate of energy flow to the surface is governed by the flame's thermal conductivity and by the distance of the high temperature regions from the combustion surface. Since the flame reaction rate is a function of pressure, consequently as the pressure increases, the energy flow to the surface of the solid state phase increases and the combustion rate increases. In the medium pressure range, the flame region is slightly separated from the solid-phase surface. Therefore a certain portion of the energy required to sustain combustion must originate from the hissing zone. Reactions in this zone are slow and to a large extent depend on the propellant's composition, as opposed to the reactions in the flame zone which are basically the same for all double-base fuels.

In view of the above, the dependence of the combustion rate on pressure, in the medium pressure range, is much less predictable. At very low pressures the quantity of energy transferred to the combustion surface from the gaseous phase is very small, and combustion rate becomes almost independent of pressure.

Changes in combustion rate with changes in initial propellant temperature are relatively small and usually amount to less than 5% per 10°C. An increase in the initial propellant temperature causes an increase in the final flame temperature. By the same token, the heat energy flowing backward from the flame zone toward the solid phase surface increases and simultaneously the combustion rate increases. This influence is taken into account by an appropriately determined change in the experimental constant b appearing in Eq. (6.17), which for this reason is called a temperature coefficient.

The temperature coefficient at a given temperature T_0 can be determined from the relation

$$b = C/(T' - T_0)$$

where C and T' are constants, characteristic for a given fuel.

The dependence of b on temperature, in the case of a propellant of the JPN type is given in Table 6.1. The composition and other properties of this material are given in Table 4.1.

TABLE 6.1

Dependence of the Temperature Coefficient b on the Initial Temperature of a Solid Propellant of the JPN Type

$t [^{\circ}\text{C}]$	-18	21	60
b	0,0683	0,0832	0,111

The influence of flame temperature (which can be determined by knowing the fuel's heating value and the composition of the combustion products) on its rate comes directly from the following relation which is applicable to the majority of solid propellants having a homogeneous structure:

$$w = 1 + p e^{-6,46 + 0,703 \cdot 10^{-3} T_g}$$

where w is combustion rate in cm/sec; p is pressure in kgf/cm^2 ; T_g is combustion temperature in $^{\circ}\text{K}$.

For this type of propellant, the flame temperature is approximately a linear function of the heating value. Furthermore, it is not surprising that the following relation exists between the heating value and the combustion rate:

$$1/2 w' = 1,47 + 0,846 \frac{H_u}{1000}$$

where w' is the double combustion rate when $p = 1000 \text{ kgf/cm}^2$, in mm/sec; H_u is the heating value in kcal/kgf.

The above relations are derived from experimental data. They are applicable solely in the high-pressure range where the combustion rate

is to a large extent governed by energy flow from the flame zone; they do not represent the actual facts in the range of low or medium pressures (below 140 kgf/cm^2), where there either is no flame region at all, or it is located at some distance from the combustion surface.

The radiation phenomenon also exhibits a certain influence on the combustion rate.

Radiant energy issuing from the flame region is absorbed by the propellant grain, thereby raising its temperature and consequently it increases the combustion rate in an analogous way to the action of an increase in initial temperature.

Radiation influence should be taken into account in the relation describing the temperature coefficient:

$$b = \frac{C}{T' - (T_0 + \Delta T_\lambda)}$$

where C and T' are constants, characteristic of the given fuel; ΔT_λ is the temperature increase due to radiation.

The increase in grain temperature due to radiation is small and may amount at most to 130°C under the most favorable conditions.

The definite addition of carbon black to the grain's material effectively decreases the influence of radiation and protects against its consequences.

REFERENCES TO CHAPTER 6

- 6.1. De Zubay: Characteristics of Disk-Controlled Flame Aero-Digest, July 1950.
- 6.2. D.B. Spalding: Theoretical Aspects of Flame Stabilization. Aircraft Engineering, September 1953.
- 6.3. B. Lewis, R. Pease, H. Taylor: Combustion Processes. Princeton University Press, 1956.
- 6.4. E. Zukoski, F. Marble: Experiments Concerning the Mechanism of Flame Blowoff from Bluff Bodies. Proceedings of the Gas Dynamics Symposium on Aerothermochemistry, 1956.

Chapter 7

PULSEJET ENGINES

Until now, the pulsejet has been a jet engine of frustrated expectations. It arose from the idea of a gas generator - without compressor - to be used in conjunction with a combustion turbine, and appeared initially as an unattainable goal of engine simplicity.

Nearly all the thermodynamic processes of a piston engine occur in a simple, but appropriately shaped channel.

Even as recently as 1953, the pulsejet was described [7.4] as the one aircraft engine having the greatest developmental possibilities. Nowadays, however, there is a widespread conviction that even the most unexpected development of the pulsejet will find only limited applications in military and civilian technology.

The idea of exploiting the phenomenon discovered by Huygens in the occurrence of an overpressure in a container due to a sudden expansion of compressed gas to the construction of engines has recurred several times during the past fifty years. However, only in 1930 did Paul Schmidt give some concrete form to these ideas. His engine, developed for over ten years in German industrial and academic laboratories, was used as the main propulsion unit of the first large scale flying missile in history.

The fundamental progress in the development of the pulsejet was achieved in 1950 by the introduction of an improved version of Bertin's idea of replacing mechanical ports with inertia gas ports. Further research aimed at reducing the engine's dimensions and improving its ef-

iciency, mainly by trying to induce detonation combustion, has failed so far to produce results.

7.1. WAVE THEORY OF PULSEJETS

The basic processes occurring in a pulsejet are most easily described by means of the wave model. Assuming a cylindrically shaped engine, instantaneous ignition of the entire mixture volume (and therefore isochronous compression of the thermodynamic agent within the mixture-filled region), isentropic expansion of the gas following the explosion and assuming that the problem is governed by laws of plane waves in a perfect gas, the following sequence of phenomena taking place during a working cycle can be discerned (Fig. 7.1).

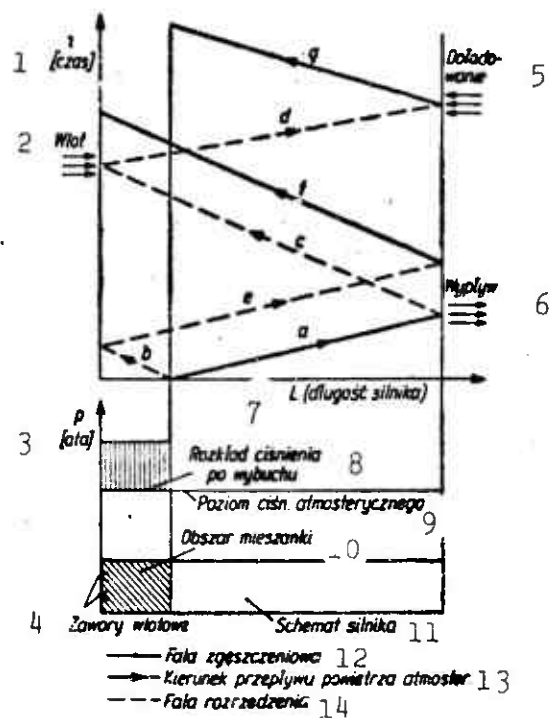


Fig. 7.1. Theory of operation for a pulsejet. 1) Time; 2) inlet; 3) atmospheres; 4) inlet ports; 5) charge; 6) outlet; 7) L (engine length); 8) pressure distribution after detonation; 9) level of atmospheric pressure; 10) mixture region; 11) engine diagram; 12) compression wave; 13) direction of atmospheric air flow; 14) rarefaction wave.

At the instant of ignition, two waves are initiated in the engine at the boundary between the regions of atmospheric and increased pres-

sure: a compression wave *a* directed toward the outlet and a rarefaction wave *b* moving toward the inlet which is closed by the inlet ports. Inflow is initiated at the instant that the compression wave reaches the engine's open end. The compression wave *a* reflects from the channel's open end as the rarefaction wave *c*. During this time, due to the outflow, the pressure in the combustion zone drops to the atmospheric level so that the incoming rarefaction wave *c* creates a partial vacuum.

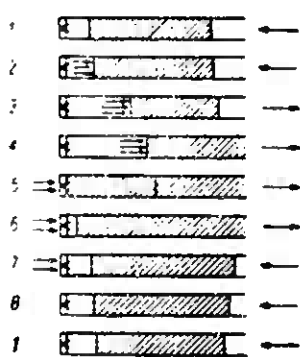


Fig. 7.2. Working cycle of a pulsejet.

The inlet ports open as a result of this partial vacuum and new mixture flows into the engine. The rarefaction wave *c* reflects from the opening inlets as the rarefaction wave *d* which causes an overpressure at the pipe's open end. As a result of this, atmospheric air flows into the engine from the outlet end.

The course of the above-described phenomena can be visualized by means of diagrams (Fig. 7.2) representing the working cycle of a pulsejet.

The top diagram, 1, represents the condition at the end of the cycle; a new mixture charge flows in through the inlet port, the tube's midsection is filled with combustion products from the previous cycle, and air is in the vicinity of the outlet, since it flowed in from the rear.

The next diagrams, 2, 3, 4, represent the conditions immediately following ignition. The small arrows indicate the action of the pressure caused by combustion: the column of gases is pushed to the rear. Due to this column's inertia (or what amounts to the same thing) due to the effect of rarefaction waves, an overpressure is created in the engine (especially in the vicinity of the inlet port) causing suction

of a new mixture charge, which is denoted by arrows in diagrams 5, 6, 7.

Air enters the engine through the outlet opening and is expelled during the next cycle (diagrams 7 and 8).

7.2. TRANSIENT FLOW OF GASES THROUGH A PULSEJET

In the analysis of isentropic unsteady flow, the starting equations are the equations of conservation of mass, conservation of momentum and the isentropy equation

$$\frac{\partial \rho}{\partial t} + \frac{\partial(\rho u)}{\partial x} = 0 \quad (7.1)$$

$$-\frac{\partial p}{\partial x} = \rho \left(\frac{\partial u}{\partial t} + \frac{\partial u}{\partial x} u \right) \quad (7.2)$$

$$p \rho^\kappa = \text{const} \quad (7.3)$$

where p and ρ are gas pressure and density; u is the flow velocity; t is time; x is the coordinate; κ is the isentropic coefficient.

Introducing the speed of sound which is given by the expression

$$a = \sqrt{\kappa \frac{p}{\rho}} \quad (7.4)$$

we obtain the following transformation of the isentropic equation

$$a \rho^{\frac{1-\kappa}{2}} = \text{const} \quad (7.5)$$

$$a p^{\frac{1-\kappa}{2\kappa}} = \text{const} \quad (7.6)$$

or in differential form

$$d\rho = \frac{2}{\kappa - 1} \rho \frac{da}{a}$$

$$dp = \frac{2\kappa}{\kappa - 1} p \frac{da}{a}$$

After substitution of the above equations into Expressions (7.1) and (7.2), we obtain the following set of equations

$$\begin{aligned} \frac{\partial a}{\partial t} + u \frac{\partial a}{\partial x} &= -\frac{2}{\kappa - 1} a \frac{\partial a}{\partial x} \\ \frac{\partial a}{\partial t} + u \frac{\partial a}{\partial x} &= -\frac{\kappa - 1}{2} a \frac{\partial u}{\partial x} \end{aligned} \quad (7.7)$$

Solutions satisfying this set of equations are:

$$\begin{aligned} u &= u_0 = \text{const} \\ a &= a_0 = \text{const} \end{aligned} \quad (7.8)$$

or

$$\begin{aligned} a &= a_0 \mp \frac{\kappa - 1}{2} u \\ u &= \frac{2}{\kappa + 1} \frac{x \pm a_0 t}{t + t_0} \end{aligned} \quad (7.9)$$

The solution given by Eq. (7.9) represents a linear wave set. The wave velocity c can be determined by appropriately transforming Eq. (7.9) and then differentiating it with respect to time. We then obtain

$$\frac{dx}{dt} = c = u \mp a \quad (7.10)$$

Therefore the wave propagation speed consists of the velocity u of the gas within which the wave travels and of the speed of sound a . Since the process under discussion is isentropic in nature, the quantity c is the velocity of propagation of weak (acoustic) waves. When this velocity is directed along the positive direction of the x -axis, the quantity $u + a$ represents the wave's propagation speed with respect to the x -axis and in the positive direction; on the other hand, the quantity $u - a$ represents the propagation velocity in the negative x direction (for the case of $u < a$).

Equations

$$\frac{dx}{dt} = u + a \quad \text{and} \quad \frac{dx}{dt} = u - a$$

in the x, t plane represent two families of lines along which the expressions

$$\begin{aligned} \frac{a}{\kappa - 1} + \frac{u}{2} &= r \\ \frac{a}{\kappa - 1} - \frac{u}{2} &= s \end{aligned} \quad (7.11)$$

remain constant and are called Riemann's invariants. These lines are

called the characteristics of the set of differential equations. Knowing the behavior of two characteristics, it is possible, based on the knowledge of the invariants s and r , to determine the flow velocity and the speed of sound from the above models by adding and subtracting Eqs. (7.11) from

$$\begin{aligned}\frac{u}{2} &= \frac{r-s}{2} \\ \frac{a}{\kappa-1} &= \frac{r+s}{2}\end{aligned}\tag{7.12}$$

7.3. ANALYSIS OF THE OUTPUT OF A PULSEJET BASED ON THE METHOD OF CHARACTERISTICS

There are a number of methods of analysis and computation of the performance of a pulsejet based on the method of characteristics [7.2, 7.3, 7.8]. They differ mainly in the assumptions made as to the course of the combustion process. In Section 7.1 the combustion process was reduced to an instantaneous pressure increase. Schultz-Grunow [7.2] proposes replacing it by a series of isentropic steps spread out in time. Each such pressure step will generate a pair of waves: a compression and a rarefaction wave which will propagate in opposite directions along the engine.

These waves, computed by Schultz-Grunow, are illustrated in Fig. 7.3. These computations were based on the following assumptions. The engine consists of a channel of constant cross section. The combustion mixture fills 1/7 of the engine's length. Atmospheric air, mixture and combustion products have the same physical properties. Pressure increase during combustion corresponds to the increase in the speed of sound (due to the isentropic compression which replaces combustion in the assumed model) $\Delta a = 0.14 a_1$ and takes place in 1/15 of the time needed by the wave to traverse the length of the engine at the speed of sound a_1 which corresponds to the temperature of the atmospheric

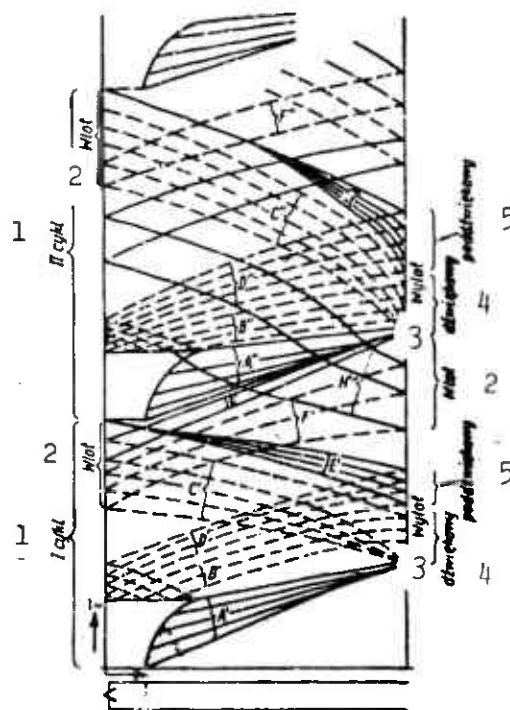


Fig. 7.3. Development of waves in a pulsejet during the first two working cycles. 1) Cycle; 2) inlet; 3) outlet; 4) sonic; 5) subsonic.

air. On that basis, a pressure increase to 2.5 times the ambient pressure level requires approximately $1/5$ of the working-cycle time. The ratio of the maximum effective inlet port area to the engine's cross section is 0.4. The coordinates were taken as dimensionless time $\tau = ta_1/L$ and dimensionless length $\zeta = x/L$, where L is the engine length, x is the coordinate and t is time.

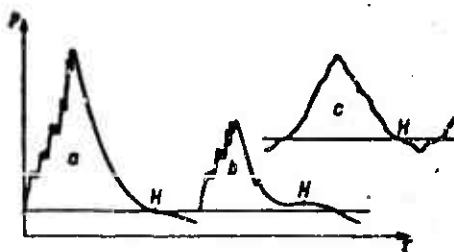


Fig. 7.4. Pressure variation as a function of time at the engine's outlet cross section. a and b) Theoretical variations during the first and second cycle; c) actual variation obtained by means of an oscilloscope.

Waves A' and A'' shown in Fig. 7.3 are caused by combustion during the first and second cycles; they initiate the outflow of combustion products at the speed of sound and at a pressure higher than atmospheric. In view of this, some of the rarefaction waves in the group B' and B'' reflect from the channel's open end with the same sign, until the overpressure is eliminated. Opening of the ports causes waves C' and C'' which initially reflect as rarefaction waves F' and F'' , and then (once the ports are fully open) as compression waves G' , except that the waves G' occur only during the first cycle. The first cycle exerts an influence on the second one mainly through waves E' and F' . Compression waves E' ignite the fresh charge. The second cycle begins with this ignition. Rarefaction waves F' reflect from the open end as compression waves H' and cause at that spot a flow of air into the engine with the maximum speed of $u/a_1 = 0.18$. This air occupies approximately $1/8$ the length of the channel. Graphs illustrating the pressure variation as a function of time at various engine cross sections can be prepared on the basis of Fig. 7.3. Figure 7.4 shows such graphs for the exit cross section.

The elevations H marked on these graphs are due to the H' waves reflecting as compression waves from the initially partly closed inlets. Therefore this phenomenon is tied to the operation of the inlets. The stiffer the ports and the greater their mass, the more pronounced these elevations.

7.4. MIXTURE GENERATION, IGNITION AND COMBUSTION DEVELOPMENT IN A PULSEJET

Figure 7.5 shows superimposed on the same graph the pressure variation as a function of time at the front engine cross section and the position of the inlet ports. These ports open and close almost instantaneously. In the open state, these ports are subjected to vibrations.

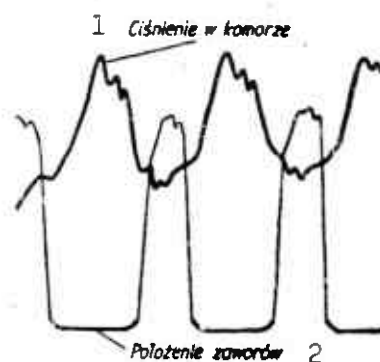


Fig. 7.5. Pressure distribution as a function of time, at the front engine cross section superimposed on the sequence of operation of the inlet ports. 1) Chamber pressure; 2) inlet port position.

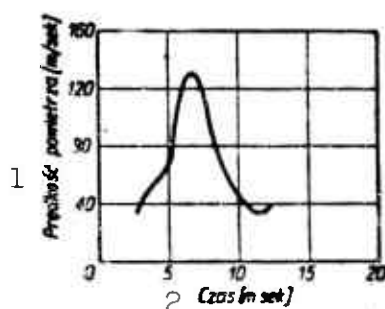


Fig. 7.6. Air velocity distribution as a function of time in the front engine cross section. 1) Air velocity (m/sec); 2) time (msec).

The inlet open time accounts for 40% of the entire cycle.

Fuel is injected into the flow of fresh air entering the engine. Due to a more or less constant injector output and a variable air velocity (Fig. 7.5), mixture composition is a function of time.

At the beginning of the charging cycle the mixture is very rich, then it gets leaner and at the end of the cycle it gets richer again.

Since each of the parameters having an effect on drop size and concentration, such as temperature, flow velocity in the vicinity of the injector and evaporation rate, vary within wide bounds, the mixture is very nonhomogeneous; it consists of two distinct layers: a highly enriched layer with fuel and combustion products from the previous cycle and a cold layer arising at the end of the suction cycle.

This mixture inhomogeneity causes a noticeable drop in its combustible properties. Proper engine operation is achieved with a mixture composition consisting of an air excess ratio $\alpha = 1.1$ to 1.4 .

There are two theories explaining the ignition mechanism in pulse-jet engines. According to the first one [7.2], ignition is initiated by the compressive waves which halt mixture entry into the engine. However, it is most unlikely that a pressure increase of the order of 0.3 kgf/cm^2 could cause ignition of a mixture which could be preheated somewhat due to intermixing with combustion products left over from the previous cycle.

According to the second hypothesis [7.6], ignition is initiated by the flame remaining from the terminal combustion of the preceding cycle. Photographs of individual phases of the engine charging process seem to confirm this hypothesis. Mean mixture temperature before ignition is at least 600°K (and often reaches 1000°C), whereas $1/3$ of the mixture volume has a higher temperature than the mean. Part of the mixture ignites even before completion of the charging process. Once the ports are closed, mixture motion ceases and the flame front surrounding the fresh mixture from all sides (also from the lateral surfaces) moves toward the inlet ports with a velocity on the order of 50 to 90 m/sec. Toward the end of the combustion process the speed of flame propagation with respect to the engine decreases because of the expansion of that part of the mixture which has not yet burned.

The combustion process most likely consists of two phases: an initial combustion which gradually takes over the entire combustion chamber and which increases the pressure and temperature in the chamber thereby facilitating the evaporation of the remaining unburned mixture, and a main combustion occurring almost instantaneously in the entire chamber and lasting about 25% of the entire cycle.

Measurements of instantaneous temperatures in the engines have shown that maximum combustion temperatures attain approximately 2000°K due to the mixture's low combustibility. Engine wall temperature (amounting to 400-500°C in the vicinity of the chamber) has no effect on combustion. During start-up, steady engine output is attained within a fraction of a second, during which wall temperature rises slightly.

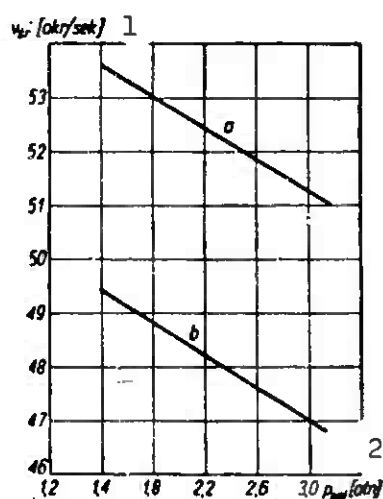


Fig. 7.7. Mean pulsation frequency ν_{sr} as a function of fuel pressure p : a) engine length is 3350 mm; b) engine length is 4300 mm. 1) (Cycles/sec); 2) (atmospheres).

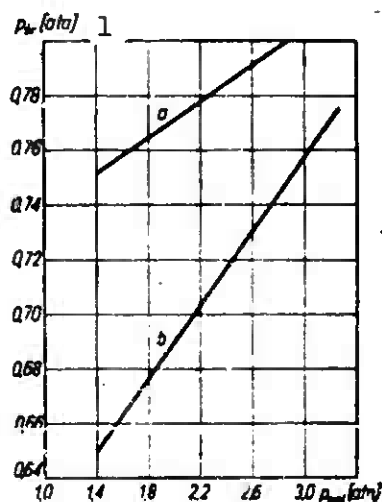


Fig. 7.8. Mean pulsation amplitude as a function of fuel pressure [same legend as in Fig. 7.7]. 1) (Atmospheres).

The second ignition hypothesis described above (from the flame remaining from the terminal combustion of the preceding cycle) is further verified by two facts:

First of all, the frequency of pulsations in the engine (Fig. 7.7) is almost insensitive to fuel quantity and is not proportional to engine length despite noticeable differences in the total pressure amplitude (Fig. 7.8).

If ignition were a function of the waves which stopped mixture motion, the pulsation frequency should be inversely proportional to engine length and should increase with an increase of added fuel (because of an increase in the mean gas temperature and pressure, and therefore an increase in the turbulence propagation rate).

Second; noticeable changes in the duration of the several engine cycles, which on the average amount to 15-20% of the entire cycle, should be taken as a rule; and this can be explained only by the probable occurrence of ignition.

It must be recognized, however, that optimum efficiency will be achieved only in that engine in which ignition occurs at the instant at which the compression waves reach the combustion chamber. In the event of a lack of synchronization between these times, low-frequency changes in pressure amplitudes take place, and these can often lead to an interruption of engine operation.

7.5. PORTLESS ENGINES

The mechanical, spring loaded type ports (Fig. 7.9) most often used in pulsejet engines have a number of disadvantages, the most important of which are:

- short life, presently amounting at most to 50 hours;
- good performance only at engine frequency corresponding to port natural frequency;

- inadequacy of adaptation to large altitude variations due to great changes in air density. Inlet port opening is caused by the absolute pressure difference across the port. Since this difference decreases with flight altitude, the width of the inlet opening decreases, which in turn decreases the fresh air charge. In addition to a number of phenomena such as drop in combustibility, as a result of a decrease in absolute pressure and temperature of the mixture in the combustion chamber, this inlet performance sets a ceiling on pulsejet engines;

- during port opening, the resistance due to its spring load must be overcome. This is especially important in the case of short engines (used, for instance, for the propulsion of propeller-driven planes) operating at high frequencies (around 150 Hz). Use of thin ports to decrease their stiffness is not indicated since it reduces their life.

These disadvantages of mechanical ports have forced designers to search for a nonmechanical method for controlling the flow in this type of engine.

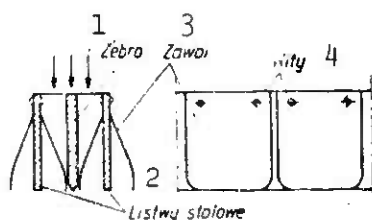


Fig. 7.9. Spring loaded ports. 1) Rib; 2) steel leaf; 3) port; 4) rivets.

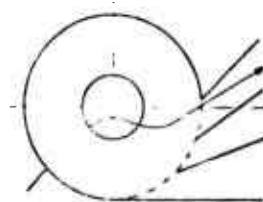


Fig. 7.10. Theory of operation of a "hydraulic flap."

Two innovations have been introduced which have completely eliminated moving parts from pulsejet engines. These are: ports of the "hydraulic-flap" type and gas inertia ports.

The first one of these is illustrated in Fig. 7.10.

Fresh mixture (or fresh atmospheric air) flows into the engine as

indicated by the arrow. On the other hand, when an overpressure exists in the engine, the combustion products are forced into rotary motion of ever-decreasing radius during the intake period. This results in a velocity increase, because of the irrotationality of the flow, thus accelerating the working fluid. In direct consequence of this phenomenon, a force is created which retards the gas outflow. Figure 7.11 illustrates an implementation based on the same principles but better adapted to practical applications.

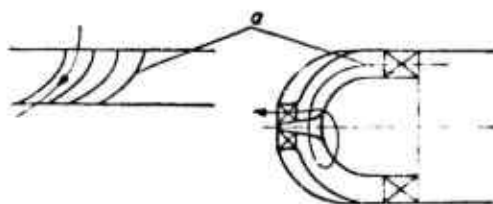


Fig. 7.11. Inlet of a pulsejet engine equipped with a "hydraulic flap":
a) jet vanes imparting rotational motion to the outflowing stream of combustion products (in the direction of the arrow).

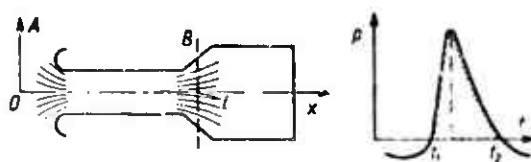


Fig. 7.12. Theory of operation of a gas inertia port.

The theory of operation of the gas inertia port is illustrated in Fig. 7.12.

Air flowing into the engine through the inlet conduit reaches a velocity u toward the end of the charging process.

In order to reverse the flow, that is, in order for that particle which at the instant of ignition is located at point A (and for which point B is the turn-around point) to be at that same spot at the end of the combustion process, an appropriate p must arise in the combustion chamber. This pressure must produce momentum (whose measure is

given by the shaded area in Fig. 7.12) capable of counterbalancing the change in momentum which will occur in the engine inlet nozzle during the time from t_1 to t_2 , that is, during the combustion time.

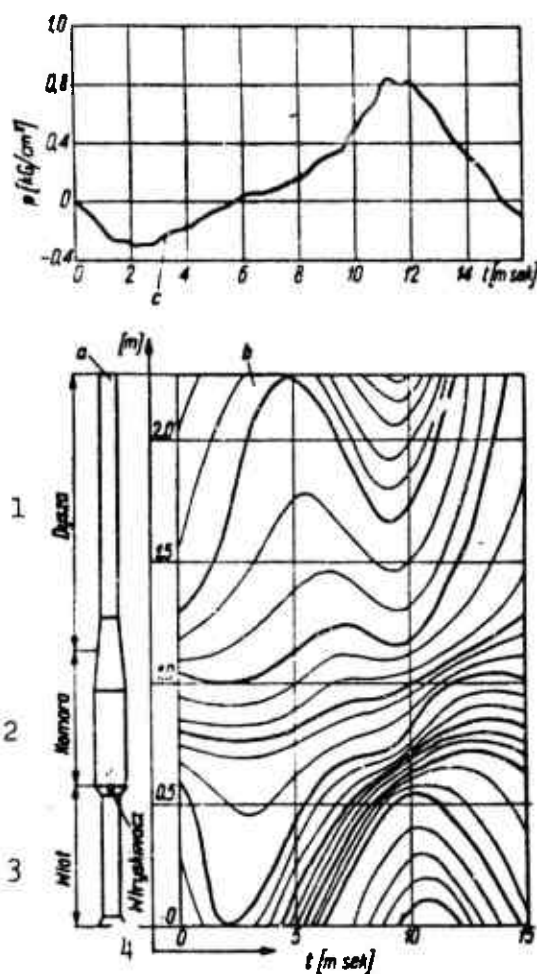


Fig. 7.13. Portless pulsejet engine: a) engine diagram; b) engine flow graph; c) pressure variation in the combustion chamber as a function of time. 1) Nozzle; 2) combustion chamber; 3) inlet; 4) injector.

Starting with the equations of conservation of momentum and flow continuity (for a constant cross section duct)

$$\frac{\partial p}{\partial x} + \rho \left(u \frac{\partial u}{\partial x} + \frac{\partial u}{\partial t} \right) = 0 \quad (7.13)$$

$$\rho \frac{\partial u}{\partial x} = 0$$

the following relation is obtained after transformation and integration:

$$p(t_2) = \rho l (u_1 - u_2) \quad (7.14)$$

where ρ is the density; u_1 and u_2 are the velocities at times t_1 and t_2 .

Substitution $\rho = 0.12 \text{ kgf-sec}^2/\text{m}^4$, $u_1 = u_2 = 100 \text{ m/sec}$ and $l = 0.5 \text{ m}$, yields

$$p(t_2) = 12 \text{ kgf-sec}/\text{m}^2.$$

Assuming that $t_2 - t_1 = 0.005 \text{ sec}$ the average combustion chamber overpressure can be computed to be 0.24 atm, which corresponds to a maximum pressure of 0.5 atm. In 1950 Bertin took advantage of this fact to build a portless pulsejet engine (that is, one without mechanical ports). A diagram of such an engine together with an illustration of the flow phenomena and pressure variation as a function of time (in the combustion chamber) is shown in Fig. 7.13 [7.4].

The theory of operation of a portless engine is the following. The combustion products created after detonation flow simultaneously through the inlet duct (called a detector) as well as through the nozzle. As a result of the inertia of both these streams, an overpressure is created in the engine's combustion chamber. But the inertia of the flow issuing through the nozzle is greater so that the outflow through the inlet port will terminate earlier and it is through this latter port that fresh air will start to flow into the engine. This air, mixing with the fuel continuously injected into the combustion chamber, forms the combustible mixture which will ignite from the smoldering combustion products remaining from the previous cycle, at an appropriate time after termination of the charging process.

7.6. CHARACTERISTICS OF PULSEJET ENGINES

7.6.1. Effect of Engine Shape on Its Output

From an aerodynamic point of view, it would be advantageous to make the pulsejet engine in the shape of a cigar (Fig. 7.14). However,

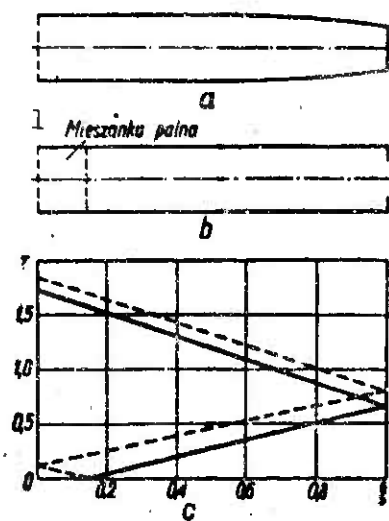


Fig. 7.14. Wave path in an aerodynamically shaped engine: a) aerodynamically shaped engine; b) substitute shape (cylindrical duct with a half open outlet; c) wave path. 1) Combustible mixture.

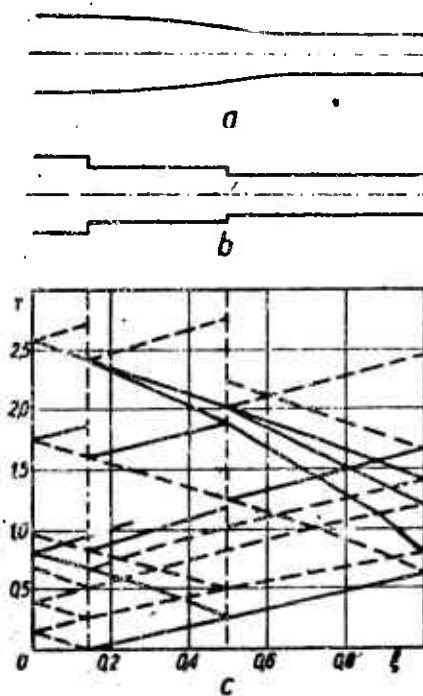


Fig. 7.15. Operation of a pulsejet engine having an enlarged combustion chamber: a) engine with enlarged combustion chamber; b) substitute shape; c) wave path.

it can be proved by means of the wave theory discussed above, that proper operation of such an engine is doubtful. The result of the wave theory is the condition for proper engine operation that upon reflec-

tion from the duct's open end two waves are generated, one being a rarefaction wave and the other a compression wave. If in order to facilitate the analysis, the aerodynamically shaped engine is replaced with a cylindrical duct terminated by a half open outlet, then as can be seen from the graphs in Fig. 7.14 the order of these waves is reversed.

This will obviously prevent suction as well as mixture ignition at the proper instant and will disturb the continuity of engine operation.

The above derivation was backed by static tests during which an attempt to start up an aerodynamically shaped engine, shown in Fig. 7.14, proved to be futile [7.2].

The shape giving proper operation without simultaneously maximizing aerodynamic drag is shown in Fig. 7.15.

Characteristic features of such an engine (with a combustion chamber wider than the outlet duct) are a longer charging time (with a lower pressure differential causing suction) and the occurrence of a weaker compression wave than in a cylindrical engine. However, as has been shown during the analysis of the ignition and combustion processes, these phenomena should not seriously affect the course of the engine operation.

Engines having the above shape have found useful applications.

7.6.2. Effect of the Size of the Inlet Cross Section on Engine Operation

The magnitude of the mixture charge sucked in during a cycle increases with an increase in the inlet cross section (Fig. 7.16).

However, at the same time the ignition and combustion conditions are impaired. Increase in mixture charge causes a drop in its temperature increase due to interaction with combustion products left over from the previous cycle. Also, the contact area between the mixture

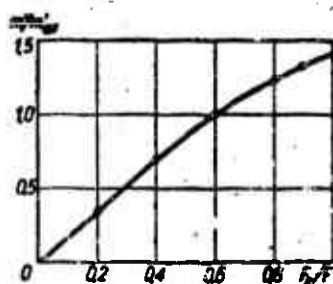


Fig. 7.16. Dependence of the charge of the new mixture sucked in during one cycle on the ratio of the engine outlet cross sectional area F_0 to the cross sectional area of the outlet duct F : $m'_{0.6}$ is the mixture charge corresponding to $F_0/F = 0.6$; m' is the mixture charge for the given ratio F_0/F .

and the remaining flame, which causes ignition, decreases. Under these conditions, as the ratio F_0/F increases, the mixture burns more and more sluggishly and the combustion process assumes an ever-increasing isobaric character (which obviously tends to decrease engine performance).

These two opposite trends: increase in the output of the working fluid and the decrease in engine performance, bring about the existence of an optimum value for the ratio F_0/F between 0.2 and 0.4 which is equally applicable to engines with and without ports.

7.6.3. Speed Characteristic of a Pulsejet Engine

Figure 7.17 illustrates schematically the characteristic operating features of a pulsejet engine at standstill and at a high flight velocity. The effect of flight velocity shows itself in an increase in charge and a decrease in supercharge.

Engine charge (Fig. 7.18) increases with an increase in flight velocity: at first slowly, and then starting at $M_0 = 0.5$ at an increasingly faster rate.

This comes about because of the increase in the pressure difference across the ports. As in the case of an improper ratio of inlet and outlet engine cross sections, this causes a drop in engine per-

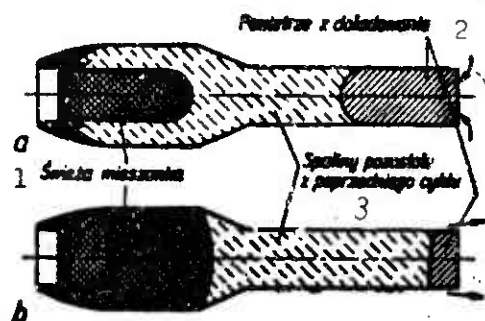


Fig. 7.17. Pulsejet engine: a) operation at standstill; b) operation in flight. The diagrams illustrate the condition immediately before ignition. 1) Fresh mixture; 2) air from supercharge; 3) combustion products left over from the previous cycle.

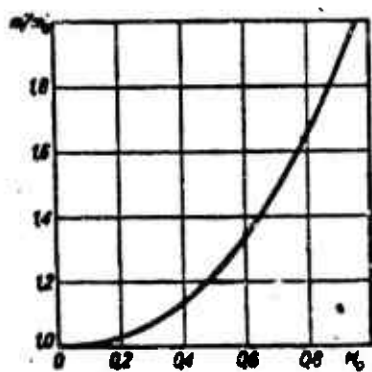


Fig. 7.18. Effect of the Mach number M_0 in free flow in front of the engine, on the latter's charge: m') charge at the given Mach number; m'_0) charge at $M_0 = 0$.



Fig. 7.19. Pulsejet engine with an inlet screen which reduces the effect of flight velocity on its performance.

formance due to sluggish combustion. The decrease in supercharge, that is, a decrease in the quantity of air which is sucked into the engine from the rear, is caused by the ejection effect of the flow streaming around the engine. Together these two phenomena cause, in conjunction with the increase in flight speed, a drop in thrust and an increase in the unit fuel consumption of the pulsejet engine. The graph in Fig.

7.22a shows the speed characteristic of a pulsejet engine using ports. Starting between $M_0 = 0.5$ and 0.8 (depending on the ratio F_0/F) the thrust of a pulsejet engine with ports begins to drop and its unit fuel consumption begins to rise.

Portless pulsejet engines are even more sensitive to the effects of speed (Fig. 7.24a). The effect of thrust decrease with increasing flight velocity can be compensated for to some extent by placing specially contoured screens at the engine inlet (Fig. 7.19). The inlet port should be so placed inside the screen that a constant dynamic pressure is present in front of the inlet ports regardless of the flight speed.

7.7. THRUST OF A PULSEJET ENGINE

The thermodynamic cycle most often used to compare the performance of pulsejet engines is Lenoir's cycle (Fig. 7.20).

Theoretical efficiency of this cycle is given by the relation:

$$\eta_t = 1 - \kappa \frac{\left(\frac{p_1}{p_0}\right)^{\frac{1}{\kappa}} - 1}{\left(\frac{p_1}{p_0}\right) - 1} \quad (7.15)$$

Since the process 0-1 is one of constant volume, then:

$$\frac{p_1}{p_0} = \frac{T_1}{T_0}$$

The isochoric compression which determines the comparative efficiency of pulsejet engines is a function of the ratio of combustion temperature to the temperature of fresh air flowing in. Since combustion temperature is a function of the excess air coefficient, it is advantageous to use nearly stoichiometric mixtures in pulsejet engines. In the case of common technical conditions and for a stoichiometric mixture, the efficiency of Lenoir's cycle is

$$\eta_t = 0.28.$$

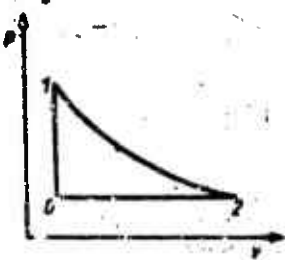


Fig. 7.20. Lenoir's cycle.

Theoretical work performed by a charge sucked in during one cycle is given by the equation:

$$L'_t = 427 B' W u \eta_i \quad (7.16)$$

where B' is the fuel weight contained in one charge; Wu is the fuel heating value.

During an actual work cycle, several energy losses occur in the engine. These losses are due to incomplete combustion, heat loss to the surroundings, friction between fluid and walls and a nonuniform velocity distribution in the stream. All these losses decrease efficiency; the resulting efficiency is called, by analogy with the efficiency of piston engines, the indicated efficiency η_i .

Useful work performed by individual charges can then be expressed by the relation:

$$L'_t = \eta_i L'_t \quad (7.17)$$

The useful energy is equal to the increase in the kinetic energy of the combustion products issuing out of the engine nozzle:

$$L'_t = \frac{G'_1 + G'_2}{2g} (\bar{w}_a)^2 \quad (7.18)$$

where G'_1 is the mixture weight (charge weight) sucked in through the engine inlet during one cycle; G'_2 is the weight of air sucked in through the engine outlet during one cycle (weight of supercharge air).

From this, the average flow velocity is

$$\bar{w}_a = \sqrt{2g \eta_i \frac{L'_t}{G'_1 + G'_2}} \quad (7.19)$$

Introducing:

the supercharge coefficient $\lambda = G'_2/G'_1$

and the work obtained from 1 kg of mixture $L_t = L'_t/G'_1$,

the relation for the mean outflow velocity is obtained in the form:

$$\bar{w}_e = \sqrt{\frac{2}{1+\lambda} g \eta_i L_i} \quad (7.20)$$

The rate of expenditure of the working fluid in a pulsejet engine amounts to

$$G = (G'_1 + G'_2) \nu = \nu G'_1 (1 + \lambda) = G_1 (1 + \lambda) \quad (7.21)$$

where ν is the pulsation frequency; G_1 is the mixture (charge) expenditure rate.

From the above equations the equation for the static thrust of the pulsejet engine is obtained:

$$S = \frac{G}{g} \bar{w}_e = G_1 \sqrt{\frac{2(1+\lambda)}{g}} \eta_i L_i \quad (7.22)$$

On the basis of experimental data, it can be assumed for computational purposes that η_i lies between 0.2 and 0.3 and λ lies between 0.25 and 0.5.

7.8. DETERMINATION OF THE CHARACTERISTIC ENGINE DIMENSIONS

Characteristic engine dimensions are computed on the basis of statistical data. The starting parameter is the thrust coefficient

$$C_g = S/pF \quad (7.23)$$

where S is the thrust (kgf); p is the atmospheric pressure (kgf/cm²); F is the nozzle cross sectional area (cm²).

It has been verified that the thrust coefficient is approximately equal to the maximum overpressure (expressed in atmospheres) in the combustion chamber. On the average it is equal to 0.25-0.35.

Assuming a value for C_g and knowing the thrust, we can compute the nozzle diameter d .

Combustion chamber diameter D and engine length L are computed on the basis of the equation

$$D/d = 1.5-1.7 \text{ and } L/d = 8-10.$$

Combustion-chamber length is determined in such a way that its volume be equal to between 1/7 to 1/5 of the volume of the entire en-

gine. The effective surface area of inlet ports should be equal to approximately 30% of the nozzle area.

Engine pulsation frequency is computed by treating it as an organ column open at one end. In view of the above assumption, the following relations are of interest

$$\nu = \frac{a}{4L}; \quad a = \sqrt{\gamma R T}; \quad T = \frac{2}{\gamma + 1} T_s$$

where ν is the frequency; R is the gas constant; a is the speed of sound in the nozzle; T_s is the combustion temperature (equal to approximately 2000°K).

7.9. DESIGN SOLUTIONS OF PULSEJET ENGINES

A dimensional diagram of a pulsejet engine with ports, having a nominal thrust of 500 kgf is shown in Fig. 7.21.

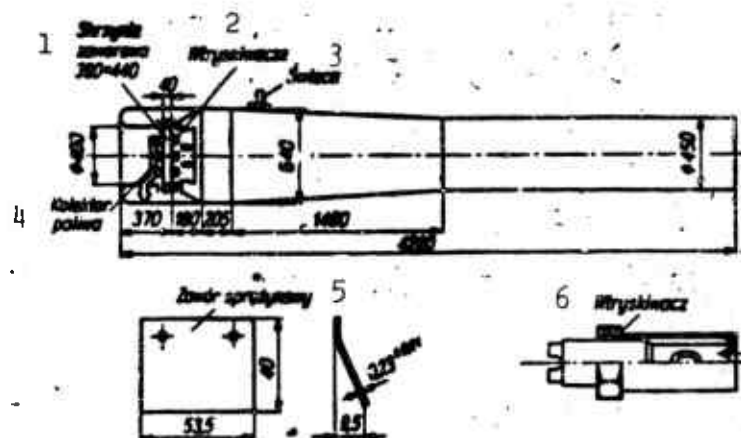


Fig. 7.21. Design diagram of a pulsejet engine with ports. 1) Inlet port manifold; 2) injectors; 3) spark plug; 4) fuel manifold; 5) spring loaded port; 6) injector.

The engine consists of the body, inlet manifold, injector and a properly shaped intake. In the body one can discern a cylindrical nozzle and a conical combustion chamber. The spark plug is located on the combustion chamber wall. In addition to the injectors, conduits feeding in compressed air which facilitates start-up have been placed in

the inlet port manifold. The inlet port manifold is in the shape of a rectangle and consists of ribs against which rest the spring inlet ports which are riveted to steel supports. The speed, altitude and choking characteristics of this engine are shown in Fig. 7.22.

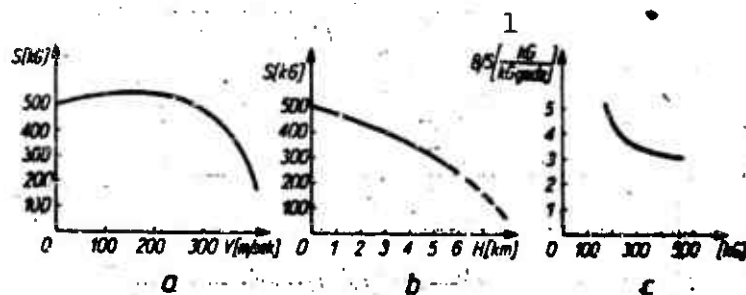


Fig. 7.22. Characteristics of the engine shown in Fig. 7.21: a) speed; b) altitude; c) choking. 1) (kg/kgf hour).

This engine is designed to propel drones and guided missiles; its nominal flight speed is 900 km/hr. The engine body is made out of corrugated steel sheet (3 mm corrugations). Total weight is 190 kg.

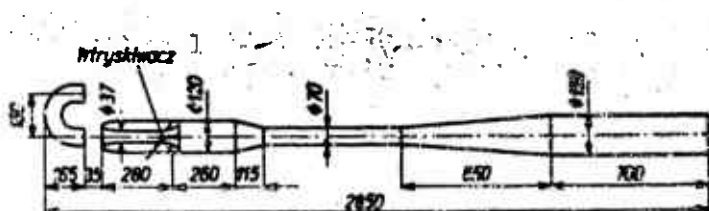


Fig. 7.23. Portless pulsejet engine having a 10 kg thrust. 1) Injectors.

Figure 7.23 shows a design diagram of a portless pulsejet engine with a nominal thrust of 10 kg. This engine is used to propel gliders. Its weight is 4.8 kg. It consists of a body, a streamlined inlet duct and of a properly shaped tube placed in front of the inlet to recover the flow of combustion products blown through the inlet during combustion in the chamber.

The exit nozzle is divergent so as to increase the supercharge flow.

Figure 7.24 shows the speed and choking characteristics of this engine.

It is seen from the speed characteristic that an engine with a divergent nozzle is very sensitive to an increase in flight velocity. However, at low velocities the unit fuel consumption of such an engine is comparatively small (1.8 compared to 3).

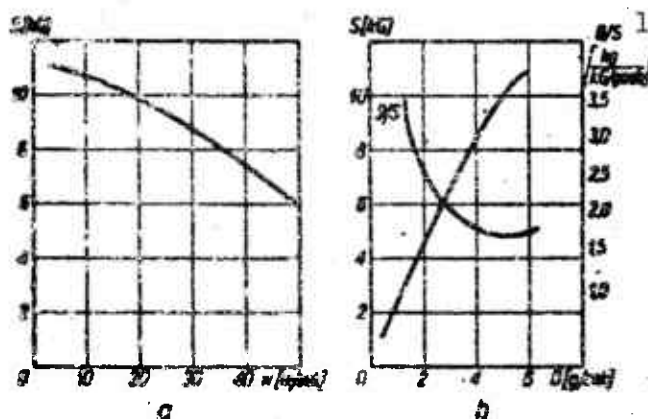


Fig. 7.24. Characteristics of a portless pulsejet engine: a) speed; b) choking. 1) (kg/kgf hour).

7.10. PULSEJET ENGINE WITH DETONATION COMBUSTION

It appears at present that the most important avenue of pulsejet engine development is indicated by the experimental achievement of detonation combustion.

The basis of operation of a detonation pulsejet engine is based on the obvious fact that a detonation wave running through a constant cross section duct can be a source of thrust. Thrust arises as a result of a pressure difference across the wave which corresponds to an increase in the momentum of the gas flowing through the duct.

A diagram of flow with combustion in a detonation wave is shown in Fig. 7.25.

The detonation wave reflecting from the open end creates a rare-

faction wave. This is based, however, on a subsonic outflow of the combustion products compressed by the wave (the condition $p_2/p_1 \leq 1.94$ must be satisfied).

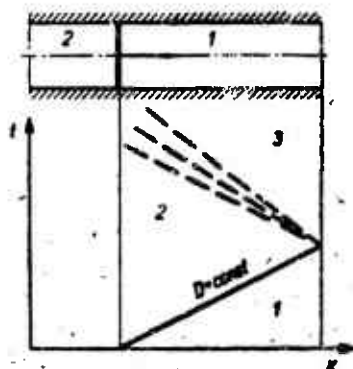


Fig. 7.25. Flow diagram in the case of detonation combustion: 1) region in front of the detonation wave; 2) region behind the detonation wave; 3) region behind the rarefaction wave.

The occurrence of intermittent detonation combustion in a constant cross section duct, one end of which is open with a spark plug which causes ignition at the other end, takes place in a fashion similar to that of conventional pulsejet engines. In a one-shot work cycle, the following processes can be distinguished: mixture injection, mixture ignition from an electrical spark, creation and motion of a detonation wave, creation and motion of a rarefaction wave, outflow of combustion products and finally the filling up of the engine with fresh mixture.

Figure 7.26 shows a detonation pulsejet engine operating as described above.

The nature of thrust variations as a function of time in this engine is shown in Fig. 7.27.

With introduction of the symbols given in Fig. 7.27, the mean thrust can be expressed by the following equation:

$$\bar{S} = \frac{\int_0^t S dt}{t_s} = \frac{F(t_d + t_r)}{t_s}$$

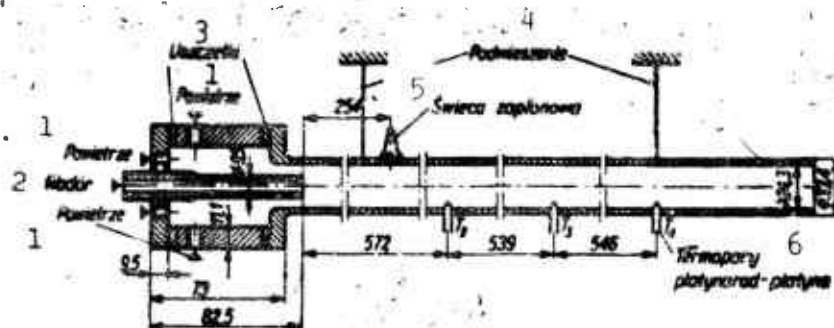


Fig. 7.26. Detonation pulsejet engine working with a hydrogen-air mixture. 1) Air; 2) hydrogen; 3) gaskets; 4) suspension; 5) spark plug; 6) thermocouples platinum rhodium-platinum.

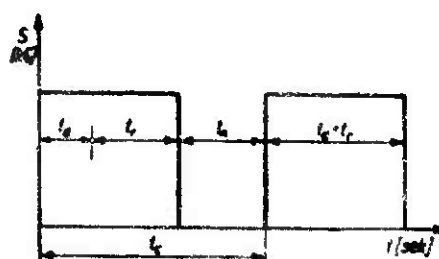


Fig. 7.27. Thrust variation as a function of time: t_e) duration of one cycle; t_d) travel time of the detonation wave; t_r) travel time of the rarefaction wave; t_n) duration of engine fill up time with fresh mixture.

whereas the thrust S is given by

$$S = F(p_2 - p_1) = F p_1 \left(\frac{p_2}{p_1} - 1 \right)$$

By appropriate transformation of this equation, the following expression for the mean thrust is obtained:

$$\bar{S} = F p_1 \frac{t_d + t_r}{t_e} \left[\frac{1 + \kappa_2 M_1^2}{1 + \kappa_2} \left(1 - \frac{\kappa_2 - 1}{2} M_2 \right)^{\frac{2\kappa_2}{\kappa_2 - 1}} \right] \quad (7.24)$$

whereas the expression for the specific impulse is:

$$I = \frac{\bar{S}}{W_p + W_0} = \frac{p_1 (t_e + t_r) \left[\frac{1 + \kappa_2 M_1^2}{1 + \kappa_2} \left(1 - \frac{\kappa_2 - 1}{2} M_2 \right)^{\frac{2\kappa_2}{\kappa_2 - 1}} \right]}{L [\gamma_p f + \gamma_0 (1 - f)]} \quad (7.25)$$

where F is the engine cross sectional area; κ_1 and κ_2 are the isen-

tropic exponents of the mixture and combustion products, respectively; M_1 and M_2 are Mach numbers in front of and behind the wave; γ_p and γ_0 are the specific weights of fuel and oxidizer (hydrogen and air); f is fuel proportion by weight, in the mixture; W_p and W_o are the weight consumption rates of fuel and oxidizer; L is engine length.

The results of studies conducted on a detonation engine built according to the drawing of Fig. 7.26 are presented in Fig. 7.28.

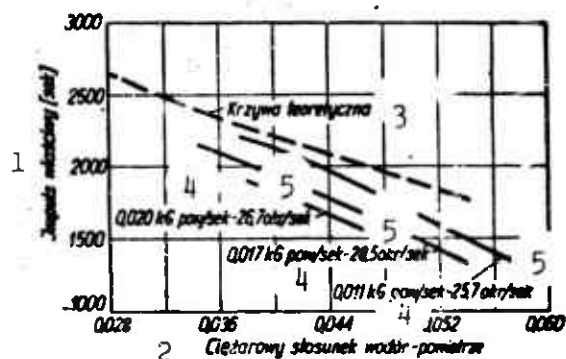


Fig. 7.28. Dependence of specific impulse of a detonation engine on the ratio of hydrogen to air. 1) Specific impulse (sec); 2) weight ratio of hydrogen-air; 3) theoretical curve; 4) kgf air/sec; 5) cycles/sec.

This graph permits a quantitative comparison of the engine under discussion with other jet engines. The value of the impulse is strikingly large, since at optimum detonation frequency and mixture composition it can amount to 2100 sec. This corresponds to a unit mixture consumption rate of 1.72 kg/kgf·hour, and a consumption of hydrogen of the order of 0.07 kg/kgf·hour. It is seen from this that a detonation engine has the lowest fuel consumption of all jet engines.

The question of thrust per unit engine frontal area does not look much worse. The 3600 kgf/cm² thrust achieved is roughly equal to the thrust obtained with turbojet engines and is 4-5 times greater than the thrust of ordinary pulsejet engines.

7.11. APPLICATIONS OF PULSEJET ENGINES

Up to the present, the applications of pulsejet engines have been limited. The reasons for this state of affairs are: noise is difficult to control; short range, especially at higher speeds, and low thrust per unit engine frontal area.



Fig. 7.29. Glider *Bocian* [Stork] in powered flight, propelled by four port pulsejet engines (photograph from the advertising brochure *World Glider Champions at Lesznie Wlkp*).



Fig. 7.30. Drone powered by a port pulsejet engine.

Remembering, however, this engine's advantages, such as thrust

generation at standstill and simple and easy design, it might be assumed that the range of its applications will not shrink. This is further evidenced by an as yet incomplete exploitation of its full developmental potential.

Figures 7.29 and 7.30 illustrate examples of contemporary applications of these engines.

Figure 7.29 shows how pulsejet engines (two on each side) power a two-seat glider of the "Bocian" [Stork] type.

Figure 7.30 shows a photograph of a drone equipped with a port pulsejet engine which is placed over the rear fuselage. This engine is provided with an inlet screen adjusted for high flight speeds (Fig. 7.21).

REFERENCES TO CHAPTER 7

- 7.1. A. Busemann: Bericht über den Paul Schmidtschen Strahlrohr-Antrieb [Report on the Paul Schmidt Jet-Tube Propulsion System]. F.B. [Aeronautical Engineering Reports] 530, 1936.
- 7.2. K. Schultz - Grunow: Gas-Dynamic Investigation of the Pulse-Jet Tube. NACA T.M. No. 1131, 1947.
- 7.3. L. Poggi: Contributo allo studio della pulsoreazione [Contribution to Study of the Pulse Jet]. L'aerotechica [Aeronautical Engineering], Nos. 5 and 6/1949.
- 7.4. M. Bertin: Das Pulso-Düsentriebwerk SNECMA Interaria [The SNECMA Interaria Pulsejet Engine]. No. 6/1953.
- 7.5. S. Wojcicki: Możliwości rozwojowe silników pulsacyjnych [Growth Potential of Pulsejet Engines]. Technika Lotnicza [Aviation Technology], No. 6/1953.
- 7.6. H. Staab: Vorgänge in pulsierenden Strahltriebwerken [Processes in Pulsejet Propulsion Systems]. Zeitschrift für Flug-

wissenschaften [Journal of the Aeronautical Sciences]. No. 3/1957.

- 7.7. A. Kowalewicz: Przepływy ze spalaniem detonacyjnym [Flows with Detonation Combustion]. Technika Lotnicza, No. 4/1958.
- 7.8. J. Chomiak: Zastosowanie teorii nieustalonego jednowymiarowego ruchu płynu ściśliwego do obliczania silników pulsacyjnych bezzaworowych [Application of Unsteady One-Dimensional Flow Theory of a Compressible Fluid to the Computation of Portless Pulsejet Engines]. Technika Lotnicza, No. 3/1958.
- 7.9. R. Foa: Intermittent Jets. 1959.
- 7.10. R. Szymanik: Silniki pulsacyjne [Pulsejet Engines]. C.M.P., Nos. 29 and 30/1960.

Chapter 8

RAMJET ENGINES

Application of ramjet engines is presently limited exclusively to the propulsion of missiles, experimental fighter planes and a certain number of helicopters. However, this field should expand in the near future to encompass passenger airliners and transport planes.

Such airplanes, powered by ramjets and flying at speeds corresponding to Mach numbers between 6 and 8 will have a lower cost effectiveness than the present subsonic airplanes.

8.1. THERMODYNAMICS AND AERODYNAMICS OF RAMJETS

Atmospheric air flowing through and around the ramjet engine exerts a static pressure on its walls (Fig. 8.1a) the resultant of which

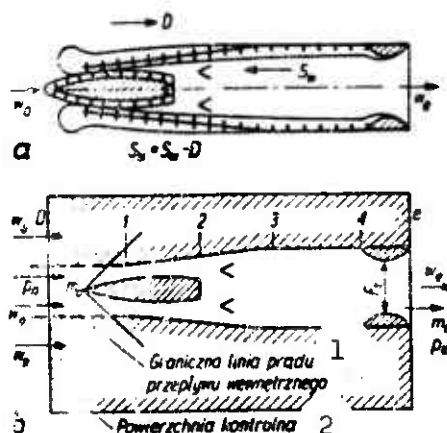


Fig. 8.1. Distribution of static pressures acting on the walls of a ramjet engine. 1) Boundary streamline of the internal flow; 2) control surface.

is called the useful thrust and is directed in a direction opposite to the flow direction. Useful thrust S_u is the resultant of two antiparal-

lel forces:

- the internal thrust S_w (being the resultant of the pressures acting on the internal engine walls),

- the external drag D (being the resultant of the pressures acting on the external walls)

$$S_u = S_w - D. \quad (8.1)$$

8.1.1. Internal Thrust

By introducing the concept of a flow thrust

$$S = mw + pF \quad (8.2)$$

the internal thrust of a ramjet engine can be described [8.4] as

$$S_w = S_e - S_0 - p_0(F_e - F_0) \quad (8.3)$$

where S_e and S_0 are the thrusts of the outlet and inlet flows; F_e and F_0 are the cross-sectional areas of the outlet and inlet flows; p_0 is the ambient pressure; m is the mass rate of flow.

Thus the internal thrust is equal to the difference of flow thrusts at engine inlet and outlet plus the force due to atmospheric pressure acting on the difference of the normal inlet and outlet flow cross-sectional areas.

Analysis of the distribution of the flow's thrust along the engine length is most instructive. Such an analysis is very useful in the selection of engine shape.

For a constant inlet-flow thrust ($S_0 = \text{const}$) the internal thrust can be increased by increasing the value of the outlet-flow thrust. This can be done only by increasing the engine outlet area, which is automatically related to an increased heating of the flow in the combustion chamber. In the limit case where the internal thrust is maximum, the adiabatic-expansion exit nozzle is replaced by the combustion chamber fulfilling the role of a thermal nozzle. However, this change reflects itself in a decrease in engine efficiency, which becomes evi-

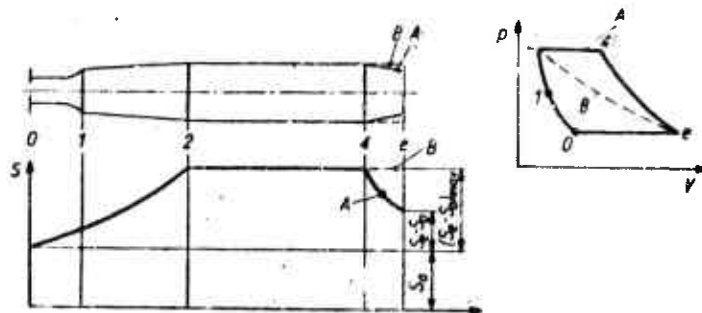


Fig. 8.2. Variation of flow thrust along the length of a ramjet engine and effect of thrust magnitude on the area of the thermodynamic cycle: A) conventional engine with adiabatic nozzle; B) engine with thermal cycle.

dent from a consideration of the engine cycles shown in Fig. 8.2 for the case of an adiabatic and thermal nozzle.

Equation (8.3) can be transformed by introducing the continuity relation:

$$S = mw + pF = F(\rho w^3 + p) = pF(1 + \kappa M^2) \quad (8.4)$$

Then one obtains successively

$$S_w = m_e w_e - m_0 w_0 + F_e (p_e - p_0) \quad (8.5)$$

and

$$S_w = p_e F_e (1 + \kappa_e M_e^2) - (p_0 F_0 M_0^2 + p_0 F_e) \quad (8.6)$$

where κ_e is the isentropic coefficient; M_0 and M_e are Mach numbers at inlet and outlet.

In order to eliminate the expressions containing pressure from the equation for the internal thrust, the concept of effective stream velocity at nozzle exit is introduced and it is defined as

$$w_e = w_e + \frac{F_e g}{m_e} (p_e - p_0)$$

In this case, Eq. (8.5) can be written in the following form

$$S_w = m_e w_e - m_0 w_0 \quad (8.7)$$

whereas Eq. (8.6) can be transformed as follows:

$$S_e = F_0 x_0 t_0 M_0^2 \left[(1 + f) \frac{M_j}{M_0} \sqrt{\frac{x_e T_e}{x_0 T_0}} - 1 \right] \quad (8.8)$$

where f is the fuel-to-air ratio; $M_j = w_j/a_e$ is the effective Mach number at nozzle exit; T_0 and T_e are the absolute temperatures of the inlet and outlet flows; a_e is the speed of sound in the outlet flow.

Flow through the engine involves pressure losses. These losses are due to:

- increase of entropy in the fluid during transition through the shock waves in the supersonic diffuser;
- friction, separation and turbulence in the subsonic portion of the diffuser;
- aerodynamic drag of injectors, flame stabilizers and other components located inside the engine;
- pressure drop due to heat transfer;
- friction in the nozzle.

The ratio of total pressures at the beginning and end of a typical ramjet is $p_e^*/p_0^* = 0.72$ under the following operating conditions: inlet Mach number $M_0 \sim 1.8$; Mach number at the entrance to the combustion chamber $M_2 \sim 0.2$; and temperature at the end of the combustion chamber $T_3 \sim 2100^\circ\text{K}$. This over-all pressure drop is subdivided in the following way among the various engine components:

- across the supersonic diffuser $p_1^*/p_0^* = 0.92$;
- across the subsonic diffuser $p_2^*/p_1^* = 0.90$;
- across flame stabilizers $p_3^*/p_2^* = 0.97$;
- across the combustion chamber $p_4^*/p_3^* = 0.92$;
- across the nozzle $p_e^*/p_4^* = 0.97$.

The over-all pressure drop causes a drop in the effective Mach number at the nozzle exit. This effect is exhibited in Fig. 8.3.

In the ideal case, the Mach numbers at engine inlet and outlet

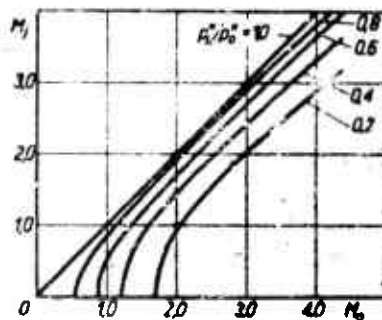


Fig. 8.3. Effect of the overall pressure drop in a ramjet engine on the value of the effective Mach number at nozzle exit.

are equal. Furthermore, if one also assumes that $\kappa_0 = \kappa_e$ and that $f = 0$, then Expression (8.8) for the internal thrust can be transformed as follows:

$$S_w = F_0 \rho_0 M_0^2 \left(\sqrt{\frac{T_4}{T_3}} - 1 \right)$$

or

$$S_w = \rho_0 F_0 w_0^2 \left(\sqrt{\frac{T_4}{T_3}} - 1 \right)$$

where ρ_0 is the air density in the inlet stream; T_4 is the temperature at the end of the combustion chamber; T_3 is the temperature at the beginning of the combustion chamber.

From this last expression it is seen that the internal thrust of a ramjet engine is proportional to:

- the density of inlet air (and therefore decreases with increasing flight altitude),
- the velocity squared (and therefore changes similarly to aerodynamic drag),
- the square root of the temperature ratio at the end and beginning of the combustion chamber minus one.

8.1.2. External Drag

External drag of a ramjet engine is expressed by the following equation:

$$D = \int_{F_s} (p_s + \tau_s) dF - p_0 (F_s - F_0) \quad (8.9)$$

or

$$D = \int_{F_s} [(p_s - p_0) + \tau_s] dF \quad (8.10)$$

where p_s and τ_s are the pressure and contact potential on the outer engine walls; p_0 is the ambient pressure.

External drag consists of:

- friction drag D_t ;
- drag D_c due to the pressures acting on the engine's outer surfaces;
- charging drag D_d .

Obviously

$$D = D_t + D_c + D_d.$$

Charging drag is due to a change in momentum resulting from a spreading of the flow in front of the inlet diffuser (Fig. 8.4). Its magnitude is mainly a function of the inlet contraction coefficient

$$\varphi_0 = \frac{F_1}{F_0} \quad (8.11)$$

where F_0 is the area of the stream flowing into the engine; F_1 is the inlet area, and can be expressed by the relationship

$$D_d = mw_1 + F_1(p_1 - p_0) - mw_0 \quad (8.12)$$

which is a calculation of the changes in momentum between cross section 0-0 and 1-1 (Fig. 8.4).

In the case where the inlet contraction coefficient is equal to unity (that is, contraction does not occur), the charging drag is zero.

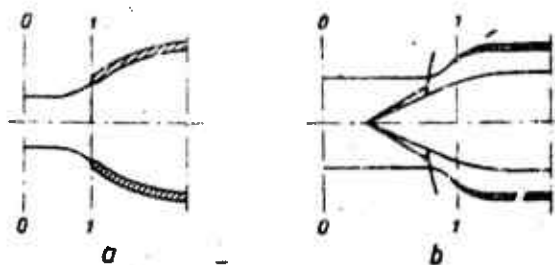


Fig. 8.4. Occurrence of charging drag as a result of the contraction of the stream flowing into a ramjet engine: a) engine with subsonic diffuser; b) engine with supersonic diffuser.

The magnitude of the charging drag is specified by means of a drag coefficient

$$C_d = \frac{L_d}{q_0 F_m} \quad (8.13)$$

where F_m is the engine frontal area; q_0 is the dynamic pressure in the inlet stream.

Figure 8.5a shows typical dependence of C_d on the Mach number and the contraction coefficient.

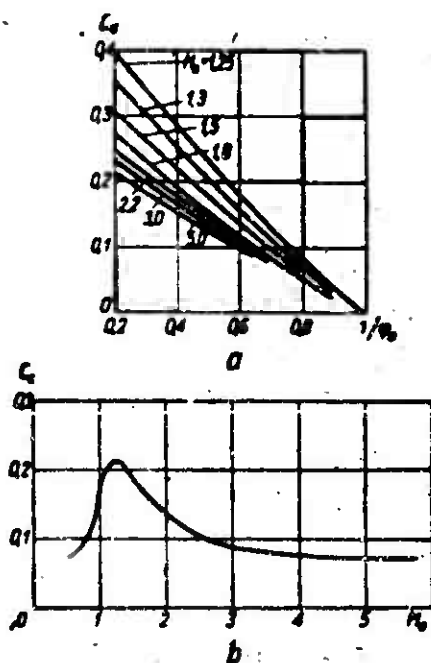


Fig. 8.5. Drag dependence on inlet Mach number: a) charging drag; b) pressure drag.

The remaining drag coefficients, friction and pressure, are expressed by analogous equations

$$C_t = \frac{D_t}{q_\infty F_b} \quad \text{and} \quad C_p = \frac{D_p}{q_\infty F_m}$$

where F_b is the transverse area of the engine.

The values of the friction-drag coefficient can be expressed by means of the following relationships:

$$C_t = \frac{0.074}{Re^{0.2}} \quad \text{for } Re \leq 10^6$$

and

$$C_t = \left(\frac{0.242}{lg Re} \right)^2 \quad \text{for } Re > 10^6$$

Coefficient C_p is a function of the Mach number, engine shape and of the inlet contraction coefficient. For preliminary computations it can be selected on the basis of the graph given in Fig. 8.5b.

8.1.3. Coefficient of Useful Thrust

The coefficient of useful thrust for a ramjet engine is expressed by the relationship

$$C_{S_s} = \frac{S_s}{q_\infty F_m} = \frac{2(S_s - D)}{\rho_\infty F_m \alpha_\infty M_\infty^2} \quad (8.14)$$

Figure 8.6a shows the dependence of the useful thrust on the inlet Mach number.

The following assumptions were made in the computations shown in this graph of characteristics:

- gasoline combustion efficiency 0.9,
- ambient temperature 20°C,
- the coefficient of total pressure recovery in the diffuser varies as shown in the graph placed in the upper left-hand corner of the figure.

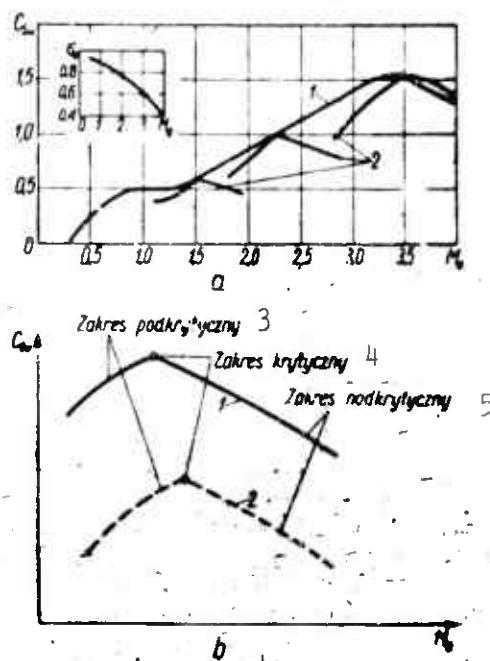


Fig. 8.6. Velocity characteristics of ramjet engines: a) dependence of the coefficient of useful thrust on the inlet Mach number; 1) characteristic of an engine of variable geometry; 2) characteristics of engines of constant geometry; b) dependence of the coefficient of internal thrust on the inlet Mach number; 1) at altitude conditions; 2) at sea level; 3) subcritical range; 4) critical range; 5) supercritical range.

8.1.4. Coefficient of Internal Thrust

The application of useful thrust and by the same token of the coefficient of useful thrust in the evaluation of the performance of ramjet engines is correct only in the case of the engine itself. However, more and more often one encounters implementations (and such is the development trend in the development of flying craft) in which the ramjet engine constitutes an integral part of the aircraft as a part of its fuselage or wing. In this case, the quantity characterizing the engine is its internal thrust and by the same token the coefficient of internal thrust is defined by the expression

$$C_{su} = \frac{S_u}{\rho_0 F_m} \quad (8.15)$$

After the necessary transformations of Eq. (8.15) we obtain

$$C_{sx} = \frac{\frac{2F_0}{F_m}}{\kappa_0 M_0^2} \left[\frac{\rho_0^*}{\rho_0} \left[\frac{1 + \kappa_0 M_0^2}{\frac{\rho_0^*}{\rho_0}} \right] - 1 \right] - \frac{2F_0}{F_m} \quad (8.16)$$

As is already known from previous considerations, the development of thrust in the engine is a consequence of the presence of an appropriately high pressure. In order to maintain this pressure it is necessary to transfer heat to the stream of air flowing through the engine.

For constant-geometry engines, the mass rate of air flow through the engine is a function of the quantity of heat transferred. Equation (8.16) presented above allows us to compute the dependence of the coefficient of internal thrust on the inlet Mach number. Typical characteristics are shown on the graph of Fig. 8.6b. Three ranges of engine operation can be discerned on these characteristics: subcritical, critical and supercritical. The critical range corresponds to the case for which the computations were made, that is, when the entire flow of the incoming air enters the engine and the normal shock wave is situated at the cross-sectional area of the diffuser inlet. The subcritical range (Fig. 3.34a) corresponds to the case in which the inlet Mach number is smaller than computed, in view of which a contraction takes place at the diffuser inlet and the mass rate of inflowing air decreases. In the supercritical range (Fig. 3.34b) the inlet Mach number is greater than computed, so that the normal shock wave is swallowed inside the diffuser. This causes an increase in over-all pressure loss across the engine and a drop in the coefficient of internal drag. The increase in the thrust coefficient with an increase in flight altitude, shown in Fig. 8.6, is explained by the drop in inlet stream temperature. In view of this, the maintenance of the assumed temperature T_4 at the end of the combustion chamber requires an increase in the heat

transferred, which in turn causes an increase in C_{Sw} .

8.1.5. Unit Fuel Consumption

Unit fuel consumption of a ramjet engine is defined by the equation:

$$b = B/S \text{ (kgf/kgf}\cdot\text{hr)} \quad (8.17)$$

where B is fuel consumption in kgf/hour; S is the thrust to which the unit fuel consumption corresponds (S_w corresponds to b_w , whereas S_u corresponds to b_u).

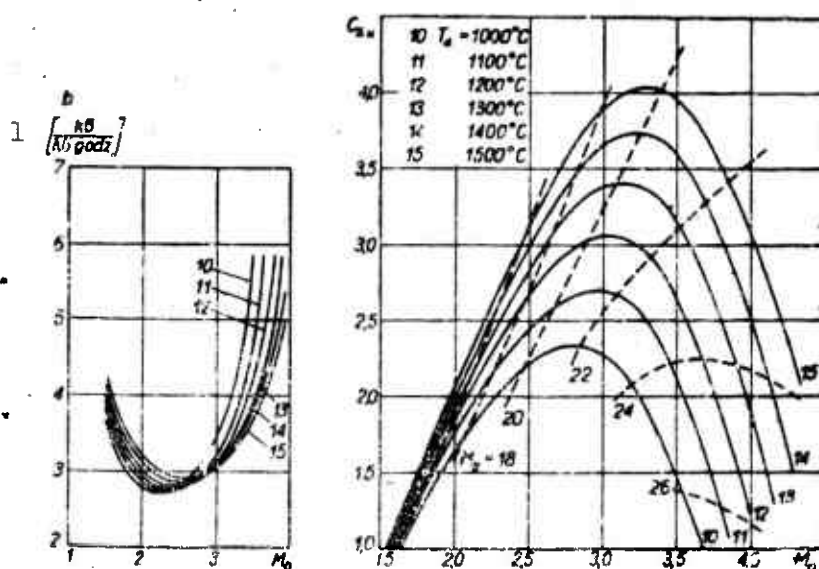


Fig. 8.7. Dependence of the coefficient of useful thrust and of unit fuel consumption on inlet Mach number for a typical, fixed-geometry ramjet engine specified by the area ratio $F_t/F_4 = 0.6$ (Fig. 8.1). 1) (kgf/kgf·hr).

After appropriate transformation of Eq. (8.17) one gets:

$$b = \frac{2g}{a_0 M_0} \left(\frac{F_2}{F_m} \right) \frac{f}{C_S} \quad (8.18)$$

where g is the acceleration of gravity; a_0 is the speed of sound in the inlet stream; f is the fuel-to-air ratio; C_S is the thrust coefficient corresponding to the unit fuel consumption.

Results of computations specifying the dependence of unit fuel consumption and of the coefficient of useful thrust on the inlet Mach

number of a typical supersonic engine are shown in the graphs of Fig. 8.7.

8.2. COMBUSTION CHAMBERS OF RAMJET ENGINES

Combustion chambers of ramjet engines constitute their basic element. Their operating conditions are much more stringent than those of the combustion chambers in turbojets. Flow velocities occurring in this case reach up to 150 m/sec and this often at very low pressures (down to 0.2 atm). The one factor which in particular makes it difficult to achieve an efficient operation of the combustion chamber is the condition of small over-all pressure drop across the chamber. The necessity of this requirement arises because of the effect of pressure losses on engine performance, as was mentioned in an earlier section.

8.2.1. Thermal Efficiency of the Combustion Chamber

The thermal efficiency of the combustion chamber is given by the relation

$$\eta_t = \frac{\Delta i_{rs}}{\Delta i_t} \quad (8.19)$$

where Δi_{rs} is the actual increase in enthalpy in the chamber; Δi_t is the theoretical enthalpy change in an ideal chamber.

By ideal chamber we mean one without thermal losses due to incomplete combustion and due to heat transfer to the surroundings. The following mixture parameters and construction details influence the thermal efficiency of the combustion chamber:

- composition, temperature and initial mixture velocity;
- length of the combustion chamber and shape of flame stabilizers.

Figure 8.8 illustrates the effect of mixture composition and initial temperature. The characteristics shown here have been obtained in a model chamber through which flowed a homogeneous and completely evaporated mixture. A conical flame stabilizer was placed on the cham-

ber's axis. Maximum thermal efficiency is achieved with a stoichiometric mixture. It follows from the above that a stoichiometric mixture composition assures optimum stability conditions and the highest speed of flame propagation from the stabilization zone toward the chamber walls. Thermal efficiency increases with temperature, which is obvious, since a temperature rise increases the combustion rate.

The effect of flow velocity on thermal efficiency is shown in Fig. 8.9.

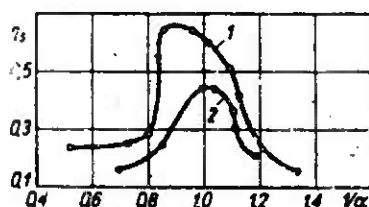


Fig. 8.8. Effect of the coefficient of air excess α and of initial mixture temperature t on the chamber's thermal efficiency: 1) $t = 210^\circ\text{C}$; 2) $t = 100^\circ\text{C}$.

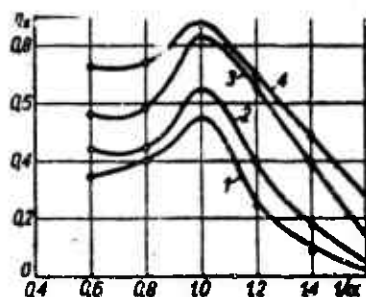


Fig. 8.9. Effect of flow velocity w on the chamber's thermal efficiency: 1) $w = 91$ m/sec; 2) $w = 76$ m/sec; 3) $w = 61$ m/sec; 4) $w = 46$ m/sec.

Turbulence intensity increases with increasing flow velocity, and by the same token the speed of flame propagation increases. However, the rate of increase in flame propagation speed is smaller than that of the flow velocity so that the flamefront angle between the stabilization zone and chamber wall (δ_{cz} in Fig. 8.14) decreases. At excessive flow velocities the flame becomes detached from the stabilizer and is

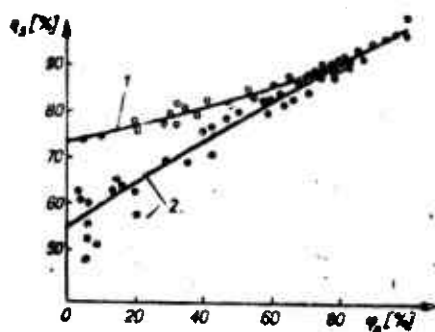


Fig. 8.10. Dependence of chamber thermal efficiency on the degree of evaporation and initial average drop diameter d_k : 1) $d_k = 90$; 2) $d_k = 290$.

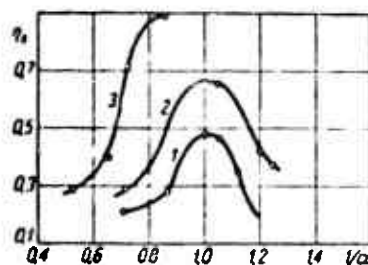


Fig. 8.11. Effect of chamber length L on its thermal efficiency: 1) $L = 254$ mm; 2) $L = 355$ mm; 3) $L = 457$ mm.

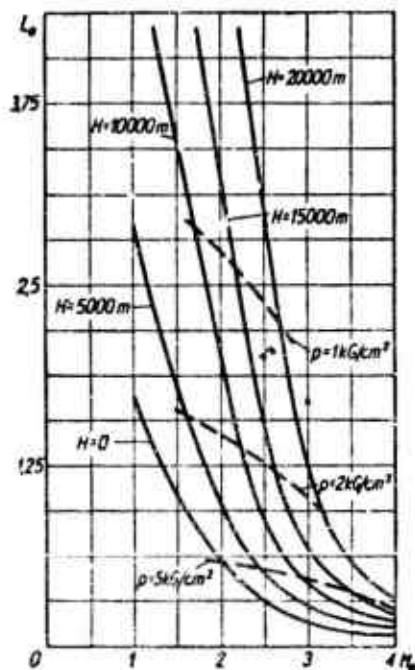


Fig. 8.12. Dependence of combustion chamber length L of a ramjet engine, corresponding to an efficiency $\eta_c = 1.0$, on altitude H and flight velocity M_0 . Coefficient of air excess $\alpha = 1$.

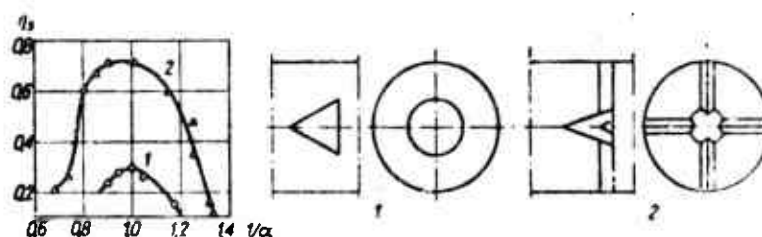


Fig. 8.13. Effect of stabilizer shape on chamber thermal efficiency: 1) conical stabilizer; 2) spider stabilizer.

blown out. During the transition stage, increase in flow velocity causes a drop in chamber thermal efficiency.

Figure 8.10 represents the results of studies on the effect of the degree of evaporation and of the size of hydrocarbon-fuel drops on chamber thermal efficiency [8.8]. The graph shows that a drop in the degree of evaporation lowers thermal efficiency. This effect is more pronounced the larger the average drop diameter. The obvious conclusion is shown in Fig. 8.11 and namely that thermal efficiency increases with chamber length. Increased chamber length increases combustion time which facilitates complete combustion of regions of unevaporated or badly mixed mixture. From a certain chamber length, thermal efficiency reaches 100%. Typical dependence of this chamber length, from the combustion point of view, is shown in Fig. 8.12. It is seen from this graph that the optimum chamber length is a function of flight altitude and speed. An increase in flight speed and a decrease in flight altitude have the beneficial effect of shortening the combustion chamber. If from hardware considerations chamber length must be shorter than the optimum length, then the drop in thermal efficiency must be taken into account.

Figure 8.13 illustrates the effect of flame-stabilizer shape on thermal efficiency.

Two stabilizers - a cone and a spider - have been compared; each one has the same coverage and the same ratio of stabilizer frontal area to the area of a transverse chamber cross section. The spider stabilizer favors the propagation of hot reaction gases, formed behind the center cone, in the direction of the walls and thus reduces the distance required for flame propagation across the entire transverse cross section of the chamber.

8.2.2. Design of Combustion Chambers

Figure 8.14 shows the configuration of the combustion chamber of a ramjet engine which is most often encountered.

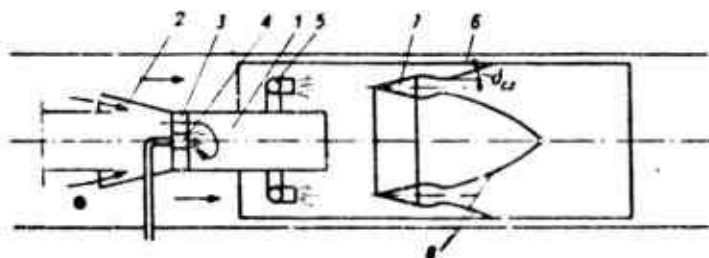


Fig. 8.14. Diagram of a combustion chamber in a ramjet engine: 1) antechamber; 2) intake of air diverted to the main chamber; 3) swirl chamber; 4) starter injector; 5) main injector; 6) liner; 7) stabilizer; 8) flame front.

The chamber consists of:

- an antechamber whose task is to facilitate the acceleration achieved by means of a spark plug or detonation ignition and to initiate the combustion process in the mixture flowing next to the main stream;
- main spray nozzles which supply fuel to the air stream flowing through;
- a flame stabilizer or a stabilizer system.

Combustion chamber walls are of the liner type so as to protect them from the effects of high temperature. An additional function of

the liner is to muffle the vibrations in the flowing mixture which arise due to combustion. The transverse cross section of the antechamber constitutes approximately 25% of the transverse cross section of the entire chamber, whereas the transverse area of the cooling jacket, protected from the chamber by the liner, amounts to approximately 10 to 15%.

The design of the antechamber is analogous to the majority of designs for the burner portion of combustion chambers in turbojet engines. A centrally located injector injects fuel into an air stream which has been set into rotation by appropriately shaped blades situated at the chamber inlet. The mixture so created burns to form a pilot flame of high intensity. In order to increase the flame's chemical activity in relation to the main mixture stream, the combustion process in the antechamber is deliberately not allowed to go to completion, leaving a certain percentage of unsaturated reaction products in the combustion products. In the design of a combustion chamber for a ram-jet engine, the following problems arise:

- design of the stabilization system;
- choice of the injection system;
- relative position of these two systems.

Before initiating the design of the stabilization system, we must find the answers to the following two questions:

- what should the stabilizer shape be?
- what should be its coverage and characteristic dimension?

Stabilizer shape is governed by chamber diameter. In the case of small chambers (up to ~250 mm) conical, circular (Fig. 8.15a and b) or spider (Fig. 8.13) stabilizers are used; in larger chambers, ring stabilizers (Fig. 8.15c), multiple ring stabilizers (Fig. 8.17) or mixed type stabilizers are used.

The coverage magnitude, a measure of which is given by the coefficient

$$\varphi_s = \frac{F_s}{F_k} \quad (8.20)$$

where F_s is the stabilizer frontal area; F_k is the area of the transverse cross section, is specified by the condition that the ratio of the characteristic stabilizer dimension to the flow velocity, in a given chamber, should be maximum; in that case, for conical and circular stabilizers $\varphi_s = 0.5$ whereas for ring stabilizers $\varphi_s = 0.35$.

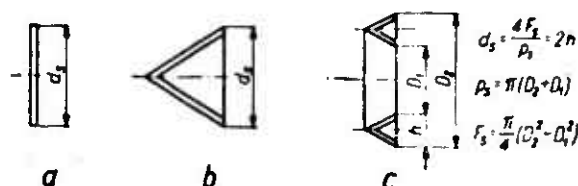


Fig. 8.15. Shape of flame stabilizers: a) circular stabilizer; b) conical stabilizer; c) ring stabilizer.

The characteristic stabilizer dimension d_s is equal, in the case of circular or conical stabilizers, to their geometric diameter, whereas in the case of ring stabilizers it is equal to the hydraulic diameter (Fig. 8.15). It is computed on the basis of De Zubay's relation

$$\alpha = F \left[\frac{w}{\rho^{0.95} d_s^{0.856}} \left(\frac{T_0}{T} \right)^{1.5} \right] \quad (8.21)$$

where α is the air-excess coefficient in the area of the stabilizer; w is the velocity at the stabilizer cross section; T_0 is the temperature at which De Zubay conducted his experiments ($T_0 = 390^\circ\text{K}$); F is the function defined by means of the curve in Fig. 6.10; T is the initial mixture temperature.

The computation is performed for the worst flight conditions (most

often for high-altitude conditions). The quantity obtained is checked against the graph of Fig. 8.16. This graph represents the effect of the characteristic ratio R/w (where $R = d_g/2$) of a flame stabilizer on the stability range of a kerosene-air mixture. It is seen from the graph that increasing the ratio R/w over 200 μsec is senseless.

In view of this, it is advantageous to replace a single ring stabilizer in larger combustion chambers by several stabilizers of smaller characteristic dimensions (Fig. 8.17).

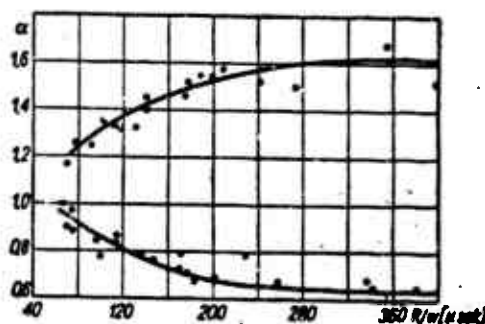


Fig. 8.16. Effect of the characteristic ratio R/w of a flame stabilizer on the range of stability of a kerosene-air mixture.

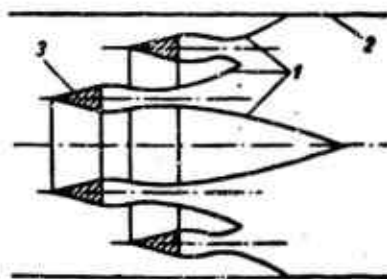


Fig. 8.17. Stabilizing system with two ring stabilizers: 1) flame front; 2) chamber wall; 3) stabilizers.

Such an arrangement decreases the flamefront path in the transverse direction and at the same time shortens the chamber. In order to eliminate interactions between the stabilization zones (which might cause vibrations dangerously affecting chamber strength), the stabilizers are spread out longitudinally in such a way that they are not

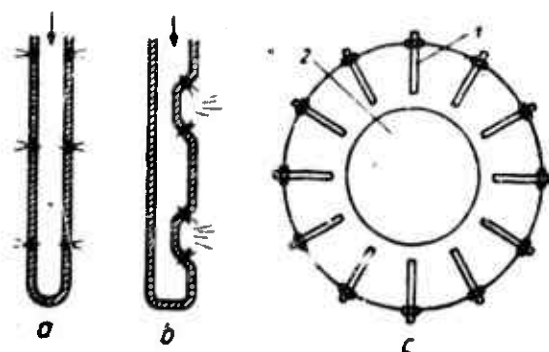


Fig. 8.18. Flow injectors: a) straight; b) spreading; c) injector position in the chamber spray zone; 1) injector; 2) diffuser core or antechamber.

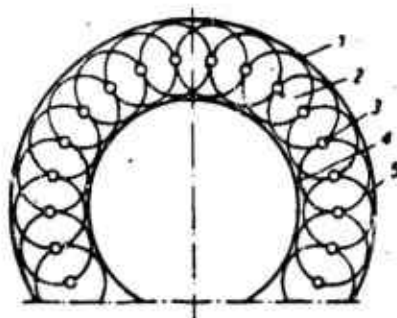


Fig. 8.19. Manifold of vortex injectors: 1) outer engine wall; 2) manifold channel; 3) vortex injector; 4) outer wall of the antechamber or of the diffuser core; 5) boundary of flow reached by a single injector.

in direct contact with the flame front produced by another stabilizer.

The injection system consists of an assembly of vortex or jet injectors.

Figure 8.18 shows two types of flow injectors. The injector sketched in Fig. 8.18a consists of a straight pipe with openings oriented perpendicularly to the flow. The injector shown in Fig. 8.18b is of the confluent type. The injection openings are located in such a way that the individual flows collide, thus improving dissemination. Figure 8.18c indicates a method of positioning such injectors in a combustion chamber. Vortex injectors are positioned on one or several circular manifolds as shown in Fig. 8.19.

In those cases where the operating conditions of the ramjet engine require a large range of fuel flow rates which cannot be handled by variation of the injection pressure, an injection system consisting of several sections (which are switched in or out as may be required) can be used or the simple vortex injectors can be replaced by vacuum injectors (Fig. 5.6).

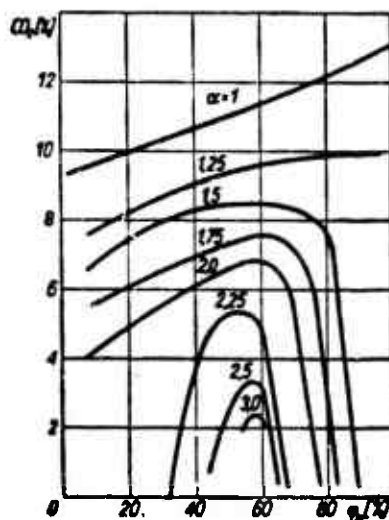


Fig. 8.20. Effect of evaporation coefficient α on flame stability.

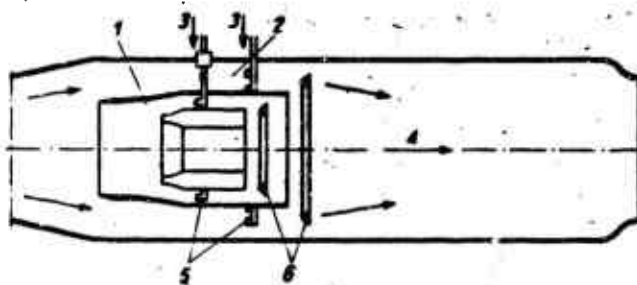


Fig. 8.21. Two-zone combustion chamber for a ramjet engine: 1) internal zone; 2) external zone; 3) fuel; 4) zone of combustion and mixing; 5) injectors; 6) stabilizers.

The next important consideration in the design of the combustion chamber is the proper positioning of injectors. They should be located

in such a way that the mixture flowing past the flame stabilizer is as close to stoichiometric composition as possible, since this increases the range of combustion stability. In theory, the distance from the injector to the stabilizer should be chosen in such a way that the fuel in the mixture reaching the stabilizer is already evaporated to a large extent. Except in special cases, such as for instance when due to the operating range one would expect lean mixtures in the stabilization zone, it is advantageous to position the injectors in such a way that the fuel in the mixture flowing past the stabilizer is only partly evaporated. Such a mixture has better stabilization properties due to the existence within it of fuel-rich microspheres. This phenomenon is illustrated in Fig. 8.20. This figure shows the dependence of mixture stabilization properties (the measure of which is the partial content of CO_2 in the stabilization zone) on the evaporation coefficient. It is seen from the figure that optimum stability of lean mixtures is achieved with evaporation coefficients $\Phi_p = 0.6$. In the case in which the range of required thrusts at constant flight velocity is such as to require such a wide range of mean temperatures at the end of the combustion chamber that it exceeds the possibility of stabilizing the mixture-flame stabilizer system, the combustion chamber should be subdivided into two zones (Fig. 8.21). The individual zones can be arbitrarily switched in or out so that three engine operating ranges can be achieved without imposing stringent requirements on the operating range of the stabilization system.

The last design parameter, namely chamber length, is chosen empirically in such a way as to maintain the combustion efficiency above 80 to 90%.

8.3. VIBRATIONS IN THE CHAMBER OF A RAMJET ENGINE

Under certain conditions, continuous combustion in the chamber

begins to pulsate. This manifests itself by an increase in noise, drop in efficiency and a pressure oscillation of various frequencies and amplitudes.

In many cases these pulsations cause destruction of chamber components or even of the entire engine. The phenomenon described above is called hard combustion. Obviously, the combustion chamber should be designed in such a way that hard combustion should not occur under its operating conditions.

Studies conducted by a number of researchers have differentiated three types of hard combustion differing in their pulsation frequency and which are caused by different factors.

8.3.1. Hard Combustion of the 35 to 60 hz Type

This type of hard combustion exhibits the following pattern (Fig. 8.22). When the flame from the stabilizer reaches the chamber walls after traversing the mixture stream, a detonation occurs in the bound-

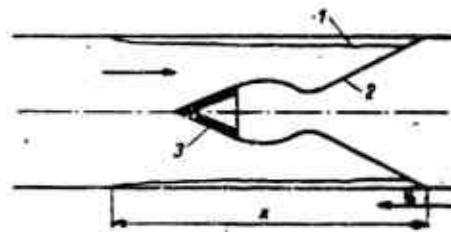


Fig. 8.22. Diagram of the occurrence of hard combustion of the 35 to 60 hz type: 1) layer of detonating mixture; 2) flame front; 3) flame stabilizer.

ary layer and adjacent layers which runs counter to the stream flow and terminates some distance from the stabilizer. When the new boundary layer of the fresh mixture reaches the flame, the process repeats. The combustion definitely is explosive in character; this has been verified by spraying water at the point of contact between the flame front and the chamber wall. This stopped the process, since as is well

known steam has antidetonation properties (whereas cooling of the wall in this same spot from the outside had no effect on the course of the process).

Under the best conditions, this type of combustion terminates in the destruction of the stabilizer.

If we denote by x the frontal path of the detonation wave, and by S_0 the initial combustion rate in the counterflow direction (6-9 m/sec), then the pulsation frequency is given by:

$$\nu = \frac{\sqrt{350 S_0}}{\arctg x \sqrt{\frac{350}{S_0}}}$$

If it is assumed that $x = 300-900$ mm, then $\nu = 35-60$ hz.

It has been verified that the occurrence of this type of hard combustion is governed by the quality of stabilizer performance and by the air-excess coefficient. Namely, it occurs in rich mixtures (coefficient of air excess $\alpha = 1.1-0.8$).

In certain cases it is sufficient to increase the characteristic dimension of the stabilizer in order to avoid this type of hard combustion.

8.3.2. Hard Combustion of the 100 to 130 hz Type

This type of combustion is governed by combustion chamber shape. The pulsations taking place are a function of the parameters of stream state.

Standing waves can occur in a gaseous stream flowing through a channel with a velocity corresponding to a Mach number M , and their pulsation frequency is given by

$$\nu = a(1 - M^2) \frac{1}{l}$$

In this equation l denotes the wavelength and a the speed of sound.

Pulsations of this type occur only in the range of 100-130 hz. Chamber length must be chosen in such a way as to avoid these vibrations.

8.3.3. Hard Combustion of the 20 to 30 hz Type

Pulsations occurring during this combustion are related to the characteristic interaction between the injector system and the chamber.

Let us assume that for certain reasons a pressure pulse appears and disappears in the chamber. This causes an increase and a decrease in fuel flow rate which of course is a function of the difference of pressures in the chamber and the injector. When a leaner mixture reaches the stabilizer, pressure in the chamber decreases. When the pressure also drops in the vicinity of the injector, the mixture becomes richer, and so on. Counterflow pressure pulsations travel at the speed of sound minus the average stream velocity.

Therefore, the period of a complete cycle consists of the time required for the pulse to travel from the stabilizer to the injector and of the time required by the portion of mixture having an increased air-excess coefficient to move from the injector to the stabilizer.

The relation between the pulsation frequency and the above-mentioned quantities is expressed by the following equation:

$$\nu = \left(\frac{x}{a} + \frac{x}{a - u} \right)^{-1} \quad (8.22)$$

where x is the distance between the injector and stabilizer; u is the flow velocity; a is the speed of sound.

The higher the pressures under which the injector operates, the smaller is the effect of this phenomenon.

8.4. SUBSONIC RAMJET ENGINES

Subsonic ramjet engines find a very limited application in aircraft and rocket technology. They are used to propel short-range mis-

siles, drone airplanes and helicopters.

The most interesting, from the design point of view, is the engine for helicopter propulsion. Its implementation is rendered difficult in view of the high requirements (low weight with high mechanical loads and limited length). Figure 8.23 shows one of many possible design solutions for such an engine. A characteristic feature of the design shown here is its compactness. In view of the small engine length requirement, a spider flame stabilizer is inserted deep into the diffuser, thus creating a cone which squeezes the stream of air flowing through it against the walls. At the end of this cone a counterflow vortex injector has been positioned. The flow of sprayed fuel is deflected to the rear, thus creating an incompletely evaporated mixture in the stabilization zone, which, as will be remembered from the previous section, increases the range of chamber stability.

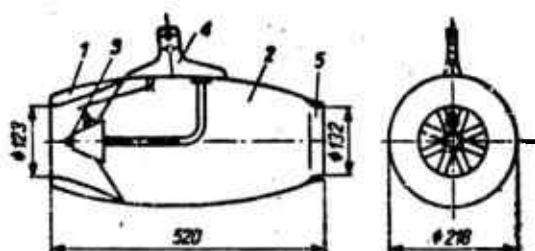


Fig. 8.23. Subsonic ramjet engine with bladed propulsion: 1) diffuser; 2) combustion chamber; 3) injector; 4) engine propeller mounting; 5) exhaust nozzle outlet ring.

The graph in Fig. 8.24 shows the engine's choking characteristic. This characteristic has been computed for the case of constant flow velocity $w_0 = 180$ m/sec. This is accomplished by reducing the mass rate of fuel flow out of the injector. A change in fuel flow rate causes a change in the temperature T_4 at the end of the combustion chamber and a change in the velocity w_1 at the engine inlet and therefore a change in the inlet contraction coefficient $\varphi_0 = F_1/F_0$. The

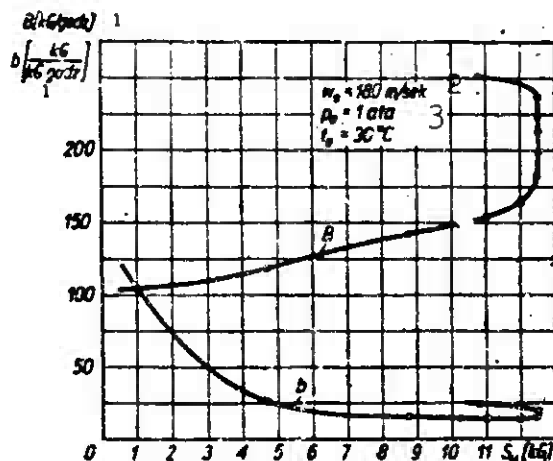


Fig. 8.24. Choking characteristic of a subsonic ramjet engine. 1) Hour; 2) m/sec; 3) atm.

mass rate G of air flow through the engine and the coefficient of air excess α at which combustion takes place also change as a result of the above changes. The optimum useful engine thrust S_u corresponding to the minimum fuel consumption b_{min} depends on the proper selection of the enumerated parameters. It is especially important to assume the proper value for the contraction coefficient φ_0 .

It is seen from the graphs in Fig. 8.25 that the unit fuel consumption b , as a function of the inlet contraction coefficient and for a constant F_e/F_1 ratio has a minimum for a certain value of φ_0 , which is different for different F_e/F_1 ratios. This minimum moves in the direction of an increasing contraction coefficient φ_0 as the F_e/F_1 ratio decreases and the value of the minimum increases during this translation. The value of F_e/F_1 is selected on the basis of the required thrust (F_e/F_1 increases as the thrust increases). An appropriately optimum contraction coefficient is selected corresponding to the chosen value of F_e/F_1 ; it is determined by the appropriately selected (optimum) excess air coefficient.

Figures 8.26 and 8.27 show a typical dependence of the optimum

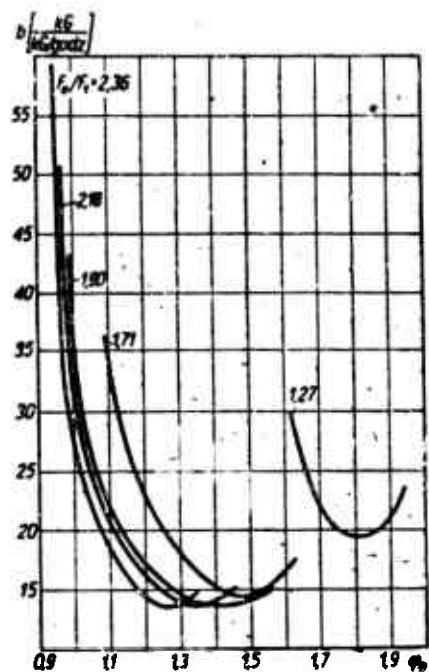


Fig. 8.25. Dependence of unit fuel consumption b on inlet contraction coefficient Φ_0 under various ratios of outlet and inlet cross sectional areas F_e/F_1 .

excess air coefficient and of the optimum contraction coefficient on the F_e/F_1 ratio.

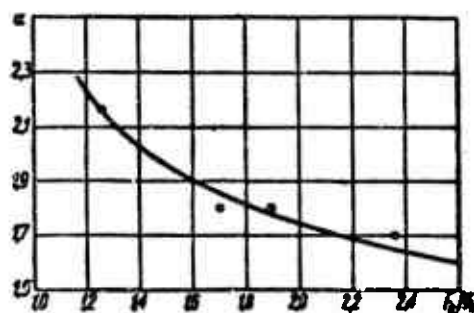


Fig. 8.26. Effect of the F_e/F_1 ratio on the optimum air excess coefficient.

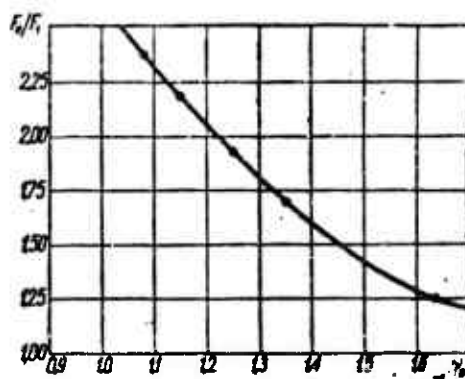


Fig. 8.27. Dependence of the F_e/F_1 ratio on the optimum contraction coefficient ϕ_0 .

8.5. SUPERSONIC RAMJET ENGINES

Supersonic ramjet engines are presently used mainly to power guided missiles (Fig. 8.28) and drone fighter planes (Fig. 8.29). Figure 8.30 illustrates a typical supersonic ramjet engine designed for flights corresponding to Mach numbers of 2 to 3.

The individual design elements of this engine are familiar from previous considerations. The subject of the following discussion will be the selection of optimum engine parameters and the optimum shape of the individual components. Figure 8.31 shows the dependence of the ratio of total pressures p_4^*/p_2^* at the end and beginning of the combustion chamber on the velocity coefficient $M_2^* = w_2/c_2^*$ at the combustion chamber inlet (where c_2^* is the critical flow velocity) under the assumption of a constant stabilizer coverage coefficient $\phi_s = 0.33$. Superimposed on the same figure is the dependence of the velocity coefficient at combustion chamber exit $M_4^* = w_4/c_4^*$ on the ratio of the critical and outlet cross sectional areas F_t/F_4 (nozzle contraction). It is seen from the graph that if the specified nozzle contraction and degree of superheat are assumed, then unique values are obtained for the velocity coefficients at combustion chamber inlet and exit, as

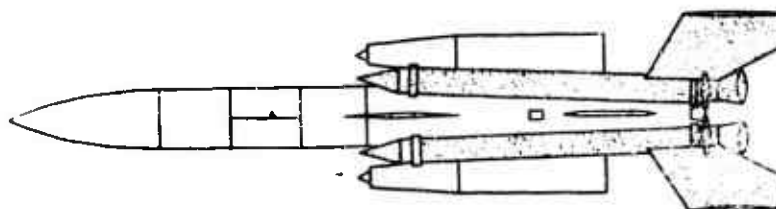


Fig. 8.28. Antiaircraft guided missile with ramjet propulsion, of the *Bloodhound* type.

well as for the coefficient of total pressure drop across the chamber. It has been verified experimentally that in order to avoid unsteady flow conditions in the combustion chamber, nozzle contraction should be selected so that $F_t/F_4 < 0.9$. A decrease of the F_t/F_4 ratio causes a drop in the Mach number at the combustion chamber inlet and outlet and an increase in the corresponding ratio of total pressures p_4^*/p_2^* .

The thrust magnitude of a ramjet engine is governed mainly by the value of the impulse J_e of the flow issuing out of the nozzle. This impulse reaches a maximum value J'_e when the expansion in the nozzle is carried out to the ambient pressure. Unfortunately this condition cannot be attained at high Mach numbers since the required cross sectional area at nozzle exit would be greater than the cross sectional

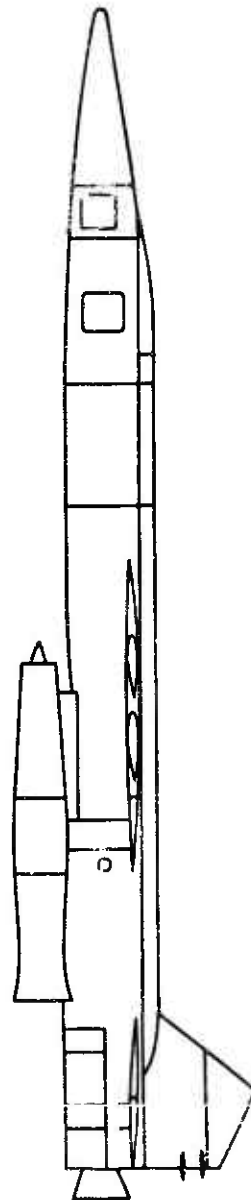


Fig. 8.29. Drone fighter airplane with ramjet propulsion, of the *Bomarc* type.

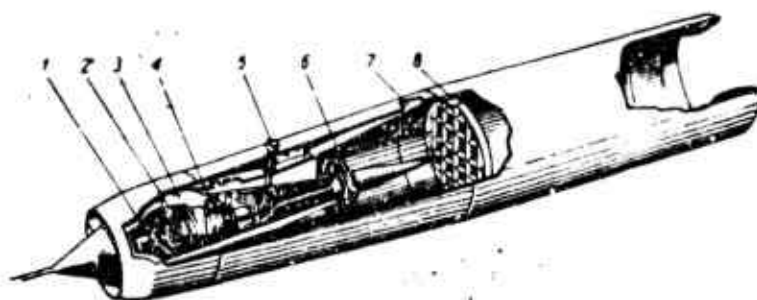


Fig. 8.30. Supersonic ramjet engine: 1) fuel control system; 2) air turbine; 3) inlet of compressed air into the turbine; 4) fuel pump; 5) fuel feed; 6) fuel manifold and injector; 7) air exit from turbine; 8) flame stabilizer.

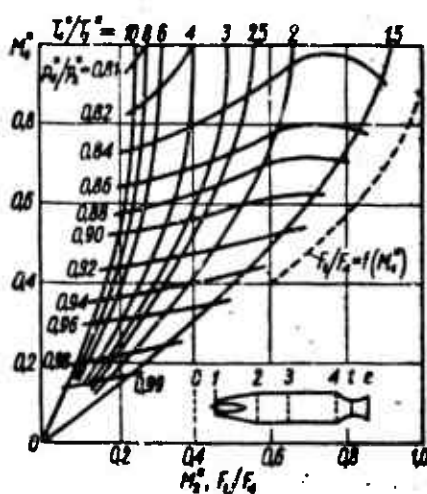


Fig. 8.31. Characteristic of a combustion chamber for a supersonic ramjet engine.

area of the combustion chamber; this obviously would greatly increase the engine's aerodynamic drag.

Limitation of the exit cross section area to that of the combustion chamber causes momentum losses which are specified by the ratio J_e/J'_e . Dependence of this ratio on the pressure ratio p_4^*/p_0^* (where p_0 is the static pressure in the exit stream) is shown in Fig. 8.32 for various ratios of cross sectional areas F_e/F_t .

Selection of engine parameters is achieved on the basis of the graphs shown in Fig. 8.33. This figure shows the dependence of useful

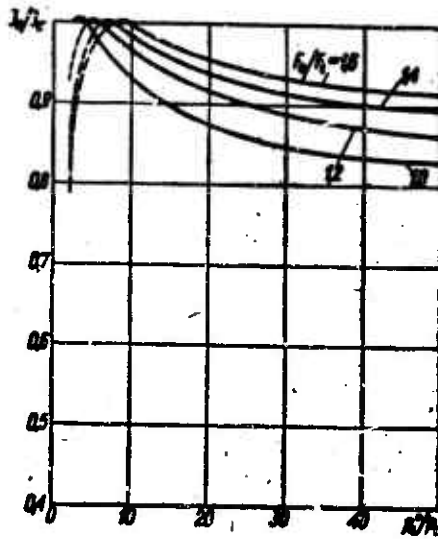


Fig. 8.32. Nozzle characteristic of a supersonic ramjet engine.

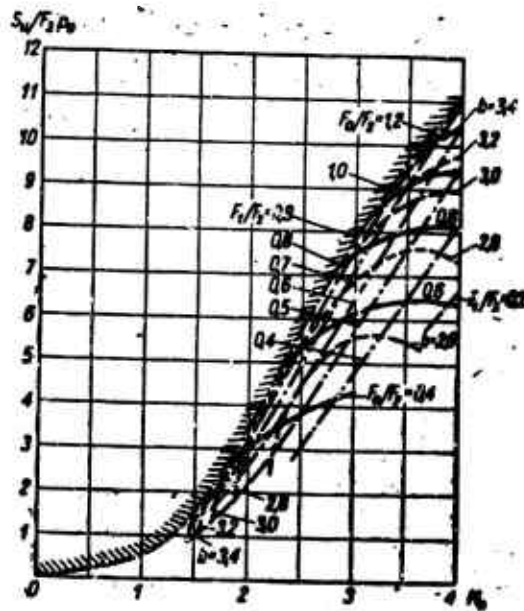


Fig. 8.33. Characteristic of a supersonic ramjet engine (flight altitude $H = 11$ km, two-stage diffuser):

$$\gamma_2 = 0.33, F_2 = F_1 = F_0, T_1 = 200^\circ K, \gamma_1 = 0.33$$

thrust per unit ambient pressure and unit combustion chamber area on the Mach number M_0 at engine inlet and on the area ratios $F_t/F_2 = F_i/F_e$.

As a result of an increase of this ratio, that is, of the degree of nozzle contraction, the following effects take place: thrust increases, the area ratio F_0/F_2 increases (and therefore an increase in the mass rate of air flow through the engine), an increase of unit fuel consumption and an increase in the Mach number at the combustion chamber inlet. The quantity F_t/F_2 is chosen with proper regard for correct operation of the combustion chamber which is governed, in the steady-state case free of vibrations, by the appropriate stability range and specific thermal efficiency. The effect of the basic total pressure losses on the performance of a ramjet engine is shown in Fig. 8.34. The source of these losses is mainly:

- nonisentropic compression in the supersonic diffuser;
- incomplete expansion in the engine nozzle.

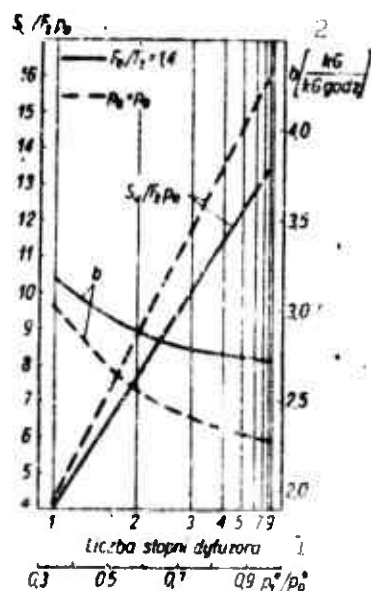


Fig. 8.34. Effect of energy losses due to nonisentropic compression and incomplete expansion on ramjet engine performance: $M_0 = 3$, $M_2 = 0.2$, $H = 11$ km, $T_H = 2000^\circ\text{C}$, $\tau_s = 0.33$. 1) Number of diffuser stages; 2) $\text{kgf/kgf}\cdot\text{hour}$.

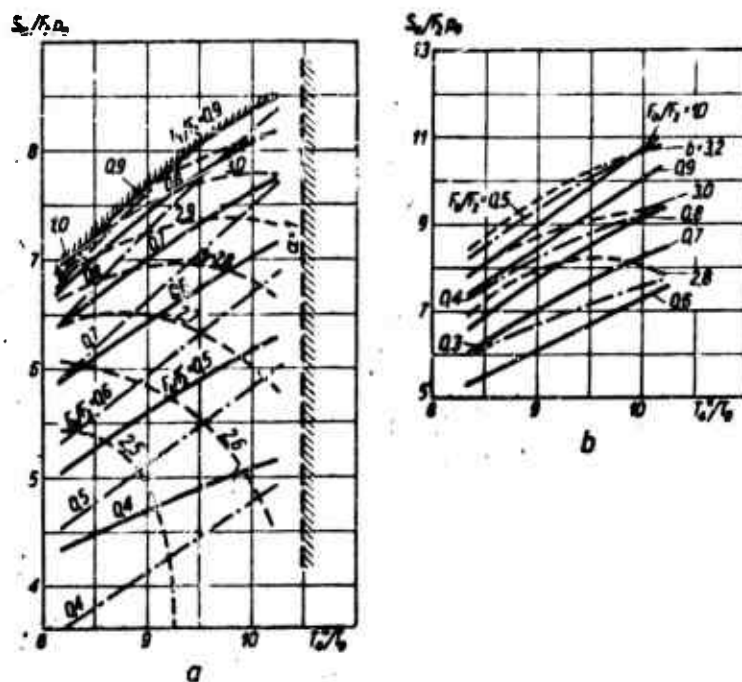


Fig. 8.35. Effect of preheating the stream of air flowing through the engine on the ramjet's characteristics: $H = 11$ km; $\varphi_s = 0.33$; a) $M_0 = 3.0$; b) $M_0 = 4.0$.

It is seen from the graph shown in the figure that the performance of a ramjet engine is governed mainly by diffuser efficiency, which in turn is a function of the number of stages. As an example, for the case under consideration a change from a two-stage to a three-stage diffuser increases thrust by $\sim 55\%$ and decreases unit fuel consumption by $\sim 6\%$.

Figure 8.35 shows the effect on thrust of preheating the stream of air flowing through the ramjet engine (the temperature ratio T_4^*/T_0^* was taken as a measure of the preheating). It is seen from the graphs that for a constant F_t/F_2 ratio an increase in the preheating causes an increase in thrust with a concomitant increase in unit fuel consumption. The range of physically attainable thrusts is limited on the one hand by preheating corresponding to the stoichiometric ($\alpha = 1$) mixture composition, and on the other hand by the area ratio $F_t/F_2 = 0.9$ which

is due to the condition of stable flow through the combustion chamber.

A third limit occurring at high Mach numbers is shown in Fig. 8.35b. A thrust increase under constant preheating causes a concurrent increase in the area ratios F_t/F_2 and F_0/F_2 . These ratios govern the mass rate of air flow through the engine. The limit ratio of the stream area entering the engine F_0 to the combustion chamber area F_2 is $F_0/F_2 = 1$ for a supersonic stream. This ratio is attained for a lower value of the ratio F_t/F_2 , the greater the magnitude of M_0 . For the case of $M_0 = 4$ and $T_4^*/T_0 = 10$ the ratio $F_0/F_2 = 1$ occurs already when $F_t/F_2 = 0.5$, that is, for a much lower value than the maximum allowable from the point of view of steady flow through the chamber. As can be seen from Fig. 8.31, for the case of supercritical pressure drop across the nozzle, the Mach number at the combustion chamber inlet indicates nozzle contraction and the temperature ratio T_4^*/T_3^* . Increasing the Mach number at the inlet for a constant nozzle contraction and constant temperature at the end of the combustion chamber increases the Mach number at the combustion chamber inlet. On the other hand, from the condition of maintenance of the optimum range of diffuser performance (Fig. 8.36), which occurs when the normal shock wave is located at the inlet engine cross section, it results that as the inlet Mach number increases, the Mach number at the end of the combustion chamber should decrease. If this does not take place, then the normal shock wave is swallowed by the diffuser (Fig. 3.33b). If, however, the ratios T_4^*/T_3^* and F_t/F_2 remain unchanged and the inlet Mach number M_0 decreases, then the ratio F_0/F_2 decreases which causes a drop in the mass rate of air flow through the engine and a translation forward of the normal shock wave (Fig. 3.33a). This increases the aerodynamic drag and threatens to shift the diffuser operation into the unsteady range which may wreck the engine and therefore should not be

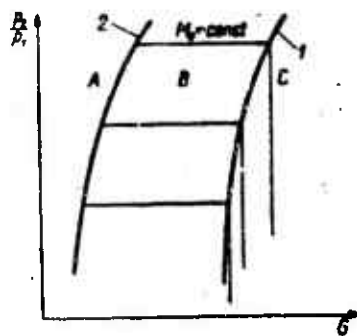


Fig. 8.36. Characteristic of a supersonic diffuser: 1) operational curve under critical conditions (normal shock wave is located in the diffuser inlet cross section); 2) stability limit; A) region of unsteady operation; B) region of operation in the subcritical range (normal shock wave is moved forward); C) region of operation in the supercritical range (normal shock wave is moved backward).

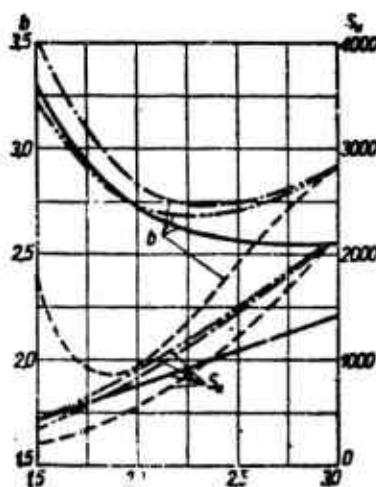


Fig. 8.37. Comparison of different methods of control of ramjet engines: $H = 11$ km, $T_3 = 2000^\circ\text{K}$ (except in the case of control by means of changes in T_4), $F_2 = F_1 = F_e = 0.1257 \text{ m}^2$. —) Nozzle control; - - -) control by changes in T_3 ; - · -) air suction; · · ·) engine with fixed geometry.

allowed to occur.

Presently there are several control systems to maintain normal operating conditions in the diffuser. These consist of:

- air suction between inlet and combustion chamber;
- change of temperature ratio at the beginning and end of the combustion chamber;

- change of diffuser geometry;
- change of nozzle geometry.

Figure 8.37 illustrates the effect of the various control methods on the engine characteristic in the case of inlet Mach number $M_0 = 3$ and a two-stage diffuser.

It is seen from the graphs shown in this figure that the thrust characteristic has a most advantageous shape in the case of control by air suction, whereas the characteristic of unit fuel consumption achieves its best shape in the case of control by changes of temperature T_4^* . However, in certain types of engines where it is necessary to achieve large changes in thrust at constant flight velocity, it is imperative that control be performed by means of changes in the area of the critical nozzle cross section, since this is the only control which will guarantee optimum conditions for diffuser operation in the presence of significant changes of temperature at the end of the combustion chamber.

8.6. HYPERSONIC RAMJET ENGINES

The characteristic feature of hypersonic flows is the high stagnation temperature. This has a fundamental effect on the performance of the combustion chamber, by facilitating on the one hand the ignition process, stabilization and mixture combustion and on the other hand by decreasing the chamber's thermal efficiency due to the strong appearance of dissociation. Figure 8.38 shows the characteristic temperatures occurring in hypersonic ramjet engines. It is apparent from the characteristics shown in the figure that the mixture of kerosene and air reaches the autoignition temperature at a Mach number $M_0 \sim 4.5$. Under these conditions, the classical methods of flame stabilization by insertion of unstreamlined bodies into the stream can be replaced by stabilization in the boundary layer or by means of aerodynamic sta-

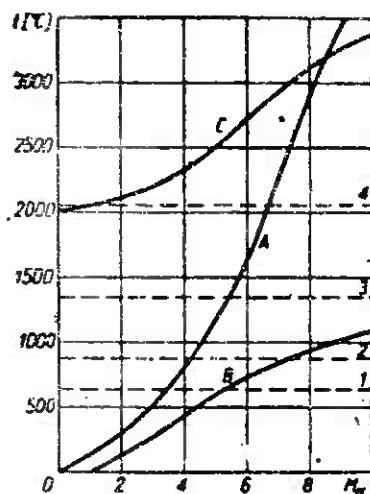


Fig. 8.38. Characteristic temperatures occurring in hypersonic ramjet engines: A) temperature at combustion chamber inlet; B) engine wall temperature taking into consideration heat loss due to radiation; C) combustion temperature of a stoichiometric mixture taking dissociation into account; 1) melting temperature of aluminum; 2) autoignition temperature of the kerosene-air mixture; 3) melting temperature of heat-resistant steel; 4) melting temperature of ceramic refractory materials.

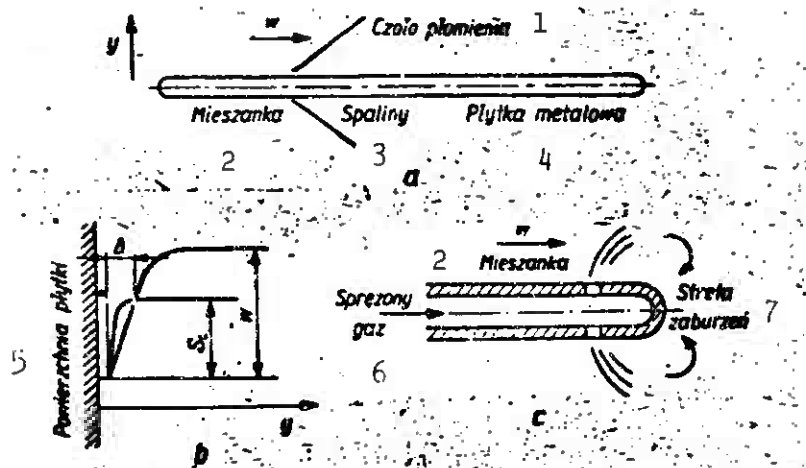


Fig. 8.39. Flame stabilization: a and b) in the boundary layer; c) by means of an aerodynamic stabilizer. 1) Flame front; 2) mixture; 3) combustion products; 4) metal plate; 5) plate surface; 6) compressed gas; 7) turbulence zone.

bilizers. Figures 8.39a and b illustrate the flame stabilization process in the boundary layer. A laminar layer is created in the mixture flowing past a plate; the distribution of flow velocity w and of laminar combustion speed S_L in this layer are shown in Fig. 8.39b. As a

result of these distributions, there exists a layer of thickness Δ where the flame propagation is greater than the combustion speed. If this layer is thick enough, it can become the point of attachment of the flame front. Layer thickness is a function of the Reynolds number, and therefore in the case of a given mixture of a given flow velocity it is a function of the distance between the flame front and the plate leading edge.

In an aerodynamic stabilizer (Fig. 8.39c) the flow disturbance, within which the flame front is initiated, is caused by introduction of compressed air in a direction perpendicular to the main mixture stream. This method is sufficient to obtain stable combustion within wide limits at the high temperatures present in hypersonic engines. Both of these stabilization methods, as opposed to combustion chambers with classical flame stabilizers, are characterized by small over-all pressure losses which has a beneficial effect on total engine efficiency. Curve C in Fig. 8.38 shows the relationship between the combustion temperature and the Mach number M_0 at engine inlet. It is seen from the shape of this curve that as M_0 increases, the loss of chemical energy due to absorption by dissociation increases at such a rate that when $M_0 > 9.0$ combustion does not even take place. And even though part of the dissociation energy is recovered in the nozzle as a result of the recombination taking place during expansion, it can nevertheless be assumed that this value of the inlet Mach number constitutes the limit of applicability of a ramjet engine with conventional combustion chamber.

In order to shift this limit in the direction of higher flight speeds, the following solutions have been proposed:

- a ramjet engine operating with an over rich mixture;
- a ramjet engine with a supersonic combustion chamber;

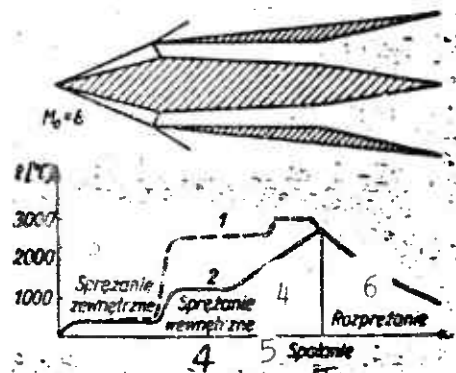


Fig. 8.40. Hypersonic ramjet engine with a supersonic combustion chamber: 1) temperature distribution in an engine with a conventional combustion chamber; 2) temperature distribution in an engine with a supersonic combustion chamber; 3) external compression; 4) internal compression; 5) combustion; 6) expansion.

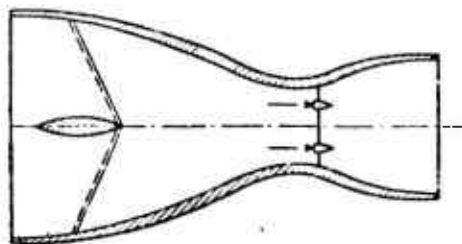


Fig. 8.41. Hypersonic engine with detonation combustion.

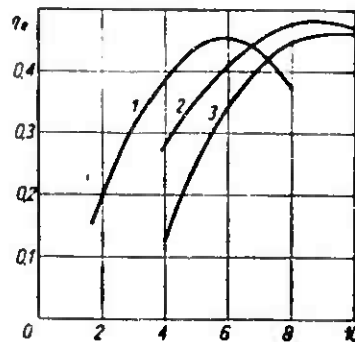


Fig. 8.42. Dependence of the over-all efficiency of hypersonic ramjet engines on inlet Mach number: 1) engine with a conventional combustion chamber; 2) engine with a hypersonic combustion engine; 3) engine with detonation combustion.

- a ramjet engine with detonation combustion;
- a ramjet engine with external combustion.

The use of fuel-rich instead of stoichiometric mixtures can in-

crease the operating range of ramjet engines even up to $M_0 = 20$. Such engines have a higher unit fuel consumption and are characterized by lower combustion temperatures and thereby by a lower energy loss due to dissociation. Furthermore, large mass rates of fuel flow can be used to advantage for cooling of combustion chamber and nozzle walls. An engine with a supersonic combustion chamber, sketched in Fig. 8.40, is a different proposition. The air stream entering the supersonic diffuser of such an engine is slowed down to an appropriate supersonic speed selected in such a way that after addition of the predicted amount of heat the flow velocity at the end of the combustion chamber would correspond to $M = 1$.

A lower initial temperature is achieved in this fashion as compared to that obtained with a conventional system. Obviously, this has a beneficial effect on the decrease of losses in fuel chemical energy due to dissociation of the products of combustion.

Figure 8.41 shows a diagram of a hypersonic engine in which detonation combustion takes place. The combustion process in this engine is implemented in a standing detonation wave which is located at the leading edge of the wedge placed in the supersonic mixture stream.

The graphs in Fig. 8.42 show a comparison of the performance of the above-mentioned engines with that of a conventional engine.

In the case of a hypersonic ramjet engine having a conventional combustion chamber, the over-all efficiency begins to decrease from $M_0 = 5-6$. At higher Mach numbers, the engine with a hypersonic combustion chamber appears to be more efficient; the detonation engine falls in between. The range of their maximum efficiency falls between $M_0 = 8$ and 10.

The hypersonic ramjet engines described above extend the operational range of ramjet engines; however, they do not solve the cooling

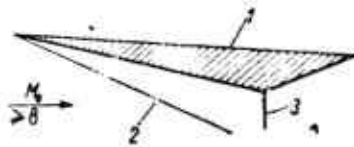


Fig. 8.43. Hypersonic ramjet engine with external combustion: 1) hypersonic flight profile; 2) oblique shock wave; 3) flame front.

problem. From this point of view, the idea of a supersonic ramjet engine with external combustion appears most interesting. Figure 8.43 shows the diagram of such an engine. The engine consists of a flying wing having a hypersonic profile. Heat transfer to the rear portion of the wing causes a deflection of the air stream flowing into the heating zone. This increases lift in the same fashion as an increased angle of attack, thereby causing the creation of thrust. If this thrust is sufficiently large then the wing can accelerate the flight. Since the larger portion of the total force due to the expansion of the combustion gases, in this case, contributes to lift rather than to thrust, the determination of engine efficiency by means of characteristics such as in Fig. 8.42 is difficult. However, from an approximate estimate, it appears that this engine's efficiency is roughly equal to that of the detonation engine. But the biggest advantage of this type of engine is primarily the solution of the cooling problem consisting of heat transfer from highly stressed points by conduction through the material of which the profile is made and also through radiation.

8.7. SOLID FUEL RAMJET ENGINES

Solid fuel ramjet engines constitute a separate group of ramjet engines. Figure 8.44 shows a design diagram of such an engine.

The engine consists of (in addition to the components of conventional ramjet engines) a solid fuel grain placed in an appropriately shaped frame. The grain is made out of compressed magnesium powder

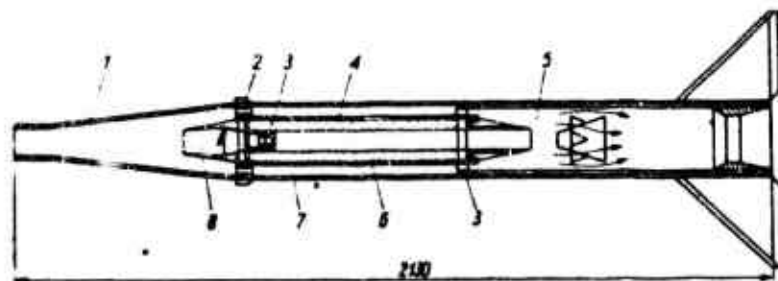


Fig. 8.44. Solid fuel ramjet engine: 1) diffuser; 2) seal; 3) igniter; 4) fuel grain made of compressed magnesium powder; 5) mixing chamber of secondary air and combustion products; 6) fuel grain frame; 7) secondary air channel; 8) primary air channel.

with a small oxidizer additive which accelerates the combustion process. Application of such engines is forecast in the propulsion of missiles of the "surface-to-surface" and "air-to-air" type having a range of 15-150 km. In this range, solid fuel ramjet engines have a better performance than rocket engines which are usually used for this purpose, if they are both restricted to the same dimensions. The fundamental disadvantage of these engines is the lack of thrust control capability during operation.

REFERENCES TO CHAPTER 8

- 8.1. M. Roy: Poussees Netes et Consommations Specifiques du Statoracteur Supersonique [Net Thrusts and Specific Fuel Consumption Rates of the Supersonic Ramjet]. 1952.
- 8.2. S. Wojcicki: Badanie wplywu charakterystycznych wielkosci poddzwiekowego silnika strumieniowego na jego osiagi [Study of the Effect of Characteristic Dimensions of Ramjet Engines on Their Performance]. Arch. Bud. Masz. [Archives of Machine Design], 1954.
- 8.3. S. Wojcicki: Termodynamiczne zagadnienia silnikow strumieniowych [Thermodynamic Problems in Ramjet Engines]. Technika Lotnicza [Aviation Technology] No. 3/1954.

- 8.4. A. Ronney, M. Zucrow, C. Besserer: Propulsion. 1956.
- 8.5. S. Wojcicki: Flame Stabilization in the Boundary Layer. Biuletyn PAN [Bull. Polish Academy of Sciences], Vol. IV, No. 4/1956.
- 8.6. M. Bondariuk, S. Iljaszenko: Priamotocznyje wozdusznoreaktywne dwigateli [Ramjet Engines]. Oborongiz [State Press for the Defense Industry], 1958.
- 8.7. G. Dugger: Recent Advances in Ramjet Combustion. ARS Journal, No. 11/1959.
- 8.8. J. Basewicz: O wlijanii predwaritielnogo isparenia na polnostiu i ustoičziwos gorenia rozpylennogo topliwa [Influence of Preliminary Vaporization on the Completeness and Stability of Combustion of Atomized Fuel]. Izd. AN SSSR [Acad. Sci. USSR Press], 1960.
- 8.9. H. Jenkins: Priamotocznyje dwigateli na twierdom topliwie [Solid-Fuel Ramjet Engines]. W.R. Tjechn. [Problems of Rocket Engineering] 7/1960.

Chapter 9

ROCKET ENGINES

The rocket engine is the oldest thermal engine and it is characterized by extremely functional simplicity and in many cases by design simplicity as well. In spite of this, its real development started relatively late, that is, in the nineteen-thirties. This can be explained mainly by manufacturing difficulties which could be overcome only as a result of the technological progress taking place before our eyes. The combustion intensity not encountered in any installations until now has raised a number of problems, the solution of which was tied to development in a number of fields in science and technology.

Also, the field of rocket-engine application, in artillery as well as aircraft, required pronounced changes in outlook before they could be successfully introduced. This had to do mainly with high flight velocities and the relatively large masses which were to be transported across larger but strictly specified ranges and altitudes.

9.1. THERMODYNAMICS OF ROCKET ENGINES

The basic thermal process which results in rocket engine thrust is an exothermal chemical reaction and expansion of the products of combustion which are created.

A characteristic feature of these processes is high temperature and high flow velocity. This becomes the source of additional thermal effects, of which heat transfer between the hot combustion gases and metal engine walls, as well as pressure fluctuations due to instability of the combustion process, give the designer the most difficulties.

9.1.1. Rocket Engine Thrust

The following equation represents the function previously derived for a rocket engine thrust:

$$S = mw_e + F_e (p_e - p_0) \quad (9.1)$$

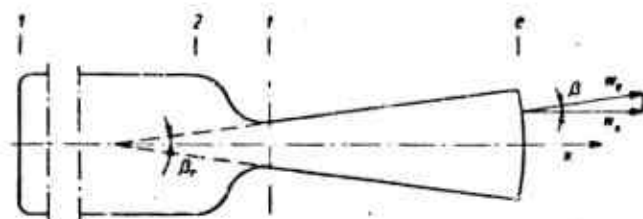


Fig. 9.1. Diagram of an ideal rocket engine: 1) initial cross section of combustion chamber; 2) terminal cross section of combustion chamber and initial cross section of the nozzle; t) critical nozzle cross section; e) cross section of nozzle exit; w_x) axial component of flow velocity; w_e , x) axial coordinates.

This equation requires correction factors due to the fact that the diverging portion of the nozzle is a truncated cone and the exit velocity cannot be parallel to the axis over the entire cross section (Fig. 9.1). Strictly speaking, the thrust equation should have the form

$$S = \int_{F_e} w_x dm + (p_e - p_0) F_e$$

where $w_x = w_e \cos \beta$; p_0 is the ambient pressure.

Transforming this equation and introducing

$$\zeta = \frac{1}{2} (1 + \cos \beta_r)$$

we get

$$S = \zeta mw_e + F_e (p_e - p_0) \quad (9.2)$$

In the case of conventional nozzles, the ζ coefficient is close to unity (e.g., for $\beta_r = 15^\circ$, $\zeta = 0.983$) and therefore it can be neglected in approximate computations. Differentiating Eq. (9.1) and taking into account the fact that the mass rate of gas flow through the

nozzle is not a function of exit conditions, we get

$$dS = mdw_e + (p_e - p_0) dF_e + F_e dp_e$$

From the law of conservation of momentum we get:

$$mdw_e = -F_e dp_e$$

and after substitution we obtain

$$dS = (p_e - p_0) dF_e$$

The thrust reaches a maximum value when

$$\frac{dS}{dF_e} = 0$$

This occurs when $p_e - p_0 = 0$. And thus maximum thrust is achieved when exit pressure is equal to the ambient pressure

$$S_{max} = mw_e, \text{ when } p_e = p_0.$$

Figure 9.2 shows the thrust loss S/S_{max} and the corresponding ratio of cross sections F_t/F_e as a function of the pressure ratio p_0/p_e .

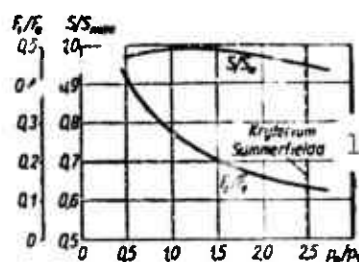


Fig. 9.2. Thrust variation as a function of exit pressure $p_2 = 20 \text{ kgf/cm}^2$; $\kappa = 1.21$. 1) Summerfield's criterion.

These characteristic curves were obtained for an engine with the following parameters: $\kappa = 1.21$; $p_2 = 20 \text{ kgf/cm}^2$ and $p_0 = 1.032 \text{ kgf/cm}^2$.

The quantities which are subject to change during the operation of the rocket engine are:

- ambient pressure, which occurs as a result of flight altitude;
- pressure existing in the combustion chamber, which occurs during regulation of thrust magnitude.

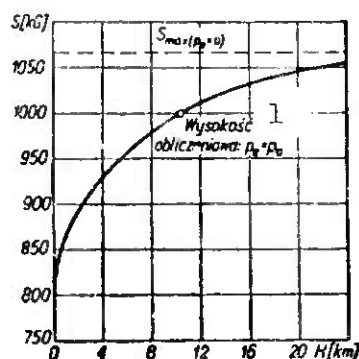


Fig. 9.3. Altitude characteristic of a rocket engine. 1) Design altitude.

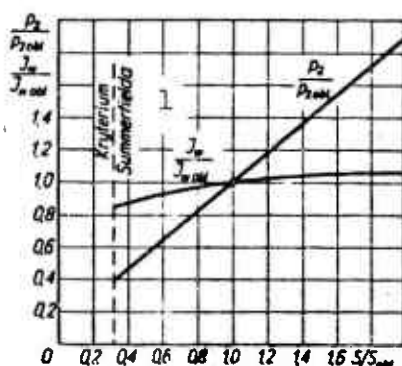


Fig. 9.4. Choking characteristic of a liquid fuel rocket engine: p_2 , J_w , S are the pressure in the combustion chamber, the specific impulse and thrust; $p_2 obl$, $J_w obl$, $S obl$ are the corresponding design quantities. 1) Summerfield's criterion.

Thrust variation as a function of altitude is due to a change in the value of p_0 in Eq. (9.1). This function is illustrated in Fig. 9.3.

Thrust regulation in a liquid fuel rocket engine is achieved by changing the flow rates of fuel and oxidizer (in general, however, preserving their weight ratio), which causes an appropriate change in the combustion chamber pressure. With constant combustion temperature and a constant nozzle geometry, this adjustment causes only a small change in the specific impulse, and it preserves the proportionality between thrust changes and combustion-chamber pressure changes. The

corresponding characteristic curve, called the choking characteristic, is shown in Fig. 9.4.

9.1.2. Mass Rate of Flow Through the Nozzle

The mass rate of fluid flow through the nozzle can be represented by the equation:

$$G = \gamma_1 a_1 F_1 = \gamma_2 a_2 \left(\frac{a_1}{a_2} \right) \left(\frac{\gamma_1}{\gamma_2} \right) F_1$$

where γ_1 , a_1 , F_1 are the specific weight, the speed of sound and the area at the critical nozzle cross section; γ_2 , a_2 are the specific weight and the speed of sound at the end of the combustion chamber.

Assuming an isentropic expansion process in the nozzle between the critical and exit cross sections and substituting the known relation for the speed of sound

$$a = \sqrt{g \kappa R T}$$

where g is the acceleration of gravity (m/sec^2); κ is the isentropic exponent; $R = 848/\mu$ is the gas constant ($\text{m}^2/\text{sec}^2 \text{K}$); μ is the molecular weight (kgf/mol), we get:

$$G = \Gamma \frac{\sqrt{g p_1^* F_1}}{\sqrt{R T_2}} [\text{kg/sec}] \quad (9.3)$$

where

$$\Gamma = \sqrt{\kappa} \left(\frac{2}{\kappa + 1} \right)^{\frac{\kappa + 1}{2(\kappa - 1)}} \quad (\text{see Table 9.1}),$$

TABLE 9.1

Γ as a Function of κ [Eq. (9.3)]

κ	Γ	κ	Γ	κ	Γ
1.14	0.6366	1.20	0.6485	1.26	0.6599
1.15	0.6386	1.21	0.6505	1.27	0.6618
1.16	0.6407	1.22	0.6524	1.28	0.6636
1.17	0.6426	1.23	0.6543	1.29	0.6655
1.18	0.6446	1.24	0.6562	1.30	0.6674
1.19	0.6466	1.25	0.6581	1.31	0.6691

p^* is the total pressure at the initial nozzle cross section; T_2 is the total temperature at the end of the combustion process, equal to

the combustion temperature of the propellants.

Substituting into Eq. (9.3)

$$m = G/g$$

an expression is obtained for the mass rate of fluid flow through the rocket engine:

$$m = \Gamma \frac{p^* F_t}{\sqrt{g} \sqrt{RT_2}} \quad (9.4)$$

9.1.3. Characteristic Parameters of Rocket Engines

The quantity characterizing the effectiveness of the flow of combustion products through the nozzle of a rocket engine has been defined in Chapter 2 as the thrust coefficient

$$C_s = \frac{S}{p^* F_t} \quad (9.5)$$

where p^* is the total pressure in the engine's combustion chamber.

This relation can be transformed by using Eqs. (9.1) and (9.3).

We then get

$$C_s = \Gamma \sqrt{\frac{2x}{x-1} \left[1 - \left(\frac{p_e}{p^*} \right)^{\frac{x-1}{x}} \right]} + \frac{F_e}{F_t} \left(\frac{p_e}{p^*} - \frac{p_0}{p^*} \right) \quad (9.5')$$

This equation is plotted in Fig. 9.5.

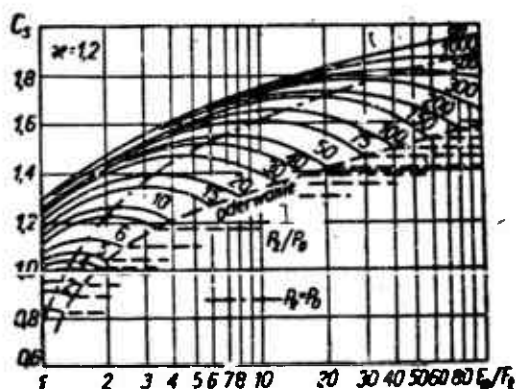


Fig. 9.5. Variation of the thrust coefficient as a function of the ratio of nozzle cross sections: of the terminal and critical areas for various expansion ratios p_2/p_0 . 1) Separation.

The region of applicability for this equation is limited by the separation phenomenon occurring in the nozzle when expansion is carried out to a pressure lower than atmospheric. This phenomenon stabilizes the magnitude of the thrust coefficient, but since it is often the cause of unsteady changes in flow direction, its occurrence should be avoided. Equation (9.5) refers to the case of isentropic flow through the nozzle. When nozzle efficiency η_d is less than unity, the maximum thrust coefficient moves in the direction of lower F_e/F_t ratios (Fig. 9.6).

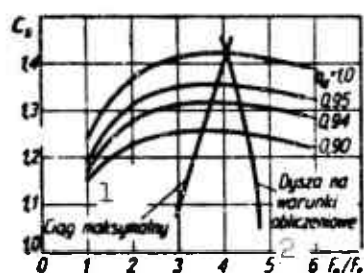


Fig. 9.6. Shift in maximum thrust coefficient as a function of nozzle efficiency. 1) Maximum thrust; 2) design nozzle.

Furthermore, taking into account that the curve of the thrust coefficient as a function of the cross-section ratio F_e/F_t is very flat in the vicinity of the maximum, it is advantageous to build the nozzle with a somewhat smaller F_e/F_t ratio than the theoretical.

The parameter characterizing the engine's combustion effectiveness is the coefficient of the mass rate of flow, defined by analogy to the thrust coefficient as:

$$C_m = \frac{\dot{m}}{p^* F_t} \text{ (sec/m)} \quad (9.6)$$

where \dot{m} is the mass rate of fluid flow through the engine.

The output coefficient has dimensions which are the inverse of the dimensions of velocity and therefore instead of C_m one very often

uses a parameter which is its inverse and which is known as characteristic velocity

$$w_c = \frac{p^* F_t}{\dot{m}} \text{ (m/sec)}. \quad (9.7)$$

Replacing \dot{m} by its value from Eq. (9.3), we get:

$$w_c = \sqrt{g} \frac{\sqrt{RT^*}}{F} \text{ (m/sec)}. \quad (9.7')$$

It is seen from Eq. (9.7) that the characteristic velocity is solely a function of the parameter RT which has been introduced in Chapter 4 and which characterizes the suitability of the propellant as a source of energy for rocket engines. The characteristic velocity defines the availability of energy from the products of combustion created in the combustion chamber and at the same time it characterizes the quality of the propellants.

Both kinds of parameters discussed above, of which the thrust coefficient defines the flow and the output coefficient (or the characteristic velocity) defines combustion, are related by a parameter introduced earlier and which characterizes the efficiency of the total engine system, namely, the thrust unit also known as the specific impulse J_w (sec). The unit of propellant consumption b (kgf/kg·hour) or the effective velocity w_j have an analogous significance, i.e., they are related with the remaining parameters characterizing the rocket engine by the equation:

$$w_j = \frac{S}{\dot{m}} = J_w g = \frac{3600 g}{b} = \frac{C_t}{C_m} = C_t w_c \text{ (m/sec)}. \quad (9.8)$$

9.1.4. Loss Coefficients

Coefficients of energy losses in a rocket engine are defined by comparing the actual values of characteristic parameters discussed in the preceding section, with the theoretical values.

These are:

- the coefficient characterizing nozzle quality, which is the ratio of the actual thrust coefficient $C_{s\text{ }rz}$ with the theoretical thrust coefficient $C_{s\text{ }t}$

$$\xi_s = \frac{C_{s\text{ }rz}}{C_{s\text{ }t}} \quad (9.9)$$

- the coefficient characterizing the quality of processes taking place in the engine chamber, that is, the quality of spray, mixture formation and primarily combustion.

This is the ratio of characteristic velocities: of the actual $w_{c\text{ }rz}$ to the theoretical $w_{c\text{ }t}$

$$\xi_w = \frac{w_{c\text{ }rz}}{w_{c\text{ }t}} \quad (9.10)$$

- the coefficient characterizing the quality of operation of the entire engine, which is the ratio of specific impulses: of the actual $J_{w\text{ }rz}$ to the theoretical $J_{w\text{ }t}$

$$\xi_J = \frac{J_{w\text{ }rz}}{J_{w\text{ }t}} \quad (9.11)$$

According to Eq. (9.8) from which we obtain the relationship

$$J_w g = C_s w_c$$

we obtain the following relation between these three loss coefficients:

$$\xi_J = \xi_w \xi_s \quad (9.12)$$

9.2. SOLID PROPELLANT ROCKET ENGINES

The characteristic feature of solid propellant rocket engines is their physical arrangement whereby the combustion chamber acts simultaneously as the propellant storage container. This eliminates automatically the fuel supply system which is indispensable in other engines, but especially in the case of larger units this increases the design weight. However, the undeniable advantage of these engines, namely their extreme simplicity, constantly assures them an expanding range of applicability.

Solid propellant rocket engines are subdivided into types according to the propellant grain shape and to the type of surface on which combustion takes place. In this way we can distinguish end-burning grains and unrestricted grains.

9.2.1. Solid Propellant Rocket Engines with End-Burning Grains

An engine with an end-burning grain is shown in the diagram of Fig. 9.20D. It consists of a cylindrical combustion chamber terminated by a nozzle; the propellant charge of constant circular cross section is located in the combustion chamber. All the propellant surfaces except the end facing the nozzle are covered with an inhibitor, that is, an inflammable substance which is also resistant to high temperature effects. The inhibitor's main component is most often talc mixed in proper proportions with polyvinyl octane in conjunction with a plasticizer, such as, for instance, butyl phthalate.



Fig. 9.7. Antitank missile.

Engines of this type are characterized by low thrust and long burning time. They are used as sustaining engines, for instance, in antitank missile and in target airplanes (Fig. 9.7).

Steady-state engine conditions are achieved when the mass rate of gas flow through the nozzle is equal to its generation rate during combustion.

Starting with the defining equation (9.6) of the output coefficient, we get:

$$m = C_m p F_t$$

This output of combustion products is generated by the combustion of the propellants

$$m = \rho_p w_s F_s$$

where ρ_p is the density of the solid propellants ($\text{kgf} \cdot \text{sec}^2 / \text{m}^4$); w_s is the combustion rate (m/sec); F_s is the combustion surface (m^2).

Assuming, as per Eq. (6.17), that

$$w_s = b p^n$$

the following equation for the equilibrium pressure in the combustion chamber is obtained after proper transformations:

$$p = \left(\frac{\rho_p b K_N}{C_m} \right)^{\frac{1}{1-n}} \quad (9.13)$$

where $K_N = F_s / F_t$ is the ratio of the combustion surface area to the nozzle critical cross sectional area; b is the temperature coefficient assumed for w_s in m/sec (in Eq. (6.17), and in Table 6.1b it is given for w_s in cm/sec).

Combustion chamber stability is illustrated in Fig. 9.8 where two characteristic curves intersect at the equilibrium point; these are the characteristic curve of the output of combustion products flowing through the nozzle and the characteristic curve of the generation of combustion products during combustion. Perturbation of equilibrium conditions by either process (combustion or flow) leads back to the equilibrium point A. Substituting the characteristic velocity w_s into Eq. (9.13) instead of the output coefficient C_m we get, according to Eqs.

(9.6) and (9.7)

$$p = (b \rho_p K_N w_c)^{\frac{1}{1-n}} \quad (9.14)$$

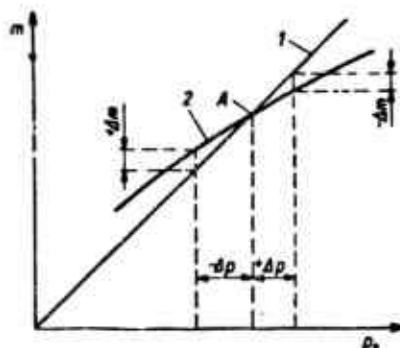


Fig. 9.8. Stability of the combustion chamber: 1) nozzle characteristic; 2) combustion characteristic; A) equilibrium point; $+\Delta m$) excess of combustion products generated during combustion with respect to the mass rate of flow of these products through the nozzle (pressure must increase); $-\Delta m$) excess of output of combustion products flowing through the nozzle with respect to the generation rate of these products during combustion (pressure must decrease).

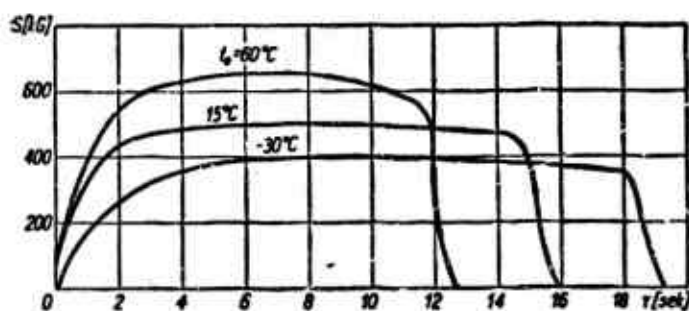


Fig. 9.9. Dependence on temperature of thrust and burn time of a solid propellant rocket engine.

In Eq. (9.14) K_N defines the engine geometry whereas b , ρ_p , w_c and n denote the properties of the solid propellant. The influence of the initial charge temperature manifests itself through the b coefficient whose variation as a function of temperature is particularly pronounced in the case of homogeneous propellants. Obviously this is related directly to thrust variations as well as burn duration. This variation for a typical booster engine is shown in Fig. 9.9.

9.2.2. Solid Propellant Rocket Engines with Unrestricted Grains

Solid propellant rocket engines with unrestricted grains are used whenever high thrust generation is required. This type of requirement occurs first of all in the case of booster engines (Fig. 9.10). The transverse cross sections of engines such as are most commonly encountered are shown in Fig. 9.11. The shape of the transverse cross section is a function of the required combustion area and of the postulated engine thrust schedule. The highest combustion area (i.e., the highest thrust and shortest burn time) is obtained in an engine (Fig. 9.11j) which is filled with several pipe-like charges. The disadvantage of such an engine (and also of engines of the types *f*, *g*, *i*, *h*) is the direct contact between engine walls and the hot combustion products. In the arrangements shown in Figs. 9.11a through *e*, on the other hand, combustion takes place only on the internal grain surface while the external grain surface in direct contact with engine walls insulates the latter from the effects of the combustion products. In order to increase thrust, the internal surface is usually made in the shape of a star.

The requirement of engine operation most often postulated is constancy of thrust. This of course is related to constancy of the grain surface during combustion.

The following phenomena, which are peculiar only to solid propellant rocket engines operating with restricted grains, seriously affect engine designs:

- pressure drop across the combustion chamber;
- erosion combustion;
- resonance combustion.

The first of these phenomena is caused by an increased output and the corresponding acceleration occurring in the combustion-product

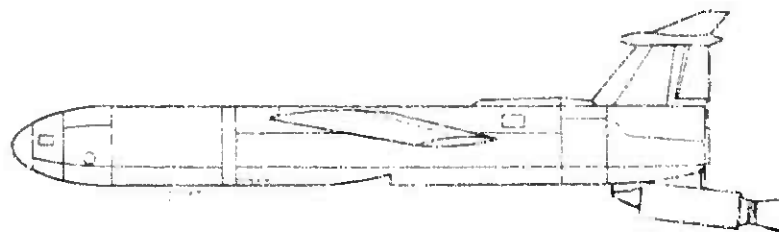


Fig. 9.10. Rocket launched by solid rocket engine.

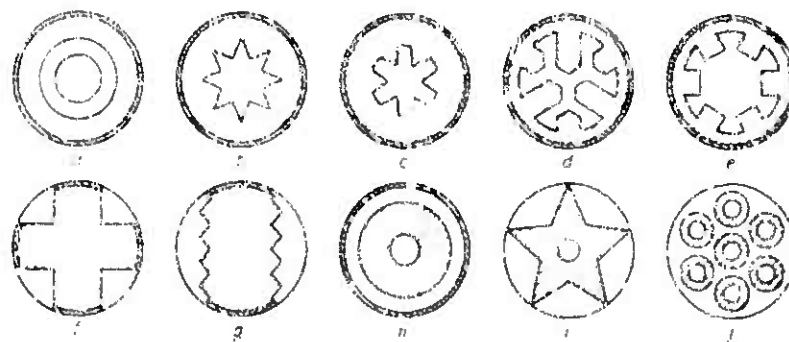


Fig. 9.11. Transverse cross sections of solid rocket propellant grains for internal burning.

stream (Fig. 9.12). Maximum pressure occurs in the initial engine cross section (Section 1, Fig. 9.12) and at the beginning of combustion when the ratio of combustion surface area to the outlet area is at its maximum. Its value can be determined by means of Eq. (9.13) in which parameter K_N is replaced by parameter $K_{N_{ef}}$ which is obtained from the expression:

$$K_{N\prime} = K_N \left[1 + \left(\frac{\Gamma^2}{2} \right) K_J^2 \right] \quad (9.15)$$

where Γ is the function defined by Eq. (9.3) and whose values are contained in Table 9.1; $K_J = F_t/F_p$; F_p is the instantaneous flow area at the terminal grain cross section (Section 2, Fig. 9.12); F_t is the area of the critical nozzle cross section.

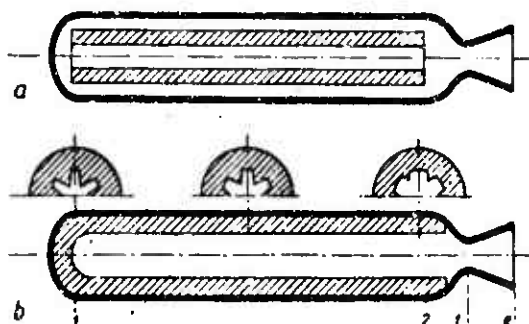


Fig. 9.12. Longitudinal cross section of rocket engines with restricted propellant grains. a) engine with a single grain of circular cross section (h of Fig. 9.11); b) engine having an internal grain combustion surface in the shape of a star (c of Fig. 9.11).

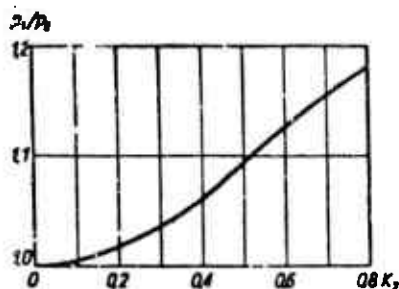


Fig. 9.13. Effect of K_J on the pressure ratio p_1/p_2 at the beginning and end of the combustion chamber.

The graph in Fig. 9.13 illustrates the effect of K_J on the ratio of pressures at the beginning and end of the combustion chamber. In order to limit the pressure changes along the combustion chamber and in order to decrease the concomitant axial loads which occur in the case of grains with circular cross section (these loads are propor-

tional to the pressure difference $p_1 - p_2$ across the grain), it is necessary to satisfy the condition

$$K_1 \leq 0,5 \quad (9.16)$$

when designing the combustion chamber of a solid propellant rocket engine. Obviously, this condition refers to the start-up condition when pressure p_1 at the chamber head reaches its maximum value. The effect of pressure variation along the chamber can be compensated for to some extent by shaping the grain in such a way as to increase the flow cross section gradually from the chamber head toward the nozzle exit. In the solution shown in Fig. 9.12b the quantity $K_{N\ ef}$ remains unchanged during the entire combustion process.

The second phenomenon, which is peculiar to the rocket engines under discussion, is the increase in combustion rate caused by the interaction of the combustion products flowing along the burning grain surface. This phenomenon, known as erosive burning, occurs when the flow velocity of the combustion products exceeds a certain limit value. The intensity of erosive burning is specified by the following erosion coefficient:

$$\varphi_E = \frac{w_{SE}}{w_S} = 1 + k(u - u_E) \quad (9.17)$$

where w_S is the combustion speed without erosion; w_{SE} is the combustion speed with erosion; u_E is the limit flow velocity of combustion products (m/sec); u is the flow velocity of combustion products (m/sec); k is a proportionality constant, and is equal to 0.002 sec/m under commonly used pressures.

In the case of homogeneous propellants, the limit velocity is around 200 m/sec.

Occurrence of erosive burning causes an increase of the combustion chamber pressure which decreases as the flow cross section in-

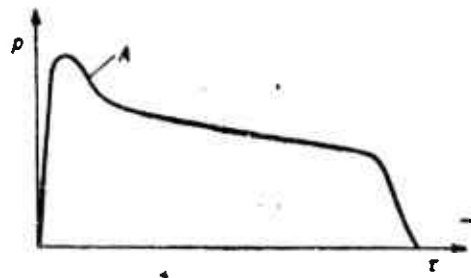


Fig. 9.14. Pressure variation during erosive burning: A) erosion peak. This graph is characteristic of regressive combustion.



Fig. 9.15. Resonant combustion.
1) atm. abs.; 2) sec.

creases and the flow velocity of the combustion products drop below the limit velocity. Due to this phenomenon an erosion peak arises, and this is illustrated in Fig. 9.14. This undesirable effect can be avoided either by increasing the initial flow cross section, which, however, reduces the size of the propellant charge, or by designing the grain shape in such a way that during the initial phase of engine operation the combustion variation be geared to the increase in flow cross section. It is thus possible to achieve in the combustion chamber a constant pressure during the entire burning time.

The third characteristic phenomenon peculiar to engines using restricted grains is resonant combustion. We mean by this the occurrence of overpressures in rocket engines, which are sometimes observed but cannot be explained by an increase in the burning surface (Fig. 9.15). This process is related to the existence of periodic pressure fluctuations in the thrust chamber and to an abnormal increase in the burning

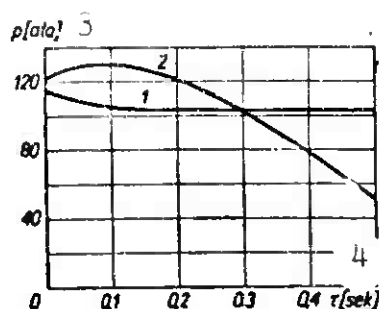


Fig. 9.16. Theoretical pressure variation as a function of time in the case of the burning of a tubular grain: 1) without openings (taking into account initial erosion); 2) with openings distributed on the grain's surface; 3) atm. abs.; 4) sec.

rate at certain points on the grain's surface. These irregularities can be eliminated by drilling a number of radial holes in the grain. Unfortunately, however, this entails a decrease in burning surface (Fig. 9.16). The radial openings are distributed on the grain's surface along the path of a screw thread so that each opening is displaced by 120° from each neighboring one. The distance between openings decreases with increasing propellant heating value. For homogeneous propellants of the JPN type, this distance amounts to 25 mm. The hole diameter should correspond to about 40% of the diameter of the inner core. Thrust chambers filled with propellant grains in the shape of pipes and in which gas flow is subdivided are particularly susceptible to resonant combustion. In this case the source of perturbations might be the dissimilarity in the pressure and rate variations along the chamber length in the various flow channels. In order to avoid this condition, the grain shape and position should be chosen in such a way as to preserve the same ratio of combustion surface area to the flow cross section for each stream of combustion products.

In the case of an engine with a single tubular grain the above condition yields the following geometric relationship:

$$\frac{d_w}{d_i} = \left(\frac{D}{d_i} \right)^2 - 1 \quad (9.18)$$

where d_o is the outside grain diameter; d_i is the inside grain diameter; D is the inside combustion chamber diameter.

Obviously, such a condition can be rigorously satisfied only during the initial combustion phase.

The reason for the instabilities described above is most likely the turbulent motion of the flowing combustion products; these turbulent motions allow the heat flux originating at the flame zone to come in direct contact with the grain surface, and this greatly increases the burning rate. This hypothesis is verified by the familiar experimental fact that the phenomenon of resonant combustion disappears with increasing pressure in the chamber, at which time the flame zone starts to supply heat to the reaction surface at a faster rate.

Over-all dimensions of a solid propellant rocket engine using a restricted grain are most often determined in such a way as to obtain minimum design weight. In general, the starting point of these calculations is the following data: thrust S (kgf); burning time τ (sec); propellant properties described by means of the characteristic velocity w_c (m/sec); and the allowable tensile stress σ (kgf/cm²) of the metal out of which the combustion chamber is manufactured. Assuming the pressure p in the combustion chamber, we can determine the thrust coefficient C_g from Eq. (9.5), and then the total propellant volume required to obtain the postulated thrust and burn time is computed:

$$V_p = \frac{1.1 S \tau}{\rho_p C_g w_c} [\text{m}^3] \quad (9.19)$$

where 1.1 is the safety factor which accounts for incomplete combustion; ρ_p is the density of the propellant (kgf·sec²/m⁴).

Next, the assumption of the K_f parameter allows us to determine the initial flow area at the terminal grain cross section:

$$F_p = \frac{1.05 \cdot S}{K_J p C_S} [\text{cm}^2] \quad (9.20)$$

where 1.05 is a coefficient which accounts for nozzle losses.

Critical nozzle cross section is given by:

$$F_t = F_p K_t [\text{cm}^2] \quad (9.21)$$

The engine's second geometric parameter is computed from Eq. (9.14).

Thus the burning surface is defined as

$$F_s = K_N F_t [\text{m}^2] \quad (9.22)$$

The following relationship is valid for the basic combustion chamber length L of radius R_k :

$$L = \frac{V_p \cdot 10^6}{\pi R_k^2 - F_p} [\text{cm}] \quad (9.23)$$

This equation allows us to determine the basic chamber dimensions if the specified combustion surface is maintained.

Engine weight G_s consists of nozzle weight G_b , combustion-chamber weight G_k and of propellant weight G_p

$$G_s = G_p + G_b + G_k$$

The individual component weights are approximated by the following equations:

- nozzle weight from the empirical equation

$$G_b = 2.5 \cdot 10^{-4} S_t [\text{kgf}] \quad (9.24)$$

- propellant weight from the obvious relation

$$G_p = V_p \gamma_p [\text{kgf}]$$

- chamber weight

$$G_k = \gamma_s \frac{p}{\sigma} (2\pi R_k^2 L + 2\pi R_k^2 - F_p R_k) \quad (9.25)$$

where γ_s (kgf/cm^3) is the specific weight of the combustion chamber wall material; $\sigma = p R_k / Z$ (kgf/cm^2) is the allowable stress in the chamber wall material; Z (cm) is the chamber wall thickness.

It is seen from the equations given above that a pressure increase in the combustion chamber of a rocket engine causes:

- a decrease in the volume of the propellant required to achieve the postulated engine performance schedule;

- a decrease in the characteristic surfaces F_t , F_p and F_s .

All these changes have a beneficial effect in reducing over-all engine dimensions. However, engine weight is a function not only of the over-all dimensions but also of wall thickness, which in turn are functions of pressure, allowable stress and chamber diameter. Therefore, it can be concluded that there is a certain optimum pressure and optimum chamber diameter for which engine weight reaches a minimum. The graph in Fig. 9.17 shows the results of such an analysis carried out for an engine having a thrust of 500 kgf and a 4-sec burning time. In the lower-portion of the graph the variations of three curves 4 are shown; these show the change in weight of an empty engine as a function of pressure in the case of three chamber diameters (10, 15 and 20 cm). The envelope of these curves is curve 5 which specifies the variation of the optimum chamber diameter R_k^* (that is, a diameter such that for a given pressure it results in the lowest weight for the empty engine). The upper part shows the effect of pressure and strength of material out of which the combustion chamber is manufactured on the over-all minimum engine weight (that is, a weight which corresponds to the optimum chamber diameter).

A solid propellant grain burns in such a way that each point on its combustion surface moves in a direction perpendicular to the tangent at that point. In view of this, grain elements which are convex toward the combustion side maintain their shape, whereas concave elements are subject to transformation and assume a bowed shape of increasing radius as the combustion process proceeds (Fig. 9.18). The

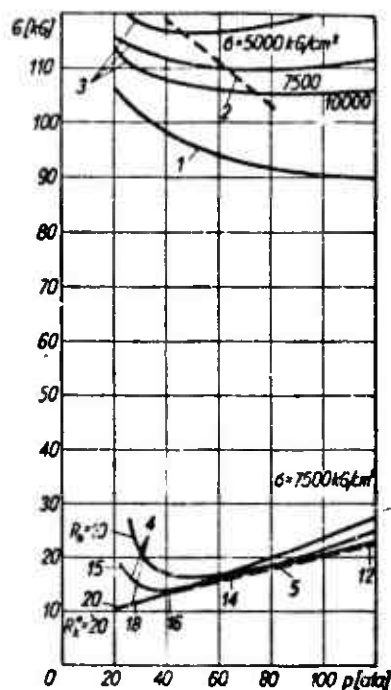


Fig. 9.17. Dependence of empty engine weight, of minimum weight of loaded engine and of weight of propellant on the pressure in the combustion chamber: 1) propellant weight; 2) curve of minimum weight of loaded engines; 3) weight of a loaded engine; 4) weight of an empty engine; 5) curve of minimum weight of empty engines; R_k^*) optimum combustion chamber diameter resulting in minimum weight for empty engine under given pressure conditions.

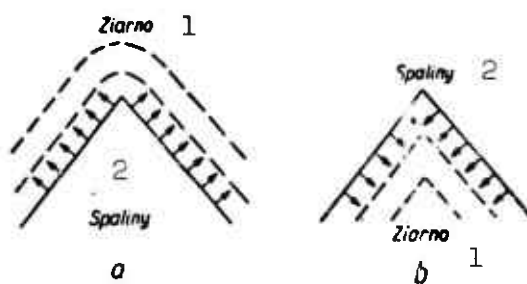


Fig. 9.18. Development of combustion in propellant elements: a) concave; b) convex. 1) Grain; 2) combustion products.

most convenient grain shape from the point of view of engine weight is a grain whose outer surface adheres to the chamber wall and which burns from the inside. This protects the walls from direct contact with the combustion products and thus allows the use of higher allow-

able stresses. Since combustion from the inside, in the case of a simple tubular grain, has a progressive character, the internal surface must be shaped in such a way that it should not change during combustion. The shape most commonly encountered which satisfies this condition to some extent is the star shape. In the segment of an 8-sided star shown in Fig. 9.19 three combustion stages can be discerned. Dur-

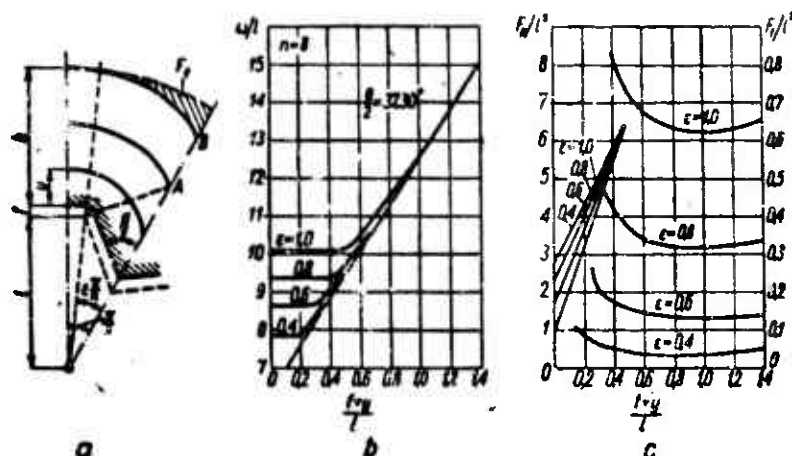


Fig. 9.19. Grain geometry having a transverse cross section in the shape of an eight-sided star.

ing the first stage, the process is in general characterized by a constant reaction surface. This lasts until the flame front reaches point A. Further combustion exhibits a progressive character. Upon reaching point B, there occurs a sudden drop in the combustion surface with a simultaneous thrust decrease. In order to avoid perturbations during this final phase of engine burn time, very often the cross-hatched area is filled out with an inert material.

Progress during the first combustion stage is a function of the choice of angle $\theta/2$. When the angle $\theta/2$ is specified by the equation

$$\frac{\pi}{2} + \frac{\pi}{n} = \frac{\theta}{2} + \operatorname{ctg} \frac{\theta}{2} \quad (9.26)$$

where n is the number of star sides, then the combustion surface is

constant.

The variation of $\theta/2$ with n is shown in Table 9.2.

TABLE 9.2
 $\bar{\theta}/2$ as a Function of n [Eq. (9.26)]

n	4	5	6	7	8	9	10	11
$\frac{\bar{\theta}}{2} [^\circ]$	28,21	31,12	33,53	35,55	37,30	38,83	40,20	42,52

If the angle $\theta/2$ is smaller than $\bar{\theta}/2$ then regression occurs during combustion. Progressive combustion occurs in the case when $\theta/2 > \bar{\theta}/2$. Figure 9.19 shows the graphs specifying all the dimensions which characterize the grain geometry, that is, ω/l , F_p/l^2 and F_f/l^2 as a function of the dimensionless combustion path $(f + y)/l$ and of the angular coefficient ϵ . The quantity ω , the so-called combustion parameter, constitutes the active length of the internal grain surface.

If the over-all grain length is denoted by L , then the combustion surface area is

$$F_g = L\omega.$$

It is seen from Fig. 7c that minimal losses are caused by the existence of the F_f surface when $f + y = l$ and when ϵ is small. This is related, however, to a large (or in the case of small ϵ to an early) progression in the second combustion stage (ω/l increases from 10.1 to 12.6).

An important problem in solid propellant rocket engines generating high thrusts is thrust control. Combining equations (9.5) and (9.14) we get:

$$S = C_s F_t (\omega_c \rho_p b K_N)^{\frac{1}{1-\alpha}} \quad (9.27)$$

It is seen from the above relations that engine thrust varies as a function of charges in:

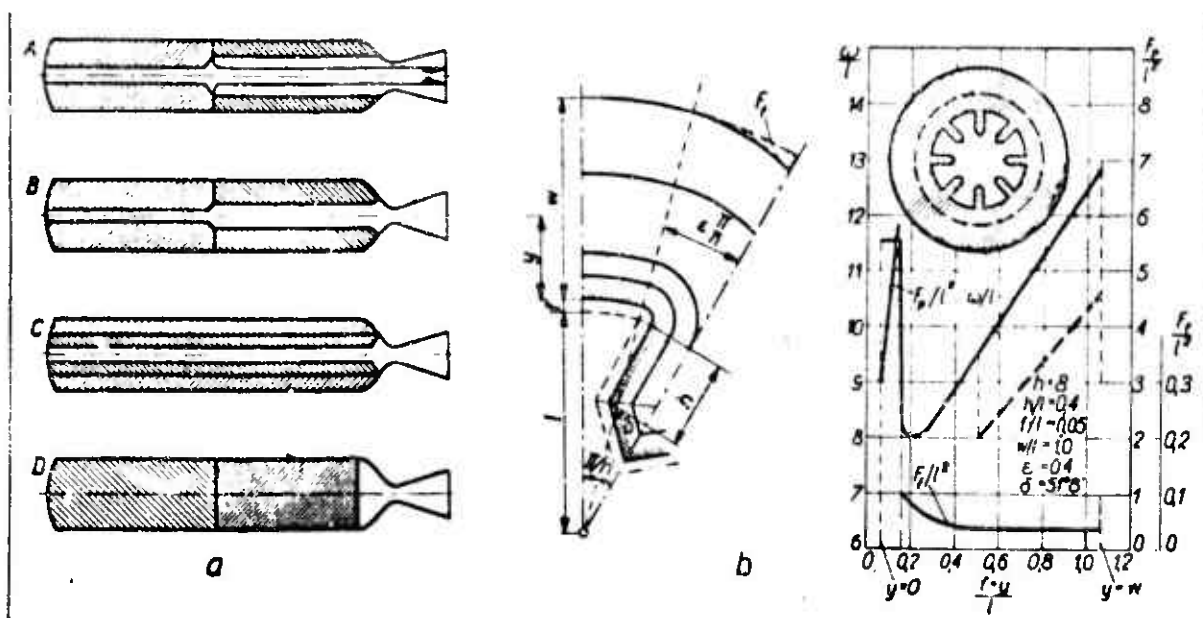


Fig. 9.20. Engines exhibiting a dual thrust range.

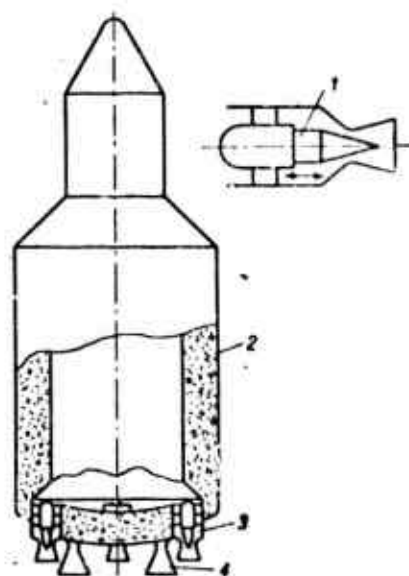


Fig. 9.21. Solid propellant rocket engine with a controllable thrust: 1) nozzle with variable cross section; 2) solid propellant; 3) controlled nozzles; 4) constant cross-section nozzles.

- type of propellant (ω_p , ρ_p , b , n);
- grain combustion surface F_B (K_N);
- area of the critical nozzle cross section F_t .

The first two methods reduce to programming the engine burn cycle;

the third method makes it possible to vary the thrust in response to definite needs. The most common case of programming occurs when the purpose of the engine is to develop high thrust during the first flight phase so as to facilitate launch, and then just to sustain the flight which requires a significantly lower thrust. The diagrams in Fig. 9.20a show sample solutions where two types of propellants were used. An engine whose cross sectional grain shape is such as to allow thrust programming is shown in Fig. 9.20b. The dashed line indicates the case in which the propellant consists of two layers, the second one of which burns more slowly.

Figure 9.21 shows the diagram of a rocket engine used to propel long-range ballistic missiles and future spaceships. Thrust control in this engine is achieved by variation of the combustion surface and by variations of the critical cross sections of the nozzles.

9.3. LIQUID FUEL ROCKET ENGINES

The combustion chamber in solid propellant rocket engines serves a dual role; it is simultaneously the fuel storage tank and the thrust chamber.

In liquid fuel rocket engines these two tasks are separated. Fuel and oxidizer are stored in two separate containers and they are introduced into the combustion chamber by means of a special pumping system. Such a thrust chamber consists of three basic zones (Fig. 9.22): injection, vaporization and combustion.

The injection zone is located directly adjacent to the injectors which are located in the forward portion of the chamber which is known as the injection head. The length of the injection zone is mainly a function of the types of injectors and the method of their emplacement. In the next zone, the injected propellants are heated by the hot combustion products, vaporized and partly mixed and even burned to some

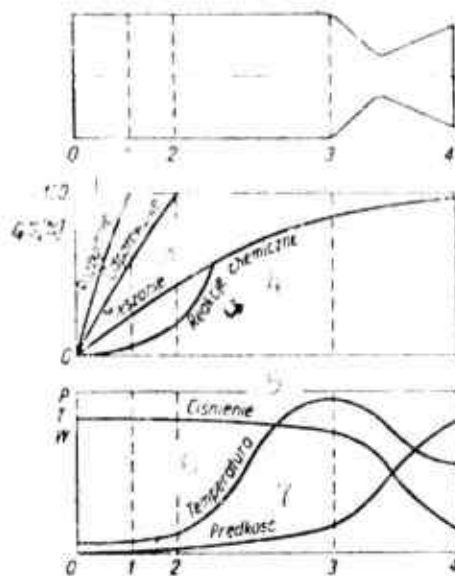


Fig. 9.22. Diagram of the development of processes in the combustion chamber of a liquid fuel engine: G'/G is the relative quantity of the injected, vaporized, mixed or burned propellant. 1) Injection; 2) vaporization; 3) mixing; 4) chemical reactions; 5) pressure; 6) temperature; 7) rate.

extent. In the third zone, the mixing process is continued and the combustion reaction is intensified. In the final portion of this zone the combustion rate is governed by the rate of mixture generation.

9.3.1. Injection System

The basic component of the injection system is the set of fuel and oxidizer injectors selected in proper number or of appropriate diameters so that they can generate a mixture of proper composition. Figure 9.23 shows a few such elementary systems. In Systems 1 and 2 injection is achieved only by atomization caused by reaction with the medium. The disadvantage of this system is a long mixing path. In Example 3 the stream injectors have been replaced by vortex injectors, which naturally complicates the design, but it accelerates mixing. In Examples 4 to 7 injection occurs as a result of collision between fuel and oxidizer streams. The resulting impact angle is determined by the equation:

$$\operatorname{tg} \theta = \frac{m_u w_u \sin \alpha_u - m_p w_p \sin \alpha_p}{m_u w_u \cos \alpha_u + m_p w_p \cos \alpha_p} \quad (9.28)$$

where m_u , m_p are the oxidizer and fuel yields; w_u , w_p are the flow velocities of oxidizer and fuel; α_u , α_p are the angles shown in Fig. 9.24.

System 8 consists of a certain variation on this method since liquid atomization is obtained as a result of its collision with a metallic wall.

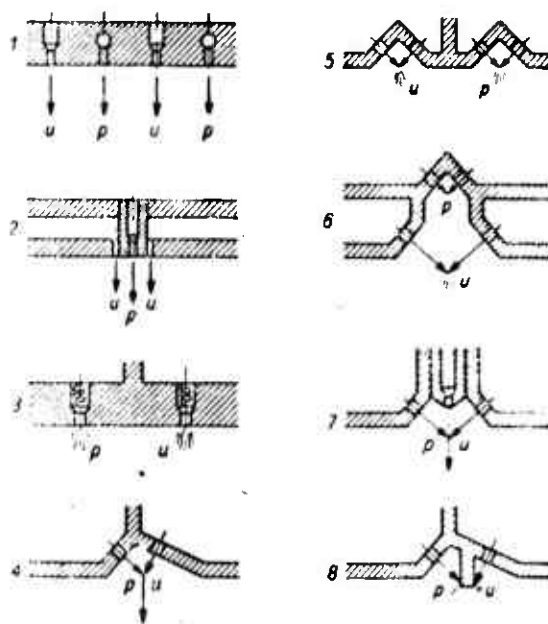


Fig. 9.23. Elementary injection systems of injection heads: u) oxidizer; p) fuel; 1 and 2) common-axis stream injectors; 3) vortex injectors; 4-7) stream injectors with colliding streams; 8) splash injectors.

The characteristic features of injection are mainly a function of the hole diameters, the angle at which the streams collide, injection overpressure and ambient pressure in the combustion chamber.

Dimensions of injection orifices vary between 0.8 and 2 mm. Excessively small orifices risk frequent clogging, whereas excessively large orifices yield an inferior spray. An injection overpressure of 4-10 kgf/cm² is commonly used. The selection of proper overpressure is

governed by finding a compromise between good spray and stress considerations.

The average diameter of the sprayed liquid is a function of injection overpressure as indicated by the expression:

$$d_m \Delta p^r = \text{const}$$

where d_m is average drop diameter; r is a constant dependent on chamber pressure ($r = 1.0$ when $p < 20 \text{ kgf/cm}^2$).

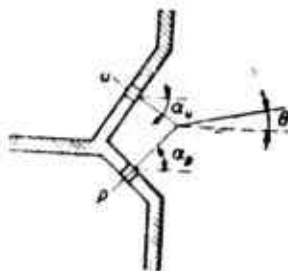


Fig. 9.24. Geometry of colliding-stream injectors.

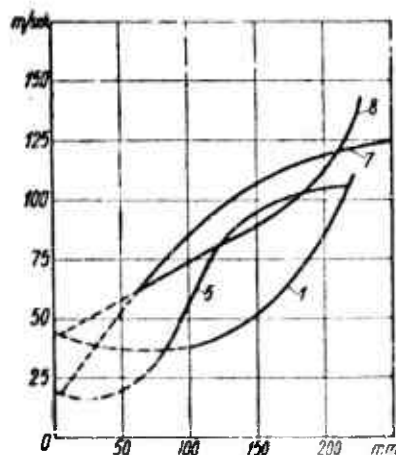


Fig. 9.25. Distribution of flow velocities for burning particles along the length of the combustion chamber. Numbers associated with the curves correspond to the particular injection systems.

The ambient pressure in the combustion chamber has a similar influence on the spray:

$$d_m p^n = \text{const}$$

where p is the pressure in the chamber; n is a constant dependent on

the diameter of the injection orifice ($\alpha = 0.35$ when $d_0 = 1.2$ and $\alpha = 0.16$ when $d_0 = 0.8$); d_0 is the orifice diameter.

In order to monitor the quality of the elementary injection systems, the velocity with which burning propellant particles move in the chamber has been determined: this velocity was obtained by measuring particle progression from the injection head to the nozzle entrance plane. The results of these measurements are shown in Fig. 9.25.

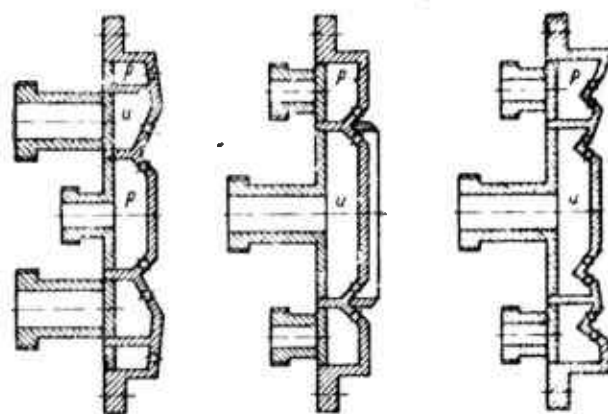


Fig. 9.26. Flat heads.

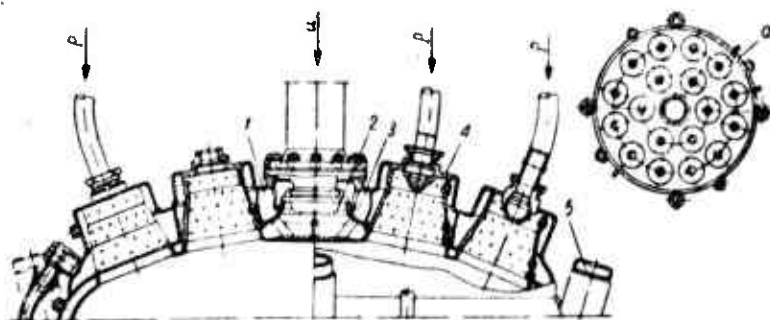


Fig. 9.27. Spherical head with antechambers: a) emplacement of antechambers on the head; 1) upper fuel manifold; 2) fuel port; 3) lower fuel manifold; 4) antechamber; 5) thrust transmitting bracket; u) oxidizer; p) fuel.

The local speed of drop motion is obviously a measure of the degree of progress in the vaporization and combustion reactions at the given chamber cross section.

The shape of the injection head and the emplacement of the elementary injection systems should be selected in such a way as to satisfy the following conditions:

- protection of walls from sudden heat transfers by emplacement of fuel and oxidizer injector orifices in such a way as to create a fuel rich zone in the vicinity of the walls;
- intensification of heat transfer between combustion products and the injected propellants;
- creation in the vicinity of the injection head of an inhomogeneous zone so as to smooth out combustion instabilities;
- creation of an antechamber in the front portion of the main combustion chamber in the case of high thrust (over 10,000 kgf) engines.

Sample head designs are shown in Figs. 9.26 and 9.27.

9.3.2. Combustion Chambers

All the fundamental processes taking place in a combustion chamber, and namely, vaporization, mass transfer, heat transfer and chemical reaction are so interdependent that one cannot select among them any one process which would govern the course of the others. This interdependence varies from case to case and makes it impossible to derive a strict analytical method of combustion-chamber design. The most typical pattern of phenomena occurring in a combustion chamber is as follows. The streams of sprayed fuel and oxidizer injected into the combustion chamber move in the direction of the combustion zone as they mix with each other and vaporize. A layer of saturated vapor is created around each drop, and the evaporation rate is governed by the diffusion rate. As a result of heat transfer from the combustion zone, the temperature of drop surface increases, and this in turn accelerates drop vaporization. If the drops do not fully vaporize by the time

they reach the combustion zone, a chemical reaction will begin on their surfaces regardless of whether it is a fuel or an oxidizer drop. The changes in mixture state, singled out above, from the instant of injection to the time of exit in the form of hot combustion gases, characterize the staytime in the chamber, which is the sum of the durations of the individual processes.

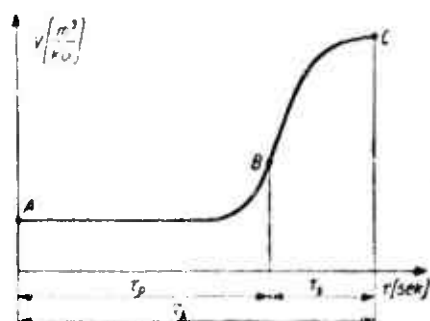


Fig. 9.28. Variation of specific mixture volume, in the combustion chamber, as a function of time.

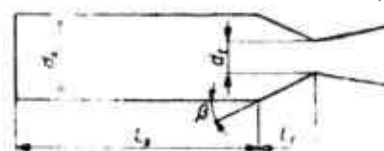


Fig. 9.29. Definition of the characteristic geometric dimensions of a combustion chamber.

If it is assumed that a measure of progress is the increase in the mixture's specific volume, then the graph in Fig. 9.28 illustrates the transformation rate in a combustion chamber. The propellant is injected at point A; then it mixes and vaporizes, igniting at point B. Combustion takes place between points B and C, and point C denotes the exit time of the hot combustion gases from the chamber. The total chamber staytime τ_k can then be treated as the sum of the following times: preparation τ_p and combustion τ_s . The magnitude of these times is a function of the injection system, the mixture properties and of the thermodynamic parameters prevailing in the chamber. They have a definite effect on the fundamental engine design parameter, and namely, combustion chamber volume.

In computations for the volume of a cylindrical combustion cham-

ber, the volume for the subsonic portion of the nozzle is added (Fig. 9.29). In this case the total volume of the combustion chamber is given by the equation:

$$V_k = F_t \left\{ L_k \left(\frac{F_k}{F_t} \right) + \frac{1}{3} \sqrt{\frac{F_t}{\pi}} \operatorname{cig} \beta \left[\left(\frac{F_k}{F_t} \right)^{3/2} - 1 \right] \right\} \quad (9.29)$$

The ratio of the chamber cross sectional area F_k to the nozzle critical cross section area F_t is selected as a function of engine thrust magnitude (Fig. 9.30). Presently there is a tendency to use the lower values of this ratio (the lower portion of the shaded region in Fig. 9.30).

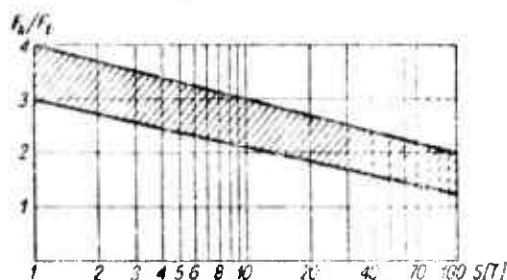


Fig. 9.30. The ratio of the cross section area of the combustion chamber to the area of the critical nozzle cross section as a function of rocket engine thrust.

Transforming Eq. (9.29)

$$L^* = \frac{V_k}{F_t} = L_k \left(\frac{F_k}{F_t} \right) + \frac{1}{3} \sqrt{\frac{F_t}{\pi}} \operatorname{cig} \beta \left[\left(\frac{F_k}{F_t} \right)^{3/2} - 1 \right] \quad (9.30)$$

we get the defining equation of the so-called characteristic chamber length.

Taking the value of L^* from the statistical data (Table 9.3), the chamber dimensions can easily be determined.

The following relation exists between the characteristic chamber length and the liquid stay time:

$$\tau_k = \frac{1}{\Gamma^2} \frac{L^*}{w_c} \quad (9.31)$$

where Γ is the function given in Table 9.1; w_c is the characteristic

TABLE 9.3

Typical Values of the Characteristic Combustion Chamber Length when Chamber Pressure $p = 20 \text{ kgf/cm}^2$

1	Material pędny	l^* [m]
2	Ciekły tlen + spirtus etylowy	1,25 - 2,00
3	Kwas azotowy + anilina	1,00 - 1,25
4	Kwas azotowy + nafta	1,25 - 1,50

1) Propellants; 2) liquid oxygen + ethyl alcohol; 3) nitric acid + aniline; 4) nitric acid + kerosene.

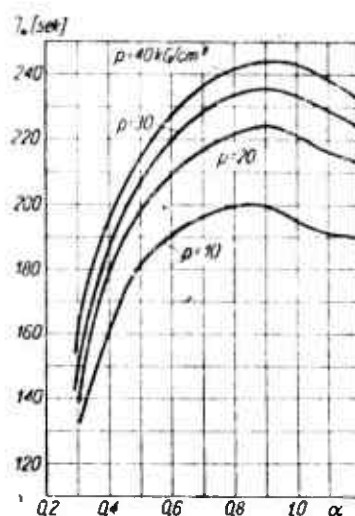


Fig. 9.31. Dependence of the specific impulse on chamber pressure and on the coefficient of oxidizer excess in the case of the mixture: 96% nitric acid + kerosene.

speed defined by Eq. (9.7').

Chamber thermodynamic parameters, that is, the coefficient of oxidizer excess (which determines the composition of the combustion products and the combustion temperature) and pressure are selected by taking into account optimum engine performance.

These effects are illustrated in Figs. 9.31 and 9.32.

It is seen from these graphs that maximum engine performance is attained with slightly rich mixtures. This is due to the fact that these mixtures are subject to dissociation to a lesser degree. Improve-

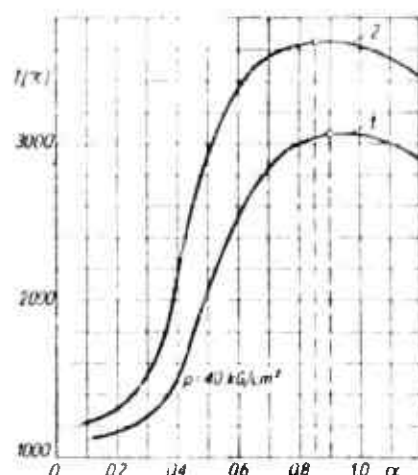


Fig. 9.32. Dependence of the combustion temperature on the coefficient of oxidizer excess: 1) nitric acid + kerosene; 2) liquid oxygen + kerosene.

ment of engine performance with increasing ambient chamber pressure can be explained on the one hand by the latter's moderating effect on disassociation and on the other hand by the increase in the thrust coefficient which is mainly a function of the ratio between the pressure inside and outside the chamber. But even in this case there is an upper bound to the pressure level which arises from its effect on the decrease of steady diffusion which in turn impairs the conditions for mass transfer. Furthermore, a pressure rise causes increased heat transfer between hot combustion gases and chamber walls and requires thicker chamber walls because of stress considerations. Thus the upper pressure bound should be taken as $p = 60 \text{ kgf/cm}^2$. Presently, however, the most commonly encountered pressures vary between 20 and 30 kgf/cm^2 .

9.3.3. Nonsteady Processes

Nonsteady combustion arises under certain operating conditions of liquid fuel engines. The results of this nonsteadiness are: fluctuations in pressure, temperature and in yield of fluid flowing through the engine; increased heat transfer to the chamber and exit nozzle

walls; and also, under certain conditions, a decrease in combustion efficiency. This has very deleterious effects on the interaction between the engine and the body being propelled; incidentally, this has been a contributory factor to the slow-down in the development of guided missiles. Two types of instabilities can be discerned in these nonsteady processes, i.e., low and high pulsation frequency. Such subdivision is due to the fluid stay time in the combustion chamber (9.31). For liquid fuel engines, this time is of the order of $\tau_k = 3 \cdot 10^{-3}$ sec.

Thus, when the instability period is greater than this time, that is, when the pulsation frequency is smaller than the corresponding frequency $\nu = 333 \text{ sec}^{-1}$, then the entire chamber participates in the oscillations. In the opposite case, when $\nu > 333 \text{ sec}^{-1}$, a pressure wave propagates through the chamber.

The fundamental reason for the occurrence of low frequency perturbations is the lag in propellant ignition due to the time required for mixing, vaporization and heating of the propellant components. They usually occur at low injector overpressures. A low overpressure in the injection system makes it very sensitive to pressure changes in the chamber, which manifests itself by a change in yield of propellants into the chamber. As has been shown, chamber pressure is stabilized because of equilibrium between the outflow of combustion products and their generation rate in the chamber as a result of the combustion reaction. If due to some cause this equilibrium is disturbed and the chamber pressure increases, the propellant output provided by the injection system decreases. During this time the chamber is cleared of combustion products since the injected propellants will not burn in time because of ignition lag; however, once it reaches combustion, this process takes place faster than under equilibrium conditions and

pressure increases sharply above the average level. In this fashion the first cycle is terminated and the next one is started.

On the basis of studies that have been conducted, the following features of combustion instability at low frequencies have been observed:

- disturbance frequency decreases with increasing chamber length;
- a rise in chamber pressure causes a drop in the pressure pulsation amplitude and an increase in its frequency;
- a rise in injector overpressure reduces frequency;
- for each liquid fuel rocket engine it is possible to determine experimentally the region of fuel-to-oxidizer ratio f and chamber pressure p in which no instabilities occur (Fig. 9.33). The minimum chamber pressure above which steady state conditions prevail, occurs in the case of a stoichiometric mixture; this pressure increases markedly as the mixture becomes lean and increases slowly when the mixture becomes rich;
- combustion efficiency decreases in the region of nonsteady chamber operation (in some cases, to as little as 20%).

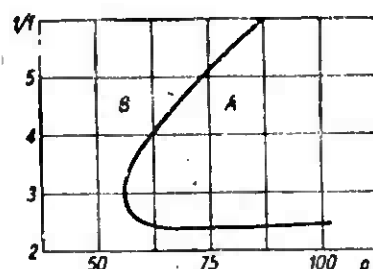


Fig. 9.33. Sample characteristic of combustion stability in liquid fuel rocket engines: A) steady operating region; B) nonsteady operating region.

High-frequency nonsteady processes are characterized by high pressure amplitudes. A secondary effect of this type of combustion instability is a twofold increase in the heat exchange rate with the cham-

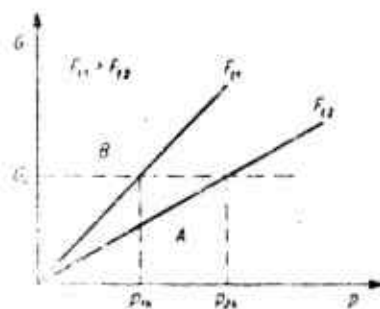


Fig. 9.34. High frequency instabilities as a function of flow rate and chamber pressure: A) region of steady state operation; B) region of nonsteady operation.

ber walls. The cause of these instabilities is the chemical ignition lag and its inverse proportionality to the chamber ambient pressure [Eq. (4.4)]. As a result of the perturbations a transverse or longitudinal standing wave is created in the chamber; in the case of longitudinal waves, the latter may transform into a strong shock wave. The frequency of these instabilities is determined, in first approximation, by the length of the standing wave and by the speed of sound in the chamber.

The following conclusions can be reached as to the effect of various parameters on the development of high frequency combustion instabilities, based on experimental evidence:

- occurrence of instabilities is a function of propellant output and of chamber pressure (Fig. 9.34). For any given engine of specified critical nozzle cross sectional area there exists a certain output and pressure above which combustion instabilities do not occur. If in the same engine the critical cross section is increased, then the limit pressure decreases ($p_{1k} < p_{2k}$, when $F_{t1} > F_{t2}$);

- pulsation frequency ν is a function of chamber length L , since the relation of interest is:

$$Lv = \text{const}$$

the transverse waves we get:

$$D_k v = \text{const}$$

where D_k is chamber diameter;

- the type of propellant also has an important effect on the pulsation frequency. Characterizing the propellant by means of the velocity w_p [Eq. (9.7)], we get the relation:

$$\nu = 0,36 \frac{w_p}{L}$$

- the injection head has an important effect on the propagation of high frequency perturbations. An inhomogeneous propellant injection and a spherical head shape with cavities have a dampening effect on the propagation of these instabilities;

-- combustion efficiency increases under the influence of high frequency instabilities because of better mass transfer conditions.

9.4. ROCKET ENGINES WITH NONCHEMICAL SOURCES OF ENERGY

The rocket engine using a chemical propellant is at the end of its developmental potential. The maximum impulses ever to be reached with this type of engine will never exceed 450 sec. This is amply sufficient to take care of all applications dealing with the propulsion of guided or ballistic missiles, but it is too small to keep pace with future needs which will arise in connection with the development of space flight. In this case, the sustaining engine will be required to supply a long burning time rather than high thrust (which is required only at launch). The applicability of the engine under this set of requirements will be governed mainly by the specific impulse. From Expression (3.11) it is seen that the exit flow velocity of the working fluid, and therefore its specific impulse, is governed by the ratio T/μ (T is the initial stream temperature, μ is the fluid's molecular weight).

Therefore, the impulse can be increased by increasing the temperature or by lowering the molecular weight of the fluid issuing from the nozzle. The fluid's temperature has an important effect on its chemical structure. Temperatures on the order of a few thousand degrees begin to cause dissociation of particles into atoms. At yet higher temperatures, the atoms give up their electrons and are thus subdivided into electrons and a positively charged remainder. As the temperature increases the number of free electrons increases and the gas becomes increasingly ionized. Such a mixture of highly ionized atoms and free electrons, generated by the effect of high temperatures, is called a plasma. By taking advantage of the plasma's electrical conductivity, it can be acted upon by means of an electromagnetic field. This has very important advantages, since physical nozzle walls are no longer required to accelerate and shape the outflowing stream. The ideas of nuclear, plasma and ion engines arose on the basis of these considerations.

9.4.1. Thermonuclear Engines

In a thermonuclear engine (Fig. 9.35) the working fluid is heated by the thermal energy liberated during the fission process. The basic problem in selecting the design parameters of such an engine is to find a compromise between specific impulse and temperature.

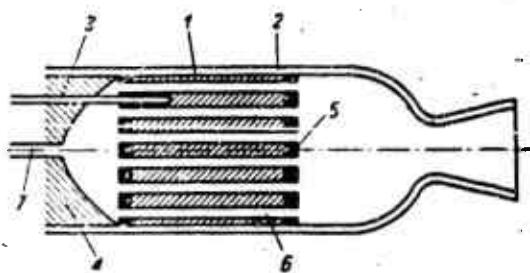


Fig. 9.35. Thermonuclear engine: 1) fission reaction; 2) containing envelope; 3) control rod; 4) screen; 5) reflector; 6) flow channels; 7) pipe bringing in the working fluid.

From the point of view of specific impulse, it is most advantageous for the outflowing gas to be dissociated into atoms since then its atomic weight is at its lowest (e.g., for atomic hydrogen $\mu = 1$). Unfortunately, the temperature for total dissociation of gas particles is around 5000°C whereas the melting temperature of most refractory materials, such as hafnium and tantalum oxides, does not even reach 4000°C . Therefore, the maximum temperature of the working fluid cannot be set any higher than 3300°C which yields a specific impulse of approximately 1000 sec. At these maximum temperatures the uranium contained in the reactor should be either in the liquid or gaseous state. With such an impulse and an engine thrust on the order of 10^6 kgf, the output of working fluid should be around 1000 kgf/sec, which corresponds to a unit consumption of $3.6 \text{ kgf/kgf}\cdot\text{hour}^2$ and thus smaller by a factor of ~ 4.5 than in present rocket engines with chemical energy sources. Thermonuclear engines will be used in the future as booster engines for space travel.

9.4.2. Electrothermal and Magnetohydrodynamic Plasma Engines

The drawing in Fig. 9.36 shows the diagram of an electrothermal plasma engine. In this engine, heating of the working fluid is accomplished by means of an electric arc. Maximum arc temperature is about $50,000^{\circ}\text{K}$. The gas flowing through the arc is heated from 3 to 12 thousand $^{\circ}\text{K}$. If hydrogen is used as the working fluid, we will get impulses up to 2500 sec. The impulse boundary value comes about because of the increase in gas conductivity with temperature rise. When this conductivity approaches that of copper, due to large losses in the external circuit, engine efficiency drops. The advantage of this engine is the ease of thrust control by varying gas output which directly influences its temperature.

A disadvantage of the engine is rapid electrode wear. Thrusts at-

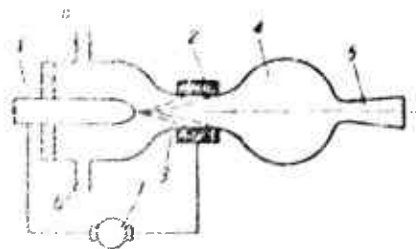


Fig. 9.36. Electrothermal plasma engine: 1) cathode; 2) anode; 3) electric arc; 4) mixing chamber; 5) supersonic nozzle; 6) pipes bringing in the working fluid; 7) voltage source 200 v.

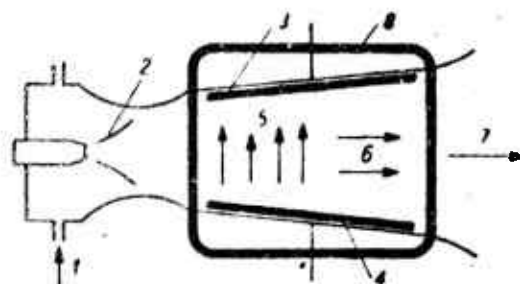


Fig. 9.37. Magnetohydrodynamic plasma engine: 1) channel bringing in the working fluid; 2) electric arc; 3) cathode; 4) anode; 5) electric current flowing perpendicularly to the direction of plasma flow; 6) plasma acceleration; 7) plasma outflow; 8) coil creating a magnetic field directed perpendicularly to the drawing surface.

Obtainable with these engines will be on the order of tenths of a kilogram. A further developmental stage of the electrothermal engine is the magnetohydrodynamic engine in which plasma acceleration is obtained not by expansion in an appropriately shaped channel, but by action upon it by a magnetic field. In this fashion, direct contact between plasma and metal engine walls is avoided. A diagram of a typical magnetohydrodynamic engine is shown in Fig. 9.37. Specific impulses up to 25 thousand sec can be obtained with such an engine.

9.4.3. Ion Engine

An ion engine (Fig. 9.38) consists of three basic components: an ion generator, an electrostatic accelerator and a neutralizer. The working fluid in an ion engine consists of cesium vapors fed in through an appropriately shaped distributor 2 onto the ionizing insert

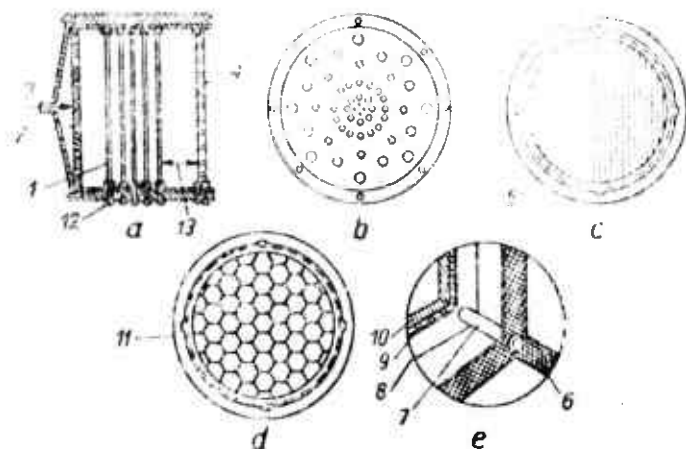


Fig. 2.38. Ion engine: a) engine cross section; b) cesium vapor distributor; c) ionizing element; d) cathode screen, perspective view of a cathode screen which produces electrons; 1) ionizing elements; 2) distributor; 3) conduit bringing in cesium vapors; 4) cathode screen; 5) incubation ring; 6) ion acceleration screen; 7) bracket; 8) thermoelectric electron generator; 9) heating element; 10) cathode screen; 11: outside steel wall; 12) terminals of electrical conductors; 13) zone of ion acceleration.

elements 1. These elements are made of porous tungsten. By coming into contact with these, the cesium vapors ionize. The efficiency of such surface ionization reaches to 100%. The positively charged particles, thus generated, are accelerated through zone 13 by means of an electrostatic field created by the cathode screen 4 shaped like a honeycomb which yields a uniform field intensity in the radial direction. In order to safeguard the system from becoming negatively charged, which would occur in a relatively short time due to the expulsion of positive particles only, the ions are neutralized in front of the last cathode screen 10 by mixing them with a beam of electrons which is generated on the surface of the thermoelectric generator 8. Similar to all other engines, the thrust of an ion engine is given by:

$$S = m v_e$$

where

$$m = \frac{\mu^2}{1000 n q N_A}$$

$$w_e = \sqrt{\frac{2000 n q N_A V}{\mu}}$$

μ is the atomic weight; n is the degree of ionization; q is the elementary ion charge; N_A is Avogadro's number; V is the voltage; I is the ion current intensity. In the case of cesium, that is, for $\mu = 133$, we get

$$S = 1,6 \cdot 10^{-4} I \sqrt{V} \text{ [kg]} \quad (9.32)$$

Impulses generated by this engine are of the order of $3 \cdot 10^7$ sec.

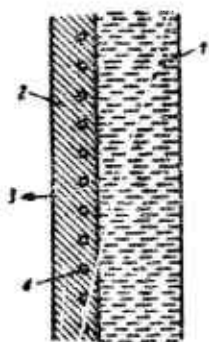


Fig. 9.39. Engine which converts nuclear energy directly into thrust: 1) reflector; 2) fission material; 3) fissioned atomic nuclei and neutrons; 4) cooling passages.

9.4.4. Engines Which Convert Nuclear Energy Directly into Thrust

It is possible to imagine the occurrence of thrust as a direct result of fission of atomic nuclei. In this case a nuclear reactor would fulfill the role of a generator of appropriately accelerated particles. Figure 9.39 illustrates the theory of operation of such an engine. A layer of fissionable material (U235) is shielded on one side by a mass of synthetic material which acts in the role of a reflector and of an absorber. The nuclear elements and the neutrons generated as a result of the fission reaction of uranium create the thrust. The attainable impulse of this engine is 10^7 sec.

9.3.3. Photon Engines

Figure 9.40 shows the diagram of a hypothetical engine presently constituting the highest achievement of the rational fantasy of a human mind. The engine's basic component is a nuclear light source filled with a gas and connected to a fission or fusion reactor, within which

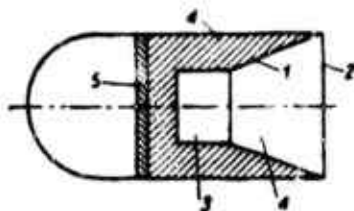


Fig. 9.40. Photon engine: 1) reflector; 2) transparent wall; 3) reactor; 4) glowing gas; 5) biological wall.

corpuscular and electromagnetic radiation energy (arising out of the nuclear reaction) would be transformed into light energy. The photons ejected by the gas filling the light source, as a result of these processes, create engine thrust. The walls of the nuclear light source are made of hypothetical materials: a hypothetically ideal reflector 1, which reflects all the photons and directs them along parallel paths in the "outflow" direction and hypothetical matter 2 which is ideally transparent and would let all these photons through. Only such hypothetical materials allow proper operation of the photon engine. Any imperfection in these bodies would cause instantaneous destruction of the engine by melting the walls. The thrust of a photon engine can be derived by starting with the Einstein equation which relates energy to the mass of a photon:

$$E = mc^2$$

and with de Broglie's equation which defines a photon's impulse:

$$J_F = mc = \frac{vh}{c} = \frac{h}{\lambda} = \frac{E}{c} = 3.06 \cdot 10^7 \text{ sec}$$

where h is Planck's constant; v is the frequency of photon radiation; c is the velocity of light; λ is the wavelength of photon radiation; E is the photon energy; m is the photon mass at rest; g is the acceleration of gravity.

From these two equations we get:

$$S = \frac{dJ_F}{dt} = \frac{d(vh/c)}{dt} = \frac{dE}{cdt} = \frac{N_F}{c} [\text{kRf}] \quad (9.33)$$

where N_F is the force of the stream of issuing photons.

In the last two years the photon engine has become the one system which most stimulates the imagination of engineers and scientists. This has come about because of the perhaps distant, but definitely genuine possibility of space flights at near the velocity of light by means of this engine.

REFERENCES TO CHAPTER 9

- 9.1. M. Zucrow: Propulsion. 1956.
- 9.2. M. Barrere, F. de Venbeke, A. Jaumotte, J. Vedonkerchhowe: La Propulsion par Fussees [Rocket Propulsion]. 1957.
- 9.3. H. Mebus: Berechnung von Raketentriebwerke [Design of Rocket Propulsion Systems]. 1957.
- 9.4. W. Corlis: Propulsion Systems for Space Flight. 1960.

Chapter 10

COMPOUND ENGINES

Compound engines consist of a system of two engines which complement each other. In such a system, the primary engine, which is usually a turbojet, a pulsejet, or a rocket motor, is supplemented with a ramjet engine.

The ramjet engine can be supplied with fuel independently or it can function merely in the role of a tunnel within which atmospheric air mixes with the combustion products generated by the primary engine.

10.1. COMBINATION OF A TURBOJET ENGINE WITH A RAMJET ENGINE

The compound engine shown in Fig. 10.1 is an example of a ramjet engine which is supplied with fuel independently of the primary engine.

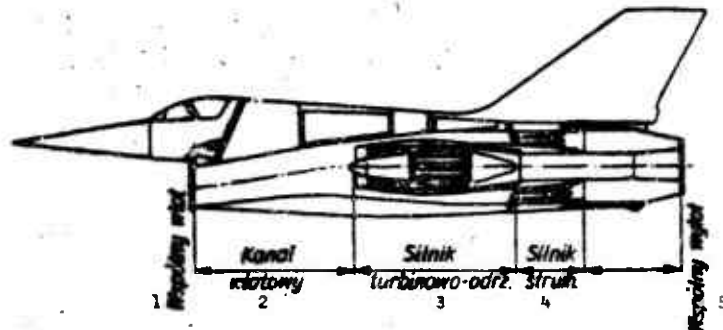


Fig. 10.1. Cross section of *Griffon 02* aircraft with compound propulsion system: a turbojet engine and a ramjet engine. 1) Common inlet; 2) inlet port; 3) turbojet engine; 4) ramjet engine; 5) common exhaust.

Figure 10.2 shows the proportion of thrust contributed by the turbojet and the ramjet engines in a compound engine system as a function of flight speed. The thrust contribution of the ramjet engine to

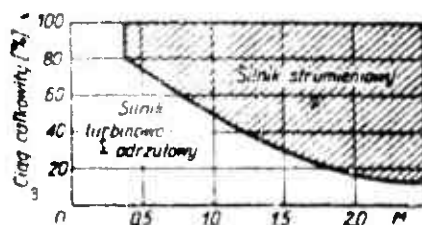


Fig. 10.2. Proportion of turbojet engine thrust in total compound engine thrust, as a function of Mach number. 1) Turbojet engine; 2) ramjet engine; 3) total thrust (%).



Fig. 10.3. Variation of compound engine thrust as a function of Mach number: 1) turbojet engine; 2) ramjet engine; 3) thrust (%).

the thrust of the combination increases from 20% at the switch-in speed corresponding to a Mach number of 0.4 to 85% at a Mach number of 2.2. Absolute changes in thrust magnitude relative to the static thrust of the turbojet are shown in Fig. 10.3 as a function of Mach number. The corresponding unit fuel consumptions are illustrated by the curves in Fig. 10.4. This type of compound engine is considered the most advantageous propulsion system for future long-range transport airplanes flying at speeds corresponding to $M = 3-5$. The starting point in the design of compound engines of this type is an existing and properly selected turbojet engine whose speed characteristics are known.

Once the required thrust variation as a function of speed is given, the ramjet engine is chosen in such a way that its thrust in the compound configuration should correspond to the stated requirements.

During the design phase, consideration should be given to the problem of cooling the turbojet engine and to guard it from interaction

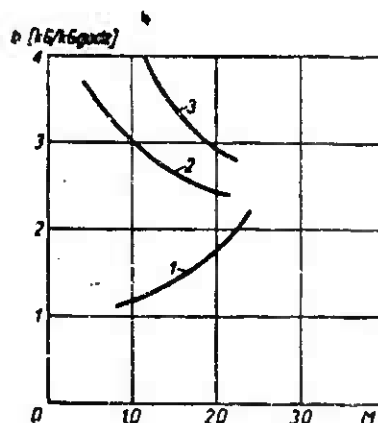


Fig. 10.4. Unit fuel consumption as a function of speed: 1) turbojet engine; 2) compound engine; 3) ramjet engine; 4) b (kgf/kgf·hr).

with the pressure pulses occurring in the ramjet combustion chamber. The study of the ramjet engine is a serious problem. In view of huge air requirements, such studies are conducted mainly on scale models or on ring segments of the actual scale combustion chamber.

10.2. TUNNELING OF PULSEJET AND ROCKET ENGINES

Emplacement of pulsejet or rocket engines in a cylindrical channel in order to increase its thrust can be accomplished in two ways:

- in an underpressure system, that is, by means of a Melot nozzle;
- in an overpressure system, that is, in combination with a ramjet engine.

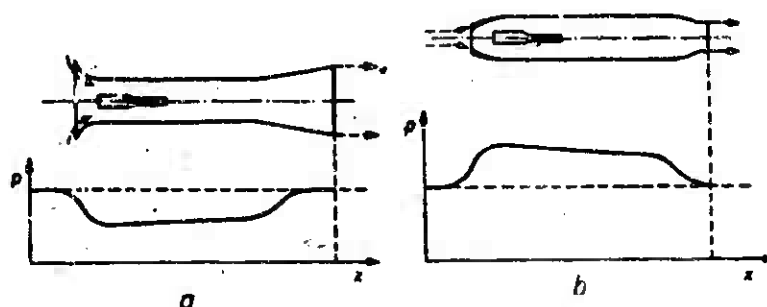


Fig. 10.5. Tunneling of pulsejet or rocket engines: a) in a system with a Melot nozzle; b) in a system with a ramjet engine.

Both these cases are illustrated in Fig. 10.5. Thrust increase, caused by tunneling, independent of the type of primary engine or of the kind of tunneling, can be determined by starting with the fundamental equations of conservation of energy, momentum and mass, by means of the following relation:

$$\frac{S}{S_0} = \frac{\sqrt{2ME \left[1 - \left(\frac{p}{p_2} \right)^{\frac{\kappa-1}{\kappa}} \right] + J^2 \left(\frac{p}{p_2} \right)^{\frac{\kappa-1}{\kappa}}}}{\rho_0 F_0 w_0^2 - \rho F_{20} w^2 \left\{ 1 + \left(2g c_p \frac{T}{w^2} \right) \left[1 - \left(\frac{p}{p} \right)^{\frac{\kappa-1}{\kappa}} \right] \right\} \left(\frac{p}{p} \right)^{\frac{1}{\kappa}}} + \frac{-\rho F_2 w^2 \sqrt{1 + \frac{2g c_p T}{w^2} \left[1 - \left(\frac{p}{p} \right)^{\frac{\kappa-1}{\kappa}} \right] \left(\frac{p}{p} \right)^{\frac{1}{\kappa}}}}{\rho_0 F_0 w_0^2 - \rho F_{20} w^2 \left\{ 1 + \left(2g c_p \frac{T}{w^2} \right) \left[1 - \left(\frac{p}{p} \right)^{\frac{\kappa-1}{\kappa}} \right] \right\} \left(\frac{p}{p} \right)^{\frac{1}{\kappa}}}$$

where

$$\begin{aligned} M &= \rho_0 F_0 w_0 + \rho (F_2 - F_{20}) \left(\frac{p}{p} \right)^{\frac{1}{\kappa}} \sqrt{w^2 + 2g c_p T \left[1 - \left(\frac{p}{p} \right)^{\frac{\kappa-1}{\kappa}} \right]}; \\ J &= \rho_0 F_0 w_0^2 + \rho (F_2 - F_{20}) \left(\frac{p}{p} \right)^{\frac{1}{\kappa}} \left[w^2 + 2g c_p T \left[1 - \left(\frac{p}{p} \right)^{\frac{\kappa-1}{\kappa}} \right] \right]; \\ E &= \rho_0 F_0 w_0 \left(\frac{w_0^2}{2} + g c_p T_0 \right) + \\ &+ \rho (F_2 - F_{20}) \left(\frac{p}{p} \right)^{\frac{1}{\kappa}} \sqrt{w^2 + 2g c_p T \left[1 - \left(\frac{p}{p} \right)^{\frac{\kappa-1}{\kappa}} \right] \left(\frac{w^2}{2} + g c_p T \right)}; \end{aligned}$$

p , T , ρ are pressure, temperature, density; F , w are the cross sectional area and flow velocity; c_p , κ are the specific heat at constant pressure (kgf-m/kgf·°K) and the isentropic exponent; M , J , E are the effective mass, impulse and energy; subscript 0 refers to the parameters at the end of the primary engine; subscript 2 refers to the parameters of the mixing chamber; no subscript refers to the surrounding parameters; S , S_0 are the thrusts of the tunneled and nontunneled engines.

Figure 10.6 shows the characteristics of tunneled engines, which were computed on the basis of the given equation. It is seen from these

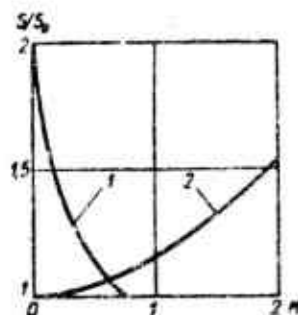


Fig. 10.6. Speed characteristics of tunneled engines: 1) in a system with a Melot nozzle; 2) in a system with a ramjet engine.

graphs that the underpressure system with a Melot nozzle results in large thrust increases only at low flight speeds. On the other hand, the system compounded with a ramjet engine has a very advantageous characteristic. In this case, thrust increases parabolically with speed. The advantages of tunneling are, however, negated to a large extent by the increase in engine weight and drag. For instance, in the case of a pulsejet engine having a thrust of 165 kgf at a speed of 200 km/hour, the internal thrust increases by 70 kgf if the flight speed increases to 800 km/hour; however, the useful thrust increases only by 20 kgf. But in certain cases, even this may prove to be beneficial, since one would expect a thrust decrease under these conditions in an untunneled engine.

In order to compare the performance of a compound rocket-ramjet engine with that of a ramjet engine, the characteristics of these engines are shown in Figs. 10.7 and 10.8. These characteristics have been computed for a flight altitude of 20 km.

In order further to stress the advantages of this type of compound engine, one should consider their great simplicity, especially in the case of a system consisting of a solid propellant rocket engine.

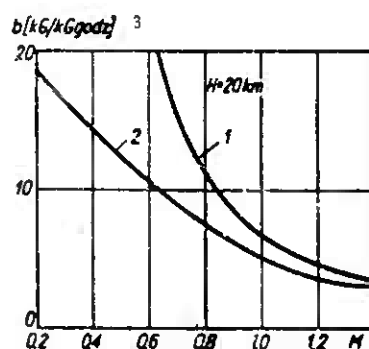


Fig. 10.7. Comparison of engine unit fuel consumption: 1) ramjet engine; 2) compound rocket-ramjet engine; 3) b ($\text{kgf/kgf} \cdot \text{hr}$).

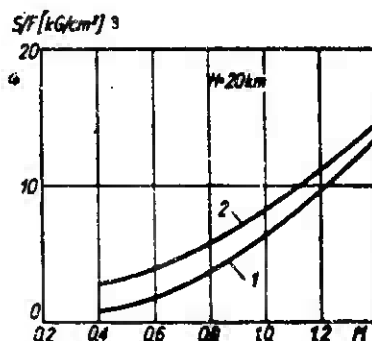


Fig. 10.8. Comparison of engine unit thrust: 1) ramjet engine; 2) compound rocket-ramjet engine; 3) S/F (kgf/cm^2).

In designing such an engine, one should consider the proper selection of the ratio of the primary stream to the secondary, seeking of course the optimum conditions with respect to thrust. The mixing chamber, which in this case functions in the role of a combustion chamber, is designed by the method given in Section 3.4.

The performance of a compound engine consisting of a ramjet engine can be greatly increased by afterburning additional fuel in the mixing chamber. However, in this process the engine's main advantage, namely its simplicity, is lost. It should be noted that afterburning fuel in a Melot nozzle not only does not increase, but decreases the compound engine's thrust.

REFERENCES TO CHAPTER 10

- 10.1. E. Sänger: Die physikalischen Grundlagen der Strahlantriebstechnik [Physical Foundations of Jet Propulsion]. 1953.
- 10.2. J. Glassmann, J. Charyk: The Ramrocket. 1960.

Chapter 11

ENGINE COOLING

The task of the cooling system is the maintenance of engine components within allowable limits which are determined by stress considerations. In view of the high temperatures and flow velocities which occur in rocket and ramjet engines, and in view of the great intensity of heat transfer which is not encountered any place else, the cooling problem has become one of the most difficult tasks in the design of these engines.

A survey of the commonly used methods of wall cooling is illustrated in Fig. 11.1. The first method (1) has the character of passive protection. The metal wall is covered with a refractory coating having a high heat-flow resistance. The heat flux which goes through the protective coating increases the metal wall temperature. The temperature increases up to the metal's melting point. Therefore, the steady state operation of an engine using this type of cooling is impossible, and the problem reduces to an answer to the questions:

- how long can the engine operate in a safe manner?
- what materials will ensure long-lasting engine operation?

This type of cooling is used mainly in solid propellant rocket engines.

The second method (2) commonly used in pulse and ramjet engines consists in transferring heat away from the heated wall by means of radiation and by convection to the atmospheric air flowing past the wall. At hypersonic flows the boundary layer is aerodynamically heated

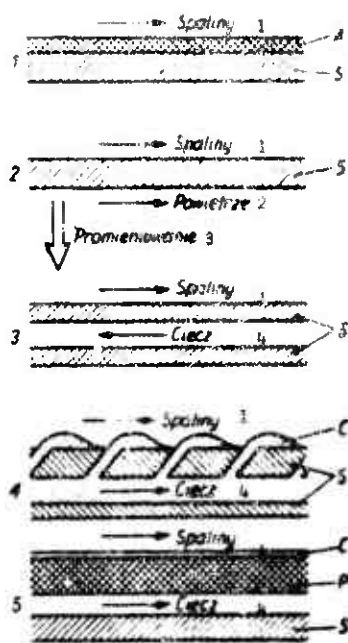


Fig. 11.1. Methods of wall cooling: A) coating of a refractory paint; S) metal wall; C) liquid; P) porous material. 1) Combustion products; 2) air; 3) radiation; 4) liquid.

so that heat transfer can take place only through radiation.

In the third system (3), which is typical for liquid fuel rocket engines, wall cooling takes place by means of the flow of one of the propellant components (most often of the oxidizer). If this type of cooling is insufficient, additional cooling (4) by means of evaporation of part of the liquid is used, this liquid being fed to the internal side of the wall to be cooled by special conduits prepared for this purpose. For a more uniform supply of the fluid to the internal wall side, it has been proposed that it be made out of a porous material (5). This method, found in animals and people, appears to have the greatest future potential.

11.1. HEAT CONDUCTION THROUGH THE WALL

Heat exchange between combustion products and the wall takes place by transfer, that is, by convection and radiation. However, the radiation contribution is small and amounts to only a few per cent of

the total heat flow.

In view of this, the process of heat flow (Fig. 11.2) from the combustion products through the wall and to the coolant consists of only three fundamental phenomena:

- heat transfer between the wall and combustion products;
- heat conduction through the wall;
- heat transfer between the wall and the coolant.

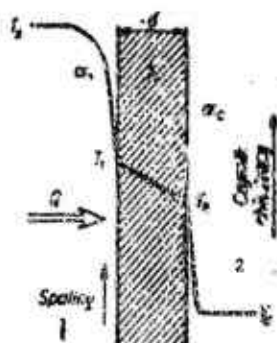


Fig. 11.2. Heat flow through the wall. 1) Combustion products; 2) coolant.

The quantity of heat flowing through the wall is given by the following equation:

$$q = \frac{Q}{F} = \frac{T_g - T_c}{\frac{1}{\alpha_g} + \frac{\delta}{\lambda} + \frac{1}{\alpha_c}} \quad (11.1)$$

where Q is the quantity of heat transferred to the surroundings per unit time (kcal/sec); F is the heat transfer area (m^2); T_g is the temperature of the combustion products ($^{\circ}K$); T_c is the temperature of the coolant ($^{\circ}K$); δ is the wall thickness (m); λ is the wall's thermal conductivity (kcal/m·sec· $^{\circ}K$); α_g is the coefficient of heat transfer between the combustion products and the wall (kcal/m 2 ·sec· $^{\circ}K$); α_c is the coefficient of heat transfer between the wall and the coolant (kcal/m 2 × sec· $^{\circ}K$).

The heat transfer coefficients are a function of the fluid type and of the conditions under which heat transfer takes place.

In general, one uses the following equations:

- for the combustion products flowing through the engine [11.1]

$$Nu = 0,0162 (Re Pr)^{0,42} \left(\frac{T_g}{T_1} \right)^{0,35} \quad (11.2)$$

where $Nu = \frac{\alpha_g d}{\lambda_1}$ is the Nusselt number; $Re = \frac{w_1 d}{\nu_1}$ is the Reynolds num-

ber; $Pr = \frac{\gamma_1 \nu_1 c_{p1}}{\lambda_1}$ is the Prandtl number; λ_1 is the thermal conductivity of the combustion products at the wall temperature (kcal/m·sec·°K); γ_1 is the specific weight of the combustion products (kgf/m³); w_1 is the flow velocity of the combustion products at a given cross section (m/sec); $\nu_1 = \frac{\mu_1 g}{\gamma_1}$ — is the kinematic viscosity (m²/sec); T^* is the stagnation temperature of the combustion products (°K); T_1 is wall temperature (°K); c_{p1} is the specific heat of combustion products at wall temperature (kcal/kgf·°K); d is the diameter of the given cross section (m).

The specific heat c_{p1} and the kinematic viscosity μ_1 of the gaseous mixture are defined by the following relations:

$$c_{p1} = \sum (m_i c_{pi})$$

$$\mu_1 = \left(\sum \frac{m_i}{\mu_i} \right)^{-1} \quad \text{or} \quad \mu_1 g = \left(\sum \frac{m_i}{\mu_i g} \right)^{-1} \quad (11.3)$$

where m_i is the weight percentage of the individual component; g is the acceleration of gravity (m/sec²).

TABLE 11.1

Specific Heat of Gases (kcal/kgf·°C)

Temperature 1 [°C]	2						
	O ₂	N ₂	H ₂	CO	NO	CO ₂	H ₂ O
0	0,218	0,248	3,390	0,248	0,238	0,194	0,444
100	0,223	0,2489	3,4509	0,2493	0,2381	0,2182	0,4515
200	0,230	0,2512	3,4643	0,2528	0,2414	0,2371	0,4635
300	0,2376	0,2554	3,4712	0,2580	0,2472	0,2524	0,4778
400	0,2445	0,2607	3,4826	0,2641	0,2534	0,2652	0,4931
500	0,2504	0,2664	3,5020	0,2704	0,2594	0,2758	0,5092
600	0,2553	0,2721	3,5298	0,2763	0,2648	0,2847	0,5258
700	0,2593	0,2774	3,5660	0,2816	0,2695	0,2921	0,5429
800	0,2627	0,2822	3,6101	0,2863	0,2736	0,2984	0,5601
900	0,2656	0,2864	3,6572	0,2904	0,2770	0,3037	0,5769
1000	0,2682	0,2902	3,7063	0,2939	0,2799	0,3081	0,5929
1100	0,2703	0,2935	3,7584	0,2970	0,2824	0,3119	0,6080
1200	0,2723	0,2964	3,8095	0,2996	0,2845	0,3152	0,6220

1) Temperature; 2) chemical symbol of gas.

Values of c_{pi} and $\mu_i g$ can be selected, for the appropriate wall

TABLE 11.2

Value of $g_u \cdot 10^5$ (kgf/msec) as a Function of Temperature

Tempe- ratura 1 [°C]	2 Symbol chemicheskyy gasu						
	O ₂	N ₂	H ₂	CO	NO	CO ₂	H ₂ O
0	1,943	1,667	0,850	1,656	1,352	1,384	0,818
100	2,460	2,101	1,052	2,067	1,825	1,846	1,208
200	2,910	2,478	1,226	2,462	2,257	2,262	1,605
300	3,312	2,815	1,381	2,797	2,653	2,642	2,000
400	3,677	3,121	1,521	3,100	3,020	2,991	2,390
500	4,014	3,402	1,651	3,380	3,362	3,316	2,772
600	4,327	3,664	1,771	3,640	3,683	3,620	3,145
700	4,622	3,911	1,884	3,885	3,986	3,906	3,510
800	4,900	4,143	1,991	4,116	4,272	4,177	3,864
900	5,164	4,364	2,093	4,336	5,546	4,435	4,21
1000	5,416	4,575	2,190	4,545	4,807	4,681	4,447
1100	5,657	4,777	2,283	4,746	5,057	4,917	4,674
1200	5,889	4,97	2,373	4,939	5,239	5,143	5,194

1) Temperature; 2) chemical symbol of the gas.

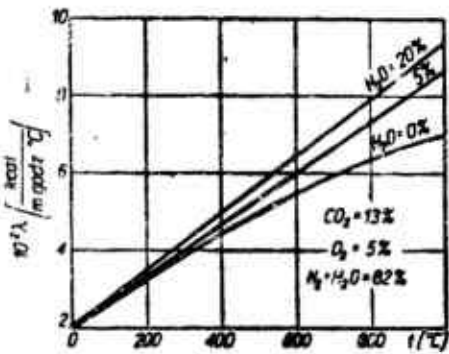


Fig. 11.3. Variation of the heat transfer coefficient for the combustion products as a function of temperature and of the percentage of water vapor. 1) [kcal/m·hour·°C].

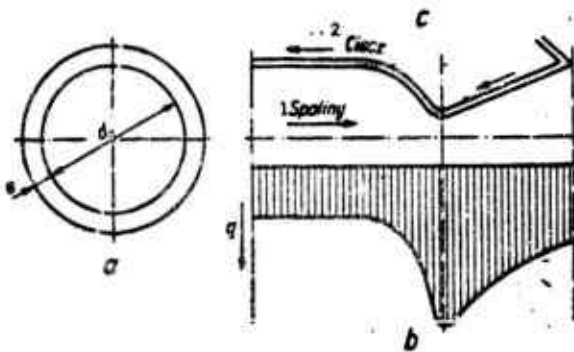


Fig. 11.4. Cooling of rocket engines by means of liquids: a) transverse cross section of the engine's combustion chamber; b) heat flow distribution along the engine; c) longitudinal engine cross section. 1) Combustion products; 2) liquid.

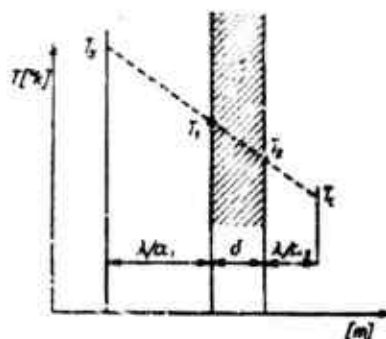


Fig. 11.5. Graphic method of determining the temperature distribution in the wall under steady state heat transfer conditions (λ is the conductivity of wall material).

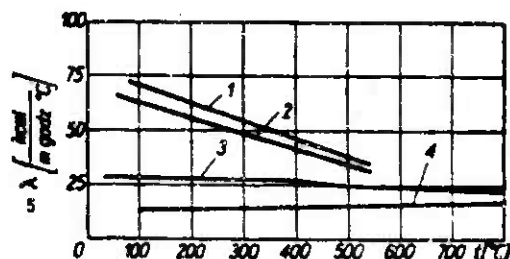


Fig. 11.6. Conductivity of steels used in the manufacture of engines, as a function of temperature: 1) steel 10; 2) steel 20; 3) steel 30 HMA; 4) steel 1 H18N9T; 5) [kcal/m·hour·°C].

temperature, from Tables 11.1 and 11.2. Unfortunately, the heat transfer coefficient cannot be determined by the method of superposition and therefore it must be obtained experimentally for each composition. Because of the lack of other data, this coefficient can be selected by means of the graphs shown in Fig. 11.3;

- for the coolant

$$Nu = 0,023 Re^{0.8} \cdot Pr^{0.33} \quad (11.4)$$

where

$$Nu = \frac{\alpha_1 d_s}{\lambda_s}$$

$$Re = \frac{w d_s}{\nu_s}$$

$$Pr = \frac{\mu_s c_{p1}}{\lambda_s}$$

$$d_s = \frac{4F}{Q}$$

$F = \pi d_z e$ (Fig. 11.4); Ω is the wetted parameter.

Viscosity and thermal conductivity data of liquids used in cooling of engines are given in Table 4.8.

— in the case of air acting as the coolant (e.g., the wall of a ramjet engine)

$$St = 0,029 \frac{Re^{-0.2}}{1 + 0,75(Pr^{0.67} - 1)}$$

where $St = \frac{\alpha}{\gamma c_p w}$ — is the Stanton number; $Re = \frac{w \cdot L}{\nu}$ — is the Reynolds number; $Pr = \frac{\gamma \nu c_p}{\lambda}$ — is the Prandtl number; L is the distance from the engine inlet edge (m); γ , c_p , ν , λ are the quantities characterizing the air at the temperature of the wall.

Wall temperature is determined by a graphic method, given the heat transfer coefficients, fluid temperatures and wall thermal conductivity.

The method is illustrated in Fig. 11.5.

Wall thermal conductivity is selected from the graphs shown in Fig. 11.6.

11.2. TRANSIENT HEAT TRANSFER BETWEEN COMBUSTION PRODUCTS AND WALL

Transient heat transfer occurs in the case of heat absorption cooling. This cooling method is usually employed in the case of solid propellant rocket engines.

The one-dimensional heat transfer equation assumes the following form:

$$\frac{\partial T}{\partial \tau} = a \frac{\partial^2 T}{\partial x^2} \quad (11.5)$$

where x is the coordinate corresponding to the direction of heat flow; $a = \lambda / \gamma c$ is the thermal diffusivity; c is the specific heat of the wall material (for steel $c = 0.11$ kcal/kgf·°C); γ is the specific weight of wall material (for steel $\gamma = 7900$ kgf/m³).

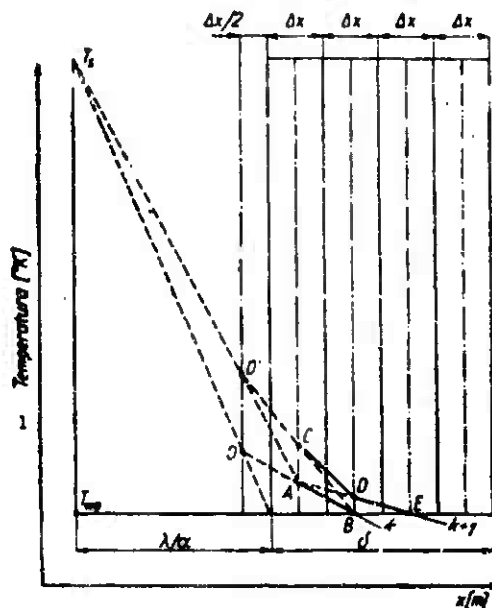


Fig. 11.7. Graphic solution of the equation of transient heat flow through the wall: T_s) temperature of combustion products; T_{w0}) initial wall temperature (at instant $k - 1$); AB) temperature distribution in the wall at time k ; CDE) temperature distribution in the wall at time $k + 1$. 1) Temperature [$^{\circ}\text{K}$].

In order to solve Eq. (11.5) by a graphic method, it must be expressed in the form of a difference equation:

$$\Delta T = a \frac{\Delta \tau}{(\Delta x)^2} \Delta^2 T \quad (11.6)$$

where $\Delta \tau$ is a time interval; Δx is a segment of wall width.

If we let $k - 1, k, k + 1, k + 2$, etc., denote the individual time intervals and let $n - 1, n, n + 1$, etc., denote the wall segments and if we further assume that

$$a \frac{\Delta \tau}{(\Delta x)^2} = \frac{1}{2} \quad (11.7)$$

we obtain the solution of Eq. (11.6) in the form:

$$T_{n,k+1} = \frac{1}{2} (T_{n+1,k} + T_{n-1,k}) \quad (11.8)$$

In words, Eq. (11.8) says: the temperature in segment n at the time $k + 1$ is equal to the arithmetic mean of the temperatures in the

neighboring segments at time k . This equation allows us to solve easily for the variation of temperature distribution in the wall under transient heat flow conditions. Figure 11.7 shows a graphic solution of this equation.

11.3. RADIATIVE HEAT EXCHANGE

As has already been mentioned, radiative heat exchange between combustion products and the wall does not play an important role.

TABLE 11.3

Radiation Path as a Function of Diameter d and of Combustion Cylinder Shape

1 Kształt komory spalania	L_e
2 Kula	$0,6 d$
3 Walec nieskończenie długi	$0,9 d$
4 Walec o wysokości $h = d$	$0,6 l$

1) Combustion chamber shape; 2) sphere; 3) infinite cylinder; 4) cylinder of height $h = d$.

From the point of view of radiation, carbon dioxide and water vapor are the only components of combustion products which are active. Heat flows due to these components are given by the following equations:

$$q_{CO_2} = 3,5 \cdot p_{CO_2} L_e \left[\left(\frac{T_g}{100} \right)^{3,5} - \left(\frac{T_1}{100} \right)^{3,5} \right] \text{ (kcal/m}^2 \cdot \text{hr)}$$

$$q_{H_2O} = 3,5 p_{H_2O} L_e \left[\left(\frac{T_g}{100} \right)^3 - \left(\frac{T_1}{100} \right)^3 \right] \text{ (kcal/m}^2 \cdot \text{hr)}$$

where p_{CO_2} , p_{H_2O} are partial pressures of CO_2 and H_2O ; L_e is the radiation path, defined in Table 11.3 as a function of combustion chamber diameter D (m); T_g is the temperature of combustion products ($^{\circ}K$); T_1 is the internal wall temperature ($^{\circ}K$).

The total heat flow due to radiation is therefore given by:

$$q_R = q_{CO_2} + q_{H_2O} \quad (11.9)$$

However, radiation plays an important role in cooling of hot walls exposed to the atmosphere. In this case the heat flow is given by:

$$\frac{Q_R}{F} = \epsilon \sigma T_2^4$$

where F is the radiating surface (m^2); T_2 is the temperature of the radiating wall ($^{\circ}K$); σ is the radiation constant of an ideal black body and is equal to $4.9 \cdot 10^{-8}$ kcal/ $m^2 \cdot hr \cdot ^{\circ}K^4$; ϵ is the emissivity (defined in Table 11.4).

TABLE 11.4
Emissivity Factors

1 Material	2 Zakres temperatur [$^{\circ}C$]	3 ϵ
3Stal szlifowana	940 ÷ 1100	0,55 ÷ 0,61
4Stal utleniona.	200 ÷ 600	0,8
5Stal o powierzchni chromowanej . . .	100 ÷ 1000	0,08 ÷ 0,26

1) Material; 2) temperature range; 3) polished steel; 4) oxidized steel; 5) chromed steel.

11.4. COMPOSITE HEAT TRANSFER

In the case of composite heat transfer, that is, when radiation and convection occur simultaneously, the heat flows add up and the total heat flow is given by:

$$q_0 = q + q_R \quad (11.10)$$

In order to simplify the computations, radiant heat is taken into account by increasing appropriately the heat transfer coefficient, which in this case is given by:

$$\alpha_0 = \frac{q_0}{\Delta t}$$

where Δt is the temperature difference between the wall and the fluid between which the compound heat transfer takes place; q is the heat

flow due to convection; q_R is the heat flow due to radiation.

REFERENCES TO CHAPTER 11

- 11.1. M. Michiejew: Osnowy ciepłopieredaczy [Fundamentals of Heat Transfer]. 1949.
- 11.2. G. Siniariew, M. Dobrowolski: Silniki rakietowe na paliwo plynne [Liquid Fuel Rocket Engines]. Wyd. MON [Publication MON], 1957.
- 11.3. M. Barrere et al.: Rocket Propulsion. 1960.
- 11.4. R. Szymanik: Analiza pracy niechlodzonego silnika rakietowego [Analysis of an Uncooled Rocket Engine]. Biuletyn WAT [Bulletin WAT], 1960.

Chapter 12

ENGINE FEED SYSTEMS

Pulsejets, ramjets and rocket engines do not contain any rotating elements so that their feed system requires an independent source of power. Such a source can consist of compressed gas which pushes the

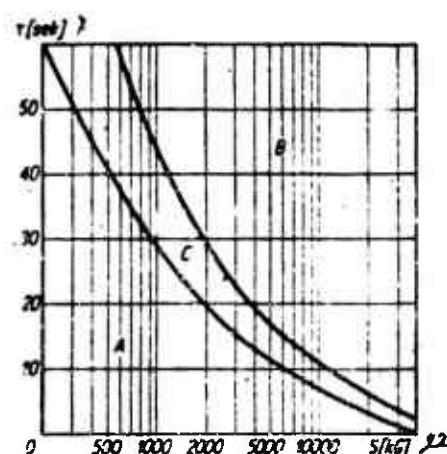


Fig. 12.1. Regions of applicability of rocket engine feed systems: A) pressure system; B) force feed system; C) transition region. 1) [sec]; 2) [kgf].

propellants out of the storage tanks and into the combustion chamber (pressure system) or it can consist of a turbine driving pump (force feed system). The first method is applicable in the case of engines of low thrust and short operating time, whereas the second method is applicable in the case of large engines having a long operating time (Fig. 12.1). In the final analysis, the selection is governed mainly by the design's weight and cost.

12.1. PRESSURE FEED SYSTEM

Figure 12.2 illustrates the pressure feed system of rocket en-

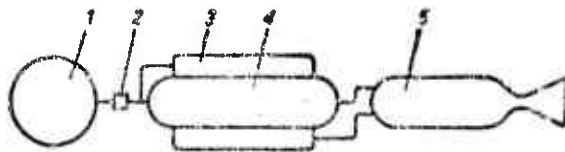


Fig. 12.2. Pressure feed system:
1) compressed gas tank; 2) valve;
3) oxidizer tank; 4) fuel tank;
5) combustion chamber.

gines. Compressed gas contained in tank 1 expands to a predetermined pressure controlled by valve 2 and by acting on the surface of the liquids in storage tanks 3 and 4, then forcing them into combustion chamber 5. Analogous systems, except that they consist of only a single tank, are used to feed pulse and ramjet engines.

12.1.1. Storage Tank Volume

The volume of the propellant tank consists of:

– the theoretical quantity of the propellants

$$V_t = \frac{G \cdot \tau}{\gamma} [\text{m}^3]$$

where G is propellant output (kgf/sec^2); τ is engine burn time (sec);
 γ is propellant specific weight (kgf/m^3);

– the volume of the safety factor excess due to injector manufacturing tolerances

$$V_b = 0.02 \div 0.05 V_t$$

– the volume of the surge tank which attenuates the starting shock and compensates for liquid expansion due to temperature variations

$$V_p = 0.03 \div 0.06 V_t$$

Therefore the total volume of the propellant tank is given by:

$$V = V_t + V_b + V_p \quad (12.1)$$

The tank volume for each propellant component is computed in the same way. The volume of all tanks is

$$V_w = \Delta V_1$$

The pressure in the tanks is necessarily greater than that in the combustion chamber because of flow losses and of the need of an overpressure for spray injection

$$p_2 = 1.15 \div 1.25 p_k$$

where p_k is the pressure in the combustion chamber.

Assuming a polytropic expansion of the feed gas, we can obtain the volume of the compressed-gas tank from the following equation:

$$V_2 = \frac{V_w}{\left(\frac{p_1}{p_2}\right)^{\frac{1}{n}} - 1} \quad (12.2)$$

where $n = 1.33$ is the polytropic expansion exponent; p_1 is the pressure of the compressed gas (it usually varies between 150 and 250 kgf/cm²).

12.1.2. Reducing Valve

The task of the reducing valve is to decrease the pressure of the compressed gas from the high value in the container, to the lower pressure required to feed the propellants. The commonly used spring reduc-

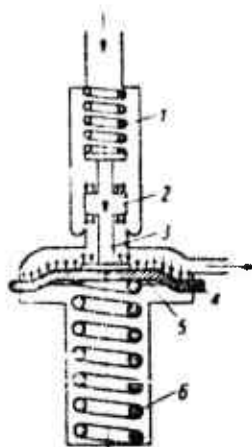


Fig. 12.3. Spring type reducing valve: 1) spring; 2) port; 3) rod; 4) diaphragm; 5) control ring; 6) control spring.

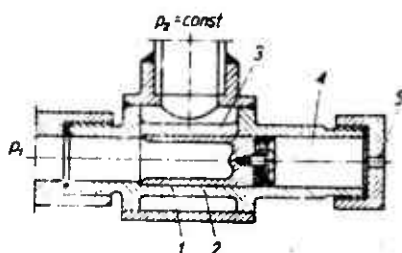


Fig. 12.4. Pressure reducing valve of the programed regulator type: 1) piston; 2) cylinder; 3) compressed air inlet orifice whose area is regulated; 4) fluid resisting piston travel; 5) liquid exhaust orifice.

ing valves (Fig. 12.3) are heavy and complicated in order to assure proper operation toward the end of the work cycle and require an overpressure of $\sim 10 \text{ kgf/cm}^2$ (which increases the volume of the compressed gas tank).

A better solution consists of the programed regulator shown in Fig. 12.4. In this regulator, the change in the primary pressure p_1 is compensated for by a change in the area of the choking orifice, which is increased as a function of time by the travel of piston 1 to the right. Piston position is controlled by the outflow of the retarding fluid through calibrated orifice 5. A serious disadvantage of this design is the necessity of experimental selection for the choking orifice shape.

12.2. FORCE FEED SYSTEM

In a force feed system the propellant is moved by a pump which in turn is powered by an axial or radial turbine. Turbine propulsion, in the case of pulse or ramjet engines, is usually accomplished by means of atmospheric air which is compressed proportionately to the flight velocity, whereas in the case of rocket engines, it is accomplished by means of a hot gas obtained most often from a cold reaction of hydrogen peroxide (see Section 4.17). As opposed to the simplicity of the pressure system, the force feed system exhibits the following advantages:

- light weight tanks and small over-all dimensions of the turbo-pump;
- the ability to feed arbitrarily large fluid outputs;
- a large dynamic range, achieved by changing the pump angular velocity.

12.2.1. Pump Characteristics

The theoretical pressure increase achievable in a pump can be described by the Euler equation (Fig. 12.5)

$$\Delta p_t = \rho (u_2 v_2 \cos \alpha_2 - u_1 v_1 \cos \alpha_1)$$

Assuming that angles α_1 and β_1 are equal to 90° , this equation can be greatly simplified:

$$\Delta p_t = \rho u_2^2$$

where ρ is the density of the pumped liquid; $u_2 = 50-80$ m/sec is the tip velocity of the pump rotor.

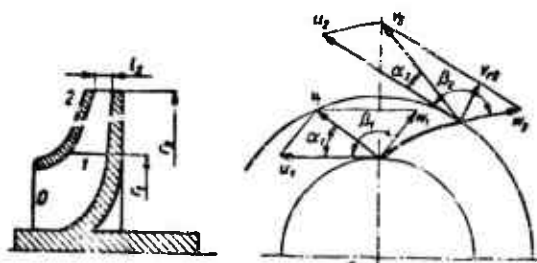


Fig. 12.5. Diagram of pump operation.

The actual pressure at pump outlet is:

$$\Delta p_a = \eta_p \Delta p_t$$

where η_p is the manometric pump efficiency, which at the point of highest pump efficiency is equal to 0.45-0.55.

Pump output is

$$G = 2\pi r_2 l_2 v_{r2} \quad (12.3)$$

where $v_{r2} = 2-4$ m/sec is the radial velocity at the tip of the rotor.

The torque applied to the rotor is given by:

$$M_p = \rho G r_2 v_2 \cos \alpha_2$$

The set of quantities characterizing pump operation includes also the useful power:

$$N_u = G \Delta p_{rx}$$

and the efficiency defined as the ratio of the useful power to the shaft power:

$$\eta = \frac{N_u}{N}$$

The characteristics of a typical pump are shown by the graphs in Fig. 12.6.

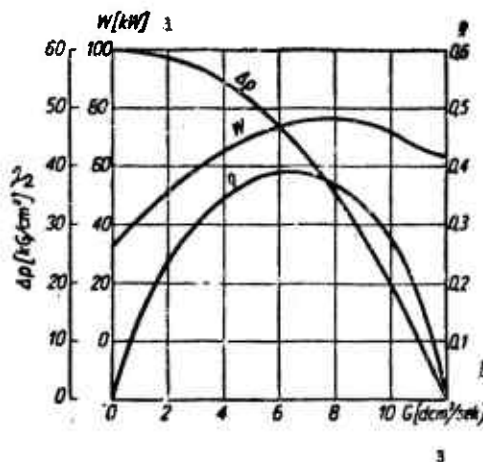


Fig. 12.6. Pump characteristic.
1) [kW]; 2) [kgf/cm²]; 3)
[d·cm³/sec].

In order to avoid the cavitation phenomenon, the pumped fuel should be fed to the pump inlet at a certain pressure greater than the limit pressure.

This pressure can be obtained by using:

- the initial tank overpressure;
- a staging pump, usually a spiral pump (Fig. 12.7);
- an ejector placed in the channel feeding the liquid to the pump, which is primed by the liquid obtained from the outlet (Fig. 12.8).

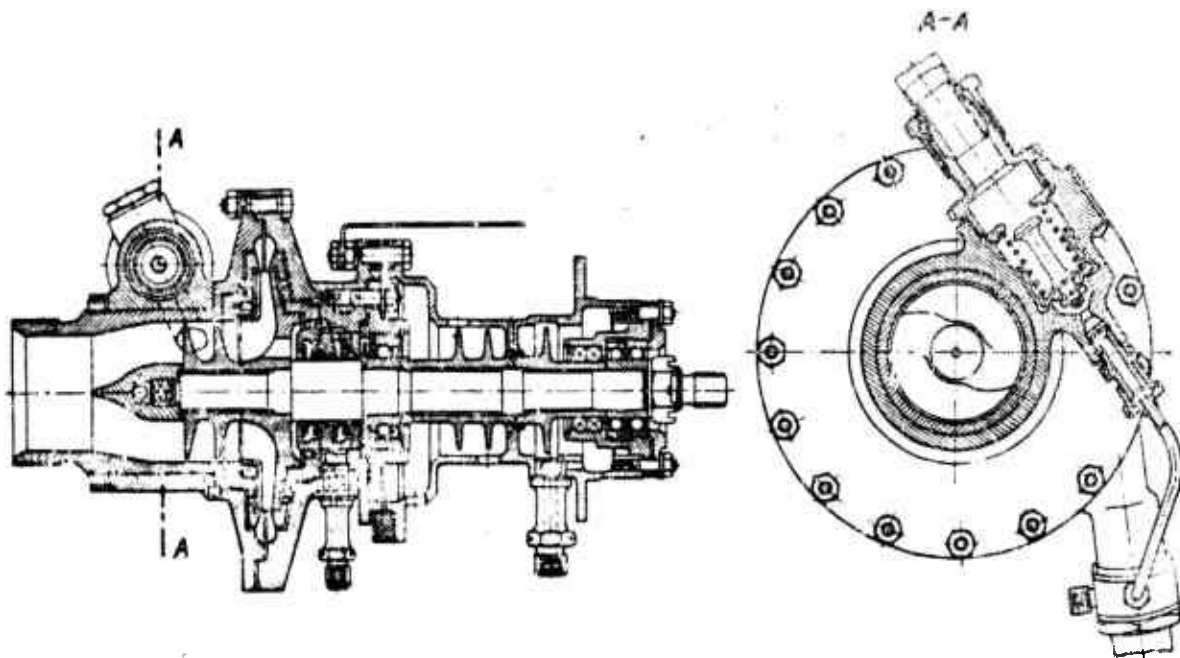


Fig. 12.7. Design schematic of a pump used in the feed system of rocket engines.

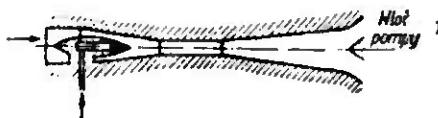


Fig. 12.8. Diagram of an ejector which increases the pressure at pump inlet. 1) Pump inlet.

12.2.2. Turbine Characteristics

The pump is powered by a turbine working on combustion products. Figure 12.9 illustrates a sample design of such a turbine. In this design, the additional combustion chamber serves as a generator of combustion products to power the axial turbine. The turbine powers the fuel and oxidizer pumps. If the auxiliary combustion chamber uses the same propellants as the main combustion chamber, then the terminal combustion temperature must be lowered by water injection. In this case, the turbine also powers a third pump, i.e., the water pump. Turbines commonly used in the design of rocket engines are of the axial type

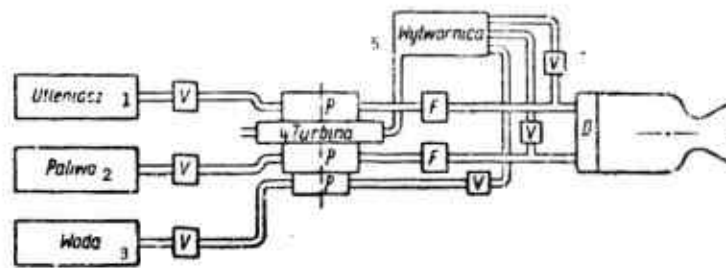


Fig. 12.9. Diagram of a feed system using a turbopump: V) valves; p) pumps; F) filters; D) manifolds. 1) Oxidizer; 2) fuel; 3) water; 4) turbine; 5) gas generator.

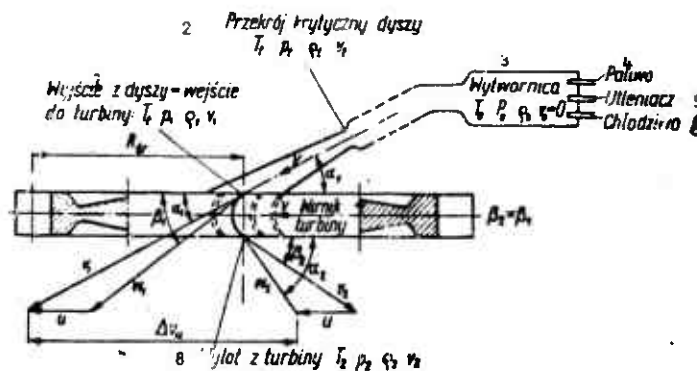


Fig. 12.10. Diagram of an axial pump used in rocket design to power pumps. 1) Nozzle exhaust = turbine inlet; 2) critical nozzle cross section; 3) gas generator; 4) fuel; 5) oxidizer; 6) coolant; 7) turbine rotor; 8) turbine exhaust.

(Fig. 12.10). The several quantities characterizing the turbine are defined by the following equations:

— turbine efficiency

$$\eta_T = \frac{2u(v_1 \cos \alpha_1 + v_2 \cos \alpha_2)}{v_1^2} \quad (12.4)$$

— power torque

$$M_T = R_{tr} q_T (v_1 \cos \alpha_1 + v_2 \cos \alpha_2)$$

where $q_T = \frac{p_0 F_t}{w_c}$, ; F_t is critical nozzle cross section; p_0 is the pressure in the gas generator; w_c is the characteristic speed of the propellant powering the turbine.

12.2.3. Interaction Between the Turbine and the Pump

In view of the simplicity of the feed system, in almost all designs the pump is mounted directly on the turbine shaft. Obviously such a system is not optimum from the point of view of efficiency and the interaction of these two components.

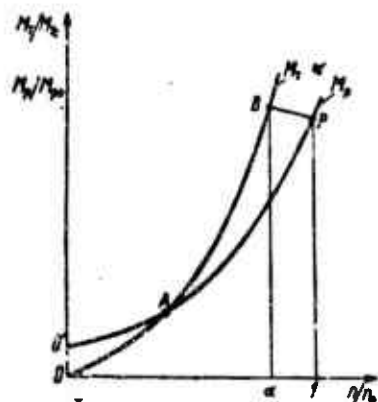


Fig. 12.11. Turbine-pump interaction.

Figure 12.11 illustrates turbine and pump characteristics expressed as a change in angular momentum as a function of angular velocity. The turbine characteristic is a hyperbola, whereas that of the pump is a parabola. These two curves intersect at a very low angle, in view of which system stability is poor. In order to remedy the situation, a bypass valve is introduced into the pipe connecting the pump to the gas generator to maintain a constant supply pressure. This pressure is achieved at point B on the turbine characteristic, which corresponds to lower angular velocities than the design velocity ($n/n_0 = \alpha < 1$, where n_0 is the design angular velocity).

Maintaining the pressure in the gas generator constant with increasing angular velocity n causes a gradual momentum decrease, which in turn causes the intersection of the turbine characteristic $OABP$ with the pump characteristic $O'AP$ to occur at point P at a large angle.

This greatly increases the stability of the turbopump system.

REFERENCES TO CHAPTER 12

- 12.1. H. Mebus: Berechnung von Raketentriebwerken [Mathematical Design of Rocket Powerplants]. 1957.
- 12.2. M. Barrere: Rocket Propulsion. 1960.

Chapter 13

FUNDAMENTALS OF ENGINE DESIGN

One of the most characteristic features of the development of contemporary civilization is the large number of prototypes never encountered until now. This is due to an ever-increasing list of requirements, necessitated by the intrusion of modern technology into increasingly varied fields of endeavor.

This situation has influenced to a large extent the stages through which each newly conceived design must pass, i.e., the prototype stages.

Until recently, the process of creating a new system was limited mainly to computations pertaining to functional and stress considerations which were performed on the basis of theoretical or experimental equations; these were collected for the use of design departments in handbooks or notes; another approach involved design at the drafting board, where attempts were made to determine, through discussions, the various configurations of the optimum design. Tests conducted on a newly designed system had the character of tests verifying the entire system. If the designer was experienced and the prototype deviated only slightly from the model, then by definition the design was a success. Some bridge builders of the past century were so sure of their designs that they stayed in a boat under the bridge arches during the latter's load carrying tests.

It could be said that the changes which took place in the methods of designing new systems were greater, and more difficult to foresee,

than the changes in the systems themselves, which are the pride of the era in which we live. Nineteenth century writers, dreamers and science-fiction authors such as Verne predicted quite accurately the conditions under which space flight would take place and the nature of the trajectories which would enable man to escape from earth. However, their heroes approached the implementation of the flight to the moon exactly in the same way as engineer Stanislaw Kierbedz approached the design of the bridge across the Vistula in Warsaw. They pored over computations and drafting boards night after night, and once their dream design was on paper, they immediately started to build it. Spaceship start-up, naturally with crew aboard, was simultaneously the system's first test and the beginning of a trip to another planet. In this method there was something of the Cartesian faith in the possibility of predicting everything on the basis of logical reasoning, backed up only by the most fundamental laws of nature.

Unfortunately, this method did not make the grade in real life; and on the basis of many experiments we must openly state the pessimistic thesis that in new situations man cannot predict everything. Therefore, in the design of prototype systems which differ greatly from the model, the process of creation should rely mainly on test results. Tests should be conducted step by step, starting from the most fundamental ones and progressing through the testing of systems up to structural and functional tests of the entire design.

In this process no skipping is allowed, since it is *a priori* doomed to failure. Unfortunately we must reconcile ourselves with this fact, just as we are reconciled to the fact that entropy increases and that a perpetual motion machine cannot be built.

The second important change in design methods, which took place in the last few years, was the increase in importance of the function

of the stress analyst. Until recently his task was limited to theoretical, and sometimes experimental, verification of some doubtful structural elements. Very often it also happened that in the case of less important designs, the designer used only his own intuition, based on his experience. At present, an efficiently organized design department, the stress analyst is a direct co-creator of the design. He selects the optimum materials and, from the structural point of view, the starting point of system development, so that the functional aspect should not suffer. And in this case the selection of the implementation technique is often governed by test results.

The process of engine design can be subdivided into the following stages:

- firming up the requirements;
- establishing the most advantageous values of thermodynamic and aerodynamic parameters, computation of the geometry of flow ducts;
- establishment of design layout, establishment of engine profile;
- load computations;
- selection of design materials, stress analysis;
- initial structural and aerodynamic tests;
- initial design;
- technical design and manufacturing drawings;
- program of experimental work;
- planning of static tests or planning the adaptation of existing test stands to the study of the new engine.

When setting down the engine requirements, we should keep clearly in mind the applications for which the design is intended. There is no such thing as a universal design; and therefore each design differs from the others in some basic characteristic feature to which all the other features should be subordinate within reasonable limits. The de-

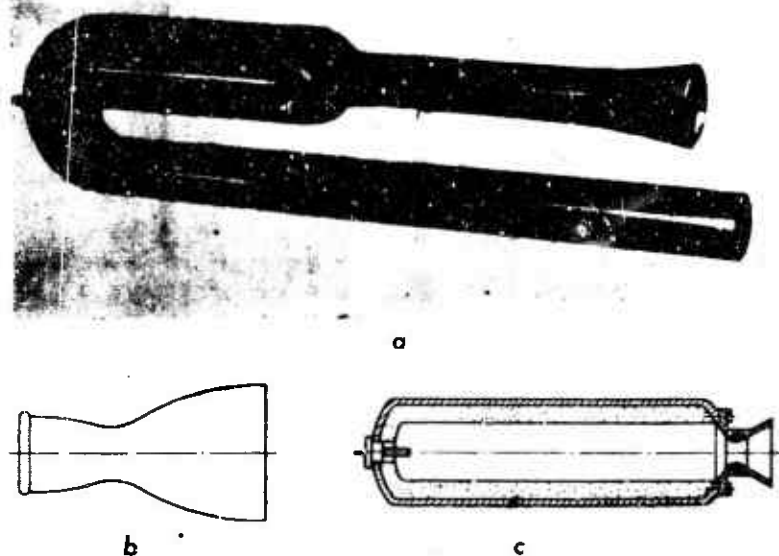


Fig. 13.1. Shapes of modern engines: a) pulse-jet; b) liquid fuel rocket engine; c) solid propellant rocket engine.

sign cannot be burdened by too great a number of conditions. It is impossible, for instance, to postulate simultaneously the unit thrust and unit fuel consumption of a projected ramjet engine. A decision must be reached as to the design's goal: high thrust per unit frontal cross section or maximum efficiency. In setting the optimum thermodynamic and aerodynamic engine parameters, most often one takes advantage of statistical data or one considers the graphical results obtained previously or found in the literature. Such an analysis is most beneficial, since in general statistical data is valid only within very narrow limits. After selecting the values of pressure, temperature and speed at the various cross sections, we choose the basic dimensions of the flow ducts in such a way as to obtain the most efficient nozzle and diffuser profiles.

The computational role of the thermodynamicist terminates with the preparation of the required theoretical engine characteristics;

then the design is handed over to the designer, who in conjunction with the stress analyst determines the optimum structural layout for the given engine. At this stage, the fundamental criterion governing the selection of the design layout should be simplicity, minimum number of parts, and an engine shape based on functional considerations and profile esthetics. Indifferent choices can be made on the premise that the one which is prettiest is best.

As an example, the shapes of a modern pulsejet engine and of a solid propellant rocket engine, as well as the profile of a combustion chamber and nozzle of a liquid fuel rocket engine are illustrated in Fig. 13.1. All the designs illustrated in this figure are characterized by far-reaching simplicity and gracefulness of the design line.

The following loads should be taken into consideration during the structural computations:

- loads during start-up. This problem is particularly evident in the case of rocket engines. Accelerations occurring at this time can reach to 40 g. One should also keep in mind, especially in the case of two-stage systems, the decelerations occurring at booster burnout can reach from 3 to 10 g's and are obviously directed in the opposite direction;

- loads during in-flight maneuvers. This requires consideration of the predicted flight program: speed, altitude as well as turn radius and type of maneuver;

- loads due to aerodynamic pressures. Obviously, the maximum value is of importance here:

$$q = \rho w^2 / 2$$

where ρ is air density, which is a function of altitude; w is flight velocity;

- loads due to pressure in the diffuser, combustion chamber and

nozzle. In the case of a ramjet engine one must consider the position of the shock and rarefaction waves whereas in the case of a pulsejet engine one must consider the propagation of these waves;

- loads due to fuel pressure, which act on the storage tanks and their supporting structures at the times of system acceleration or deceleration.

Selection of the material to be used in the engine design is governed mainly by:

- engine operating time;
- temperature and pressure;
- type of propellant.

In the case of engines whose operating time is of the order of tens of seconds, low carbon and low alloy structural steels having improved thermal characteristics can be used. Steels 15 and 20 belong to the first category and can be used in the case of light loads; on the other hand steels 30 HGSA and 30 HMA belong to the second category (see Tables 13.1 and 13.2).

TABLE 13.1

Chemical Composition of Low Carbon and Low Alloy Structural Steels

1 Stal	2 Udział składników [%]							
	C	Si	Mn	P	S	Cr	Ni	Mo
15	0,12÷0,20	0,17÷0,37	0,35÷0,65	0,040	0,045	0,30	0,30	—
20	0,17÷0,25	0,17÷0,37	0,35÷0,65	0,040	0,045	0,30	0,30	—
30 HMA	0,25÷0,33	0,17÷0,37	0,40÷0,70	0,035	0,030	0,80÷1,10	0,40	0,15÷0,25
30 HGSA	0,28÷0,35	0,90÷1,20	0,80÷1,10	0,035	0,030	0,80÷1,10	0,40	—

1) Steel; 2) composition.

Combustion chambers of ramjet and rocket engines having a longer operating time are manufactured out of refractory and acid resistant steels or out of alloys of the EJ group. These latter are used under elevated temperatures (Tables 13.3 and 13.4).

TABLE 13.2

Strength Properties of Low Carbon and Low Alloy Structural Steels

Steel		Temperature [°C]			
		20	300	400	600
15	R_p a_{10}	37÷50 27	31,9 20,8	29,7 35	9,1 42,6
20	R_p a_{10}	41÷50 25	45,5 19,7	40,5 35,7	16 49,4
30 HMA	R_p a_5	108 12	105* 12*	92 16	63 20
30 HGSA	R_p a_5	108 12	105* 12*	92 17,5	53 25

R_p) Yield strength [kgf/mm²]; a) elongation [%]; *) for 200°C.

1) Steel; 2) temperature.

TABLE 13.3

Chemical Composition of Refractory and Acid Resistant Steels

Steel	Udział składników [%]							
	C	Mn	Si	P	S	Cr	Ni	Ti
1H18N9T	0,12	2,0	1,2	0,035	0,030	17,0-20,0	8,0-11,0	0,8
1H13	0,15	0,6	0,6	0,035	0,030	12,0-14,0	0,6	—
EJ435	0,12	0,7	0,8	—	—	19-23	75	0,4
EJ437	0,08	0,5	1,0	—	—	19-23	reszta 3	2,0

1) Steel; 2) composition; 3) remainder.

Nozzles of solid propellant rocket engines are manufactured with inserts made out of high-melting materials such as tungsten, molybdenum or graphite. In selecting materials, one should keep in mind the important effect of temperature on the physical properties of structural steel. A temperature increase lowers appreciably the yield strength and the modulus of elasticity; it also changes the expansion coefficient and the thermal conductivity. Recently, titanium alloys and synthetic materials which exhibit very advantageous strength-to-

TABLE 13.4

Strength Properties of Refractory and Acid Resistant Steels

		Temperatura [°C]				
		20	200	400	600	800
1H10N9T	R_T	62	57	50	40	12
	a_b	58	42	33	39	56
1H13	R_T	60-70	35	50	18	—
	a_b	20	18	20	26	—
EJ435	R_T	75	74	72	60	24
	a_b	50	—	—	—	29
EJ437	R_T	97,7	100	102,3	79,9	35,7
	a_b	19,3	21,5	23,3	6,9	6,8

*Oznaczenia — patrz tabela 13.2.

Symbols — see Table 13.2.

1) Temperature.

TABLE 13.5

Safety Factors [9.1]

Lp.	11 Z c z e s t o t e	12 Współczynnik
1	Wszystkie konstrukcje pozr. wymienionymi oddzielnie	1,0
2	Obciążenia przy obsłudze	1,13
3	Odlewy	1,0
4	Połączenia	
5	obliczone, lecz niesprawdzone	1,15
6	sprawdzone za pomocą prób	1,00
7	nity, śruby, kolki	1,13
8	Zbiorniki pod ciśnieniem:	
9	niebezpieczne dla obsługi	2,0
10	pracujące z dala od obsługi	1,0

1) All structures except those specifically called out; 2) loads during servicing; 3) castings; 4) connections; 5) computed, but not verified; 6) checked out by means of tests; 7) rivets, screws, pins; 8) tanks under pressure; 9) dangerous to the servicing crew; 10) operating away from the crew; 11) component; 12) factor.

weight ratios are being introduced. Before undertaking the stress analysis computations, one must select the allowable stresses which will be a function of the type of design, of engine application, and of time and other operating conditions. In the selection of allowable stresses, safety factors collected in Table 13.5 should be used.

The safety factor is defined as the ratio of the destructive load to the maximum predicted load.

TABLE 13.6

Typical Manufacturing Tolerances

Lp.	Z e s p ó ł	Odchyłki	U w a g i
11	12	13	
1	Dyfuzory	$\pm 0,8$	na promieniu
2	Dysze	$\pm 1,6$	na średnicy
3	Rozmieszczenie elementów wewnątrz kadłuba, współśrodkowość względem krawędzi dyfuzora	$\pm 0,8$	5
4	Błąd kątowy wewnątrz kadłuba	$\pm 0,5^\circ$	
5	Położenie wzdłużne wlotów kadłuba	$\pm 0,8$	
6	Położenie wzdłużne powierzchni wlotów i wy- lotów	$\pm 0,6$	
7	Piętospadłość powierzchni współpracujących	$\pm 0,5^\circ$	
8	Średnica powierzchni współpracujących	$\pm 0,25$	
9	Owalizacja powierzchni współpracujących	$\pm 1,5$	
10	Grubość blach	$\pm 2\%$	

1) Diffusers; 2) nozzles; 3) placement of components inside the fuselage, concentricity with respect to diffuser edge; 4) angular error inside the fuselage; 5) longitudinal position of fuselage junctions; 6) longitudinal position of inlet and exhaust surfaces; 7) perpendicularity of interacting surfaces; 8) diameter of interacting surfaces; 9) oval shape of interacting surfaces; 10) metal sheet thickness; 11) component; 12) tolerances; 13) remarks; 14) on the radius; 15) on the diameter.

The maximum predicted load should not cause excessive permanent strains in the engine. This is usually the largest load which is predicted to exist during engine operation; it is usually multiplied by unity to obtain the design load.

In the preparation of manufacturing drawings, one should consider proper selection of tolerances, which from a cost point of view, should not be too tight. Table 13.6 lists the optimum values of the most important tolerances occurring during construction of engines discussed in this book.

REFERENCES TO CHAPTER 13

- 13.1. C. Besserer: Structures and Design Practice. 1956.
- 13.2. J. Lipka: Analiza własności wytrzymałościowych w wysokich temperaturach stali konstrukcyjnych niskowęglowych w zastosowaniu do komór spalania i silników strumieniowych [Analysis

of Strength Properties of Low Carbon and Low Alloy Structural Steels Used in Combustion Chambers and Ramjet Engines].
Za y I.L. [Notes of the Foreign Literature Press]. 1961.

Chapter 14

ENGINE TESTING

Testing is the basic sustaining force during the prototype design process. However, a test program conducted in an efficient manner requires large material and human resources.

The significant progress which has been achieved in recent years in rocketry and jet propulsion is due mainly to the unprecedented stress put on the expansion of research centers specializing in this very field. The most important technical problem in pulsejet, ramjet and rocket engines is the mastery of the combustion phenomena, which are characterized by very high temperatures (often reaching to 3000°K) and by serious instabilities which can, in the case of rocket engines, lead to engine destruction endangering service personnel.

This has created the emergence of new experimental methods particularly suited to the operating conditions of these engines.

14.1. GENERAL PRINCIPLES OF CONDUCTING DEVELOPMENTAL TESTS

The engine test-effort can be subdivided into the following parts:

- component testing;
- developmental tests;
- control tests;
- flight tests.

The first two types of tests have the greatest effect on engine design philosophy, and it is mainly these tests that will be discussed below.

The cardinal principle of developmental research is to start the

experimental work with the simplest components.

The engine under investigation is subdivided into systems and these in turn are subdivided into individual components which are first tested from a functional point of view and then from a structural point of view on separate test stands under conditions approximating as much as possible those to be encountered in the field.

Therefore, as an example, it would seem that the very simple system shown in Fig. 8.23 and consisting of a ramjet engine powering a helicopter rotor should pass the following tests before being subjected to a test simulating actual operating conditions:

- an injector test under static conditions. This test will consist of preparing the injector characteristic, that is, determination of the relationship between injection pressure and output, the determination of the injection angle and the study of the zonal distribution, i.e., the distribution in a plane perpendicular to the direction of injection;

- a test of mixture generation behind the counterflow injector under conditions increasingly approximating the actual operating conditions in the engine;

- a diffuser test with the flame stabilizer placed inside;

- combustion-chamber test or test of whether injector operation is stable;

- test of the entire engine on a test stand;

- a structural engine test, i.e., a test which damages the interconnection between engine wall and the supporting strut;

- a dynamic test on a rotating stand consisting of a rotating arm to one end of which the engine is attached and a counterweight attached to the other.

Only an engine tested in this fashion should be installed on an

actual helicopter rotor to study the interaction between the helicopter and the engines.

All tests whose goal it is to determine the effect of various parameters on the system's performance should be conducted under extreme conditions so as to accentuate the manifestation of these effects. For instance, the effect of temperature, speed or pressure on the efficiency of the combustion chamber is most easily exhibited in the vicinity of the lean-flame extinction limit, i.e., flame extinction due to lack of fuel. Under these conditions any parameter change whatsoever will cause a definite change in the efficiency.

Test results are the more certain and the more general, the simpler the system being tested from the point of view of eliminating any side effects. If it is desired to test the effect of flame stabilizer shape on the range of air excess coefficients for which combustion remains stable, it is necessary in view of the above (i.e., to eliminate the side effect of mixture distribution in the stream and of drop size on the occurrence of the phenomenon) to place the injectors in such a way that the mixture in the stabilizer zone is always vaporized and homogeneous.

In order to shorten testing time and decrease its cost, it is often practical to use indirect and simplified testing methods. Thus instead of determining combustion efficiency by means of measurements of speeds, pressures and temperatures at chamber exhaust from which the mean enthalpy rise can be computed and which is then compared with the theoretical rise to obtain the efficiency, it is simpler to define the efficiency as the ratio of the actual pressure drop across the chamber to the theoretical, for instance, and thus to obtain by means of direct measurements without any additional computations the characteristic of the combustion chamber. For the same reason, it is simpler to measure

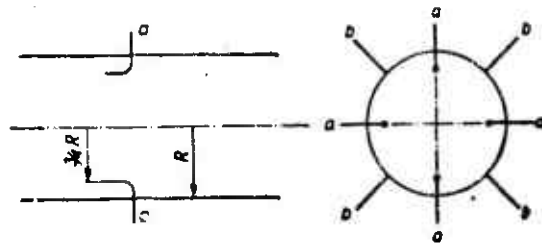


Fig. 14.1. Method of flow rate measurement by means of 4 Pitot tubes set up at $3/4$ of the radius: a) tubes measuring stagnation pressure; b) tubes measuring static pressure.

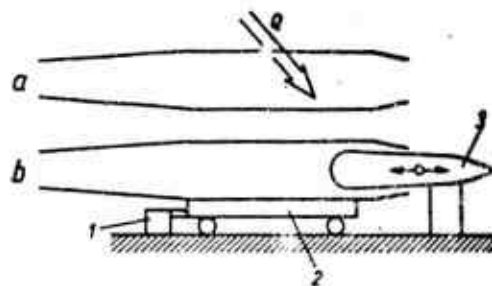


Fig. 14.2. Testing of a ramjet engine by the probe method: a) ramjet engine with combustion in the chamber; b) ramjet engine with exhaust choking by means of a probe; 1) thrust measuring system; 2) carriage to which the ramjet engine is attached; 3) engine exhaust probe.

the mass rate of flow through a pipe by means of a constriction than by means of measurements of speed distribution through the cross section. However, if due to excessive pressure losses a constriction cannot be used, then it is still possible to place 4 Pitot tubes in the pipe, $3/4$ of the radius from the center, and by connecting them, to read the mean flow velocity with very good accuracy (Fig. 14.1). Similarly, while testing systems under laboratory conditions, it is possible to replace the effects of a given process by the effects of another with the same end results, but which from certain points of view are easier to use. As an example of such an exchange of processes is the study of a ramjet engine (Fig. 14.2) in which heat generation in the combustion chamber has been replaced, in the exhaust nozzle, by

the placement of a probe which is solidly connected to the test stand. Therefore, if the engine is mounted in such a way that it can be moved with respect to the probe, by changing their relative positions, engine thrust can be changed. This method is particularly well suited to the determination of optimum engine inlet shape.

14.2. PRINCIPLES OF ENGINE MODELING

In view of the huge test costs due to high propellant costs and to the often huge costs of the test stands used in full-scale engine tests, it is often advantageous to conduct model tests.

In order to maintain complete similitude of the processes occurring in the model and in the prototype, the following parameters should be preserved in both systems:

- geometrical similitude;
- similitude of thermodynamic fields and of speed at the points unaffected by the chemical reaction;
- similitude of mixture distribution;
- similitude of the course of the chemical reaction.

This implies the preservation of the following similitude groups:

- (a) ratio of specific heats: $\kappa = c_p/c_v$;
- (b) Mach number: $M = w/a$;
- (c) Reynolds number: $Re = \rho w d/\mu$;
- (d) Prandtl number: $Pr = \mu c_p/\lambda$;
- (e) Schmidt number: $Sc = \mu/\rho D$;
- (f) Damköhler's first similitude parameter:

$$D_1 = \frac{d}{w \tau_{ch}}$$

- (g) Damköhler's second similitude parameter:

$$D_{II} = \frac{\Delta h}{c_p T}$$

where w , a are flow velocity and speed of sound; ρ , T are density and

temperature; d is a characteristic dimension; μ , λ , D are viscosity, thermal conductivity and diffusion constant; c_p , c_v are specific heats at constant pressure and constant volume; Δh is heat released during the chemical reaction; τ_{ch} is the duration of the chemical reaction.

Similitude parameters (a) to (e) are dimensionless similitude parameters of classical thermodynamics and aerodynamics; Damköhler's parameters, on the other hand, come about from the analysis of chemical processes, and the first one takes into account the kinematic aspect and the second the energy aspect of the phenomenon.

14.2.1. Modeling of Solid Propellant Rocket Engines

Solid propellant rocket engines are the simplest example of the application of modeling principles.

If the geometrical similitude of the model and prototype is preserved and if the same material is used, then the following relations are obtained between the parameters of engine operation and the characteristic dimension d :

- operating time: $\tau \sim d$;
- thrust: $S \sim d^2$;
- total impulse: $J_c = S\tau \sim d^3$.

Chamber pressure and the quantities K_N and K_J are not functions of the value of d .

Model tests of solid propellant rocket engines enable one to determine with great accuracy and at low cost the optimum grain shape.

14.2.2. Modeling of Ramjet Engines

It is not always possible to carry out a model study of an entire ramjet engine because of the difficulty of simultaneously preserving two dimensionless groups, namely, the Mach and Reynolds numbers. However, since the Mach number mainly affects diffuser operation, whereas the Reynolds number affects the operation of the combustion chamber,

all conflicts can be easily resolved by separating the tests of diffuser and combustion chamber.

The most important problem in the diffuser study is the determination of the position of shock waves on the inlet cone under various operating conditions (Fig. 14.3), the delineation of stable operating limits and the preparation of characteristics, i.e., of the relation between the output and the pressure generated as a function of flow velocity.



Fig. 14.3. Diffuser inlet under two operating ranges: a) supercritical flow; b) subcritical flow.

Great simplification in model tests of combustion chambers can be introduced if the same initial temperature and the same fuel-to-air ratio are used for both the model and the prototype.

It results from the above assumptions that:

$$D_{11} = \text{idem}$$

and

$$Pr = \text{idem}$$

In order to maintain similar fuel distribution in the stream, the injection angle must be constant

$$\alpha_v = \text{idem}$$

and the speed ratio of fuel and air must also be constant, which leads

to:

$$\frac{\Delta p^{0.5}}{w} = \text{idem}$$

where Δp is injector overpressure.

In order to assure similitude of the phenomena of diffusion, heat transfer and reaction kinetics we must have:

$$Sc = \frac{\mu}{\rho D} = \text{idem}$$

$$Re = \frac{\rho w d}{\mu} = \text{idem}$$

$$D_I = \frac{d}{w \tau_{ch}} = \text{idem}$$

Instead of using the time of chemical reaction in Damköhler's parameter, we could use the time of ignition lag as being the most representative parameter characterizing the combustion process. Furthermore, if we let the initial flow velocity be constant

$$w = \text{idem}$$

- if we let the diffusion constant and the ignition lag time be inversely proportional to pressure

$$D \sim p^{-1} \quad \tau_{ch} \sim p^{-1}$$

- if we let the kinematic viscosity be constant independent of pressure

$$\mu = \text{idem}$$

and if we replace the density by pressure according to the equation of state

$$p = \rho R T$$

then we obtain a simple law for modeling the combustion chambers of ramjet engines

$$p d = \text{const.}$$

Equation (14.1) is very useful in modeling combustion chambers of ramjet engines designed to operate at high altitudes. In this case,

with an appropriate choice of scale, it is possible to conduct tests on the model chamber while supplying it with air at near atmospheric pressure, which is most advantageous since it requires a low-powered fan to supply the combustion chamber.

14.2.3. Modeling of Pulsejet Engines

The method of modeling pulsejet engines should satisfy the following basic condition, if it is to be of much help in the testing process:

- the model and the prototype should be tested on the ground under atmospheric conditions, i.e., the initial temperature and pressure of supply air should be identical. Fulfillment of this condition is important from the point of view of test cost. However, its imposition makes impossible a strict modeling of the phenomena.

Assuming:

- the same mixture composition containing a fuel of the same heating value;
- the same flow velocities, which can be achieved with the same instantaneous pressure fields;

we get

$$M = \text{idem}, \quad D_{11} = \text{idem} \quad Pr = \text{idem} \quad \text{and} \quad Re \neq \text{idem}$$

It appears that failure to keep the Reynolds number constant is not dangerous from the flow point of view; however, it is most significant as far as the vaporization rate of fuel injected into the chamber is concerned.

One way or another, the following conditions must be maintained in order to preserve the similitude of the combustion process

$$D_1' = \frac{d}{w\tau_f} \quad D_1'' = \frac{d}{w\tau_{ch}}$$

where d is the characteristic engine dimension; w is similarly the

characteristic flow velocity; τ_f is the physical ignition lag; τ_{ch} is the chemical ignition lag.

The law of modeling of pulsejet engines is obtained from the above conditions

$$\frac{d}{\tau_f} = \text{const}; \quad \frac{d}{\tau_{ch}} = \text{const} \quad (14.2)$$

It is possible to satisfy this law only by

— supplying the model and prototype engines with different fuels having the same heating value but different kinetic properties. Selection of such fuels is not difficult especially if fuel preheating at the inlet is used in the case of the model engine.

14.2.4. Modeling of Liquid Fuel Rocket Engines

In order to preserve geometrical and mechanical similitude in the combustion chambers of the model and prototype engines, the following relations should be satisfied

$$n_d = \frac{d}{d_M}, \quad n_w = \frac{w}{w_M} \quad (14.3)$$

where n_d , n_w are similitude constants; d , w are dimension and speed; M is a subscript referring to the model.

Assuming that the fundamental time characterizing the chemical process is the ignition lag time, we get from the above equations:

$$\frac{n_d}{n_w} = \frac{\tau_k}{\tau_{kM}} = \frac{\tau}{\tau_M} \quad (14.4)$$

where τ_k is the combustion chamber stay time; τ is the ignition lag time.

Ignition lag is a function of chamber pressure p and of injector overpressure Δp , as shown in the equation:

$$\tau = k p^{-n} \Delta p^{-r} \quad (14.5)$$

where k , n and r are experimental constants.

Substituting this equation into Eq. (14.4) we get:

(14.6)

Since

$$\frac{n_d}{n_w} = \frac{\rho_M}{\rho} \cdot \frac{\Delta p_M}{\Delta p}$$

where w_{wtr} is the velocity of the liquid stream injected into the chamber, Eq. (14.6) can be transformed into

$$\frac{\Delta p}{\Delta p_M} = \left(\frac{w_{wtr}}{w_{wtr M}} \right)^2 = n_w^2$$

Combining the above equations with the condition of constancy of the Reynolds number expressed by:

$$\left(\frac{\rho_M}{\rho} \right)^2 = n_d n_w^{2r-1}$$

we get the law of modeling of liquid fuel rocket engines:

$$\begin{aligned} \frac{\rho_M}{\rho} &= n_d^{\frac{2(1-r)}{1+n-2r}} \\ \frac{w}{w_M} &= n_d^{\frac{1-n}{1+n-2r}} \end{aligned} \quad (14.7)$$

In the case of a mixture of nitric acid and furfuryl alcohol, we get

$$n_d = 0.3 \text{ and } r = 1.5.$$

By physically interpreting Eqs. (14.5) and (14.7) the following two limit cases are obtained:

- assuming that $r = \infty$ we get

$$\begin{aligned} \frac{w}{w_M} &= 1 \\ \frac{\rho_M}{\rho} &= n_d \end{aligned}$$

This case applies to chamber operating conditions for which ignition lag is governed by the chemical lag that is the kinetics of the chemical reaction.

- assuming that $n = \infty$ we get

$$\frac{P_{11}}{p} = 1$$

$$\frac{n}{n_0} = \frac{n_0^{-1}}{n_0^{-1}}$$

This case occurs under chamber operating conditions such that ignition lag is governed by the physical lag, i.e., the rate of drop vaporization.

14.3. TEST FACILITIES

In the planning of test facilities, the following factors should be taken into account:

- crew safety;
- ease of erection and of dismantling and the provision for stand modification;
- facility equipped with proper instrumentation rather than for the comfort of location.

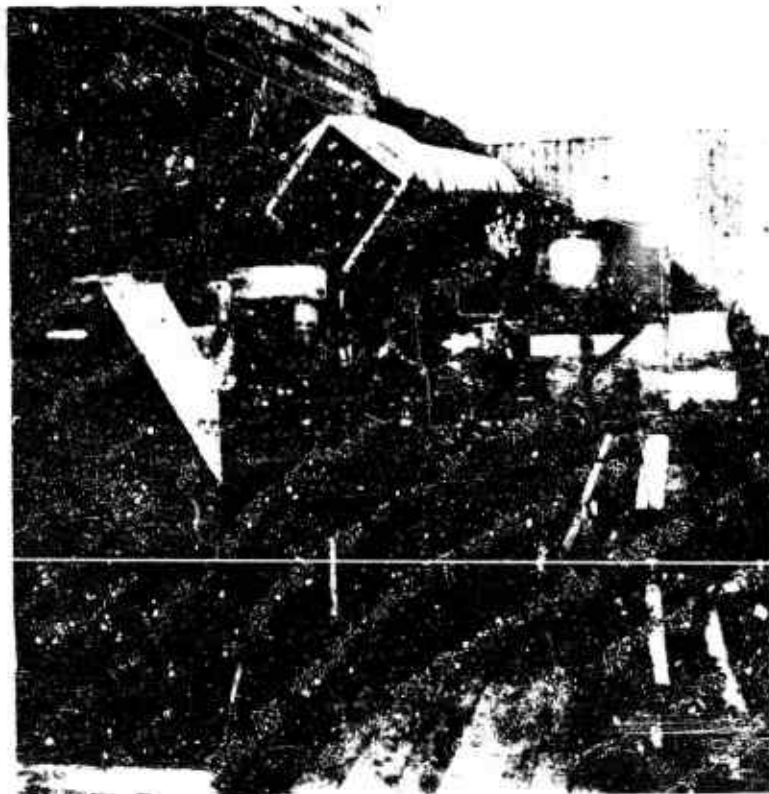


Fig. 14.4. Pulsejet engine test facility.

Figure 14.4 shows a photograph of a facility for testing pulsejet engines. The engine is fastened to a mobile carriage which facilitates thrust measurement. In front of the engine there is a spherical fuel tank. Next to it there are two tanks of compressed air: one to start the engine and the other to feed the fuel. Simplicity of the instrumentation and lack of laboratory comfort are surprising. Those who conducted tests on this stand must have had more brains than money. This is the more perplexing, since it is there that the first useful pulsejet engine was created.

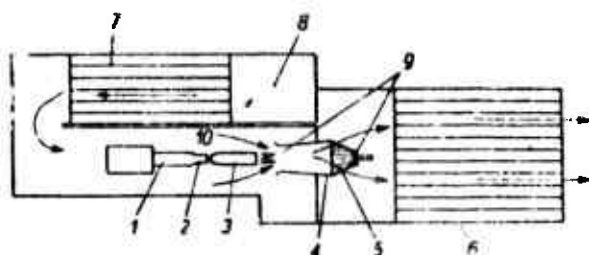


Fig. 14.5. Test facility for studying ramjet engines: 1) compressed air conduit; 2) Laval nozzle; 3) ramjet engine; 4) diffuser for exhausting combustion products; 5) mixing chamber; 6) exhaust muffler; 7) inlet muffler; 8) cooling air inlet; 9) water injection; 10) cooling air.

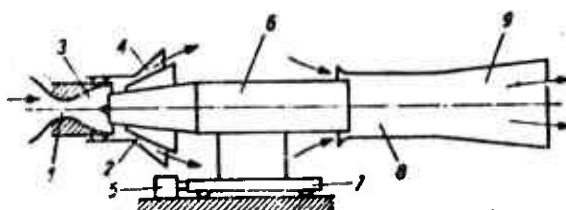


Fig. 14.6. Test facility for studying ramjet engines under high altitude conditions: 1) first critical cross section (transition of subsonic flow to supersonic); 2) second critical cross section (transition of supersonic flow to subsonic); 3) supersonic nozzle; 4) supersonic diffuser; 5) thrust measuring instrumentation; 6) ramjet engine; 7) mobile engine carriage; 8) mixing chamber of combustion products and ambient air; 9) diffuser.

Figure 14.5 shows a test facility for the study of ramjet engines. In this case, flight velocity is modeled by means of precompressed air flowing out of the nozzle. Combustion products arising in the engine

are cooled by water injection. If the pressure of the compressed air is insufficient to create the appropriate Mach number, then appropriate conditions should be maintained at nozzle exhaust to permit expansion below atmospheric pressure. In this fashion, due to a higher expansion, an appropriately higher Mach number can be achieved. Figure 14.6 represents a test stand built along these ideas. Operating conditions to which the engine is subjected correspond to altitude conditions. Inlet overpressure is obtained by means of an appropriate ratio of the area of nozzle exhaust cross section to the area of the critical cross section. The supersonic diffuser prevents the occurrence of shock waves inside the nozzle, by compressing the remaining air which cannot attain atmospheric pressure while flowing through the engine. The area of the second critical cross section occurring in a supersonic diffuser (of the type of an inverted Laval nozzle) must be properly selected as a function of output of the supply nozzle and of engine flow resistance. Overpressure at engine exhaust is obtained by means of an ejector diverging in the flow direction and which consists of a mixing chamber and a diffuser which compresses the mixture of combustion products and atmospheric air to the ambient pressure.

The test facility for studying rocket engines, and shown in Fig. 14.7, consists of three parts: a measurement room, a test room and a room in which are located (and properly segregated) tanks containing compressed air, fuel oxidizer and water. Water is used to cool the combustion products exiting from the nozzle and to wash off the floor the propellants which spill from the engine at start-up.

All measuring instruments and systems are located in the observation room.

Obviously engine start and stop is also accomplished from the observation room. In this room, the following quantities as indicated by

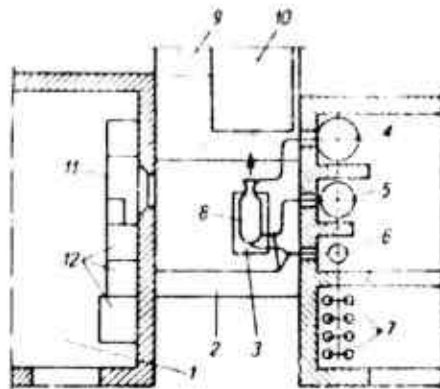


Fig. 14.7. Test facility for studying rocket engines: 1) measurement room; 2) test stand room; 3) engine carriage; 4) water tank; 5) oxidizer tank; 6) fuel tank; 7) bottle of compressed nitrogen; 8) rocket engine; 9) water tank; 10) muffling and exhausting of combustion products; 11) observer console; 12) measurement and recording instrumentation.

meter readings are recorded by the method of photography or automatic printout:

- rate of oxidizer and fuel flow (measurement by means of a contraction or of a rotating flowmeter whose revolutions are recorded by an electrooptical or a magnetic system);

- engine thrust (measured by the tensometer method);

- pressures at all characteristic engine points and in the pipe feeding the propellants (measured by means of properly cooled capacitive or inductive transducers whose outputs are recorded on an oscillographic tape);

- wall temperature and propellant temperature (measured with thermocouples);

- flame temperature (measured by optical means);

- velocity of combustion products in the chamber (measurement of the translation of burning propellant particles by means of a high-speed camera. The photographs are taken through a slit in the combustion chamber, specially fitted for this purpose).

REFERENCES TO CHAPTER 14

- 14.1. R. Jamison: Journal of the Royal Aeronautical Society. 61, No. 558, 1957.
- 14.2. T. Karman: Fundamental Equations in Aerothermodynamics. Selected Combustion Problems II, 1958.
- 14.3. M. Barrere, A. Jaumotte: Rocket Propulsion. 1960.

APPENDICES

APPENDIX 1

Equilibrium Constants

T (K)	$K_1 = \frac{P_{CO} P_{H_2O}}{P_{CO_2}}$	$K_2 = \frac{P_{H_2} P_{H_2O}}{P_{H_2O}}$	$K_3 = \frac{P_{H_2} P_{H_2O}}{P_{H_2O}}$	$K_4 = \frac{P_{H_2} P_{H_2O}}{P_{H_2O}}$	$K_5 = \frac{P_{H_2} P_{H_2O}}{P_{H_2O}}$	$K_6 = \frac{P_{H_2} P_{H_2O}}{P_{H_2O}}$	$K_7 = \frac{P_{H_2} P_{H_2O}}{P_{H_2O}}$	$K_8 = \frac{P_{H_2} P_{H_2O}}{P_{H_2O}}$
300	0.1825 · 10 ⁻⁴	0.1637 · 10 ⁻⁴	0.1637 · 10 ⁻⁴	0.1637 · 10 ⁻⁴	0.1637 · 10 ⁻⁴	0.1637 · 10 ⁻⁴	0.1637 · 10 ⁻⁴	0.1637 · 10 ⁻⁴
400	0.3895 · 10 ⁻⁴	0.5759 · 10 ⁻⁴	0.5759 · 10 ⁻⁴	0.5759 · 10 ⁻⁴	0.5759 · 10 ⁻⁴	0.5759 · 10 ⁻⁴	0.5759 · 10 ⁻⁴	0.5759 · 10 ⁻⁴
500	0.9806 · 10 ⁻⁴	0.1302 · 10 ⁻⁴	0.1302 · 10 ⁻⁴	0.1302 · 10 ⁻⁴	0.1302 · 10 ⁻⁴	0.1302 · 10 ⁻⁴	0.1302 · 10 ⁻⁴	0.1302 · 10 ⁻⁴
600	0.6624 · 10 ⁻⁴	0.2333 · 10 ⁻⁴	0.2333 · 10 ⁻⁴	0.2333 · 10 ⁻⁴	0.2333 · 10 ⁻⁴	0.2333 · 10 ⁻⁴	0.2333 · 10 ⁻⁴	0.2333 · 10 ⁻⁴
700	0.2900 · 10 ⁻⁴	0.2614 · 10 ⁻⁴	0.2614 · 10 ⁻⁴	0.2614 · 10 ⁻⁴	0.2614 · 10 ⁻⁴	0.2614 · 10 ⁻⁴	0.2614 · 10 ⁻⁴	0.2614 · 10 ⁻⁴
800	0.1277 · 10 ⁻⁴	0.5156 · 10 ⁻⁴	0.5156 · 10 ⁻⁴	0.5156 · 10 ⁻⁴	0.5156 · 10 ⁻⁴	0.5156 · 10 ⁻⁴	0.5156 · 10 ⁻⁴	0.5156 · 10 ⁻⁴
900	0.1445 · 10 ⁻⁴	0.3105 · 10 ⁻⁴	0.3105 · 10 ⁻⁴	0.3105 · 10 ⁻⁴	0.3105 · 10 ⁻⁴	0.3105 · 10 ⁻⁴	0.3105 · 10 ⁻⁴	0.3105 · 10 ⁻⁴
1000	0.6331 · 10 ⁻⁴	0.8728 · 10 ⁻⁴	0.8728 · 10 ⁻⁴	0.8728 · 10 ⁻⁴	0.8728 · 10 ⁻⁴	0.8728 · 10 ⁻⁴	0.8728 · 10 ⁻⁴	0.8728 · 10 ⁻⁴
1100	0.1389 · 10 ⁻⁴	0.1314 · 10 ⁻⁴	0.1314 · 10 ⁻⁴	0.1314 · 10 ⁻⁴	0.1314 · 10 ⁻⁴	0.1314 · 10 ⁻⁴	0.1314 · 10 ⁻⁴	0.1314 · 10 ⁻⁴
1200	0.1014 · 10 ⁻⁴	0.1267 · 10 ⁻⁴	0.1267 · 10 ⁻⁴	0.1267 · 10 ⁻⁴	0.1267 · 10 ⁻⁴	0.1267 · 10 ⁻⁴	0.1267 · 10 ⁻⁴	0.1267 · 10 ⁻⁴
1300	0.1591 · 10 ⁻⁴	0.8448 · 10 ⁻⁴	0.8448 · 10 ⁻⁴	0.8448 · 10 ⁻⁴	0.8448 · 10 ⁻⁴	0.8448 · 10 ⁻⁴	0.8448 · 10 ⁻⁴	0.8448 · 10 ⁻⁴
1400	0.1620 · 10 ⁻⁴	0.4401 · 10 ⁻⁴	0.4401 · 10 ⁻⁴	0.4401 · 10 ⁻⁴	0.4401 · 10 ⁻⁴	0.4401 · 10 ⁻⁴	0.4401 · 10 ⁻⁴	0.4401 · 10 ⁻⁴
1500	0.5087 · 10 ⁻⁴	0.1607 · 10 ⁻⁴	0.1607 · 10 ⁻⁴	0.1607 · 10 ⁻⁴	0.1607 · 10 ⁻⁴	0.1607 · 10 ⁻⁴	0.1607 · 10 ⁻⁴	0.1607 · 10 ⁻⁴
1600	0.2074 · 10 ⁻⁴	0.6615 · 10 ⁻⁴	0.6615 · 10 ⁻⁴	0.6615 · 10 ⁻⁴	0.6615 · 10 ⁻⁴	0.6615 · 10 ⁻⁴	0.6615 · 10 ⁻⁴	0.6615 · 10 ⁻⁴
1700	0.7131 · 10 ⁻⁴	0.2005 · 10 ⁻⁴	0.2005 · 10 ⁻⁴	0.2005 · 10 ⁻⁴	0.2005 · 10 ⁻⁴	0.2005 · 10 ⁻⁴	0.2005 · 10 ⁻⁴	0.2005 · 10 ⁻⁴
1800	0.2135 · 10 ⁻⁴	0.5983 · 10 ⁻⁴	0.5983 · 10 ⁻⁴	0.5983 · 10 ⁻⁴	0.5983 · 10 ⁻⁴	0.5983 · 10 ⁻⁴	0.5983 · 10 ⁻⁴	0.5983 · 10 ⁻⁴
1900	0.5687 · 10 ⁻⁴	0.1301 · 10 ⁻⁴	0.1301 · 10 ⁻⁴	0.1301 · 10 ⁻⁴	0.1301 · 10 ⁻⁴	0.1301 · 10 ⁻⁴	0.1301 · 10 ⁻⁴	0.1301 · 10 ⁻⁴
2000	0.1371 · 10 ⁻⁴	0.2892 · 10 ⁻⁴	0.2892 · 10 ⁻⁴	0.2892 · 10 ⁻⁴	0.2892 · 10 ⁻⁴	0.2892 · 10 ⁻⁴	0.2892 · 10 ⁻⁴	0.2892 · 10 ⁻⁴
2100	0.3035 · 10 ⁻⁴	0.5954 · 10 ⁻⁴	0.5954 · 10 ⁻⁴	0.5954 · 10 ⁻⁴	0.5954 · 10 ⁻⁴	0.5954 · 10 ⁻⁴	0.5954 · 10 ⁻⁴	0.5954 · 10 ⁻⁴
2200	0.1240 · 10 ⁻⁴	0.1149 · 10 ⁻⁴	0.1149 · 10 ⁻⁴	0.1149 · 10 ⁻⁴	0.1149 · 10 ⁻⁴	0.1149 · 10 ⁻⁴	0.1149 · 10 ⁻⁴	0.1149 · 10 ⁻⁴
2300	0.1203 · 10 ⁻⁴	0.2094 · 10 ⁻⁴	0.2094 · 10 ⁻⁴	0.2094 · 10 ⁻⁴	0.2094 · 10 ⁻⁴	0.2094 · 10 ⁻⁴	0.2094 · 10 ⁻⁴	0.2094 · 10 ⁻⁴
2400	0.2195 · 10 ⁻⁴	0.3634 · 10 ⁻⁴	0.3634 · 10 ⁻⁴	0.3634 · 10 ⁻⁴	0.3634 · 10 ⁻⁴	0.3634 · 10 ⁻⁴	0.3634 · 10 ⁻⁴	0.3634 · 10 ⁻⁴
2500	0.3810 · 10 ⁻⁴	0.6037 · 10 ⁻⁴	0.6037 · 10 ⁻⁴	0.6037 · 10 ⁻⁴	0.6037 · 10 ⁻⁴	0.6037 · 10 ⁻⁴	0.6037 · 10 ⁻⁴	0.6037 · 10 ⁻⁴
2600	0.6332 · 10 ⁻⁴	0.1609 · 10 ⁻⁴	0.1609 · 10 ⁻⁴	0.1609 · 10 ⁻⁴	0.1609 · 10 ⁻⁴	0.1609 · 10 ⁻⁴	0.1609 · 10 ⁻⁴	0.1609 · 10 ⁻⁴
2700	0.1013	0.1412 · 10 ⁻⁴	0.1412 · 10 ⁻⁴	0.1412 · 10 ⁻⁴	0.1412 · 10 ⁻⁴	0.1412 · 10 ⁻⁴	0.1412 · 10 ⁻⁴	0.1412 · 10 ⁻⁴
2800	0.1565	0.2233 · 10 ⁻⁴	0.2233 · 10 ⁻⁴	0.2233 · 10 ⁻⁴	0.2233 · 10 ⁻⁴	0.2233 · 10 ⁻⁴	0.2233 · 10 ⁻⁴	0.2233 · 10 ⁻⁴
2900	0.2345	0.3256 · 10 ⁻⁴	0.3256 · 10 ⁻⁴	0.3256 · 10 ⁻⁴	0.3256 · 10 ⁻⁴	0.3256 · 10 ⁻⁴	0.3256 · 10 ⁻⁴	0.3256 · 10 ⁻⁴
3000	0.3417	0.4628 · 10 ⁻⁴	0.4628 · 10 ⁻⁴	0.4628 · 10 ⁻⁴	0.4628 · 10 ⁻⁴	0.4628 · 10 ⁻⁴	0.4628 · 10 ⁻⁴	0.4628 · 10 ⁻⁴
3100	0.4054	0.6436 · 10 ⁻⁴	0.6436 · 10 ⁻⁴	0.6436 · 10 ⁻⁴	0.6436 · 10 ⁻⁴	0.6436 · 10 ⁻⁴	0.6436 · 10 ⁻⁴	0.6436 · 10 ⁻⁴
3200	0.6744	0.0770 · 10 ⁻⁴	0.0770 · 10 ⁻⁴	0.0770 · 10 ⁻⁴	0.0770 · 10 ⁻⁴	0.0770 · 10 ⁻⁴	0.0770 · 10 ⁻⁴	0.0770 · 10 ⁻⁴
3300	0.9179	0.1173	0.1173	0.1173	0.1173	0.1173	0.1173	0.1173
3400	1.2260	0.1544	0.1544	0.1544	0.1544	0.1544	0.1544	0.1544
3500	1.6100	0.2000	0.2000	0.2000	0.2000	0.2000	0.2000	0.2000
3600	2.9810	0.2556	0.2556	0.2556	0.2556	0.2556	0.2556	0.2556
3700	2.6520	0.3222	0.3222	0.3222	0.3222	0.3222	0.3222	0.3222
3800	3.3340	0.4017	0.4017	0.4017	0.4017	0.4017	0.4017	0.4017
3900	4.1410	0.4951	0.4951	0.4951	0.4951	0.4951	0.4951	0.4951
4000	5.6870	0.6042	0.6042	0.6042	0.6042	0.6042	0.6042	0.6042
4100	6.1810	0.7303	0.7303	0.7303	0.7303	0.7303	0.7303	0.7303
4200	7.4420	0.8750	0.8750	0.8750	0.8750	0.8750	0.8750	0.8750
4300	8.8740	1.0400	1.0400	1.0400	1.0400	1.0400	1.0400	1.0400
4400	10.5000	1.2280	1.2280	1.2280	1.2280	1.2280	1.2280	1.2280
4500	12.5300	1.4370	1.4370	1.4370	1.4370	1.4370	1.4370	1.4370
4600	14.3600	1.6730	1.6730	1.6730	1.6730	1.6730	1.6730	1.6730
4700	16.6200	1.9340	1.9340	1.9340	1.9340	1.9340	1.9340	1.9340
4800	19.1100	2.2240	2.2240	2.2240	2.2240	2.2240	2.2240	2.2240
4900	21.8400	2.5110	2.5110	2.5110	2.5110	2.5110	2.5110	2.5110
5000	24.8300	2.8010	2.8010	2.8010	2.8010	2.8010	2.8010	2.8010
5100	28.0600	3.2760	3.2760	3.2760	3.2760	3.2760	3.2760	3.2760
5200	31.5800	3.6640	3.6640	3.6640	3.6640	3.6640	3.6640	3.6640
5300	35.3700	4.1040	4.1040	4.1040	4.1040	4.1040	4.1040	4.1040
5400	39.4100	4.6110	4.6110	4.6110	4.6110	4.6110	4.6110	4.6110
5500	43.7500	5.1000	5.1000	5.1000	5.1000	5.1000	5.1000	5.1000
5600	48.3700	5.7270	5.7270	5.7270	5.7270	5.7270	5.7270	5.7270
5700	53.2700	6.3330	6.3330	6.3330	6.3330	6.3330	6.3330	6.3330
5800	58.4600	6.9810	6.9810	6.9810	6.9810	6.9810	6.9810	6.9810
5900	63.9600	7.6700	7.6700	7.6700	7.6700	7.6700	7.6700	7.6700
6000	69.7400	8.4050	8.4050	8.4050	8.4050	8.4050	8.4050	8.4050

APPENDIX 2

Total Enthalpy h_{ci} of Combustion Products of Fuels for Rocket Engines
[cal/mol·°C]

T [°K]	CO ₂	H ₂ O	CO	OH	NO	H	O ₂	N ₂	H	O	N	T [°K]
300	-93990,0	-57731,4	-26375,1	10107,9	21615,2	16,9	47,9	47,4	52115,6	5011,1	10591,6	300
400	-93049,8	-56919,4	-25676,8	10015,0	21399,2	711,9	7,6,0	714,9	52012,1	50701,0	10608,4	400
500	-92021,8	-56007,9	-24970,6	11520,1	23002,1	119,9	169,1	1117,5	53109,2	60211,5	10535,2	500
600	-90922,2	-55231,2	-24251,1	12226,2	23819,6	2131,6	2244,4	2160,5	53006,0	60717,8	87002,0	600
700	-89763,3	-54341,9	-23511,8	12932,3	24570,0	2811,9	3022,3	2637,3	51102,0	61221,6	107578,8	700
800	-88555,2	-53423,8	-22760,8	13613,8	25347,0	3477,0	3819,9	3631,1	51099,6	61723,5	108075,6	800
900	-87304,7	-52478,7	-21990,0	14300,8	26138,9	4253,1	4631,0	4486,0	50996,1	62221,5	108572,4	900
1000	-86022,6	-51505,4	-21204,1	15001,4	26941,4	4976,3	5461,5	5165,0	50893,2	62721,9	109082,2	1000
1100	-84709,6	-50505,1	-20404,6	15800,0	27762,9	5702,7	6300,3	5953,2	50790,0	63221,5	109566,0	1100
1200	-83371,8	-49477,2	-19593,3	16579,6	28592,1	6430,5	7138,6	6753,7	50690,8	63723,7	110062,8	1200
1300	-82013,4	-48423,2	-18771,7	17340,3	29430,5	7161,5	8005,1	7565,1	50583,6	64222,5	110539,6	1300
1400	-80637,2	-47344,3	-17941,0	18112,0	30276,7	7910,0	8893,0	8386,0	50480,1	64721,0	111056,4	1400
1500	-79245,6	-46242,2	-17102,1	18891,1	31129,6	8707,7	9799,6	9215,1	50377,2	65219,3	111553,2	1500
1600	-77840,4	-45118,3	-16257,6	19666,8	31988,3	9484,6	10616,5	10051,6	50274,0	65717,4	112050,0	1600
1700	-76423,0	-43974,5	-15406,8	20408,7	32852,0	10271,3	11491,4	10894,5	50170,8	66215,4	112546,8	1700
1800	-74995,0	-42812,4	-14550,7	21299,6	33720,1	11060,3	12388,1	11713,0	50067,6	66713,2	113043,6	1800
1900	-73557,4	-41633,7	-13690,1	22118,9	34592,1	11875,8	13292,6	12586,6	50004,4	67211,1	113540,5	1900
2000	-72111,2	-40440,1	-12825,5	22915,9	35467,6	12690,4	14218,7	13454,7	50061,2	67708,8	114037,4	2000
2100	-70657,4	-39232,8	-11957,3	23780,2	36346,2	13514,0	15098,3	14316,8	50110,0	68206,6	114534,3	2100
2200	-69196,4	-38013,1	-11085,9	24621,3	37227,6	14345,5	15993,5	15182,5	50155,8	68704,4	115031,3	2200
2300	-67723,0	-36782,1	-10211,5	25468,6	38111,6	15184,5	16891,1	16051,5	50201,6	69202,3	115528,5	2300
2400	-66255,6	-35540,7	-9334,4	26321,9	38997,9	16030,8	17795,2	16923,4	50248,4	69700,4	116025,8	2400
2500	-64776,6	-34289,9	-8454,5	27180,6	39886,4	16883,9	18705,7	17798,0	50304,5	70198,6	116523,4	2500
2600	-63292,4	-33030,3	-7573,2	28044,5	40776,8	17743,5	19698,1	18675,1	50354,0	70697,1	117021,4	2600
2700	-61803,2	-31762,6	-6689,5	28913,1	41669,1	18609,5	20676,4	19554,5	50403,8	71195,9	117519,8	2700
2800	-60309,3	-30487,6	-5803,9	29786,4	42563,2	19481,3	21579,6	20436,0	50453,6	71695,0	118018,9	2800
2900	-58811,1	-29295,7	-4916,6	30664,0	43458,9	20350,9	22522,3	21319,5	50503,2	72194,6	118518,6	2900
3000	-57308,8	-27917,4	-4027,6	31545,8	44356,3	21242,1	23480,0	22204,7	50552,9	72694,8	119019,2	3000
3100	-55802,6	-26623,4	-3136,0	32431,6	45255,1	22130,6	24437,1	23091,6	50602,6	73195,5	119520,9	3100
3200	-54292,7	-25324,1	-2244,0	33321,1	46155,4	23024,4	25399,1	23980,2	50652,8	73696,8	120023,3	3200
3300	-52779,2	-24020,0	-1350,7	34214,2	47057,1	23923,3	26365,2	24870,2	50701,6	74198,9	120528,0	3300
3400	-51262,4	-22711,4	-456,2	35110,7	47960,2	24827,2	27335,5	25761,6	50751,6	74701,8	121033,9	3400
3500	-49742,4	-21398,7	+479,6	36010,6	48864,5	25736,0	28309,7	26651,3	50801,3	75205,4	121541,6	3500
3600	-48219,2	-20082,2	1336,4	36913,7	49770,0	26649,6	29287,8	27548,3	50851,0	75710,0	122051,4	3600
3700	-46693,2	-18762,1	2234,4	37819,9	50676,7	27568,0	30265,5	28441,5	50900,8	76215,5	122563,3	3700
3800	-45164,4	-17438,7	3133,4	38729,1	51584,6	28491,0	31254,7	29332,3	50950,6	76722,0	123077,7	3800
3900	-43632,8	-16112,2	4033,4	39641,2	52493,6	29418,5	32243,2	30227,2	51000,4	77229,5	123594,8	3900
4000	-42098,6	-14782,8	4934,4	40556,0	53403,8	30350,5	33234,8	31125,6	51049,2	77738,1	124114,7	4000
4100	-40561,8	-13450,7	5836,3	41473,6	54315,0	31286,9	34229,4	32035,0	51099,0	78247,8	124637,7	4100
4200	-39022,6	-12116,1	6739,2	42393,8	55227,3	32227,6	35226,8	32935,4	51149,8	78758,6	125164,0	4200
4300	-37480,9	-10779,1	7643,0	43316,6	56140,6	33172,5	36226,8	33836,6	51197,6	79270,6	125693,8	4300
4400	-35936,8	-9439,9	8547,7	44241,9	57054,9	34121,7	37229,3	34738,8	51248,4	79783,8	126227,3	4400
4500	-34390,5	-8098,6	9453,2	45169,7	57970,2	35074,9	38234,1	35641,9	51298,1	80298,1	126764,6	4500
4600	-32841,8	-6755,2	10359,5	46099,9	58886,5	36032,1	39211,2	36545,8	51347,8	80813,7	127305,9	4600
4700	-31291,0	-5405,3	11260,5	47032,5	59803,8	36993,4	40250,4	37450,6	51397,8	81330,5	127851,4	4700
4800	-29737,8	-4062,4	12174,3	47967,5	60722,1	37958,6	41261,6	38356,2	51447,6	81848,5	128401,1	4800
4900	-28182,6	-2713,2	13082,9	48904,8	61641,4	38927,7	42271,4	39262,0	51498,4	82367,7	128955,4	4900
5000	-26625,0	-1362,0	13992,1	49844,3	62561,7	39900,5	43289,3	40169,8	51549,2	82888,1	129514,1	5000
5100	-25065,4	-9,0	14902,1	50786,0	63483,0	40877,2	44305,7	41077,8	51600,0	83409,7	130077,6	5100
5200	-23503,4	+1346,0	15812,7	51729,1	64405,3	41857,6	45323,7	41986,5	51650,8	83932,5	130645,8	5200
5300	-21939,4	2702,6	16724,1	52675,6	65328,5	42811,6	46343,1	42896,1	51701,6	84456,6	131218,9	5300
5400	-20373,0	4061,1	17636,1	53623,5	66252,6	43829,3	47363,9	43806,3	51752,1	84981,8	131796,9	5400
5500	-18804,6	5422,0	18548,7	54573,4	67177,7	44820,5	48386,0	44717,4	51802,9	85508,2	132380,0	5500
5600	-17233,8	6784,3	19462,1	55525,3	68103,8	45815,1	49409,9	45629,1	51854,0	86035,8	132968,1	5600
5700	-15661,0	8148,5	20376,1	56478,1	69030,9	46813,5	50433,8	46541,6	51905,2	86564,0	133561,4	5700
5800	-14085,8	9514,5	21290,7	57434,3	69958,9	47815,1	51459,4	47454,9	51956,4	87094,5	134159,9	5800
5900	-12508,6	10932,3	22206,0	58392,5	70887,8	48820,1	52485,9	48368,8	52007,6	87625,5	134763,7	5900
6000	-10929,0	12351,9	23121,9	59351,8	71817,7	49826,5	53513,4	49283,5	52058,8	88157,7	135373,8	6000

Note: Values of total enthalpy are given in cal/mol·°C. In order to convert them to [kcal/mol·°C], the tabular entries should be divided by 1000.

DISTRIBUTION LIST

<u>Organization</u>	<u>Nr. Cys.</u>	<u>Organisation</u>	<u>Nr. Cys.</u>
<u>AIR FORCE</u>		<u>OTHER DOD AGENCIES</u>	
Hq USAF (AFNIEBA)	1	DDC	20
AFNIEBE	1	Hq USAREUR	1
ACIC (ACDEL-7)	2	Army Map Service	1
AFRIF		U.S. Army (EMTC)	4
Rend (Calif)	1	Harry Diamond Lab	1
OAR (BRYA)	2	Army Security Agency	1
AFORL (CRCLR)	1	U.S. Navy (STIC/NSE)	1
ARI. (ARB) WF, AFB	1	NOTS China Lake	1
SAC (DISC)	1	PAC Msl Range	1
Hq AFSC (SCFT)	1	<u>OTHER GOVERNMENT AGENCIES</u>	
AEDC (AEY)	2	AEC (Tenn)	2
AFETR (ETW)	1	AEC (Wash)	2
AFRPL (RPT)	1	FAA (Med Lib)	2
APGC (PGFR/APGCC)	1	FAA (SS-10)	1
ASD (ASFUS-2)	9	NAFEC	1
EED (ESY/ESDSI)	1	NASA (ATSS-T)	1
SAMSO (SMFA)	5		
RTD			
TDBDI -2	2		
TDETL	2		
TDBXF	3		
ATD (2)			
PHS (1)			
TDBXT	1		
TDCT	3		
CTE (1)			
CTP (1)			
TDDEI	1		
TDDP	1		
TDE (PHE)	15		
PRA (1)			
PRE (1)			
PV (1)			
PW1 (1)			
PW2 (1)			
PW3 (1)			
PW4 (1)			
PW5 (1)			
PW7 (1)			
PW9 (1)			
PW10 (1)			
PW12 (1)			
PW13 (1)			
PW (1)			
PX (1)			
		DIA (DIACO-3)	18
		DIAAP-1C1 (1)	
		DIAAP-1H2 (1)	
		DIAS-A (1)	
		DIAS-5C (1)	
		U.S. Navy (ONR) (1)	
		OP922F2 (1)	
		CIA (SD) (5)	
		NSA (CREF/CDB) (5)	

DISTRIBUTION LIST

<u>Organisation</u>	<u>Nr. Cys.</u>	<u>Organization</u>	<u>Nr. Cys.</u>
<u>AIR FORCE</u> (Continued)		<u>OTHER DOD AGENCIES</u>	
FTD (Continued)			
TDSC	3		
ESP	(1)		
ESP/B	(1)		
ESP/S	(1)		
TDET	9		
ETT4/B	(1)		
ETT4/D	(1)		
ETT4/G	(1)		
ETT4/H	(1)		
ETT4/R	(1)		
ETT8/M	(1)		
ETT8/R	(1)		
ETC/Roberts	(2)		
TDFA	1		
TDFC	2		
FCC	(1)		
TCC/2	(1)		
TDGS	1		
TDT	2		
Det #4 (FTD)	1		
		<u>OTHER GOVERNMENT AGENCIES</u>	
		<u>DISTRIBUTION TO BE MADE BY</u>	